ISSN 2636-8498

Environmental Research & Technology

Year 2022
Volume 5
Number 1

YTU PRESS

www.ert.yildiz.edu.tr

ISSN 2636-8498

Environmental Research & Technology

Volume 5 Number 1 Year 2022

ISSN 2636-8498

Environmental Research & Technology

Volume 5 Number 1 Year 2022

ISSN 2636-8498

Environmental Research & Technology

Volume 5 Number 1 Year 2022

CONTENTS

Research Articles

Environ Res Tec, Vol. 5, Issue. 1, pp. 1–10, March 2022

Environmental Research and Technology
https://ert.yildiz.edu.tr - https://dergipark.org.tr/tr/pub/ert
DOI: https://doi.org/10.35208/ert.860623

Environmental Research & Technology

Research Article

Lime stabilization of clayey landfill base liners: Consolidation behavior and hydraulic properties

Tanay KARADEMİR*

Department of Civil Engineering, İstanbul Bilgi University, İstanbul, Türkiye

ARTICLE INFO

Article history
Received: 13 January 2021
Revised: 14 September 2021
Accepted: 04 January 2022

Key words:
Clayey soils; Consolidation behavior; Hydraulic properties; Landfill base liners; Lime stabilization

ABSTRACT

Lime soil treatment is a chemical process in which lime (quicklime, hydrated lime or lime slurry) is mixed with the in place subgrade soil and a chemical reaction takes place. The lime reacts with the clay particles in the soil to create a cementitious matrix. The design of landfill base liners including a clay layer as a fluid barrier (i.e. water-resistant impervious layer) requires a neat engineering approach considering, in particular, consolidation behavior as well as hydraulic properties of the clay contained. For sake of safe and stable design of such baseliners under the landfills, the reduction of consolidation settlement in clay when subjected to the accumulated waste load (i.e. superposed action) during operation as well as the accomplishment for ensuring the waterproof of those composite base liners (comprised of multiple different layers) not to allow the penetration of the contaminated water - produced as a result of exothermic reactions occurring in the waste body in landfills – by enabling enhanced isolation from the natural ground is of importance. In light of this, in order to address those two most important design concerns (i.e. Consolidation and Hydraulic Properties of Clay) as well as to in an attempt to develop an enhanced clay layer system for landfill baseliners that has a greater bearing capacity (i.e. load resistance), and hence, more robust against settlements, and additionally, possessing improved hydraulic properties by being relatively more water-resistant and greatly impermeable, a series of consolidation tests were performed in the laboratory at different lime contents (lime/lime-clay mixture proportions by weight: 0%, 10%, and 20%) on clay specimens to investigate the stabilization and improvement of clayey landfill baseliners. Lime treatment on clay specimens has shown as a result of the experimental program that the strength of clay against loading improves, and further, exhibits less vertical deformation (settlement) under the load owing to an increase in lime content. Moreover, the clay becomes highly impermeable and displays substantially larger water-resistant properties because of increased lime mass proportion in clayey soil. The findings of the experimental program demonstrate that lime stabilization of the clayey soils in landfill baseliners will benefit the bearing capacity and the imperviousness (water tightness) engineering design properties as compared to standard composite multi-layered landfill baseliner systems.

Cite this article as: Karademir T. Lime stabilization of clayey landfill base liners: Consolidation behavior and hydraulic properties. Environ Res Tec 2022;5:1:1–10.

***Corresponding author.**
*E-mail address: tanay.karademir@bilgi.edu.tr

This paper has been presented at EurAsia Waste Management Symposium 2020, İstanbul, Turkey

Published by Yıldız Technical University Press, İstanbul, Turkey

INTRODUCTION AND LITERATURE REVIEW

Lime stabilization is a chemical process established through physical mixing with the in-place soil along with the addition of a limited amount of water to facilitate (i.e. catalyze) and accelerate the chemical reaction for the formation of clay-lime cementitious matrix as well as to prevent dust emission during construction. In this perspective, over decades, lime has been used as a modifier as well as a binder for fine grained soils such as clay. Further, the treatment of clays with high plasticity results in a decrease of the plasticity index, and thus, the clay becomes possessing less affinity with water to exhibit substantial volume changes (dilation and/or expansion) which may cause the endangerment of the stability of the infrastructure constructed using that clay layer. Additionally, the pozzolanic action in fine grained soils accompanies strength increment in soil. Moreover, lime also provides binding action even for course grained soils.

The improvement of the engineering design properties of soil up to desired values to satisfy the project requirements is called soil stabilization for which the principal objective is to increase load carrying resistance (i.e. bearing capacity) as well as to enhance hydraulic properties of the soil layers designed in infrastructural projects in order to fulfill the constructional purpose. Landfills are one of the commonly constructed geo-environmental infrastructure applications throughout the world, particularly in the developed countries to protect the environment from the damaging impact of the contaminants that exist in the stacked and stored industrial and/or municipal waste bodies. To this end, base, side slope and cover liners of the landfill applications requires a neat engineering approach in design and development to accomplish a proper performance in terms of sufficient bearing capacity and superior hydraulic properties by enabling improved compressive strength against accumulated waste load and by providing enhanced imperviousness against infiltration of contaminated water leaking out from the waste. Within this scope, lime treatment of clay layers, essential part (component) of multi-layered composite landfill liners, leads to building and establishing a strengthened and highly water-resistant cementitious matrix in clay so as that the desired bearing capacity and hydraulic properties are achieved in the landfill liners. Furthermore, the main advantages of lime stabilization method in comparison to the other techniques including mechanical (i.e. compaction) and chemical (i.e. cement stabilization) stabilization methods are; (i) soil becomes more workable, (ii) strength is substantially improved, (iii) compressive strength is increased as high as 60 times, (iv) it is effective for most soil types. On the other hand, the disadvantages of lime stabilization could be described as follows; (i) lime is produced by burning of limestone in kilns, therefore it is harmful for the environment, (ii) the burning of limestone requires more cost, (iii) it is not effective for gravelly soils [1, 2].

Over the decades, several soil stabilization techniques including physical stabilization, chemical stabilization and mechanical stabilization have been used by the engineers in order to reinforce soil by improving mechanical strength characteristics (i.e. consolidation behavior of clayey soils) as well as by enhancing hydraulic properties (i.e. hydraulic conductivity or imperviousness characteristics) [1]. To this end, the lime-treatment process (i.e. being a chemical stabilization method) comprised mainly of chemical reactions in between lime and soil particles such that an improvement for the performance of soil layer is achieved by controlling volume change, and also, by increasing strength. The mineralogical properties of the soils, as per stabilization, determines their degree of reactivity with lime, and hence, the ultimate strength that the stabilized layers will develop. Owing to pozzolanic action in fine grained soils such as clays, the strength increment (i.e. gaining resistance against loads) is particularly expected in clayey soils so that the stabilization of the soil layer is accomplished.

In the lime-treatment process, there are two stages of the soil-lime chemical reaction. The initial stage – categorized as immediate or short-term treatment – develops within a few hours or days after the lime is admixed with soil in which three primary chemical reactions, namely; cation exchange, flocculation-agglomeration and carbonation are observed. The latter stage – categorized as long-term treatment – requires several months or years for completion in which a principal chemical reaction, namely as a pozzolanic reaction is detected [2, 3]. During lime-treatment process, the increase in soil workability as a result of drying of wet soil is attributed to immediate treatment and the increase in soil strength and durability is associated with long-term treatment [4]. As such, the calcium ions (Ca^{+2}) and the hydroxide anions (OH^{-}) are produced as a result of the addition of lime into the soil multiphase system including water in pore space. Then, during the process of cation exchange in soil, bivalent calcium ions (Ca^{+2}) are replaced by monovalent cations. The Ca^{+2} ions link to the soil minerals possessing negative charges in the encapsulation of diffused double layer, and thus, resulting in a reduction of the repulsion forces leading to the shrinkage of thickness of the diffused double layer (i.e. water layer) around clay particles so as that the bonds between the soil particles are strengthened. The reduction in the thickness of diffused double layer results in the proximity (i.e. closeness) of clay particles, thereby the soil texture changes and the multiphase soil matrix becomes densified causing a strength increment in the soil. The remaining hydroxide anions (OH-) in the solution existing in the voids (i.e. pore spaces) of soil media catalyze and induce an increment in alkalinity. This physiochemical process is called flocculation and agglomeration which is the main

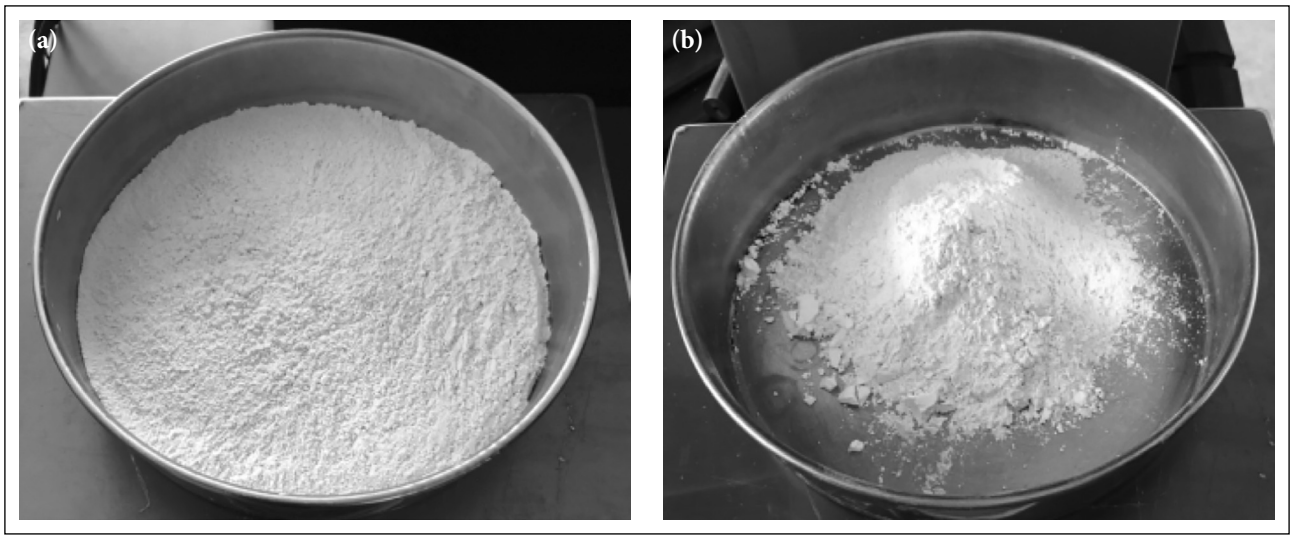

Figure 1. **(a)** Clay (Bentonite). **(b)** Lime.

factor of the increase in the strength of soil or the enhancement of the bearing capacity to exhibit better performance and greater resistance against loadings [5]. As such, the mineral particles re-arrange in the flocculated/aggregated structure, giving rise to an intra-aggregate porosity and an apparent change in texture, with clay particles clumping together into larger-sized aggregates [6]. The above-described reactions are commonly identified as short-term reactions and they reduce the soil plasticity index (PI) and its water affinity [7]. The swelling potential decreases while hydraulic conductivity usually increases [8]. In the long-term, pozzolanic reactions develop between calcium ions and the silica or alumina of the lattices of clay minerals, improving strength and compressibility of the soil [6–8].

The clayey soils mostly have soft and sensitive nature that is related to and controlled by depositional and post-depositional factors [9]. As such, the main depositional factor is the inter-particle flocculation that creates an open micro-structure in such soils. As a consequence of different environmental depositional conditions, the soft, sensitive nature clay deposits located worldwide are characterized by different mineralogical and mechanical characteristics [10]. In this regard, lime is a stabilizing agent capable of improving properties of fine-grained soils to obtain proper hydraulic and mechanical characteristics for earthen structures (e.g., dikes, road embankments) [11]. Lime stabilization is acknowledged as an environmentally sound and cost-effective application because costs of high-quality material from quarries and of disposal of the unsuitable in situ soil are eliminated, and therefore, it is widely applied worldwide [12]. In this regard, the soil stabilization utilizing lime has also been practically applied in the field for important infrastructural projects in Turkey including roadway constructions conducted by General Directorate of Highways (i.e. KGM) in Marmara Region (Tekirdag), Central Anatolia (Konya). To this end, this paper will extend the understanding regarding the effect of lime stabilization on the consolidation behavior, mechanical characteristics and hydraulic properties of soils.

MATERIAL PROPERTIES AND TESTING PROGRAM

In this section, the experimental method followed in the laboratory for performing the comprehensive testing program will be explained along with the information provided on the engineering properties of the testing materials as well as the description given regarding the testing device and the experimental procedures conducted for the preparation of test specimens, installation of the equipment and the placement of the specimen in the experimental set-up.

Materials

The clayey soil selected to be used throughout the entire experimental program was the natural calcium Bentonite (i.e. has a very high proportion of exchangeable calcium whereas including a very low proportion of exchangeable sodium) (Fig. 1a) that is industrial clay for which the physical, chemical and index properties are suitable for the engineering standards. The lime (Fig. 1b) admixed into clay as a stabilizing agent was slaked lime of which the chemical composition is comprised mainly of Calcium (CaO) that transforms to a white powder and constitutes $Ca(OH)_2$ by reacting with water vapor in the air, thereby leading to obtain white amorphous material as shown in Figure 1b.

Testing Equipment

A floating ring cell consolidometer (UTS – 0300 Oedometer) in which the ring containing the soil sample is unrestrained in the container was utilized in the laboratory to perform consolidation tests on clayey soil – lime admixture

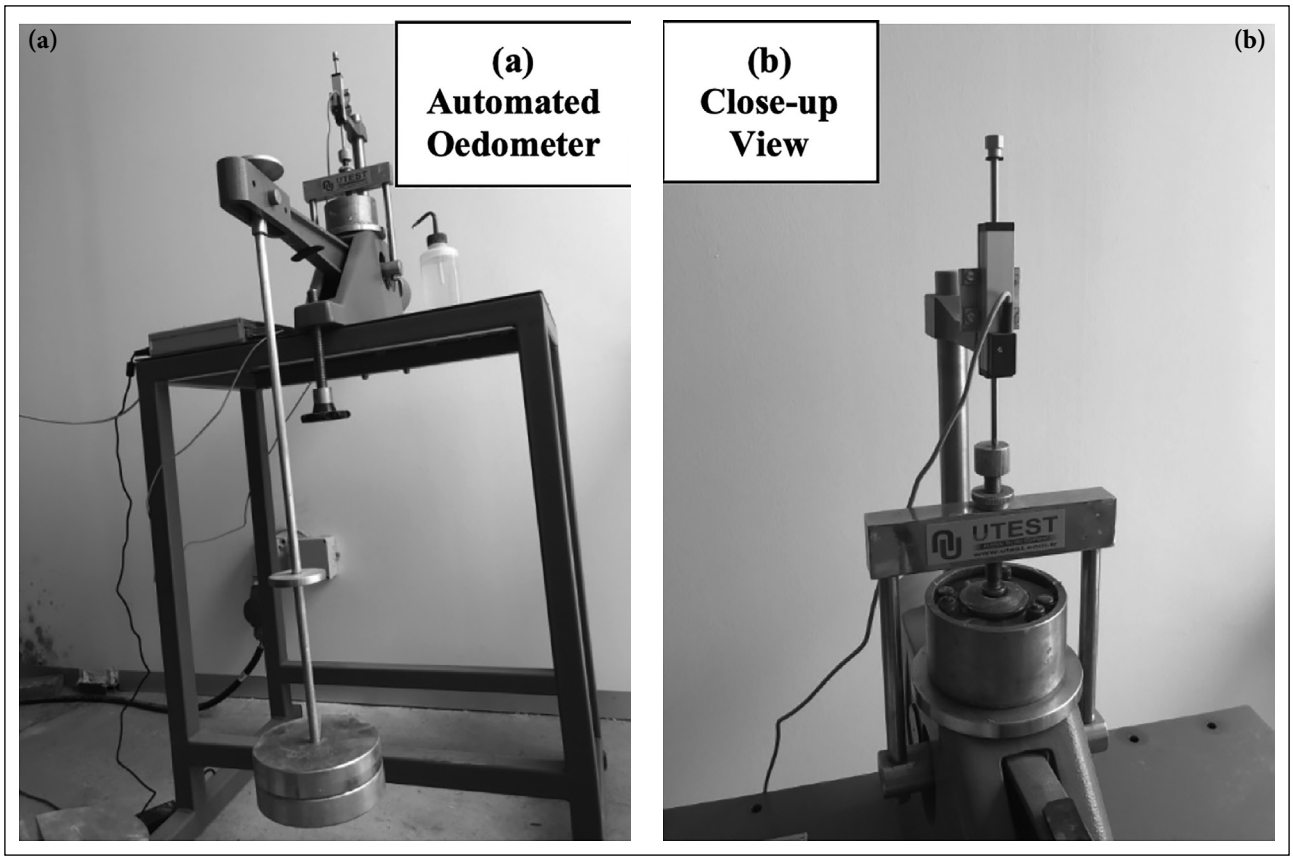

Figure 2. **(a)** Automated consolidation device. **(b)** Close up view of consolidation device.

Table 1. Laboratory testing program and dry mass proportions of different test specimens

Samples	Test specimen I	Test specimen II	Test specimen III
Mass proportions	100% Clay – 0% Lime	90% Clay – 10% Lime	%80 Clay 20% Lime

specimens (Fig. 2). A linear variable differential transformer (LVDT) was employed in the system to measure vertical displacement in evaluating the deformations developing in the soil specimen under the application of load during the tests. The displacement readings are logged into a computer through a multi-channel data logger such that the communication with the computer is enabled using RS-232 ports.

Testing Program

In this study, a series of consolidation tests [13] were performed in the laboratory at different lime contents (lime: lime-clay-mixture proportions by dry weight: 0%, 10%, and 20%) on the test specimens prepared in the laboratory to investigate the lime-stabilization (Table 1). Those different lime contents were mixed with clayey soil specimens such that the required weights of slaked lime were properly and completely admixed with batches of air-dried clay soil specimens to achieve lime-soil admixtures containing 0%, 10%, 20% lime contents on a dry weight basis. Further, the reconstituted consolidation test specimens were prepared at a dry unit weight of 13 kN/m^3 with a optimum moisture content of 30%. The results of consolidation tests conducted were used to determine the engineering consolidation parameters including; coefficient of consolidation (c_v), compression index (C_c), recompression index (C_r) for evaluating strength-deformation characteristics as well as to identify an important hydraulic property such as coefficient of permeability (k) for assessing hydraulic characteristics. The test specimens (cylindrical: 6.0 cm in diameter and 2.5 cm in height) were prepared by admixing lime into clay at different dry mass proportions, and then, by enclosing in a stiff metal ring and placing between two porous stones in a cylindrical container filled with water. Later, A metal load platen mounted on top of the upper porous stone transmits the applied vertical stress (vertical total stress) to the soil sample. Both the metal platen and the upper porous stone can move vertically inside the ring as the soil settles under the applied vertical stress.

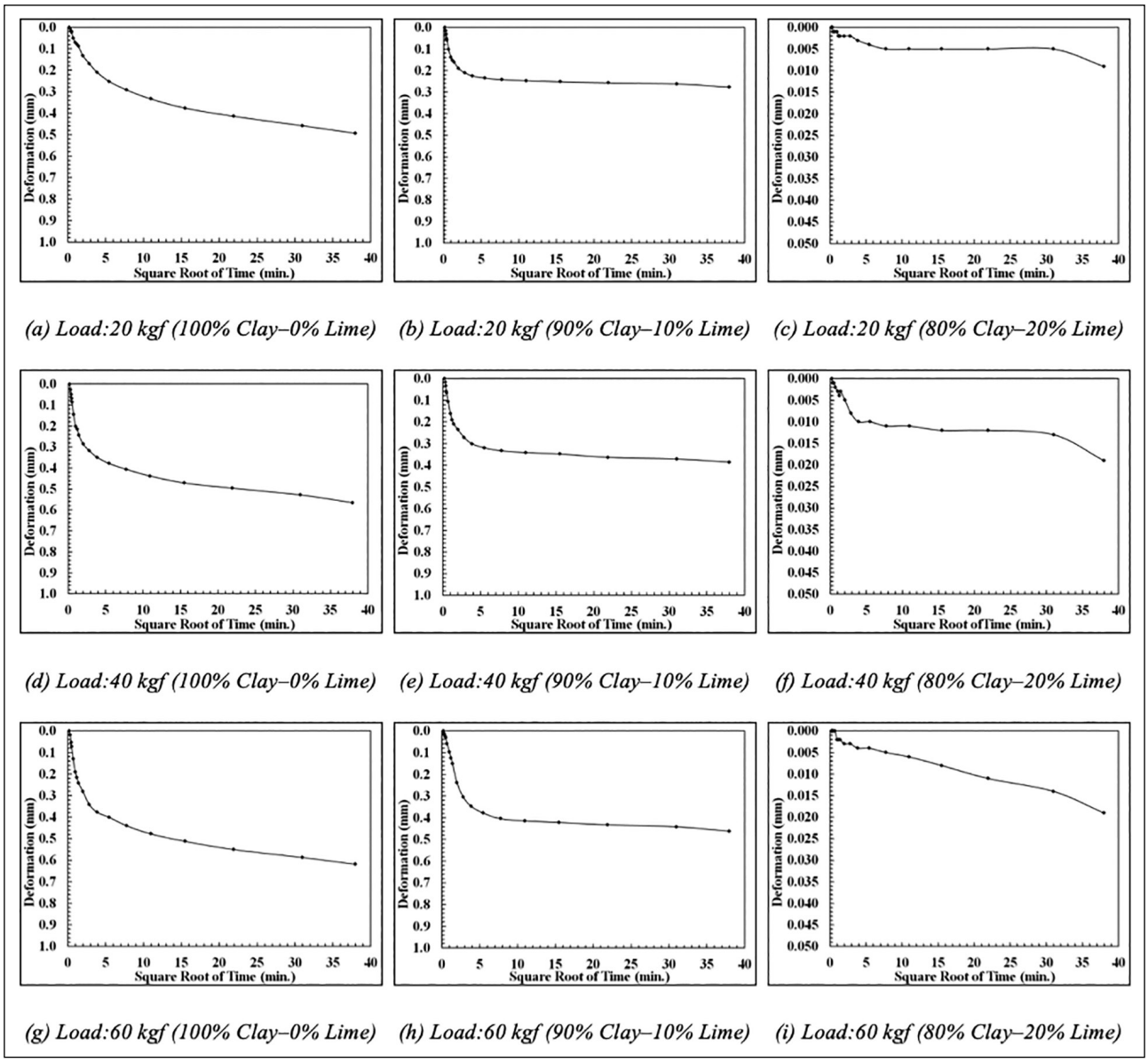

Figure 3. Deformation versus square root of time curves.

Incremental loads are applied to the platen, and the settlement of the soil at various fixed times under each load increment is measured by the transducer (LVDT) described in Testing Equipment Section. Each test continued six days with sequential incremental loads of 5, 10, 20, 40, 60, and 80 kgf, successively. As such, each load increment was doubled and allowed to remain on the soil until the change in settlement is negligible and the excess porewater pressure developed under the current load increment has dissipated. For many soils, this usually occurs within 24 hours [14]. Therefore, the vertical displacements (i.e. deformations) occurred in the specimen at every load increment were measured and recorded automatically in the computer over 24 hours (i.e. 1 day) at time intervals of logged data as follows: 0.05, 0.1, 0.2, 0.25, 0.5, 1, 2, 4, 8, 15, 30, 60, 120, 240, 480, 960, 1440 minutes, successively. Further, it should be emphasized that the ratio of the load increment to the previous load called as the load increment ratio (LIR) was selected as two conventionally. Similarly, the measurement time interval for reading the deformations develeoped in the specimen under loading were also selected as two purposefully to examine consolidation behavior in a comprehensive manner.

RESULTS

The experimental findings of consolidation tests performed at different lime contents (0%, 10%, and 20%) on the test specimens prepared in the laboratory to investigate the lime-stabilization will be presented in this Section along with supplementary theoretical descriptions and technical

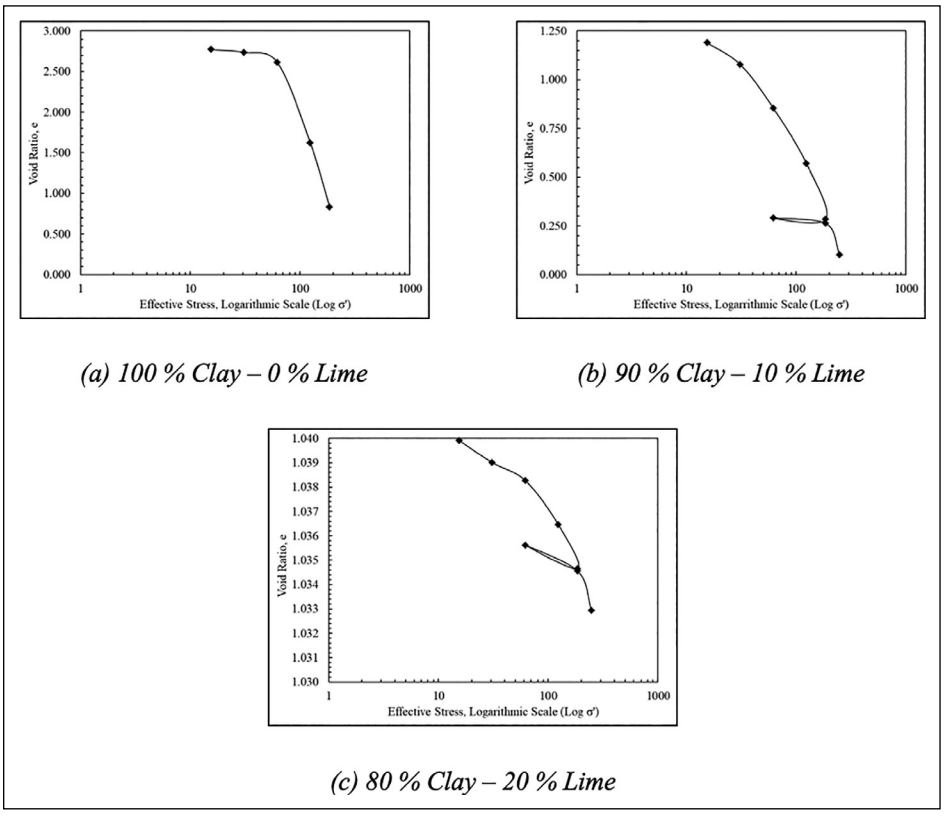

Figure 4. Void ratio (e) versus effective stress, logarithmic scale (Log σ') curves.

explanations. One purpose for changing lime content (i.e. dry mass percentage) in clay soil is to examine and unveil the mass proportion of lime content required to change the characteristics of the clayey soils, and thus, dominating the consolidation behavior and engineering properties.

Deformation Readings with Time

Three different loading conditions (20, 40 and 60 kgf) among distinct loads ranging 5 kgf up to 80 kgf incrementally applied during the course of each consolidation test were selected representatively to show the deformation readings with time, that is to say, the developed displacements measured in the tests with time for different clay – lime admixtures. As such, the generated displacement versus square root of time curves based on experimental measurements are presented in Figure 3 in the sequence of incremental loads successively.

Volumetric Compression and Loading

Soil is a multiphase material that consists of solid soil particles and void space filled by fluid and/or occupied by air exhangeably. The relative proportion of the volume of void space with respect to the volume of the solid soil particles is called void ratio (e) [15]. This engineering parameter is used very commonly to examine the change in volume of soil (i.e. volumetric compression) because of loading. To this end, the change in void ratio of the clay–lime admixtures (at different dry weight proportions) measured in the consolidation tests due to load increment, that is to say, an increase in the effective stress (applied load/specimen area) are presented in Figure 4. The compression and the recompression stages are evident in the curves such that the soil specimens exhibited elastoplastic behavior. That is, some part of the volumetric compression under the load (i.e. settlement under loading) is recoverable quantized through an engineering design parameter called recompression index (C_r), while the other part is permanent quantized through a consolidation property called compression index (C_c). Additionally, the unloading-reloading cycle has been performed in the tests of the 90% Clay-10% Lime and the 80% Clay-20% Lime specimens to clearly detect and evidently reveal recompression stage, and thus, accurately determine the important consolidation parameter; recompression index (C_r).

Both C_c and C_r consolidation parameters (from Fig. 4) helps us extend the understanding on the estimation of the amount of consolidatiton settlement the soil will undergo due to application of overburden in the field, and thus, the bearing capacity of the soil under loading. As such, the load-deformation behavior of the clayey soil is assessed through these important engineering parameters; C_c and C_r. Further, the coefficient of consolidation (c_v) (from Fig. 3) aids in the evaluation of the rate of consolidation settlement, and thus, time characteristics of the soil subjected

Table 2. Consolidation strength and deformation as well as hydraulic properties

Engineering Design Parameters (Consolidation Strength, Deformation, Hydraulic Properties)				
Clay - Lime Admixture	**Compression Index (C_c), [ ]**	**Recompression Index (C_r), [ ]**	**Coefficient of Consolidation (C_v), [cm^2/min]**	**Coefficient of Permeability (k), [cm/min]**
100% Clay - 0% Lime	1.439E-02	3.364E-03	0.19781	3.920E-04
90% Clay - 10% Lime	5.122E-03	4.787E-05	0.12036	1.151E-04
80% Clay - 20% Lime	3.085E-05	7.776E-06	0.03565	2.229E-06

to loading in the field as leading to comprehend strength performance of the clayey soil under loading.

Determination of Consolidation Engineering Design Parameters

The following theoretical methods were carried over to detemine the engineering design parameters including consolidation strength-deformation-time properties:

(i) The compression index (Equation 1) that is the average slope of compression stage in the e versus log(σ') plots – was determined using the void ratio and effective stress curves as presented in Figure 4 for different clay – lime admixtures.

$$(C_c = \Delta e/(\log \sigma'_2/\sigma'_1)) \quad (1)$$

Where:

Δe: Change in void ratio

$\log(\sigma'_2/\sigma'_1)$: Change in vertical effective stress

(ii) Similarly, the recompression index (Equation 2) that is the average slope of recompression stage in the e versus log(σ') plots – was determined using the void ratio and effective stress curves as presented in Figure 4 for different clay – lime admixtures.

$$(C_r = \Delta e/(\log \sigma'_2/\sigma'_1)) \quad (2)$$

Where:

Δe: Change in void ratio

$\log(\sigma'_2/\sigma'_1)$: Change in vertical effective stress

(iii) The coefficient of consolidation (c_v) was determined by applying "*Root time method*" (*Taylor's method*) on displacement versus square root of time curves as presented in Figure 3 at distinct loads for different clay – lime admixtures. According to Taylor's method, the cv can be calculated as follows:

$$c_v = \frac{T_v.(H/2)^2}{t_{90}} \quad (3)$$

Where:

T_v: Time factor

H: The specimen height at the beginning of the test (i.e. 2.5 cm)

t_{90}: Time required for 90% of consolidation has occurred

Determination of Hydraulic Properties

The hydraulic conductivity characteristics (i.e. coefficient of permeability, k) of clayey soils are associated with the time rate of consolidation properties (i.e. coefficient of consolidation, c_v) through Terzaghi's one dimensional consolidation theory as follows:

$$k = c_v.m_v.\gamma_w \quad (4)$$

Where:

c_v: Coefficient of consolidation

m_v: Coefficient of volume change or compressibility

γ_w: Unit weight of water

Using Equation 4, the important engineering parameter that is coefficient of permeability (k) employed to assess hydraulic properties of clayey soils was calculated for different clay – lime admixtures.

COMPARATIVE ANALYSIS ON EXPERIMENTAL FINDINGS

The engineering design parameters for clayey soils aiding in quantification and qualification of consolidation strength, deformation and hydraulic properties are listed in Table 2 to explore, and thus, to evaluate their values as well as to gauge the changes in clayey soil as a result of adding lime content on a purpose for stabilization. Substantial variations in the values of compression index (C_c), recompression index (C_r), coefficient of consolidation (c_v) and coefficient of permeability (k) have been investigated positively such that the consolidation strength-deformation characteristics have been enhanced as well as the hydraulic properties of the clayey soil have been improved owing to the contribution (favorable influence) of lime addition to the soil.

Moreover, a comparative analysis was performed on the computed values of engineering design parameters regarding consolidation strength-deformation characteristics (C_c, C_r, c_v) assisting in evaluating load bearing capacity of clayey soil (i.e. load resistance performance), and additionally, regarding hydraulic properties (k) assisting in assessing imperviousness features of clayey soil layer in the field

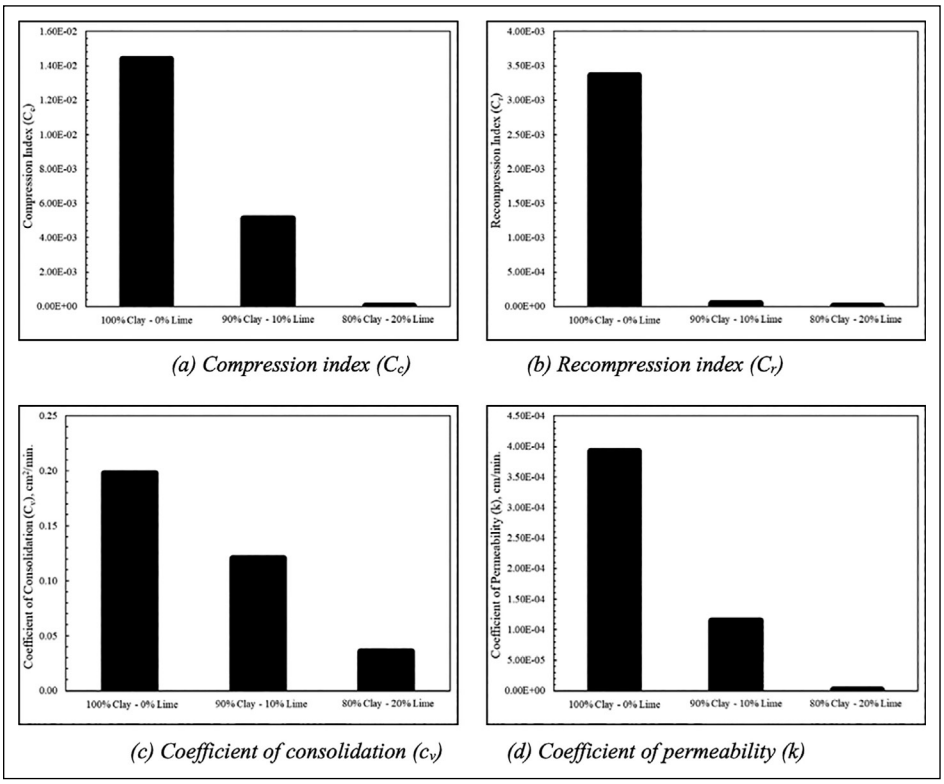

Figure 5. Comparative analysis on engineering design parameters.

(Fig. 5). The decrease in both compression index (C_c) and recompression index (C_r) (Fig. 5a, b, respectively) with an increase in lime content shows that the strength of clay becomes greater exhibiting smaller amount of deformation (consolidation settlement) against loading, and hence, displaying higher bearing capacity (greater load-carrying resistance). This is attributed to the lime treatment of the clay resulting in stabilization of soft soil through possible reactions including base-exchange, coagulation, and flocculation, reduction in thickness of water film around clay particles, cementing action and carbonation. As such, fine platy-like clay particles react with lime, and thus, get flocculated or aggregated into larger particle groups that are moderately stable even under subsequent soaking.

Since the bentonite clay used throughout the experimental program possesses inherent plastic constitution, the higher the agglomeration, the larger the strength increment was investigated compared to the other soil types such as sandy or silty soils. Therefore, lime treatment on clay specimens has shown as a result of the experimental program that the strength of clay against loading enhances, and further, exhibits less vertical deformation (settlement) under the load owing to an increase in lime content.

As per hydraulic properties, the values of coefficient of permeability (k) (Fig. 5d) have decreased such that the clay has become highly impermeable and displayed substantially improved water-resistant properties because of the increased lime content of the clayey soil. On the other hand, the coefficient of consolidation (c_v) (Fig. 5c) – showing quantitatively the time rate of consolidation deformation process (i.e. time rate of consolidation settlement in the field) – has decreased with an increase in lime content in soil. This results in extension of time duration required for the completion of consolidation settlement process of the clayey soil when subjected to loading that could be overcome by inserting wick drains in the constrcution area to facilitate and accelerate the expulsion (i.e. escape) of pore water from void space so that the progress of consolidation settlement has been eased and sped up to normal level. Similar results regarding the change in consolidation design parameters (Fig. 5) owing to the addition of lime into fine grained soils were also shown by the Reference [16] such that there observed a general increase in hydraulic conductivity (k), an evident decrease in consolidation engineering properties including coefficient of consolidation (c_V), compression as well as recompresion indices (C_c, C_r, respectively). Such finding for lime-treated soils is attributed to the aggregation of clay particles due to lime addition [6, 11, 12]. Further, as previously investigated and revealed by the Reference [6, 8], the reduction in hydraulic conductivity (i.e. k) as well as the enhancement in compressive strength properties against loading (i.e. C_c, C_r) are related and governed by the growth of pozzolanic products that are capable of partially filling the inter-aggregate porosity. As such, the significant reduction in compressibility of the tested clayey soil owing

to the lime-treatment as evidently detected from the decrease in the values of C_c, C_r (Fig. 5a, b) confirms the eaerlier findings of the References [7, 8,]. Moreover, as already indicated by the References [12, 16] and verified through the experimental results of the testing program as reported in this paper, the clayey soil – lime admixtures exhibit similar behavior analogous to over-consolidated soils attributed to and associated with the cementation characteristics induced by pozzolanic reactions being able to create a more rigid structure. Therefore, low deformations in the range of pressure typical of geo-environmental earthworks including landfills, embankments could be deemed to be ensured when soil–lime mixtures are selected to be utilized in their construction [11, 12].

The effectiveness of lime treatment can evidently be observed from the improvement of the consolidation engineering properties as shown in Figure 5. This type of enhancements in the consolidation design parameters were also reported by the References [17, 18]. In particular, for the case of soils characterized by high water contents (i.e. sensitive clayey soils), a proper design of soil–lime mixtures is based on a preliminary investigation of the soil to be used to verify its suitability to lime treatment as earlier indicated by the References [18–20]. The extensive laboratory testing program carried out on the soil–lime admixtures in the current study revealed the effect of mix proportion taking into account the specific in situ construction procedures and curing conditions in order to verify the effectiveness of quicklime treatment on a typical soft, sensitive, clayey soil for assessment at a laboratory scale.

CONCLUSION

On a purpose to address the two most important design concerns (i.e. Consolidation and Hydraulic Properties of Clay) as well as to in an attempt to develop an enhanced clay layer barrier system for landfill base liners that has enhanced bearing capacity (i.e. load carrying resistance), and hence, being robust, stable and durable against settlements, and additionaly, possesing improved hydraulic properties by being relatively more water-resistant and highly and favorably impermeable, a series of consolidation tests were performed in the laboratory at different lime contents on clay specimens to investigate the stabilization and improvement of clayey landfill base liners. The test results showed that the detected values of C_c, C_r, k decreased approximately 1/10 of the original value of the pure clayey soil, while the measured values of c_v decreased roughly 1/4 of the original magnitude as a result of an increase in lime content up to 20% by dry weight. As such, the findings of the experimental program demonstrates that lime stabilization of the clayey soils in landfill base liners will benefit the bearing capacity and the imperviousness (watertightness) engineering design properties as compared to standard compostite multi-layered landfill base liner systems. For sake of safe and stable design of base liners, containing clay layer barriers, under the landfills, the reduction of consolidation settlement in clay by enabling more stability, and thus, larger bearing capacity (i.e. greater load-carrying resistance) when subjected to the accumulated waste load (i.e. superposed action) during landfill operation could be achieved by lime stabilization. Furthermore, the accomplishment for ensuring the waterproof of those composite base liners (comprised of multiple different layers) not to allow the penetration of the contaminated water - produced as a result of exothermic reactions occurring in the waste body in landfills – by enabling enhanced isolation from natural ground could be realized in design. To this end, lime-treatment, filling voids, leads to reduction of porosity, and consequently, the reduction of permeability and the improvement of the imperviousness of clay layer. Further, the increase in bonding between soil grains as a result of lime-treatment produces mechanical strength increase, and hence, the enhancement of bearing capacity to demonstrate higher load-resistant performance of clayey soil layers in the field when employed in geo-environmental infrastructural projects.

DATA AVAILABILITY STATEMENT

The author confirm that the data that supports the findings of this study are available within the article. Raw data that support the finding of this study are available from the corresponding author, upon reasonable request.

CONFLICT OF INTEREST

The author declared no potential conflicts of interest with respect to the research, authorship, and/or publication of this article.

ETHICS

There are no ethical issues with the publication of this manuscript.

REFERENCES

[1] F. G. Bell, “Lime stabilization of clay minerals and soils,” Engineering Geology,Vol. 42, pp. 223–237, 1996.

[2] S. K. Dash and M. Hussain, “Lime stabilization of soils: reappraisal,” Journal of Materials in Civil Engineering, Vol. 24, pp. 707–714, 2012. [CrossRef]

[3] M. R. Abdi and S. Wild, “Sulphate expansion of lime-stabilized kaolinite: Physical characteristics,” Clay Minerology, Vol. 28, pp. 555–567, 1993. [CrossRef]

[4] C. M. Geiman, “Stabilization of soft clay subgrades in Virginia; Phase I laboratory study,” Master thesis, Virginia Polytechnic Institute and State University, Blacksburg, 2005. [CrossRef]

[5] J. E. Barker, C. D. F. Rogers, and D. I. Boardman,

"Physiochemical changes in clay caused by ion migration from lime piles," Journal of Materials in Civil Engineering, Vol. 18, pp. 182-189, 2006. [CrossRef]

[6] M. Di Sante, E. Fratalocchi, F. Mazzieri, and E. Pasqualini, "Time of reaction in a lime treated clayey soil and influence of curing conditions on its microstructure and behaviour," Applied Clay Science Vol. 99, pp. 100–109, 2014. [CrossRef]

[7] T. C. De Brito Galvão, A. Elsharief, and F. Simões, "Effects of lime on permeability and compressibility of two tropical residual soils," Journal of Environmental Engineering, Vol. 130, pp. 881–885, 2004. [CrossRef]

[8] N. C. Consoli, L. S. Lopes, Jr., and K. S. Heineck, "Key parameters for the strength control of lime stabilized soils," Journal of Materials in Civil Engineering, Vol. 21, pp. 210–216, 2009. [CrossRef]

[9] M. D'Ignazio, T. Lunne, K.H. Andersen, S. Yang, B. Di Buò, and T. Länsivaara, "Estimation of preconsolidation stress of clays from piezocone by means of high-quality calibration data," AIMS Geoscience Vol. 5, pp. 104–116, 2019. [CrossRef]

[10] H. F. Winterkorn, S. Pamukcu, "Soil stabilization and grouting," In Foundation Engineering Handbook, F. Hsai-Yang, editors, Van Nostrand Reinhold: New York, NY, USA, pp. 317–378, 1991. [CrossRef]

[11] H. M. Greaves, "An introduction to lime stabilization," In Lime Stabilisation; Roger, C.D.F., Glendinning, S., Dixon, N., editors, Thomas Telford: London, UK, pp. 5–12, 1996.

[12] P. Beetham, T. Dijkstra, N. Dixon, P. Fleming, R. Hutchinson, J. Bateman, "Lime stabilisation for earthworks: A UK perspective," ICE Proc. Ground Improvising, Vol. 168, pp. 81–95, 2014. [CrossRef]

[13] ASTM 2435, "Standard test method for one-dimensional consolidation properties of soils," ASTM International, West Conshohocken, PA, USA, 2003.

[14] R. D. Holtz, W. D. Kovacs, and T. C. Sheahan, "An Introduction to Geotechnical Engineering," 2nd ed., Pearson Prentice Hall, Upper Saddle River, NJ, USA, 863p, 2011.

[15] M. Budhu, "Soil Mechanics and Foundations," 3rd ed., John Wiley & Sons, Inc., New York, NY, USA, p. 761, 2011.

[16] M. R. A. Asgari, D. Baghebanzadeh, and M. Bayat, "Experimental study on stabilization of a low plasticity clayey soil with cement/lime," Arabian Journal of Geosciences, Vol. 8, pp. 1439–1452, 2015. [CrossRef]

[17] M. Di Sante, E. Fratalocchi, and F. Mazzieri, "Effects of variation in compaction water content on geotechnical properties of lime-treated clayey soil," Procedia Engineering, Vol. 158, pp. 63–68, 2016. [CrossRef]

[18] E. Fratalocchi, I. Bellezza, M. Di Sante, and E. Pasqualini, "Mix-design, construction and controls of lime stabilized embankments," In Proceedings of the 17th International Conference on Soil Mechanics and Geotechnical Engineering, Alexandria, Egypt, Vol. 3, pp. 2248–2251, 5–9 October 2009.

[19] M. Di Sante, "The Contribution of Microstructural Investigation to the Study of Lime-Treated Soils," In Proceedings of the 1st International Workshop on Metrology for Geotechnics, IMEKO TC-4, Benevento, Italy, pp. 16–21, 17–18 March 2016.

[20] M. D'Ignazio, B. Di Buò, and T. Länsivaara, "A study on the behaviour of the weathered crust in the Perniö failure test," In Proceedings of the XVI European Conference on Soil Mechanics and Geotechnical Engineering, XVI ECSMGE, Edinburgh, Scotland, UK, ICE Publishing: London, UK, pp. 3639–3644, 13–17 September 2015.

[21] M. Di Sante, "On the compaction characteristics of soil-lime mixtures," Geotechnichal Geological Engineering Vol. 38, pp. 2335–2344, 2020. [CrossRef]

[22] I. Bellezza, E. Fratalocchi, "Effectiveness of cement on hydraulic conductivity of compacted soil-cement mixtures," ICE Proc Ground Improv Vol. 10, 77–90, 2006. [CrossRef]

Environ Res Tec, Vol. 5, Issue. 1, pp. 11–23, March 2022

Environmental Research and Technology
https://ert.yildiz.edu.tr - https://dergipark.org.tr/tr/pub/ert
DOI: https://doi.org/10.35208/ert.998705

Environmental Research & Technology

Research Article

Investigating ambient air quality of a shooting range during official national competitions

S. Yeşer ASLANOĞLU*[1], Fatma ÖZTÜRK[2], Gülen GÜLLÜ[1]

[1]*Department of Environmental Engineering, Hacettepe University, Ankara, Türkiye*
[2]*Department of Environmental Engineering, Bolu Abant İzzet Baysal University, Bolu, Türkiye*

ARTICLE INFO

Article history
Received: 21 September 2021
Revised: 08 December 2021
Accepted: 17 December 2021

Key words:
EC; Elements; OC; PM_{10}; Shooting range; .22-cal

ABSTRACT

Shooting is among nine sports branches that formed the first modern Olympic Games in Athens in 1896. A professional shooting athlete shoots millions of bullets throughout their sports life to commune with their gun dedicatedly. The number of simultaneous shots per unit time depends on the capacity of the range. It can enormously increase when a national match is a case. Shooting can cause gunshot residue exposure, including lead, other elements, and their by-products accumulate in ambient air and reveal significant health risks. This study aims to find the levels of PM_{10} and its chemical composition during official three-day 50 m 22-cal competitions in May 2016, Mersin, Turkey. To this end, PM_{10} samples were collected on quartz-fiber filters and analyzed for elements by ICP-MS and carbonaceous material by Thermal-Optical EC/OC analyzer. The total PM_{10} mass concentration average is 28.7±7.3 μg/m^3 within the indoor threshold values of different countries. The ambient mass concentrations of PM_{10}, OC, EC, TC, Cd, and Pb were higher during once pistol matches instead of rifle matches. Although Pb values did not exceed the indoor limits for shooting ranges, it has the highest concentration among the analyzed elements. Additionally, Cr poses cancer risk potential. Except for Zn, Sr, and Cu, all the measured parameters have higher calculated emission factor (EF) values during pistol shots. To our best knowledge, this study reports the airborne mass concentrations of EC, OC, and TC from indoor shooting ranges and investigates indoor air quality for shooting sport for the first time.

Cite this article as: Aslanoğlu SY, Öztürk F, Güllü G. Investigating ambient air quality of a shooting range during official national competitions. Environ Res Tec 2022;5:1:11–23.

INTRODUCTION

Air pollution, which accounts for 1 in 8 deaths in 2012 according to WHO [1], is one of the most significant environmental issues in terms of human health. People are prone to high exposure risk from air pollution in indoor and outdoor environments, even at low concentrations [2]. Indoor air quality (IAQ) has been paid attention to by researchers due to the time spent in indoor environments. IAQ has been considerably influencing on well-being and productivity of people, while indoor air pollutants are increasing the risks for a variety of diseases. Jenkins et al. [3] reported that people spend 87% of their time indoors while only 6% outdoors and 7% in transit. The performed

***Corresponding author.**
*E-mail address: yaslanoglu@hacettepe.edu.tr

studies starting in the middle of the 1970s put forward that indoor concentrations of several pollutants were significantly higher than their corresponding outdoor concentrations [4].

Considerable IAQ studies on schools [5–8], elderly care centers [9, 10], homes [11–15] hospitals and nursing homes [9, 16, 17], and offices [18, 19]. On the other hand, researchers recently paid attention to the IAQ of environments used for physical exercise and sports [20–25]. Like other indoor places, construction materials, maintenance, and ventilation types form IAQ in sports centers. Moreover, higher human occupancy and the type of acts performed in the centers make them peculiar. During exercise, the respiratory ventilation per minute rises, which leads to inhalation of more air and pollutants existing in the air. Consequently, metabolic reactions to physical exercise open the human body to an elevated amount of pollutants [26]. The nasal particle-filtering system is not used during training since air is inhaled through the mouth. This process causes an increase in airflow velocity, which results in the movement of pollutants to most parts of the respiratory system and produces more risk to human health [26]. According to Ramos et al. [24], people who conduct physical exercise in polluted environments put their health at risk. Shooting is a bit tricky at this point. It is well known that a shooter's heart rate is considerably lower during shooting than in daily life. They use abdominal breathing; additionally, they inhale and exhale by their nose during aiming and triggering, not their mouth.

IAQ studies performed in sports centers revealed that occupants expose to various air pollutants, including particulate matter (PM), combustion-related emissions such as carbon monoxide (CO) and nitrogen dioxide (NO_2), carbon dioxide (CO_2). Additionally, biological pollutants such as dust mites, molds, fungus, and bacteria; volatile organic compounds (VOCs), for instance, formaldehyde and benzene; inorganic chemicals, for example, chlorinated compounds (mainly in swimming pools); heavy metals such as lead and mercury; and asbestos, which is primarily due to the building materials [27–29]. These studies focus on fitness centers [24, 30, 31] and gymnasiums and sports facilities in educational premises [32–35]. Andrade and Dominski [20] reviewed the studies performed on IAQ of places used for sports. Authors reported that the gymnasium, fitness and sports centers, and ice-skating rinks, were the most investigated places in the reviewed studies. Moreover, CO, NO_2, and PM were the IAQ parameters primarily measured in these indoor environments. On the other hand, the literature on the level and composition of emissions from firing ranges as indoor sport and recreational activity is scarce except for a few studies [36–44]. Shooting at firing ranges has become very popular among people as a recreational activity in many countries. 16,000–18,000 indoor firing ranges in the United States alone and 20 million people nationwide exercise target shooting for leisure [45]. Recreational, in other words, private sector pistol shooting ranges are about 30 thousand currently in Turkey [46]. Despite this, ranges for licensed athletes are very rare. The only world-cup standard shooting range in Turkey is located in Mersin, Erdemli. Including Erdemli shooting range, there are about 70 shooting ranges in Turkey in different cities and, these shooting ranges are operated by the Turkish Ministry of Youth and Sports [47]. A large number of these are outdoor shotgun ranges also used for recreational purposes. Only a few indoor shooting ranges are used by licensed shooting athletes, primarily for training. Operational liabilities, including ventilation, cleaning, transportation of athletes, belong to the provincial directorates. In order to reduce operating costs, unfortunately, electricity expenses such as ventilation are the first items to be reduced.

Indoor firing ranges are enclosed facilities, which have a unique operation. Improper use and design of indoor firing ranges could lead to adverse effects on human health even though military and civilian personnel prefer them for their controlled environment to outdoor counterparts. Well documented in the literature that mainly metals and gaseous compounds increase to high concentrations in the air and floor during shooting activities [38, 42, 48]. Not only major combustion gases such as carbon dioxide (CO_2) and water vapor (H_2O) but also carbon monoxide (CO), hydrogen cyanide (HCN), ammonia (NH_3), nitrous oxides (NO_x), sulfur dioxide (SO_2), and hydrogen chloride (HCl) are released during shooting [49, 50]. In addition, particulate matter (PM) consists of soot and metals, for instance, lead (Pb), copper (Cu), zinc (Zn), and iron (Fe), along with trace quantities of chromium (Cr) and molybdenum (Mo) are emitted to the indoor environment as a result of shooting activities [49]. Elevated concentrations of these airborne compounds in indoor environments cause serious health issues in occupants of indoor firing ranges.

Precisely at this point, we need to explain deeper the mechanism when a shooter pulls the trigger. A professional shooting athlete shoots millions of bullets, cartridges, or pellets throughout their shooting life, approximately starting at 13. Ammunition differs among shooting branches as lead pellets for air guns, cartridges for shotguns (rifle), and bullets for rifled guns. As in our case, in 50 m and 25 m competitions, .22-cal bullets are suitable for specialized rifles and pistols. According to the gun type, when the shooter pulls the trigger, the firing pin drops to the bullet jacket, bullet core leaves from the jacket. Due to the rifling inside the gun, the core aerodynamically travels through the shooting line till it hits the target. If the firing pin hits the jacket from the center, it is called center-fire. Otherwise, if it hits from the side part, it is called rim-fire. Compared to the center-fire bullet, less gunpowder and bullet

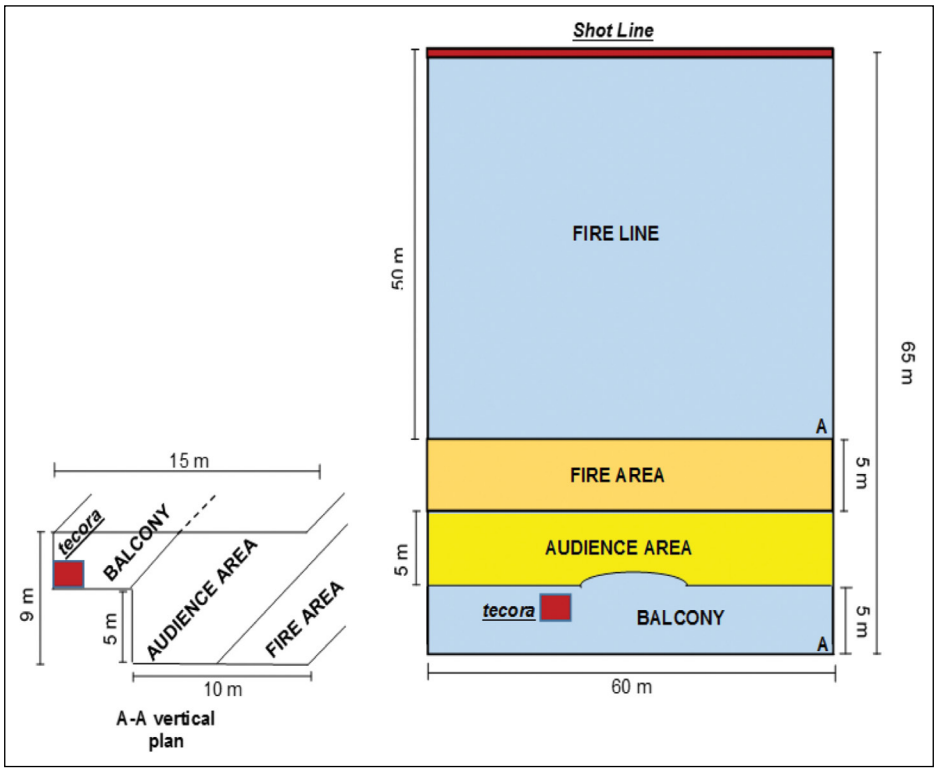

Figure 1. Schematic description of the shooting range.

materials are used in the rim-firing system. As the explosion is more efficient between jacket and core, emission rates and residues are reduced in rim-fire bullets. RWS R 50® rim-fire bullets are officially used at Turkish Shooting & Hunting Federation's competitions [51, 52].

In order to explain the health effects of shooting, Laidlaw et al. [45] reviewed thirty-six articles published in the literature and evaluated the shooters' blood lead levels (BLLs) at firing ranges. Researchers revealed that all BLL measurements exceeded the reference level of 5 µg/dL recommended by the U.S. Centers for Disease Control and Prevention/National Institute of Occupational Safety and Health (CDC/NIOSH). There is sufficient evidence that BLLs <10 µg/dL are caused to essential tremors, hypertension, cardiovascular-related mortality. Additionally, electrocardiography abnormalities and decreased kidney glomerular filtration rate among adult men and women while that <5 µg/dL leads to decreased fetal growth for an adult woman. Moreover, there is "sufficient evidence" that BLL <5 µg/dL caused several problems in children, such as declined academic achievement and intelligence quotient (IQ), reduced perinatal growth [53]. Most studies focused on the Pb because projectiles and primers contain a considerable Pb, and a huge Pb becomes airborne during shooting activities [54, 55]. International Agency for Research on Cancer (IARC) [56] classified Pb as class II (B) carcinogens, that is, possible human carcinogens. Similar to Pb, other metals emitted during shooting activities are associated with adverse health effects. Arsenic, Ni, Cd, and Cr were classified as class I carcinogenic contaminants by the IARC, while Zn, Cu, and Mn were classified as non-carcinogenic contaminants [57]. Residential exposure to a low level of Cd is related to renal toxicity, osteoporosis, and bone fractures [58]. People exposed to As by inhalation depicted an excess risk of lung cancer [59]. Moreover, upon inhalation, Zn may destroy plasmid DNA [60]. Based on epidemiological studies, it has been revealed that elemental carbon (EC) is correlated with cardiovascular and respiratory hospitalizations [61], preterm birth [62], and mortality [63]. Likewise, studies that measured organic carbon (OC) have found associations between respiratory outcomes and OC [64] and associations between cardiovascular outcomes and OC [65].

24-hr indoor PM_{10} samples were collected in three-day official competitions in this study. Collected samples were analyzed for elements and elemental and organic carbon (EC and OC, respectively). To our best knowledge, this is the first study reporting the airborne concentrations of elements, EC, and OC in a firing range in our country. This study is also unique since no indoor EC, and OC data from shooting activities have yet been produced in the literature. Another critical point is that the Mersin/Erdemli shooting range is neither commercial, recreational, nor military. So, occupants are licensed shooting athletes, their families, official coaches, referees, and audiences.

Table 1. Figures of merit of EC/OC analysis

Parameter	RSD (%) (n=3)	DL (μg/cm²) (n=7)	Sunset Lab. PES (μg/cm²) (n=5)		This study PES (μg/cm²) (n=5)	
			Avg	SD	Avg	SD
OC	4.60	0.31	16.75	0.94	13.37	1.33
EC	5.02	0.06	2.05	0.20	1.88	0.34
TC	4.65	0.34	18.80	1.14	15.26	1.67

MATERIALS AND METHODS

Sample Collection

24-hr PM_{10} samples were collected in this study during 50 m-range 22-cal rifle and pistol competitions, organized between 12 and 15 May 2016 in Erdemli (Mersin, Turkey) by the Turkish Shooting and Hunting Federation to investigate the air quality from firearms. Figure 1 depicts the schematic of the shooting range and the place where the Tecora Skypost PM_{10} sampler, which is working by the EN 12341:2014 norm, was located. According to the statutes, rules, and regulations of the International Shooting Sport Federation (ISSF), athletes cannot go beyond the 5 m distance at the shooting line, where only the referees can cross this border. Entry and exit of the athletes to the shooting area can only be performed under the supervision of referees, and all the supporters and coaches should obey this rule of ISSF during match and training times. In addition, even if referees should keep quiet during all shooting competitions except for the final match. Otherwise, supporters are invited to out of the range by the referees. Since a high-volume sampler produces an appreciable degree of noise during sampling, it was placed 10 m behind and 5 m above the fire area during the matches. Three match samples and one blank sample were collected on the pre-fired Whatman quartz fiber filter during the shooting activities. Quartz filters were pre-conditioned at 25°C and 25% relative humidity for one day before sampling, weighted and stored at -18°C until sampling. The sampler was operated only for 5 min at the sampling flow rate of 34 L/sec for the blank sample. All the samples were kept in the Petri slides in the freezer till analysis. Before analysis, the samples were pre-conditioned for one day under the same conditions stated previously, and PM load was determined by subtracting the tare of the filter. Rifle matches took place on the first and second day of the competitions, while pistol matches were last.

EC/OC Analysis

A 1.5 cm^2 punch was cut from the collected filters and analyzed utilizing Sunset Lab. (Oregon, USA) thermal-optical transmission EC/OC analyzer for elemental, organic, and total carbon (EC, OC, and TC=EC + OC). National Institute of Occupational Safety and Health (NIOSH) 870 protocol was followed during the analysis [66]. The details of the EC/OC analysis were provided in Öztürk and Keleş [67]. Briefly, the analyzer uses thermal, optical, and chemical principles to determine the carbon content of the filter samples. Firstly, an inert atmosphere is created by purging 100% He inside the oven, and OC formed during this step is converted to CO_2. Then, EC is transformed to CO_2 under oxidizing medium by purging a mixture of gas composed of 10% O_2 and 90% He (vol/vol). Afterward, generated CO_2 is reduced to CH_4, which is detected by a flame ionization detector (FID). The performance of FID is checked at the end of each run by injecting a fixed volume of methane (5% CH_4 plus 95% He, vol/vol) as an internal standard. As a part of the quality assurance and quality control (QA/QC) protocol, a known amount of sucrose solution was spiked over the pre-fired blank filters. Analysis was conducted under the same conditions as the filter samples. The measured sucrose concentrations have deviated only 0.10% from the standard sucrose solution based on n=14 repeated measurements. In addition, the instrument was operated without putting any sample at the beginning of each analysis day. The average OC levels determined in the instrument blanks were less than 0.02 μg/cm^2 while no EC was detected.

The detection limit (DL) and precision as relative standard deviation (RSD) of EC/OC measurements were also calculated in this study. DL values (three times the standard deviation of the blank filter measurements) were calculated based on the repeated blank measurements, and RSD values were estimated by analyzing the performance evaluation standard (PES) provided by the Sunset Lab. Moreover, the accuracy of the EC/OC measurements was calculated based on the data provided by Sunset Lab. for PES measurements. Table 1 summarizes figures of merit of EC/OC analysis.

As given in Table 1, the percent RSD values were almost ≤5, indicating that repeatability of the analysis is acceptable. DL values of measurements were 0.31, 0.06 and 0.34 μg/cm^2 for OC, EC and TC, respectively. The accuracy of the measurements was found to be 20, 8, and 18%, respectively (Table 1). The EC/OC results provided in this paper were corrected for filter blank. Since no carbonate carbon (CC) peak was detected during analysis, CC correction was not performed.

Table 2. Figures of merit of EC/OC analysis

	Step			
	I	**II**	**III**	**IV**
Ramp time (min)	3	2	2	1
Hold time (min)	5	10	30	10
Temperature (°C)	140	160	200	50
Pressure (bar)	30	30	35	25
Power (%)	75	85	90	0

Elemental Analysis

The rest of the filters from EC/OC analysis were digested in a mix of high purity acids (5 mL HNO_3 + 1 mL HF + 0.5 mL H_2O_2 + 1 mL de-ionized (DI) water using Berghof (speed wave-2, Germany) Microwave Digestion Oven. The steps of the digestion program are tabulated in Table 2. Acid and field filter blank were also digested along with the filter samples and treated similarly. After digestion, all the samples and blanks were diluted to 50 mL with DI water, transferred to HDPE bottles, and kept in the refrigerator till analysis. After micro-wave digestion only, samples that showed visible residues of soot carbon were filtered through 0.45 µm pore size Millipore brand mixed esters of cellulose filter (Sartorius AG).

Agilent 7700 Model Inductively Coupled Plasma Mass Spectrometry (ICP-MS) (California, USA) was employed in this study to perform the trace element analysis of the samples. Samples were analyzed for 15 elements using ICP-MS (Be, Cd, Co, Cr, Cu, Hg, Mn, Ni, As, Ba, Pb, Se, Sr, V, and Zn). 100-ppb germanium and terbium were used as internal standards during the analysis of samples. Agilent internal standard mix for ICP-MS systems (part number 5188-6525) calibrated the instrument. Calibration standards, blanks, and samples were spiked with this internal standard to overcome instrumental and sample-related variations. Internal standard element recovery was monitored closely by following the procedure described in EPA Method 200.8, section 9.4.3 [68]. Recoveries tried to be kept between 70% and 120%. In addition, the method detection limit (MDL) of the analysis was also calculated based on the same method as described in section 9.2.4 [68]. Moreover, instrument detection limit (IDL) values were estimated following the procedure provided in the same method under section 9.2.5. The accuracy of the measurements was also monitored closely as a part of the quality assurance and quality control (QA/QC) procedure. To this end, Standard Reference Material (SRM) 2783 obtained from the National Institute of Standard and Technologies (NIST) was digested by following the procedure used to extract filter samples. The obtained results were compared with the certificate sheet of the SRM. The precision of the measurements was also estimated based on the relative standard deviation of repeated SRM analysis. The values corresponding to SRM measurements, precision, MDL, IDL, and recovery for the measured parameters are summarized in Table 3 below.

Except for the Cd, the recoveries were >70% for all of the elements. Thus, the measured concentrations were not cor-

Table 3. Figures of merit of ICPMS measurements

	SRM 2783 Certified values (mg/kg)		**Obtained values (mg/kg)**		**Precision (%)**	**IDL (µg/kg)**	**MDL (µg/kg)**	**Recovery (%)**	
Parameter	**Avg**	**SD**	**Avg**	**SD**				**Avg**	**SD**
As	7.0	1.6	5.8	0.3	17.1	4.2	112	79.4	2.82
Ba									
Be									
Cd	7.3	3.7	7.5	0.5	3.1	2.5	7.5	57.8	2.27
Co						6.1	163.2	75.6	2.5
Cr	80	22	54.5	4.1	24.7	32.2	125.6	79.6	5.02
Cu						20	122.5	73.3	2.24
Hg						7.5	22.6	74.9	6.05
Mn						89.8	172.2	72.8	2.51
Ni						135.5	406.5	77.2	3.46
Pb	85.9	7.2	64.6	11.7	31.9	20.8	33.3	87.0	6.83
Se									
Sr									
V						34.9	122.8	78.3	2.22
Zn						90.6	941.4	78.1	5.19

Table 4. The average concentration of parameters measured in PM10 samples during the competitions

Parameter	Unit	1st-day rifle	2nd-day rifle	3rd-day pistol	Avg	SD
PM_{10}	μg/m³	25.4	21.9	38.8	28.7	7.3
OC	μg/m³	4.02	3.72	6.47	4.74	1.23
EC	μg/m³	0.197	0.194	0.349	0.247	0.072
TC	μg/m³	4.24	3.92	6.82	4.99	1.30
As	ng/m³	0.334	0.432	0.251	0.339	0.074
Ba	ng/m³	21.9	13.8	19	18.2	3.4
Be	ng/m³	0.026	0.035	0.032	0.031	0.004
Cd	ng/m³	0.28	0.117	0.495	0.297	0.155
Cr	ng/m³	1.06	3.39	2.13	2.19	0.95
Cu	ng/m³	3.18	1.51	1.27	1.99	0.85
Mn	ng/m³	1.81	2.55	2.24	2.20	0.30
Ni	ng/m³	2.18	3.03	2.27	2.49	0.38
Pb	ng/m³	221	110	259	197	63
Se	ng/m³	1.34	2.81	1.6	1.92	0.64
Sr	ng/m³	0.266	1.349	0.548	0.721	0.459
V	ng/m³	6.35	6.7	5.86	6.30	0.34
Zn	ng/m³	4.72	4.55	1.15	3.47	1.64

rected with the recovery values. If IDL values <0 for the parameter of concern, the corresponding value was replaced with one-third of the associated MDL value. Moreover, if the measured concentration of the parameter is less than both IDL and MDL, the analyte concentration was replaced with half its corresponding MDL value to use the data in the statistical analysis. Furthermore, the metal levels reported in this study were field blank corrected.

RESULTS AND DISCUSSION

The concentration of parameters measured during 3-day competitions is summarized in Table 4, including the average (Avg) and standard deviation (SD) of measured concentrations for the whole field study. On the third day, when the pistol athletes were competing, almost two times higher PM_{10} mass concentration was measured compared to the previous two days. The PM_{10} mass concentrations for three days were measured as 25.4, 21.9, and 38.8 μg/m³, respectively. The highest concentration was measured for OC (4.02 μg/m³), while the minimum concentration was obtained for Be (0.026 ng/m³) on the first day when rifle matches took place. The maximum and minimum concentrations were obtained for the same parameters on the second and third days of the competitions, as tabulated in Table 4.

It is also worthy to note that the highest PM_{10}, OC, EC, TC, Cd, and Pb levels were measured in the samples while the pistol was being used for shooting in the third-day competitions. Grabinski et al. [48] revealed that PM mass emissions when the shooters used rifle is about an order of magnitude lower than the emissions released from pistols. This situation can be attributed to the greater barrel diameter and shorter barrel length used in pistols.

During the matches, the measured PM_{10} mass concentration was found as 25.4, 21.9, and 38.8 μg/m³, respectively, for the first, second, and third day, while the average of the whole event was 28.7±7.3 μg/m³. The measured values were below the American Society of Heating, Refrigerating and Air-Conditioning Engineers (ASHRAE) and England indoor PM_{10} limit, 75 and 50 μg/m³, respectively. Hong Kong's first level value for indoor PM_{10} is 20 μg/m³ [69]. Table 4 revealed that during the matches, this limit value was exceeded. Wingfors et al. [38] reported that most of the particles released from indoor firing ranges fall to nanoparticle size regime, which is more critical in terms of human health point of view since these particles are capable of penetrating deep into the human respiratory tract by inhalation [70]. Consequently, the mass concentration and the size distribution of PM are significant for indoor shooters.

The measured PM_{10} concentrations in this study were comparable with the ones reported by Orru et al. [71]. The average PM concentration in one of the shooting ranges in which pistols were used is 28.9 μg/m³. Researchers collected size-segregated PM samples at indoor military shooting ranges and analyzed the collected samples in terms of metals, including Pb, Cu, Ni, and Zn. In contrast to PM_{10} levels, significantly higher metal concentrations were reported in this military shooting range.

Grabinski et al. [48] reported Cu and Zn concentration in a ventilated, indoor firing range, where PM samples were collected in cases both pistol and rifle used for firing. The airborne mass concentration of Cu was reported to vary from ≤1 to 16 μg/m^3, which is considerably higher than one measured in this study (average of the competition 1.99 ng/m^3). In addition, researchers found that Zn levels ranged from 0.5 to 1.8 μg/m^3, which is again much higher than the competition average value (Table 4).

Indoor EC and OC levels were published in some studies in the literature. For example, Na and Cocker [72] determined concentrations of these two parameters inside the 20 residential settings and one local high school in CA, USA. In the homes with smokers, OC levels ranged from 9.3±1.6 to 229±67.6 μg/m^3 while EC concentrations were between 1.7±0.7 and 4.0±1.5 μg/m^3 in $PM_{2.5}$ samples. Authors claimed that there are no indoor EC sources while OC considerably contributed to indoor $PM_{2.5}$ levels. In a similar study, Ho et al. [73] collected $PM_{2.5}$ samples inside the five buildings near roadsides in Hong Kong. The average inside OC and EC levels were found as 11.3±5.5 and 4.8±3.4 μg/m^3. The significant sources determining the indoor concentrations of these pollutants were attributed to the penetration of outdoor pollution. Seleventi et al. [74] performed $PM_{2.5}$ sampling inside an apartment in Athens. The researchers reported the indoor average OC and EC levels as 9.6 and 1.9 μg/m^3, respectively. The indoor source of OC was thought to be several activities performed by the residents, such as smoking, cooking, and cleaning. However, all these studies were conducted inside the residential places, and reported values cannot be compared to those measured in a shooting range. To our best knowledge, there is only one study in the literature reporting black carbon (BC) concentration for indoor air during sportive activities. Bisht et al. [75] monitored the indoor air quality for stadiums during the 19th Common Wealth Games (CWG) at Delhi (India). It is good to mention that BC determination relies on optical methods, and thermal-optical methods determine EC. Although co-located measurements showed that BC data could be 20% higher than EC levels [76], EC can be used as a surrogate measure of BC [77] In Bisht et al. [75], BC levels inside the three sports venues during CWG were reported to range about from 12 to 14 μg/m^3. Unfortunately, there is no information about the nature of sports competitions provided in the study. Researchers revealed that BC showed a positive correlation with CO, a pollutant released from incomplete combustion. Once the EC data generated in the shooting range were compared with the BC levels reported by Bisht et al. [75], it can be concluded that BC data was at least 50 times higher than EC measured in the shooting range.

Among the elements analyzed in the PM_{10} samples collected during the competitions and listed in Table 4, Cr is paying attention. Cr presents in the ambient atmosphere as Cr (III) and Cr (VI). Cr (III) is essential in trace levels for the proper functioning of living organisms. On the other hand, Cr (VI) is known as a pulmonary carcinogen by the International Agency for Research on Cancer and US Toxicology Program [78]. Indoor exposure to Cr (VI) is related to elevated lung and nasal cancer risk [79]. US Environmental Protection Agency listed Cr (VI) compounds as one of the 18 core Hazardous Air Pollutants (HAPs) [80]. It has been estimated that one in a million-cancer risk threshold for Cr (VI) is 0.083 ng/m^3. The average Cr (VI) to total Cr ratios ranged from 1 to 30% for the ambient air [81]. By taking a ratio of 15% on average, Cr (VI) values for this study can be estimated to vary from 0.159 to 0.509 ng/m^3 for the first and second day, respectively. Consequently, the emitted Cr during the competitions has cancer risk potential.

Once Table 4 is evaluated in terms of elements, it can be seen that the highest level was measured for Pb compared to other metals. The average Pb concentration for the whole study was 197±63 ng/m^3. Several guidelines regulate occupational Pb exposure in the world. For example, OSHA (Occupational Safety and Health Administration) (USA) set 30 μg of Pb per cubic meter of air as an action level for indoor environments. In addition, the time-weighted average (exposure over an eight-hour average) for Pb was set to 50 μg/m^3 in the same regulation. Furthermore, NIOSH recommended exposure limit (8-hour average) for Pb is 50 μg/m^3 while increasing Pb exposure to 100 μg/m^3 indicates the level that is Immediately Dangerous to Life and Health (IDLH) [82]. When these limit values were compared with the data generated in our study, none of the days' Pb exposure limits were exceeded. However, it should be kept in mind that the samples collected in this study for 24-hr long. Consequently, the measured Pb levels that we reported in this study were smoothed out.

The shooters are exposed to Pb from three different sources during the shooting activity. The first source is ammunition primer, composed of lead styphnate, which initiates the mercury fulminate explosion and lead azide propellant, released to the ambient air upon firing. The second one is burning propellant in the cartridge, which vaporizes the Pb due to extreme temperatures as high as 1100 °F. The last is associated with the dust and lead oxide fumes, which are emitted when the bullet hits to target [83]. Once the Pb is released to the indoor environment, the occupants inside the firing range are exposed to this metal through dermal contact [84], ingestion [85], and inhalation [84]. The adverse health impacts of elevated Pb exposure are well documented in the literature [36]. International Agency for Research on Cancer (IARC) declared inorganic lead as a probable human carcinogen (group 2A) [86]. Conversely, limited evidence has been found in human studies. In contrast, there is adequate data on the carcinogenicity of Pb in experimental animal studies [56]. Gulson et al. [87] suggested using non-lead primers to reduce the uptake of lead by recreational shooters.

Emission factors (EF) for the measured parameters were also calculated by dividing the mass concentrations of the parameters by the number of shots each day. Table 5 below summarizes the EF values for the corresponding parameters for rifle (average of first two days) and pistol (third day).

Once the normalized values were compared for rifle and pistol, it was found that Cd mass emission per bullet from pistol shooting is about four times higher than the one measured for the rifle. Similarly, about three times higher EF values were calculated for PM_{10}, TC, OC, EC, and Pb when pistol matches took place instead of the rifle. Estimated EF values for Mn, Cr, Ni, V, and Ba are about 1.5 times higher for pistol emissions than for the rifle. Zinc was the only pollutant that had a higher EF value in rifle emissions. EF values calculated for Sr and Cu are comparable.

In addition to the parameters listed herein, ammunition during shooting activities may release other stressors to the indoor environment. For example, nitrogen (NO_x) oxides are among these pollutants and irritate the eyes and respiratory system. Carbon monoxide (CO), another pollutant released into the indoor atmosphere due to firing, is known to reduce the ability of blood to carry oxygen and leads to headaches and nausea. Moreover, polycyclic aromatic hydrocarbons (PAHs), hydrogen cyanide (HCN), ammonia (NH_3), sulfur dioxide (SO_2), and hydrogen chloride (HCl) are other air pollutants released to indoor air upon firing. The literature has well reported the detrimental health impacts associated with these pollutants on humans and the environment.

Limitations

Since the competition was officially three days, PM_{10} samples, including two in rifle and one in pistol, were collected during this study, which prevents us from making a comprehensive assessment about the differences or similarities in the chemical compositions of the collected samples. In addition, 24-hr PM_{10} samples were collected during the study through the matches were performed from 09.00 am to 08.00 pm. Shooting range opening and closing times are spread over a wider range. After the scheduled matches, shooters may perform small training shots in order to adjust guns, shooting position, and other equipment revealed to prolonged shooting hours. In regular training conditions, samples may have been collected in shorter time windows. However, it should be noted that this is a well-attended national organization. Also, there is no other example in the literature on a measurement related to sports-shooting competition cases. Additionally, the ratio of Cr (VI) to Cr was used in this study based on the ambient PM data, and no value was found for the indoor environments. Consequently, one should consider these limitations while interpreting the generated data in this study.

Table 5. Calculated emission factor (EF) values for PM_{10}, carbonaceous materials, and elements for rifle and pistol shots (PM_{10}, OC, EC & TC in ng/bullet and elements in pg/bullet)

Parameter	Rifle	Pistol
PM_{10}	116	321
TC	20	56
OC	19	54
EC	0.959	2.890
Be	0.149	0.267
Cd	0.972	4.087
As	1.88	2.07
Sr	3.96	4.52
Se	10	13
Mn	11	18
Cr	11	18
Cu	11	11
Ni	13	19
Zn	23	10
V	32	48
Ba	87	157
Pb	810	2134

CONCLUSION

This study was conducted during a three-day-long official national shooting competition. To our best knowledge, we report first-time EC, OC, and TC concentrations associated with the indoor firing ranges. Another critical point is that the Mersin/Erdemli shooting range is neither commercial, recreational, nor military. So, occupants are licensed shooting athletes, their families, official coaches, referees, and audiences. It was demonstrated here that shooting activities produce a considerable amount of particulate matter, carbonaceous material, and many toxic elements associated with it. Lead was the most dominant metal component of a PM that we measured during the competitions regardless of pistol or rifle used. However, its concentration did not exceed the permissible levels for indoor firing ranges.

Another crucial point is that lead-free bullets have reduced precision and accuracy at the shot point on the target. On the other hand, in terms of athlete and environmental health, green or "lead-free" bullets should be encouraged to use during indoor shooting to reduce the risk of Pb exposure. Among the elements analyzed, Cr was one of the elements that have cancer risk potential. Additionally, there are some technical differences between a .22-cal rifle and pistol. The pistol bore length is shorter, and the bore radius is larger than the rifle. Also, the rifle has a higher bullet core release speed than the pistol can cause more pollutant ac-

cumulation close to the shooter in pistol matches. It should also be considered that pollutants can accumulate in the environment for three days and repeatedly be resuspended from the ground. Ventilation is another critical point that should not be negligible. It should be kept out of the operational cost savings. Indoor air quality in terms of PM and all these pollutants should be closely monitored at indoor firing ranges to take more proactive actions against these pollutants. Furthermore, the operator should regularly check the ventilation system of indoor air firing ranges to ensure acceptable air quality. Personal sampling provides a more accurate evaluation of human exposure during shooting activities. Consequently, personal sampling and indoor air quality monitoring should be coupled to understand better the impact of indoor air firing ranges on the occupants.

ACKNOWLEDGMENT

The first author of this study is a national shooting athlete supported by the Turkish Shooting and Hunting Federation in each process of the sampling campaign. Special thanks to the main office and Mersin-Erdemli shooting range staff. Moreover, we acknowledge the Ministry of Environment and Urbanization for providing the PM_{10} sampler used during this study.

DATA AVAILABILITY STATEMENT

The authors confirm that the data that supports the findings of this study are available within the article. Raw data that support the finding of this study are available from the corresponding author, upon reasonable request.

CONFLICT OF INTEREST

The authors declared no potential conflicts of interest with respect to the research, authorship, and/or publication of this article.

ETHICS

There are no ethical issues with the publication of this manuscript.

REFERENCES

[1] WHO. World Health Organization releases country estimates on air pollution exposure and health impact. http://www.who.int/news-room/detail/27-09-2016-who-releases-country-estimates-on-air-pollution-exposure-and-health-impact, (2016, accessed 30 September 2018).

[2] K.H., Kim, E., Kabir, S. Kabir, "A review on the human health impact of airborne particulate matter. Environment International, Vol. 74, pp. 136–143, 2015. [CrossRef]

[3] P.L. Jenkins, T.J. Phillips, E.J. Mulberg, and S.P. Hui, "Activity patterns of Californians: use of and proximity to indoor pollutant sources." Atmospheric Environment. Part A. General Topics, Vol. 26, pp. 2141–2148, 1992. [CrossRef]

[4] A.A. Roy, S.P. Baxla, T. Gupta, R. Bandyopadhyaya, and S.N. Tripathi, "Particles emitted from indoor combustion sources: Size distribution measurement and chemical analysis" Inhalation Toxicology, Vol 21, pp. 837–848, 2009. [CrossRef]

[5] P.N. Pegas, M.G. Evtyugina, C.A. Alves, T. Nunes, M. Cerqueira, M. Franchi, C. Pio, S.M. Almeida, and M.D.C. Freitas, "Outdoor/indoor air quality in primary schools in Lisbon: a preliminary study," Quim Nova, Vol. 33, pp. 1145–1149, 2010. [CrossRef]

[6] N. Canha, S.M. Almeida, M. do Carmo Freitas, H.T. Wolterbeek, J. Cardoso, C. Pio, and A. Caseiro, "Impact of wood burning on indoor PM2. 5 in a primary school in rural Portugal," Atmospheric Environment, Vol. 94, pp. 663–670, 2014. [CrossRef]

[7] D. Ekmekcioğlu, and S. Keskin, "Characterization of indoor air particulate matter in selected elementary schools in Istanbul, Turkey," Indoor Built Environment, Vol. 16, pp. 169–176, 2007. [CrossRef]

[8] H. Aydogdu, A. Asan, M.T. Otkun, and M. Ture, "Monitoring of fungi and bacteria in indoor air of primary schools in Edirne City, Turkey," Indoor Built Environment, Vol. 14, pp. 411–425, 2005. [CrossRef]

[9] M. Almeida-Silva, H.T. Wolterbeek, and S.M Almeida, "Elderly exposure to indoor air pollutants," Atmospheric Environment, Vol. 85, pp. 54–63, 2014. [CrossRef]

[10] C. Viegas, M. Almeida-Silva, A.Q. Gomes, H.T. Wolterbeek, and S.M. Almeida, "Fungal contamination assessment in Portuguese elderly care centers," Journal of Toxicology and Environmental Health, Part A, Vol. 77, pp. 14–23, 2014. [CrossRef]

[11] L.M. Osman, J.G. Douglas, C. Garden, K. Reglitz, J. Lyon, S. Gordon, and J.G. Ayres, "Indoor air quality in homes of patients with chronic obstructive pulmonary disease," American Journal of Respiratory and Critical Care Medicine, Vol. 176, pp. 465–472, 2007. [CrossRef]

[12] S. Langer, G. Bekö, E. Bloom, A. Widheden, and L. Ekberg, "Indoor air quality in passive and conventional new houses in Sweden," Build Environment, Vol. 93, pp. 92–100, 2015. [CrossRef]

[13] S. Menteşe, and G. Güllü, "Variations and sources of formaldehyde levels in residential indoor air in Ankara, Turkey," Indoor Built Environment Vol. 15, pp. 273–281, 2006. [CrossRef]

[14] A. Zararsız, and F. Öztürk, "Estimation of health risks associated with household dust contamination in Bolu (Turkey)," Duzce University Journal of Science and Technology, Vol. 18, pp. 2245–2265, 2020.

[15] S. Lakestani, B. Karakas, S. Acar Vaizoglu, B. Guciz Dogan, C. Guler, B. Sekerel, A. Taner, and G. Gullu, "Comparison of indoor and outdoor air quality in children homes at prenatal period and one year old," World Academy of Science, Engineering and Technology, Vol. 78, pp. 143–147, 2013.

[16] M.F. El-Sharkawy, and M.E. Noweir, "Indoor air quality levels in a University Hospital in the Eastern Province of Saudi Arabia," Journal of Family & Community Medicine, Vol. 21, pp. 39, 2014. [CrossRef]

[17] E. Özlü, Assessment of exposure effects of indoor particles in different microenvironments, Air Quality, Atmosphere & Health, Vol 14, pp. 2029–2046, 2021. [CrossRef]

[18] C. Mandin, M. Trantallidi, A. Cattaneo, N. Canha, V.G. Mihucz, T. Szigeti, R. Mabilia, E. Perreca, A. Spinazze, S. Fossati, Y. Kluizenaar, E. Cornelisse, J. Sakellaris, D. Saraga, O. Hanninen, D.O. Fernandes, G Ventura, P. Wolkoff, P. Carrer, and Y. De Kluizenaar, "Assessment of indoor air quality in office buildings across Europe–The OFFICAIR study," Science of the Total Environment, Vol. 579, pp. 169–178, 2017. [CrossRef]

[19] P. Carrer, and P. Wolkoff, "Assessment of indoor air quality problems in office-like environments: Role of occupational health services," International Journal of Environmental Research and Public Health, Vol. 15, pp. 741, 2018. [CrossRef]

[20] A. Andrade, and F.H., Dominski, "Indoor air quality of environments used for physical exercise and sports practice: Systematic review," Journal of Environment Management, 196, pp. 188–200, 2017.

[21] A. Andrade, F.H. Dominski, and D.R. Coimbra, "Scientific production on indoor air quality of environments used for physical exercise and sports practice: bibliometric analysis," Journal of Environment Management, 196, pp. 188–200, 2017. [CrossRef]

[22] C. Cianfanelli, F. Valeriani, S. Santucci, S. Giampaoli, G. Gianfranceschi, A. Nicastro, F. Borioni, G. Robaud, N. Mucci, and V.R. Spica, "Environmental quality in sports facilities: perception and indoor air quality," Journal of Physical Education and Sports Management, Vol. 3, pp. 57–77, 2016. [CrossRef]

[23] M. Hajian, and S. Mohaghegh, "Indoor air pollution in exercise centers," International Journal of Medical Toxicology and Forensic Medicine, Vol. 5, pp. 22–31, 2015.

[24] C.A. Ramos, H.T. Wolterbeek, and S.M. Almeida, "Exposure to indoor air pollutants during physical activity in fitness centers," Build Environment, Vol. 82, pp. 349–360, 2014. [CrossRef]

[25] C.A. Alves, A.I Calvo, A. Castro, R. M. Fraile, M. Evtyugina, and E.F Bate-Epey, "Indoor air quality in two university sports facilities," Aerosol and Air Quality Research, Vol. 13, pp. 1723–1730, 2013. [CrossRef]

[26] A.J. Carlisle, and N.C.C. "Sharp, Exercise and outdoor ambient air pollution," British Journal of Sports Medicine, Vol. 35, pp. 214–222, 2001. [CrossRef]

[27] R. Pérez-Padilla, A. Schilmann, and H. Riojas-Rodriguez, "Respiratory health effects of indoor air pollution, The International Journal of Tuberculosis and Lung Disease, Vol. 14, pp. 1079–1086, 2010.

[28] USEPA, An Introduction to Indoor Air Quality (IAQ), Available at: http://www.epa.gov/iaq/ia-intro.html. Accessed on Jul 15, 2018.

[29] USEPA, Indoor Air Pollution. An Introduction for Health Professionals. Available at: https://www.epa.gov/sites/production/files/2015-01/documents/indoor_air_pollution.pdf, Accessed on Jul 15, 2018.

[30] Slezakova, K., Peixoto, C., Oliveira, M., Delerue-Matos, C., do Carmo Pereira, M., Morais, S., Indoor particulate pollution in fitness centres with emphasis on ultrafine particles. Environ Pollut, 2018; 233: 180–193. [CrossRef]

[31] C.A., Ramos, J.F., Reis, T., Almeida, F. Alves, H.T. Wolterbeek, S.M. Almeida, "Estimating the inhaled dose of pollutants during indoor physical activity," Science of the Total Environment, Vol. 527, pp. 111–118, 2015. [CrossRef]

[32] Torkmahalleh, M.A., Kabay, K., Bazhanova, M., Mohiuddin, O., Obaidullah, M., Gorjinezhad, S., "Investigating the impact of different sport trainings on particulate matter resuspension in a sport center using well-characterized reference instruments and a low-cost monitor," Science of the Total Environment, Vol. 612, pp. 957–965, 2018. [CrossRef]

[33] P. Kic, "Dust pollution in the sport facilities," Agronomy Research, Vol. 14, pp. 75–81, 2016.

[34] M. Zitnik, K. Bucar B. Hiti, Z. Barba, Z. Rupnik, A. Zaloznik, E. Zitnik, L. Rodrìguez, I. Mihevc, J. Zibert, "Exercise-induced effects on a gym atmosphere," Indoor Air, Vol. 26, pp. 468–477, 2016. [CrossRef]

[35] A. Castro. A.I. Calvo, C. Alves, E. Alonso-Blanco, E. Coz, L. Marques, T. Nunes, J.M. Fernandez-Guisuraga, and R. Fraile, Indoor aerosol size distributions in a gymnasium. Science of the Total Environment, Vol. 524, pp. 178–186, 2015. [CrossRef]

[36] B.A. Abudhaise, M.A. Alzoubi, A.Z. Rabi, and R.M. Alwash, "Lead exposure in indoor firing ranges: environmental impact and health risk to the range users," International Journal of Occupational Medicine and Environmental Health, Vol. 9, pp. 323–329, 1996.

[37] T.T. Chau, W.Y. Chen, T.M. Hsiao, and H.W. Liu, "Chronic lead intoxication at an indoor firing range in Taiwan," Clinical Toxicology, Vol. 33, 371–372, 1995. [CrossRef]

[38] H. Wingfors, K. Svensson, L. Hagglund, S. Hedenstierna, and R. Magnusson, "Emission factors for gases and particle-bound substances by firing lead-free small-caliber ammunition," Journal of Occupational and Environmental Hygiene, Vol. 11, pp. 282–291, 2014. [CrossRef]

[39] R. Dams, B. Vandecasteele, M. Desmet, M. Helsen, M. Nagels, Z. Vermeir, and Q., Yu, "Element Concentrations in the air of an indoor shooting range," Science of Total Environment, Vol. 77, pp. 1–13, 1988. [CrossRef]

[40] C. Vandecasteele, G. Vermeir, and R. Dams, "Element concentrations in the air of an indoor shooting range," Environmental Technology, Vol. 9, pp. 1287–1294, 1988. [CrossRef]

[41] G. Sujetovienė, and J. Česynaitė, "Assessment of Air Pollution at the Indoor Environment of a Shooting Range Using Lichens as Biomonitors," Journal of Toxicology and Environmental Health, Part A, Vol. 84, pp. 273–278, 2021. [CrossRef]

[42] B.G. Svensson, A. Schütz, A. Nilsson, and S. Skerfving, "Lead exposure in indoor firing ranges," International Archives of Occupational and Environmental Health, Vol. 64, pp. 219–221, 1992. [CrossRef]

[43] W.J. Park, S.H. Lee, S.H. Lee, H.S. Yoon, and J.D. Moon, "Occupational lead exposure from indoor firing ranges in Korea," Journal of Korean Medical Science, Vol. 31, 497–501, 2016. [CrossRef]

[44] I. Olmez, J.P. Kotra, S. Lowery, and W.H. Zoller, "Airborne lead and trace elements in an indoor shooting range: A study of the DC National Guard Armory Pistol Range," Environmental Toxicology and Chemistry, Vol. 4, pp. 447–452, 1985. [CrossRef]

[45] M.A Laidlaw, G., Filippelli, H Mielke, B., Gulson, and A.S. Ball, "Lead exposure at firing ranges—a review," Environment Health, Vol 16, pp. 34, 2017. [CrossRef]

[46] Türkiye'dekiatışpoligonları,Availableat:https://www.google.com/search?client=firefox-b-e&q=t%C3%B-Crkiyedeki+at%C4%B1%C5%9F+poligonlar%C4%B1, Accessed on Nov 5, 2021.

[47] Turkish Shooting and Hunting Federation, Branches, Available at: https://www.taf.gov.tr/, Accessed on Sept 15, 2021.

[48] C.M. Grabinski, M.M. Methner, J.M. Jackson, A.L Moore, L.E. Flory, T. Tilly, S.M. Hussain, and D.K. Ott, "Characterization of exposure to byproducts from firing lead-free frangible ammunition in an enclosed, ventilated firing range," Journal of Occupational and Environmental Hygiene, Vol. 14, pp. 461–472, 2017. [CrossRef]

[49] P. Ase, W. Eisenberg, S. Gordon, K. Taylor, and A. Snelson, "Propellant combustion product analyses on an M16 rifle and a 105mm caliber gun," Journal of Environmental Science and Health, Part A, Vol. 20, pp. 337–368, 1985. [CrossRef]

[50] B. Quémerais, E. Diaz, I. Poulin, and A. Marois, "Characterization of Atmospheric Emission Produced by Live Gun Firing: Test on the M777 155 mm Howitzer (No. DRDC-T-TR-2007-102)," Defense Research and Development Toronto, Canada; 2007.

[51] RWS R 50. Available at: https://rws-ammunition.com/en/products/rimfire-cartridges/rws-r-50, Accessed on Nov 10, 2021.

[52] ELEY. Available at: https://eley.co.uk/ammunition/. Accessed on Nov 10, 2021.

[53] NTP, National Toxicology Program Monograph on Health Effects of Low-level Lead, June 2012. Available at: https://ntp.niehs.nih.gov/pubhealth/hat/noms/lead/index.html. Accessed on Aug 10, 2018.

[54] C.K. Haw, P.T. Jayaprakasha, Y.C. Hooib, and A.F. Abdullaha, "Health concern on lead encountered during firing practices: a review," Journal of Environmental Health, Vol. 1, pp. 24–29, 2010.

[55] H.H. Meng, and B. Caddy, "Gunshot residue analysis—a review," Journal of Forensic Sciences, Vol. 42, pp. 553–570, 1997. [CrossRef]

[56] IARC, "Inorganic and Organic Lead Compounds: Summary of Data Reported and Evaluation," International Agency for Research on Cancer monographs on the evaluation of carcinogenic risks to humans, 87, 2006.

[57] K. Liu, Q. Shang, and C. Wan, "Sources and Health Risks of Heavy Metals in PM2.5 in a Campus in a Typical Suburb Area of Taiyuan, North China," Atmosphere, Vol. 9, pp. 46, 2018. [CrossRef]

[58] Y. Yang, L. Liu, C. Xu, N. Li, Z. Liu, Q. Wang, and D. Xu, "Source apportionment and influencing factor analysis of residential indoor PM2.5 in Beijing," International Journal of Environmental Research and Public Health, Vol. 15, pp. E686, 2018. [CrossRef]

[59] L. Järup, "Hazards of heavy metal contamination," British Medical Bulletin, Vol. 68, pp.167–182, 2003. [CrossRef]

[60] L. Shao, Z. Shi, T.P. Jones, J. Li, A.G. and Whittaker, K.A. Berube, "Bioreactivity of particulate matter in Beijing air: results from plasmid DNA assay," Science of the Total Environment, Vol. 367, pp. 261–272, 2006. [CrossRef]

[61] R.D. Peng, M.L. Bell, A.S. Geyh, A. McDermott, S.L. Zeger, J.M. Samet, and F. Dominici, "Emergency admissions for cardiovascular and respiratory diseases and the chemical composition of fine particle air pollution," Environmental Health Perspectives, Vol. 117, pp. 957–963, 2009. [CrossRef]

[62] K.M. Rapazzo, J.L. Daniels, L.C. Messer, C. Poole, and D. Lobdell, "Exposure to elemental carbon, or-

ganic carbon, nitrate, and sulfate fractions of fine particulate matter and risk of preterm birth in New Jersey, Ohio, and Pennsylvania (2000–2005)," Environmental Health Perspectives, Vol. 123, 1059–1065, 2015. [CrossRef]

[63] S. Cakmak R.E. Dales, and C.B. Blanco Vida, "Components of particulate air pollution and mortality in Chile," International Journal of Occupational and Environmental, Vol. 15, pp. 152–158, 2009. [CrossRef]

[64] A.H. Sinclair, E.S. Edgerton, R. Wyzga, and D. Tolsma, "A two-time-period comparison of the effects of ambient air pollution on outpatient visits for acute respiratory illnesses," Journal of the Air & Waste Management Association, Vol. 60, pp. 163–175, 2010. [CrossRef]

[65] J.A. Sarnat, A. Marmur, M. Klein E. Kim, A.G. Russell, S.E. Sarnat, J.A. Mulholland, P.K. Hopke, and P.E. Tolbert, "Fine particle sources and cardiorespiratory morbidity: An application of chemical mass balance and factor analytical source-apportionment methods," Environmental Health Perspectives, Vol. 116, pp. 459–466, 2008. [CrossRef]

[66] M.E. Birch, and R.A. Cary, "Elemental carbon-based method for monitoring occupational exposures to particulate diesel exhaust," Aerosol Science Technology, Vol. 25, pp. 221–241, 1996. [CrossRef]

[67] F. Öztürk, and M. Keleş, "Wintertime chemical compositions of coarse and fine fractions of particulate matter in Bolu, Turkey," Environmental Science and Pollution Research, Vol. 23, pp. 14157–14172, 2016. [CrossRef]

[68] U.S. EPA., Method 200.8: Determination of Trace Elements in Waters and Wastes by Inductively Coupled Plasma-Mass Spectrometry," Revision 5.4. Cincinnati, OH., 1994.

[69] Z. Argunhan, and Avci, A.S. "Statistical evaluation of indoor air quality parameters in classrooms of a university," Advances in Meteorology, Vol. 2018, Article ID 4391579, 2018. [CrossRef]

[70] H. Qiao, W. Liu, H. Gu, D. Wang, and Y. Wang, "The transport and deposition of nanoparticles in respiratory system by inhalation," Journal of Nanomaterials, Vol. 2015, Article ID 394507, 2015. [CrossRef]

[71] H. Orru, M. Pindus, H.R. Harro, M. Maasikmets, and K. Herodes, "Metallic fumes at indoor military shooting ranges: lead, copper, nickel, and zinc in different fractions of airborne particulate matter," Propellants, Explosives, Pyrotechnics, Vol. 43, pp. 228–233, 2018. [CrossRef]

[72] K. Na, and D.R. Cocker III, "Organic and elemental carbon concentrations in fine particulate matter in residences, schoolrooms, and outdoor air in Mira Loma, California," Atmospheric Environment, Vol. 39, pp. 3325–3333, 2005. [CrossRef]

[73] K.F. Ho, J.J. Cao, R.M. Harrison S.C. Lee and K.K. Bau. Indoor/outdoor relationships of organic carbon (OC) and elemental carbon (EC) in PM2.5 in roadside environment of Hong Kong. Atmospheric Environment," Vol. 38, pp. 6327–6335, 2004. [CrossRef]

[74] M.K. Seleventi, D.E. Saraga, C.G. Helmis, K. Bairachtari, C. Vasilakos, and T. Maggos, "PM 2.5 indoor/outdoor relationship and chemical composition in ions and OC/EC in an apartment in the center of Athens," Fresenius Environment Bulletin, Vol. 21, pp. 3177–3183, 2012. [CrossRef]

[75] D.S. Bisht, S. Tiwari. A.K. Srivastava, and M.K. Srivastava, "Assessment of air quality during 19th common wealth games at Delhi, India," Natural Hazards, Vol. 66, pp. 141–154, 2013. [CrossRef]

[76] K. Ram, M.M. Sarin, and S.N. Tripathi, "Inter-comparison of thermal and optical methods for determination of atmospheric black carbon and attenuation coefficient from an urban location in northern India," Atmospheric Reseaech, Vol. 97, pp. 335–342, 2010. [CrossRef]

[77] N.L. Briggs, and C.M. Long, "Critical review of black carbon and elemental carbon source apportionment in Europe and the United States," Atmospheric Environment, Vol. 144, pp. 409–427, 2016.

[78] D.G. Barceloux, Chromium. Clinical Toxicology, Vol. 37, pp. 173–194, 1999. [CrossRef]

[79] C. Crump, K, Crump, E, Hack, R, Luippold, K. Mundt, E.J. Liebig, D. Panko, D. Paustenbach, "Proctor 'Dose-response and risk assessment of airborne hexavalent chromium and lung cancer mortality,'" Risk Analysis, Vol. 23, pp. 1147–1163, 2003. [CrossRef]

[80] USEPA, Air Quality Criteria for Particulate Matter (Final Report), U.S. Environmental Protection Agency, Washington, DC, EPA 600/P-99/002aF-bF, 2004. [CrossRef]

[81] M.A. Torkmahalleh, C.H. Yu, L. Lin, Z. Fan, J.L. Swift, L. Bonanno, D.H. Rasmussen, T.M. Holsen, and P.K. Hopke, "Improved atmospheric sampling of hexavalent chromium," Journal of the Air & Waste Management Association, Vol. 63, pp. 1313–1323, 2013. [CrossRef]

[82] M.A. Torres, "Characterizing lead exposure at a US Coast Guard Indoor Firing Range," [Doctoral Thesis], Department of Environmental and Occupational Health Sciences, University of Washington, USA, 2014.

[83] A. Fischbein, C. Rice, L. Sarkozi, S.H. Kon, M. Petrocci, and I.J. Selikoff, "Exposure to lead in firing ranges," JAMA, Vol. 241, pp. 1141–1144, 1979. [CrossRef]

[84] H. Abadin, A. Ashizawa, Y.W. Stevens, F. Llados,

G. Diamond, G. Sage, M. Citra, A. Quinones, S.J. Bosch, and S.G. Swarts, "Toxicological profile for lead, Atlanta: Agency for Toxic Substances and Disease Registry, Avaialble at: https://www.atsdr.cdc.gov/toxprofiles/tp13.pdf. Accessed on Aug 10, 2018.

[85] L.A. Verbrugge, S.G. Wenzel, J.E. Berner, and A.C. Matz, Human exposure to lead from ammunition in the circumpolar north. In: R.T. Watson, M. Fuller, M. Pokras, and W.G. Hunt, (Eds.). "Ingestion of lead from spent ammunition: Implications for wildlife and humans," The Peregrine Fund, Boise, Idaho, USA. pp. 126–136, 2009. [CrossRef]

[86] H. Löfstedt, A. Seldén, L. Storéus, and L. Bodin, "Blood lead in Swedish police officers," American Journal of Industrial Medicine, Vol. 35, pp. 519–522, 1999. [CrossRef]

[87] B.L. Gulson, J.M. Palmer, and A. Bryce, "Changes in blood lead of a recreational shooter," Science of the Total Environment, Vol. 293, pp. 143–150, 2002. [CrossRef]

Environ Res Tec, Vol. 5, Issue. 1, pp. 24–32, March 2022

Environmental Research and Technology
https://ert.yildiz.edu.tr - https://dergipark.org.tr/tr/pub/ert
DOI: https://doi.org/10.35208/ert.917337

Environmental Research & Technology

Research Article

Application of an airlift internal circulation membrane bioreactor for the treatment of textile wastewater

Abdulkadir ÇAĞLAK, Nouha Bakaraki TURAN*, Hanife SARI ERKAN, Güleda ÖNKAL ENGİN

Department of Environmental Engineering, Yıldız Technical University Civil Engineering Faculty, İstanbul, Türkiye

ARTICLE INFO

Article history
Received: 16 April 2021
Revised: 11 December 2021
Accepted: 04 January 2022

Key words:
Airlift internal circulation membrane bioreactor; Color; Reactive red; Textile wastewater

ABSTRACT

A large amount of water is used in the textile industry during the finishing and dyeing processes leading to the production of what is known as textile wastewaters. Textile wastewater is highly rich in COD and color and is characterized by relatively low biodegradability. This study aimed to investigate the treatability of reactive red dye-rich textile wastewater with the application of an airlift internal circulation membrane bioreactor (AIC-MBR). Experimental results demonstrated that high removal efficiencies of COD, NH_3-N, and reactive red up to 99.70%, 97.83%, and 97.23%, respectively, can be achieved using the AIC-MBR system. Besides, EPS and SMP analyses reflected an SMP polysaccharide (PS) and protein (PN) membrane rejection that reached 88% and 72.6%, respectively. Finally, the capillary suction time measurement highlighted a good dewatering capacity of the sludge with a low membrane fouling tendency at the end of the operating period.

Cite this article as: Çağlak A, Turan NB, Sarı Erkan H, Önkal Engin G. Application of an airlift internal circulation membrane bioreactor for the treatment of textile wastewater. Environ Res Tec 2022;5:1:24–32.

INTRODUCTION

Textile industry is recognized as one of the most wastewater producing manufacturing sectors. Textile wastewater is colored with a composition, which varies according to the type of fiber and chemicals used, the techniques applied, and the machines operated [1]. It is known that approximately 6900 additives and 8000 dying agents used in the sector increase the organic and inorganic pollution load of textile wastewater [2]. Therefore, it is characterized by a high total dissolved solid (TDS), COD/BOD5, salt and color. Color is usually studied as an important parameter in textile wastewater because if not removed effectively, it reduces light scarcity in the receiving water affecting in turn aquatic organisms [3]. Different types of dyes are used in the textile industry classified as reactive, dispersive, basic, acidic, azoic, direct and sulfuric dyes. Azoic, sulfuric and dispersive dyes are easily removed from effluents as they are insoluble in water. However, highly soluble dyes, namely direct, basic, acidic and reactive dyes, are hardly removed by conventional separation and treatment methods. Furthermore, the most problematic dye group used in the textile industry is reactive dyes. Because these dyes may form complexes with heavy metals such as nickel, copper and chromium, thus,

***Corresponding author.**
*E-mail address: nahnoouha87@hotmail.com

posing a further risk when released into the environment [4]. Thus, different treatment processes including physical [5], chemical [6], electrochemical [7], and biological [8] are applied before its discharge to the environment.

Membrane bioreactors (MBRs) are proven to ensure higher effluent quality due to the complete retention of contaminants by the microbial community. However, membrane fouling is one of the limitations that affect MBR operation, increasing energy demand and reducing membrane permeability. Different reactor configurations have been developed to reduce this disadvantage of membrane bioreactors. An example of these is airlift membrane bioreactor which is characterized by a simple configuration [9]. The bioreactor is divided into a fully gassed riser and two ungassed downcomers. The density difference between them will result in the liquid circulation, which will positively affect the membrane fouling [10]. Airlift membrane bioreactors were successful in reducing the fouling processes by the rising air bubbles that generate shear stress and remove, in turn, the deposited particle along the membrane surface [11]. Besides, airlift membrane bioreactor was proved to reduce membrane fouling enhancing a better filtration performance with a lower energy consumption [12–14].

In this study, an airlift internal circulation membrane bioreactor (AIC-MBR) was tested for the treatability of Reactive Red dye-rich textile wastewater. Three different concentrations of the reactive dye were tested in the AIC-MBR. Operational parameters such as COD, NH_3-N and EPS/SMP were monitored throughout the study. Besides, the removal of reactive red dye was investigated.

MATERIALS AND METHODS

Airlift Membrane Bioreactor System and Operating Conditions

An airlift membrane bioreactor was used in this study for the treatment of synthetic textile wastewater. The reactor design is shown in Figure 1. The reactor was made of plexiglass (32 cm x 9 cm) with an effective volume of 1.5 L. Two vertical plates, having a height of 27.7 cm and placed 4.8 cm apart, were mounted inside reactor creating a riser and two downcomers. Each plate was perforated creating a hole opening of 1.8 cm. The air diffuser is located at the bottom of the reactor supplying air inside the riser. The holes on each plate ensured the circulation of air bubbles between the riser and downcomers. A hollow fiber membrane module having a pore size of 0.2 µm and an effective area of 0.0170 m^2 was used in the AIC-MBR system. The membrane was made of polyvinylidene fluoride (PVDF)-based microporous membrane containing a small quantity of polyethersulfone (PES). The system was operated continuously based on the Archimedes theory where the same volume filtered from the membrane module was fed with synthetic wastewater to the reactor.

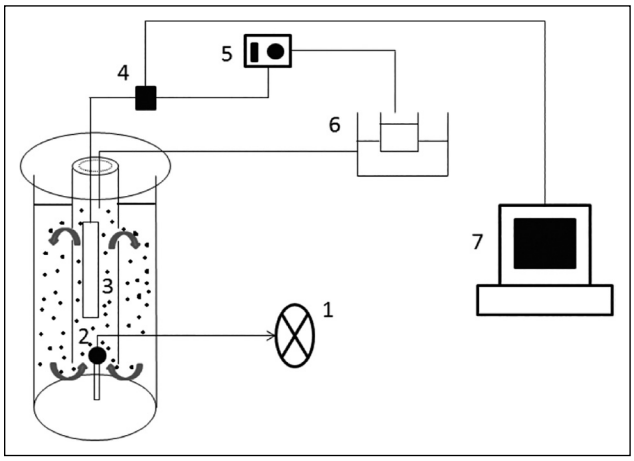

Figure 1. Schematic representation of the AIC-MBR system, air compressor (1), air diffusor (2), hollow fibre membrane module (3), manometer (4), peristaltic pump (5), feed tank (6), permeate tank, computer (7).

Table 1. Operating conditions of the AIC-MBR

Operating parameter	Value
pH	8.48
Dissolved oxygen, mg/L	8.65
Temperature, °C	18.28
SRT, days	20
HRT, hours	24
F/M (mg COD/mg MLSS.day)	0.26
Lorg, mg COD/L.day	1.095
Effective membrane area (m^2)	0.017
Net flux (LMH)	3.70

Table 2. Operational Periods in the AIC-MBR

Periods	Concentration of reactive red in feed (mg/L)	Duration (day)
1	0	1–13
2	10	14–34
3	20	35–66
4	40	67–95

AIC-MBR was operated at a steady-state condition under a sludge retention time of 20 days and an organic loading rate of 1.095 L/m^2.d. The operating conditions are summarized in Table 1. Oxygen was provided continuously through an air diffuser. The trans-membrane pressure (TMP) was measured using a pressure gauge.

The concentration of the reactive red dye was increased every 30 days as 10, 20 and 40 mg/L, in order to monitor the treatability of three different concentrations of the colorant. The operational periods are shown in Table 2.

Characterization of Textile Synthetic Wastewater and Inoculum

Real textile wastewater is characterized by a high concentration of biochemical oxygen demand (BOD) and chemical oxygen demand (COD), in addition to high values of chlorides, nitrates, suspended solids and metals [15]. However, synthetic wastewater is usually preferred because of its simplicity in evaluating results. The recipe used in this study was previously used by Yurtsever et al. (2016) as shown in Table 3 [16]. About 1000 mg/L of glucose as a source of biodegradable carbon source and different inorganics were added to meet the characteristics of real textile wastewater. Activated sludge seeded to the reactor was taken from a municipal wastewater treatment plant in İstanbul having an MLSS concentration of 5800 mg/L.

Sampling and Analyses Procedure

Chemical oxygen demand (COD), ammonium-nitrate NH_3-N, mixed liquor suspended solids (MLSS) and mixed liquor volatile suspended solids (MLVSS) were measured three days per week based on the Standard Methods [17]. COD was analyzed in both the filtrate and the supernatant taken from the activated sludge. The dissolved oxygen (DO) and pH were monitored daily in the bioreactors using a WTW Multiline P4 multimeter (CellOx 325 DO probe and SenTix 41 pH probe). Extracellular polymeric substances (EPS) and soluble microbial products (SMP) with their protein and polysaccharide fractions were analyzed once per week from both the activated sludge and filtrate samples. EPS and SMP analyses were performed following the formaldehyde extraction method [18] where the protein (PN) and polysaccharide (PS) fractions were tested using the Lowry [19] and phenol-sulphuric acid methods [20]. The capillary suction time (CST) and sludge volume index (SVI) were analyzed every 15 days. CST was measured using a capillary suction timer (Triton type 304M) and a standard filter paper obtained from Triton. EPS, SMP and CST analysis were measured at steady-state conditions. Reactive red color treatability was monitored by analyzing its concentration in both the filtrate and the supernatant from the activated sludge. Reactive red was measured at a wavelength of 455 nm using Hach Lange DR 5000 spectrophotometer.

Table 3. Composition of the synthetic textile wastewater used in this study [16]

Added chemical	mg/L
$C_6H_{12}O_6.H_2O$	1000
$NaHCO_3$	1000
NH_4Cl	230
K_2HPO_4	37
KH_2PO_4	67
$CaCl_2.2H_2O$	4
$MgCl_2.H_2O$	3.4
$FeSO_4.7H_2O$	5.92
$MnSO_4.2H_2O$	0.4289
$ZnSO\pm.7H_2O$	0.1053
Na_2SO_3	0.2811
$NiSO_4.6H_2O$	0.1
$CoCl_2$	0.5457
Reactive red	10, 20 and 40

RESULTS AND DISCUSSION

Evaluation of AIC-MBR System Performance

Figure 2 shows the variations in the MLSS and MLVSS concentrations in addition to MLVSS/MLSS ratio. The

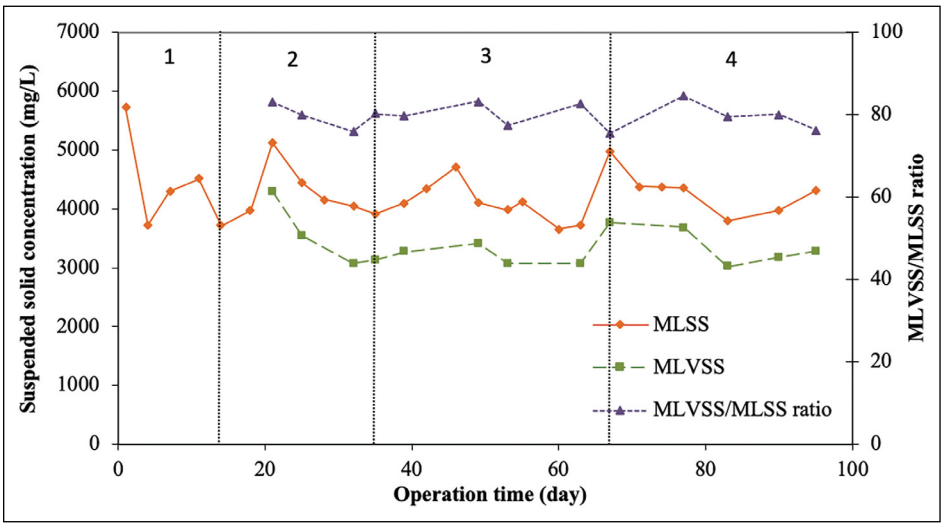

Figure 2. Variation of MLSS and MLVSS concentration and ratio.

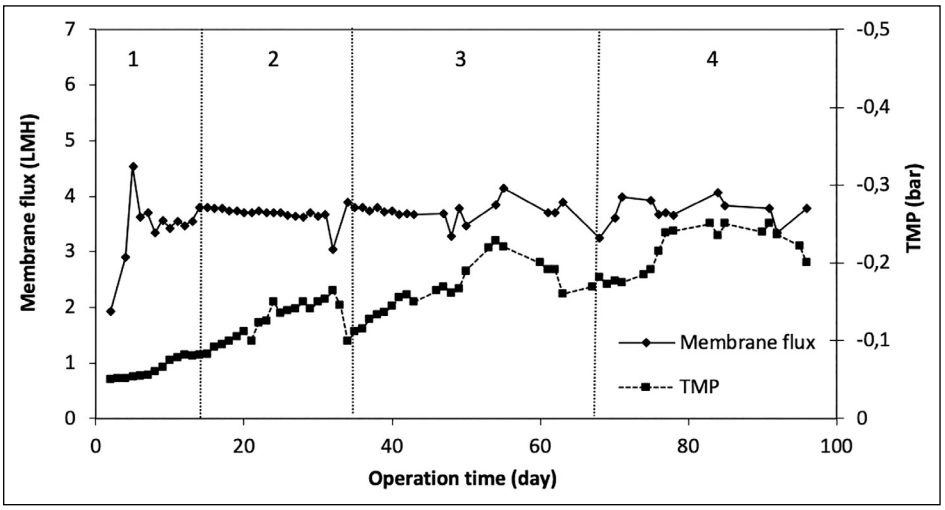

Figure 3. Variation of membrane flux and TMP values throughout AIC-MBR operation.

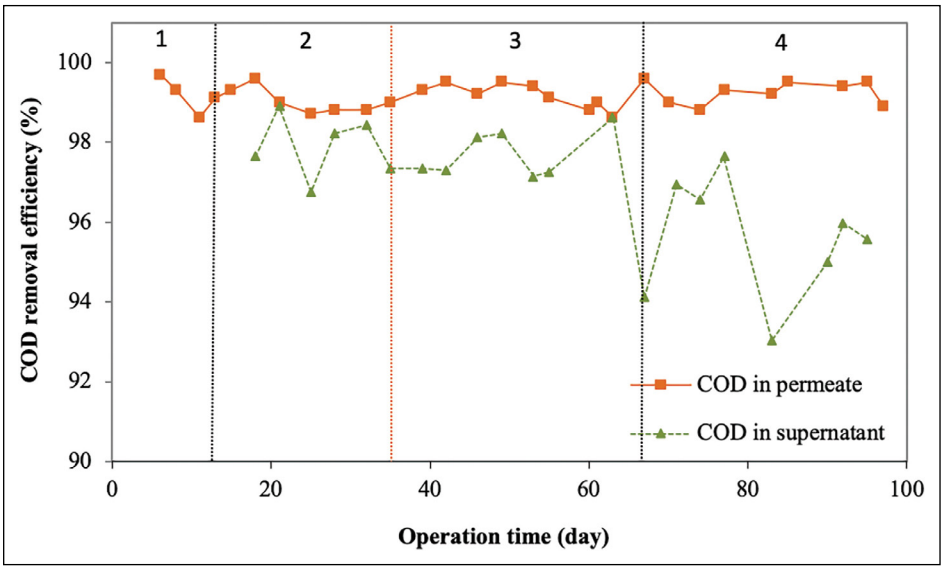

Figure 4. COD removal efficiencies in the supernatant and permeate over time.

initial MLSS concentration was 5800 mg/L which fluctuated until it reached its steady-state conditions after about 20 days. MLSS was then kept stable between 4000 to 5000 mg/L for the remaining 80 days of operation. Similarly, the MLVSS and MLVSS/MLSS ratio changed in the range of 4000 to 3000 mg/L and 75.5 to 85.5%, respectively. This high MLVSS/MLSS ratio reflected the microbial activity in the reactor. An SRT value of 20 days was kept by drawing a daily sludge volume of 75 mL from the AIC-MBR. The SRT in aerobic MBRs is usually preferred to be between 20 and 50 days, which confirms the suitability of the operating SRT in this study [21].

The average membrane flux was about 3.70 L/m^2.h (LMH) where the transmembrane pressure (TMP) decreased from zero to -0.2 bar at the end of the operating period (Fig. 3). Membrane flux and TMP were directly affected by the aeration rate influencing in turn membrane fouling. In this study, no back-washing or chemical washing was applied to the membrane. Therefore, the minimal reduction occurred in TMP is acceptable.

COD Removal Efficiency by AIC-MBR

COD removal efficiency was measured in both the permeate and the supernatant during the operating period of the reactor. As can be seen from Figure 4, the COD removal efficiency in the supernatant fluctuates in the range of 93.02–98.91% while in the permeate it registered a removal efficiency of about 98.62 to 99.70%. Thus, COD removal efficiency was higher in the permeate then in the supernatant noting that both demonstrated great removal efficiencies. This is in correspondence with Lee

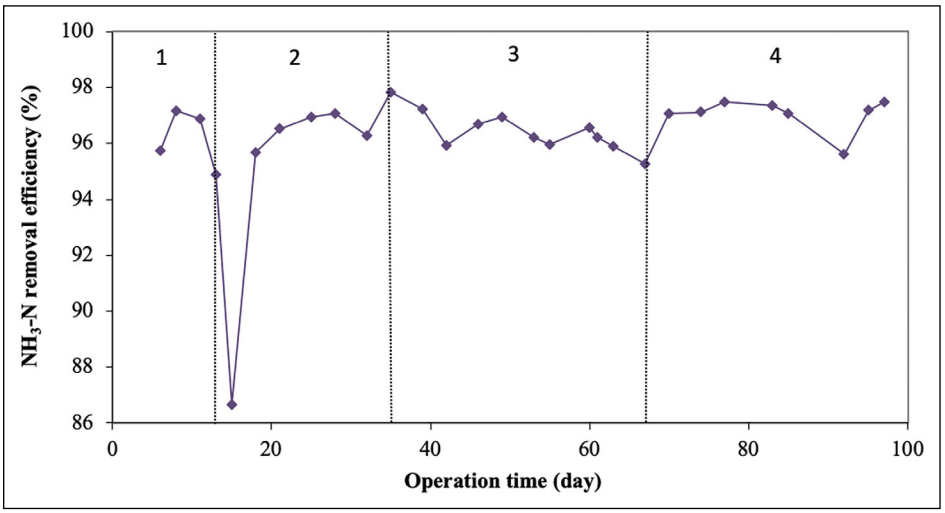

Figure 5. NH_3-N removal efficiencies over time.

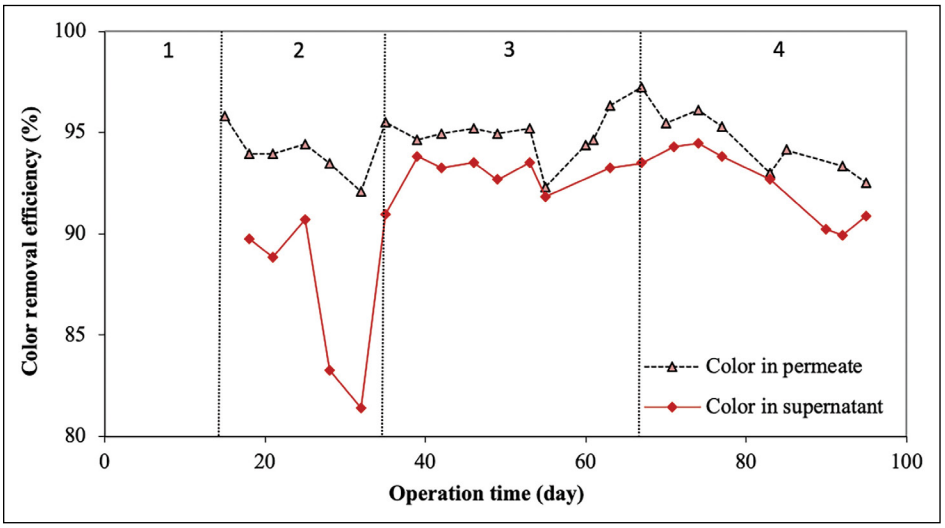

Figure 6. Color removal efficiencies over time.

et al. (2003) who found out that the COD removal in the permeate was higher than the supernatant [22]. Besides, Yurtsever et al. (2016) reported in their study that COD concentrations of 54±14 mg/L and 47±12 mg/L were recorded for the supernatant and permeate, respectively [16]. Berube et al., (2010) reported that the COD removal efficiency in a conventional activated sludge process may typically reach about 95%, however, this value may increase to reach a range of 96 to 99% in a membrane bioreactor process [23]. This can be explained by the fact the colloids and soluble compounds can be attached to the suspended solids which can be retained in MBR system giving a better COD removal and particle-free effluent [24, 25]. The average removal efficiency of 90% was obtained in another study that used airlift external circulation membrane bioreactor (AEC-MBR) for the treatment of toilet wastewater [26].

NH_3-N Removal Efficiency by AIC-MBR

The laboratory prepared synthetic textile wastewater had a NH_4^+ concentration of 77.4 mg/L. The removal efficiency of NH_3-N in the permeate from an AIC-MBR was studied and the experimental results are presented in Figure 5. NH_3-N removal efficiency changed between 95.73 and 97.83% during the operating period. However, an important decrease in NH_3-N removal was observed after the addition of reactive red color to the reactor which affected the performance of the microorganisms. The adaptation time of microorganisms to any new component entering the reactor medium may differ in COD values, which may explain the reason behind the sudden decrease observed on the day of dye addition [27]. The removal efficiency of 96.6% was obtained using a draft tube MBR without carriers for the treatment of mixed wastewater [28]. The COD/TN ratio with the dissolved

Table 4. Typical characteristics of textile effluents

	Ghaly et al. (2014) [32]	Kehinde and Aziz (2014) [33]	Tavangar et al. (2019) [34]	Bhuvaneswari et al. (2016) [35]	Yurtsever et al. (2020) [36]
pH	6–10	6.95–11.8	7.03±0.01	8.6–9.2	8–9.5
Color (Pt-Co)	50–2500	50–2500	2100±5	N/A	500–1250
COD (mg/L)	150–12000	150–30000	2690±10	3880–4400	700–1250
TSS (mg/L)	15–8000	15–8000	280±2	550–650	200–450

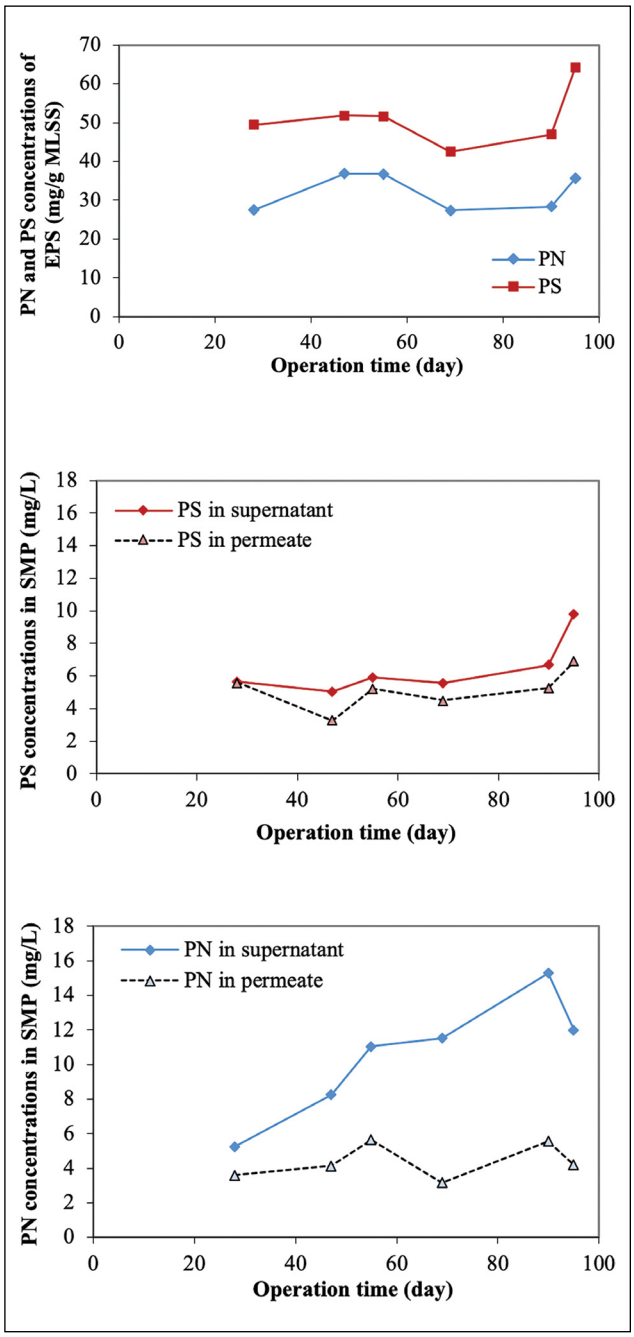

Figure 7. Variance in the protein and polysaccharide concentrations of EPS **(a)**, polysaccharide **(b)** and protein **(c)** concentrations in SMP in both supernatant and permeate.

oxygen level was found to affect the simultaneous nitrification and denitrification in an airlift membrane bioreactor. A COD/TN level in the range of 4.77 to 10.04 leads to a nitrogen removal that exceeds 70% which is comparable to the results in this study taking into consideration that COD/TN is about 12.92 [29].

Reactive Red Removal Efficiency by AIC-MBR

Reactive red was used in this study as the type of colorant to be removed. As mentioned earlier, three different concentrations of reactive red were added subsequently to the reactor. The color removal efficiency was monitored in both permeate and supernatant and the obtained results are shown in Figure 6. The removal efficiency in the supernatant varied between 83.25 and 94.47% where it increased to 89.29 and 97.23% in the permeate. A slight decrease occurred after the addition of the third concentration of reactive red of 40 mg/L. Color removal was performed using different methods in the literature. The removal efficiency varied according to the initial concentration and the treatment process applied [30]. In an anaerobic/aerobic sequential batch reactor system, 20 mg/L of reactive black 5, reactive blue 19 and reactive blue 5 was treated and the removal efficiencies were found to be 63, 64 and 66%, respectively [31]. Color may be removed through different processes through cleavage of the chemical bonds or adsorption to the microbial flocs. The removal occurred in supernatant reflects the role of the microbial activity in reducing or adsorbing the dye molecules [30]. Besides, the higher removal efficiencies obtained in the permeate is in close relationship with the membrane used which blocks the passage of any particle, as mentioned earlier.

The composition of textile industry wastewater varies from factory to factory and from country to country, depending on the process, the equipment used, the type of fabric produced and the chemicals applied [30]. Table 4 shows the real textile wastewater characteristics reported from different sources and countries. As seen from Table 4, the pH value of real textile wastewater varies in a wide range between 5.5–11.8. This wide pH or COD variations may lead to negative effects in MBR operation, especially on active biomass, making it impossible to achieve a stable biological treatment in terms of pollutant removal and membrane fouling.

Variation in EPS and SMP Components

Extracellular polymeric substances (EPS) are divided into bound EPS and soluble EPS [mainly named soluble microbial products (SMP)]. Major constituents of EPS consist mainly of proteins and polysaccharides [37]. The results regarding the variation in EPS and SMP concentrations are presented in Figures 7, respectively. An overall evaluation of both plots in Figure 7a shows a general increasing trend in EPS and SMP level with time noting that EPS values were higher than SMP ones. The increase in these values may be attributed to the increase in MLSS concentration in the reactor. Besides, the increasing trend may be related to the increase in the TMP levels discussed above and thus to membrane biofouling [38]. It was stated by researchers that EPS concentration and characteristics are directly affected by multiple parameters such as the sludge composition, sludge retention time (SRT) and aeration [39, 40]. The comparison between the polysaccharide and protein fractions of EPS and SMP reflected a superiority of polysaccharide levels in both EPS and SMP. Polysaccharide fractions usually affect fouling in membrane bioreactors, as reported by Yigit et al. [41]. SMP polysaccharide (PS) and protein fractions (PN) were measured in both the supernatant and permeate. The corresponding results are presented in Figure 7b and 7c. It can be seen clearly than PS and PN of SMP shows higher and increasing values in the supernatant than in the permeate. The PS rejection of SMP by the hollow membrane was found to be 0.88% at 28th day, while the PS rejections by the membrane increased in the next operation period and were determined between 64 and 88%. On the other hand, PN rejection of SMP was found 31.4% at 28th day, while after this point, the rejection rates were found to vary between 49.7 and 72.6%. The obtained results can be explained by the membrane filterability which blocks the soluble part of EPS that may be adhered to microbial flocs or other particles in the sludge [38]. However, the minimal part of the SMP appearing in the permeate is caused by the membrane permeability that may enhance the passage of the soluble and non-adhesive part of the SMP [42].

Variation in CST Levels

The capillary suction time (CST) of the sludge was measured in order to test the dewatering properties of the activated sludge. As can be seen from Figure 8, CST values showed fluctuations between 5.5 and 9.6 s with a minimal increase at the end of the operating period. Additionally, an increase observed in the CST may be related to the increase occurred in the polysaccharide values of EPS. However, CST values were still in an acceptable range reflecting a good dewatering capacity of the sludge [43].

On the 69th day of operation, CST value decreased from 6.9 s to 5.5 s and then increased to 9.6 s on the 90th day.

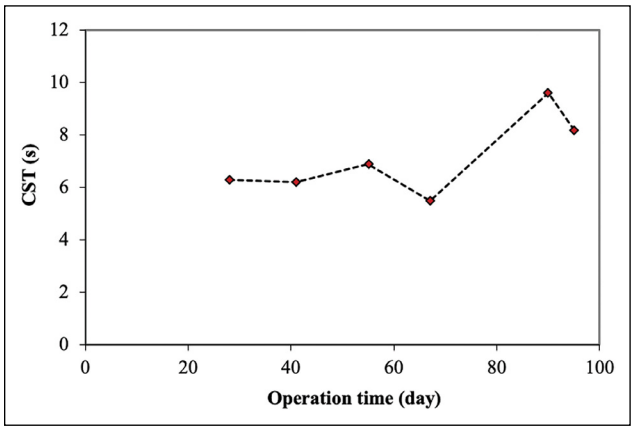

Figure 8. CST values obtained from activated sludge samples over time.

These results could be related to the concentrations of PN and PS of SMP, as the CST values presented a similar trend with SMP concentrations of supernatant. It was reported by Zhang et al. (2015) [44] that there is a significant relationship between SMP and membrane fouling and SMPs are the main soluble components in a gel layer and cake layer on the membrane surface and pores. Higher specific filtration resistance occurred in the gel layer due to the adsorption of SMP [45].

CONCLUSION

The application of an AIC-MBR demonstrated quite high COD, NH_3-N and reactive red removal efficiencies up to 99.70%, 97.83%, and 97.23%, respectively. Moreover, the proposed system ensures satisfactory results even with increased initial concentrations of the reactive dye. Additionally, a relatively low membrane fouling tendency was observed in this technology based on the results from EPS, SMP and CST. The overall results indicated that the AIC-MBR can be applied for the treatment of real textile wastewater, after necessary preliminary tests were carried out.

DATA AVAILABILITY STATEMENT

The authors confirm that the data that supports the findings of this study are available within the article. Raw data that support the finding of this study are available from the corresponding author, upon reasonable request.

CONFLICT OF INTEREST

The authors declared no potential conflicts of interest with respect to the research, authorship, and/or publication of this article.

ETHICS

There are no ethical issues with the publication of this manuscript.

REFERENCES

[1] V. Jegatheesan, B.P. Pramanik, J. Chen, D. Navaratna, C-Y. Chang, L. Shu, "Treatment of textile wastewater with membrane bioreactor: a critical review," Bioresource Technology,. Vol. 204, pp. 202–212, 2016. [CrossRef]

[2] K.M. Shah, "Handbook of synthetic dyes and pigments," Multi-tech Publishing Company, North Dakota, 1998.

[3] C.R. Holkar, A. J. Jadhav, D. V. Pinjari, N. M. Mahamuni, A.B. Pandit, "A critical review on textile wastewater treatments: possible approaches," Journal of Environmental Management, Vol. 182, pp. 351–366, 2016. [CrossRef]

[4] M.M Hassan, and C.M. Carr, "A critical review on recent advancements of the removal of reactive dyes from dyehouse effluent by ion-exchange adsorbents," Chemosphere, Vol. 209, pp. 201–219, 2018. [CrossRef]

[5] G. Walker, and L. Weatherley, "Textile wastewater treatment using granular activated carbon adsorption in fixed beds. Separation Science and Technology," Vol. 35, pp. 1329-1341, 2000. [CrossRef]

[6] S.H. Lin, and M.L. Chen, "Treatment of textile wastewater by chemical methods for reuse, Water Research, Vol. 31, pp. 868–876, 1997. [CrossRef]

[7] J. Naumczyk, L. Szpyrkowicz, and F. Zilio-Grandi, "Electrochemical treatment of textile wastewater," Water Science and Technology, Vol. 34, pp. 17–24, 1996. [CrossRef]

[8] S. Andleeb, N. Atıq, M. I. Ali, R.R. Husnain†, M. Shafique, B. Ahmad, P.B. Ghumro, M. Hussain, A. Hameed, and S. Ahmad, "Biological treatment of textile effluent in stirred tank bioreactor," International Journal of Agriculture and Biology, Vol, 12, pp. 256–260, 2010.

[9] H.S. Erkan, N.B. Turan, and G.O. Engin, "Fouling control in MBR in a sustainable perspective, in Current Developments in Biotechnology and Bioengineering," Elsevier, Oxford, pp. 21–57. 2020. [CrossRef]

[10] J. Merchuk, A. Contreras, F. Garcia, and E. Molina, "Studies of mixing in a concentric tube airlift bioreactor with different spargers," Chemical Engineering Science, Vol. 53, pp. 709–719, 1998. [CrossRef]

[11] T.-H. Kim, S.-R. Lee, Y.-K. Nam, J. Yang, C. Park, and M. Lee. "Disintegration of excess activated sludge by hydrogen peroxide oxidation," Desalination, Vol. 246, pp. 275-284, 2009. [CrossRef]

[12] R. Liu, X. Huang, C. Wang, L. Chen, and Y. Qian. "Study on hydraulic characteristics in a submerged membrane bioreactor process," Process Biochemistry, Vol. 36, pp. 249–254, 2000. [CrossRef]

[13] A. Sofia, W. Ng, and S. Ong, "Engineering design approaches for minimum fouling in submerged MBR," Desalination, Vol. 160, pp. 67–74, 2004. [CrossRef]

[14] F. Yang, S. Bick, S. Shandalov, and G. Oron, "Optimal performance of an immersed membrane bioreactor equipped with a draft tube for domestic wastewater reclamation," Water Science and Technology, Vol. 54, pp. 155–162, 2006. [CrossRef]

[15] P. Pal, "Industrial water treatment process technology," Butterworth-Heinemann, Oxford, 2017.

[16] A. Yurtsever, B. Calimlioglu, M. Görür, Ö. Çınar, and E. Sahinkaya, "Effect of NaCl concentration on the performance of sequential anaerobic and aerobic membrane bioreactors treating textile wastewater," Chemical Engineering Journal, Vol. 287, pp. 456–465, 2016. [CrossRef]

[17] A. Eaton, "Standard Methods for the Examination of Water and Wastewater," 21st American Public Health Association, American Water Works Association, Water Environment Federation, ed.(Washington DC, APHAAWWA-WEF). ΣΧΟΛΗ, ΤΜΗΜΑ ΧΗΜΙΚΩΝ ΜΗΧΑΝΙΚΩΝ, 2005.

[18] T. Li, R. Bai, and J. Liu, "Distribution and composition of extracellular polymeric substances in membrane-aerated biofilm," Journal of Biotechnology, Vol. 135, pp. 52–57, 2008. [CrossRef]

[19] O.H. Lorwy, N.J. Rosebrough, A.L. Farr, and R.J. Randall, "Protein measurement with the Folin phenol reagent," Journal of Biological Chemistry, Vol. 193, pp. 265–275, 1951. [CrossRef]

[20] M. Dubois, K.A. Gilles, P.A. Rebers, and F. Smith, "Colorimetric method for determination of sugars and related substances," Analytical Chemistry, Vol. 28, pp. 350–356, 1956. [CrossRef]

[21] F. Meng, S.R. Chae, A. Drews, M. Kraume, H.S. Shin, and F. Yang, "Recent advances in membrane bioreactors (MBRs): membrane fouling and membrane material," Water Research, Vol. 43, pp. 1489–1512, 2009. [CrossRef]

[22] W. Lee, S. Kang, and H. Shin, "Sludge characteristics and their contribution to microfiltration in submerged membrane bioreactors," Journal of Membrane Science, Vol. 216, pp. 217–227, 2003. [CrossRef]

[23] P. Bérubé, "Membrane bioreactors: Theory and applications to wastewater reuse," Sustainability Science and Engineering, Vol. 2, pp. 255–292, 2010. [CrossRef]

[24] S. Judd, "The status of membrane bioreactor technology," Trends in Biotechnology, Vol. 26, pp. 109–116, 2008. [CrossRef]

[25] F. Meng, H. Zhang, Y. Li, X. Zhang, and F. Yang, "Application of fractal permeation model to investigate membrane fouling in membrane bioreactor," Journal of Membrane Science, Vol, 262, pp. 107-116, 2005. [CrossRef]

[26] Y. Fan, G. Li, L. Wu, W. Yang, C. Dong, H. Xu, and W. Fan, "Treatment and reuse of toilet wastewater by

an airlift external circulation membrane bioreactor," Process Biochemistry, Vol. 41, pp. 1364–1370, 2006. [CrossRef]

[27] B.A. Poursat, R.J.M. van Spanning, P. De Voogt, and J.R. Parsons, "Implications of microbial adaptation for the assessment of environmental persistence of chemicals," Critical Reviews in Environmental Science and Technology, Vol. 49, pp. 2220–2255, 2019. [CrossRef]

[28] F. Yang, Y. Wang, A. Bick, J. Gilron, A. Brenner, L. Gillerman, M. Herzberg, and G. Oron, "Performance of different configurations of hybrid growth membrane bioreactor (HG-MBR) for treatment of mixed wastewater," Desalination, Vol. 284, pp. 261–268, 2012. [CrossRef]

[29] Q. Meng, F. Yang, and F. Meng, et al, "Effects of COD/N ratio and DO concentration on simultaneous nitrification and denitrification in an airlift internal circulation membrane bioreactor," Journal of Environmental Sciences, Vol. 20, pp. 933–939, 2008. [CrossRef]

[30] D. Yaseen, and M. Scholz, "Textile dye wastewater characteristics and constituents of synthetic effluents: a critical review," International Journal of Environmental Science and Technology, Vol. 16, pp. 1193–1226, 2019. [CrossRef]

[31] Panswad, T. and W. Luangdilok, "Decolorization of reactive dyes with different molecular structures under different environmental conditions," Water Research, Vol. 34, pp. 4177–4184, 2000. [CrossRef]

[32] A.E. Ghaly, R. Ananthashankar, M. Alhattab, and V.V. Ramakrishnan, "Production, characterization and treatment of textile effluents: a critical review," Journal of Chemical Engineering & Process Technology, Vol. 5, pp. 1-19, 2014.

[33] F. Kehinde, and H.A. Aziz, "Textile waste water and the advanced oxidative treatment process, an overview," International Journal of Innovative Research in Science, Engineering and Technology, Vol. 3, pp. 15310–15317, 2014. [CrossRef]

[34] T. Tavangar, K. Jalali, M.A.A. Shahmirzadi, and M. Karimi, "Toward real textile wastewater treatment: Membrane fouling control and effective fractionation of dyes/inorganic salts using a hybrid electrocoagulation–Nanofiltration process," Separation and Purification Technology, Vol. 216, pp. 115–125, 2019. [CrossRef]

[35] A. Bhuvaneswari, B. Asha, and D. Selvakumar, "Start up and enhancement granulation in an anaerobic baffled reactor for the treatment of textile wastewater," International Journal of Civil Engineering, Vol. 9, pp. 645–652, 2016.

[36] A. Yurtsever, E. Sahinkaya, and Ö. Çınar, "Performance and foulant characteristics of an anaerobic membrane bioreactor treating real textile wastewater," Journal of Water Process Engineering, Vol. 33, pp. 101088, 2020. [CrossRef]

[37] H. Lin, M. Zhang, F. Wang, F. Meng, B.Q. Liao, H. Hong, J. Chen, and W. Gao.et al., A critical review of extracellular polymeric substances (EPSs) in membrane bioreactors: characteristics, roles in membrane fouling and control strategies. Journal of Membrane science, 2014. 460: p. 110-125. [CrossRef]

[38] S. Rosenberger, C. Laabs, R. Gnirss, G. Amy, M. Jekel, and J.-C. Schrotter, "Impact of colloidal and soluble organic material on membrane performance in membrane bioreactors for municipal wastewater treatment, Water Research, Vol. 40, pp. 710–720, 2006. [CrossRef]

[39] P. Le-Clech, V. Chen, and T.A. Fane, "Fouling in membrane bioreactors used in wastewater treatment," Journal of Membrane Science, Vol. 284, pp. 17–53, 2006. [CrossRef]

[40] M.E. Hernandez Rojas, R. Van Kaam, S. Schetrite, and C. Albasi, "Role and variations of supernatant compounds in submerged membrane bioreactor fouling," Desalination, Vol. 179, pp. 95–107, 2005. [CrossRef]

[41] N.O. Yigit, I. Harman, G. Civelekoglu, H. Koseoglu, N. Cicek, and M. Kitis, "Membrane fouling in a pilot-scale submerged membrane bioreactor operated under various conditions," Desalination, Vol. 231, pp. 124–132, 2008. [CrossRef]

[42] L.-C. Juang, D.-H. Tseng, Y.-M. Chen, G. Uy Semblante, and S.-J. You, "The effect soluble microbial products (SMP) on the quality and fouling potential of MBR effluent," Desalination, Vol. 326, 96–102, 2013. [CrossRef]

[43] B. Durmaz, and F. Sanin, "Effect of carbon to nitrogen ratio on the physical and chemical properties of activated sludge," Environmental Technology, Vol. 24, pp. 1331–1340, 2003. [CrossRef]

[44] X. Wang, Y. Chen, B. Yuan, X. Li, and Y. Ren, "Impacts of sludge retention time on sludge characteristics and membrane fouling in a submerged osmotic membrane bioreactor," Bioresource Technology, Vol. 161, pp. 340–347, 2014. [CrossRef]

[45] T. Stephenson, S. Judd, B. Jefferson and K. Brindle, "Membrane bioreactors for wastewater treatment." IWA Publishing, London, 2000.

Environ Res Tec, Vol. 5, Issue. 1, pp. 33–43, March 2022

Environmental Research and Technology
https://ert.yildiz.edu.tr - https://dergipark.org.tr/tr/pub/ert
DOI: https://doi.org/10.35208/ert.1014814

Environmental Research & Technology

Research Article

Optimization of the effect of copper electrodes on the removal efficiency of 4-clorophenol from aqueous solution by electrocoagulation

Gülizar KURTOĞLU AKKAYA*[1], Muhammed Kamil ÖDEN[2]

[1]*Department Environmental Engineering, Necmettin Erbakan University, Konya, Türkiye*
[2]*Department of Environmental Protection Technology, Selcuk University Sarayönü Vocational High School, Konya, Türkiye*

ARTICLE INFO

Article history
Received: 26 October 2021
Revised: 14 December 2021
Accepted: 04 January 2022

Key words:
Copper; Electrocoagulation; MINITAB; 4-clorophenol

ABSTRACT

In this study, the investigation of 4-clorophenol (CP) removal from aqueous solutions using copper electrodes by electrocoagulation (EC) process was done. The effects of various experimental parameters such as pH, current density and exposure time, which affect the EC process, on 4-CP removal were investigated. To optimize the process, response surface methodology (RSM) Box Behnken Design was used by MINITAB program, a series of experimental sets were obtained and carried out. Afterward, 4-CP removal was analyzed and calculated. Results were entered into the MINITAB program as a response. At the end of the optimization, optimum operating conditions were determined as 74 mA/cm^2, 45 min, 4.24 for current density, exposure times and pH, respectively. When the results were evaluated, approximately 92% phenol removal efficiencies were obtained. Additionally, according to the model results, it was understood that the factors with the greatest effect on 4-CP removal were the exposure time and current density and these had a linear effect, but the pH value did not have a significant effect.

Cite this article as: Kurtoğlu Akkaya G, Öden MK. Optimization of the effect of copper electrodes on the removal efficiency of 4-clorophenol from aqueous solution by electrocoagulation. Environ Res Tec 2022;5:1:33–43.

INTRODUCTION

With the developing technology and increasing population, the reequipments of people have changed and increased. Uncontrollable increase in production and consumption has caused rapid depletion of resources and increased pollution. As a consequence, it increases the consumption of water, which is one of the most important natural resources and rapidly causes pollution of water resources.

Water is necessary for developing countries [1, 2]. Agricultural irrigation uses water resources the most with 70% of the total water consumption. This is followed by electricity generation, steam-based electricity generation and cooling waters [1].

The wastewaters are identified as waters, which are used in various processes in people activities and in some industries, are discharged to the receiving environments. They disrupt the ecological balance in the receiving environment where they are discharged or they cause great destruction. For this reason, they must be treated before been discharged into the receiving water environments and must obtain the legal discharge limit values [3].

***Corresponding author.**
*E-mail address: ka.gulizar@gmail.com

Wastewaters are treated using conventional processes such as biological processes [4], physico-chemical processes [5], as well as developing technologies, namely membrane filtration [6] and adsorption [7], advanced oxidation processes [8]. Advanced oxidation processes require strong oxidizers, which makes wastewater treatment safe and cost-effective. Biological processes, on the other hand, require tightly controlled conditions with long retention times. Chemical processes require extensive chemical addition, which not only increases the cost of the process but also complicates downstream processes with an increased risk of secondary contamination. Membrane filtration and adsorption methods alone cannot effectively treat wastewater unless integrated with extensive pretreatment processes, especially in the treatment of phenolic compounds. Therefore, wastewater treatment research using electrochemical processes is highly attractive [9, 10].

Recently, electrochemical treatment methods such as electrooxidation and electrocoagulation (EC) have drawn attention due to their environmental importance and economic efficiency [11, 12]. High removal efficiencies have been achieved for treating different wastewaters and drinking water using the EC process [3]. EC is a complex process in which sacrificial electrodes are used to form ions that act as coagulants in wastewater, including many removal mechanisms such as adsorption, co-precipitation, chemical oxidation-reduction and flotation [13]. Metal hydroxides are formed by the anodic dissolution and hydrolysis of metal anodes, such as aluminum and iron [14].

There are many pollutants in wastewater that needs to be treated, depending on the variety of activities. Pollutants such as color, hardness, dissolved oxygen, detergent types, heavy metals, oil-grease, polycyclic aromatic hydrocarbons (PAH) and volatile organic compounds and similar toxic and/or carcinogenic pollutants, nitrogenous compounds, biological hazards and phenols are available in water and wastewater [15].

Phenolic compounds have significant effects on the environment and people health [16]. They are easily taken into the body by respiratory, oral and dermal routes. Phenol and phenol forms are contained in products such as nylon, epoxy resins, surfactants, synthetic detergents, plasticizers, antioxidants, phenolic resins, cyclohexanol, aspirin, dyes, wood preservatives, drugs, fungicides, gasoline additive, inhibitors, explosives and pesticides. Phenol causes excessive irritation and corrosion if it comes into contact with the skin and other tissues. Absorption of phenol can cause cyanosis, shock, weakness, liver and kidney damage, coma and death [17, 18].

The industry wastewaters are one of the sources of industrial phenolic pollutants. There are wastewaters containing high amounts of phenol in the world and in Turkey. These are mainly found in iron and steel factories, coke ovens, petrochemical facilities, pharmaceutical factories, socks factories, plastic factories, paper industry, photographic industry, explosive industry, paint, pharmaceutical and resin production facilities [19, 20].

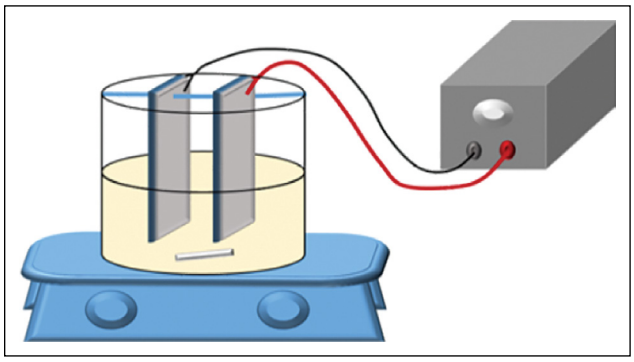

Figure 1. Schematic representation of EC in the laboratory.

Besides phenol which is a common research pollutant model, 4-chlorophenol (4-CP) is a highly toxic chemical compound which is difficult to degrade and is commonly found in industrial wastewater. Because of these properties, 4-CP was chosen as the target pollutant for this study. The treatment of it by EC was investigated. Here, the effects of operational parameters that significantly affect the EC process such as initial pH, current density and electrolysis time on 4-CP removal efficiency in a reactor using monopolar parallel connected copper electrodes were investigated.

EXPERIMENT

Material and Methods

Stock solutions of 4-CP were prepared by dissolving 1 g of analytical reagent grade (Merck, Germany) in 1 L of distilled water without pH adjustment. Experiments were conducted on 4-CP solutions with 50 mg/L concentration prepared during the experiment. 2 mg/L NaCl was added to increase the ionic strength of the solution. Each run volume was 250 ml. In Figure 1, a schematic representation of the laboratory scale system used in the EC process is given. The EC reactor, made of Plexiglas, has a diameter of 19 cm and a height of 15 cm. In the study, the copper plate electrodes were used on the anode and cathode (6 cm wide, 11 cm high and 0.2 cm wall thickness) and the distance between the electrodes was 2 cm. The total effective electrode areas were determined as 24 cm^2. The reactor was supplied with a direct current power supply. A homogeneous mixture of the solution was provided by means of a magnetic stirrer at 150 rpm. The electrodes were washed 2 times before each run. After run was completed, samples were waited for a 1-hour settling period. Supernatants of samples were collected and the remaining 4-CP concentration was determined according to the Direct photometric method (Standard Methods 5530-D) [21]. The method

Table 1. Experiment design input and factors

Factors	Factor	-1	0	1
Initial pH	X_1	4	7	10
Exposure time (min)	X_2	5	25	45
Current density (mA/cm²)	X_3	10	42	74

based on the spectrophotometric analysis of the developed color resulting from the reaction of 4-CP with 4-aminoantipyrine. The absorbance of colored samples was measured at 500 nm by the Hach UV/Vis DR5000 spectrophotometer after 15 min of reaction. To find the 4-CP concentration, 11 standard solutions (0.5, 1, 2, 3, 4, 5, 6, 7, 8, 9, 10 mg/L) were prepared and a calibration curve was drawn. After the analysis, the absorbances of 4-CP were read by spectrophotometer and put in the calibration equation. Afterwards, the 4-CP concentrations were calculated. 4-CP removal efficiency were obtained using equation 1.

$$R\% = \frac{100(C_0 - C_1)}{C_0} \quad (1)$$

where C_0 and C_1 are initial and final concentration, respectively.

Experimental Study and System Design

4-CP removal by EC process was optimized using the Response-Surface Method (RSM). The current density, exposure time and pH affecting the EC process were optimized using RSM. The Box-Behnken design model included in Minitab 17 (Trial version) software is used to determine the individual and combined effects of operating parameters on pollutant removal efficiency. In this study, experiments for 4-CP removal were designed by the Box-Behnken design. As shown in Table 1, the three-factor Box-Behnken response surface was used in the optimization and investigation of the process variables, namely initial pH (4–10), exposure time (5–45 mins), current density (10–74 mA/cm²). With the runs created in the program, 15 batch EC processes were conducted and the effects of initial pH (X_1), current density (X_2) and exposure time (X_3) changes on 4-CP removal efficiency were determined. Depending on the responses, the relationships between the criteria affecting the removal efficiency were determined.

The effects of the selected independent variables and their interactions on responses according to BBD were described using the second order polynomial equation 2.

$$Y_i = \beta_0 + \sum_{i}^{k} \beta_i x_i + \sum_{i=1}^{k} \sum_{j \geq i}^{k} \beta_{ij} x_i x_j + c \quad (2)$$

where β_0 , β_i , β_{ii}, and β_{ij} are constant, linear, quadratic, and cross-factor interaction coefficients, respectively; X_i and X_j represent the independent variables; Y_i is the predicted response; and k and C are the number of factors and the residual terms, respectively [22].

Table 2. Experimental results

Run order	pH	Current density (mA/cm²)	Exposure time (min)	Efficiency (%)
1	4	10	25	1
2	10	10	25	7
3	4	74	25	44
4	10	74	25	73
5	4	42	5	1
6	10	42	5	4
7	4	42	45	83
8	10	42	45	41
9	7	10	5	1
10	7	74	5	1
11	7	10	45	11
12	7	74	45	81
13	7	42	25	44
14	7	42	25	50
15	7	42	25	48

RESULTS AND DISCUSSION

Response Analysis and Interpretation using BBD Three factors in the three-level Box-Behnken response surface design (BBD) is used to optimize and examine the effect of process variables. Table 1 shows the BBD matrix of the independent variables and the response values. Then, the experimental results for 4-CP removal efficiency (Table 2) were entered to software Minitab 17 (trial version). The calculated response functions correspond to the experimental data for Y (Efficiency) R^2=92.51.

Regression Equation in Uncoded Units

$$Y=-58{,}7+7{,}2\ X_1+0{,}624\ X_2+2{,}94\ X_3-0{,}366\ X_1{*}X_1-0{,}01215\ X_2{*}X_2-0{,}0290\ X_3{*}X_3+0{,}0591\ X_1{*}X_2-0{,}189\ X_1{*}X_3+0{,}0273\ X_2{*}X_3 \quad (3)$$

The adequacy of the quadratic model and the quality of the correlation between parameters and responses were examined by analysis of variance (ANOVA) at 95% confidence interval (CI). For a term to be meaningful in ANOVA, its p-value must be less than 0.05. The p-value is used as a tool to check the significance of each factor [23]. The ANOVA table of the factors is given in Table 3. When the Table 3a, b is examined, it is seen that the factors that have the greatest effect on 4-CP removal, exposure time and current density factors have a linear effect, and the p-values are 0.007 and 0.003. However, the p-value of the pH is 0.935 and it does not have a significant effect.

Generally, the coefficient of determination (R-square-adj) explains the total variability taken into account by the independent variables in the regression model. In

Table 3a. ANOVA table for 4-CP removal (analysis of variance)

	Analysis of variance				
Source	**DF**	**Adj SS**	**Adj MS**	**F-value**	**P-value**
Model	9	12443.7	1382.63	6.87	0.024
Linear	3	9575.7	3191.91	15.85	0.005
X1	1	1.5	1.46	0.01	0.935
X2	1	4027.4	4027.42	20	0.007
X3	1	5546.8	5546.85	27.55	0.003
Square	3	999.8	333.27	1.66	0.29
X1*X1	1	40	40	0.2	0.674
X2*X2	1	571.1	571.14	2.84	0.153
X3*X3	1	495.4	495.37	2.46	0.178
2-way interaction	3	1868.1	622.71	3.09	0.128
X1*X2	1	129	128.98	0.64	0.46
X1*X3	1	515.9	515.91	2.56	0.17
X2*X3	1	1223.2	1223.24	6.07	0.057
Error	5	1006.8	201.36		
Lack-of-fit	3	986.9	328.95	32.96	0.03
Pure error	2	20	9.98		
Total	14	13450.5			

Table 3b. ANOVA table for 4-CP removal (continued-coded coefficients)

	Coded coefficients					
Term	**Effect**	**Coef**	**SE coef**	**T-value**	**P-value**	**VIF**
Constant		47.14	8.19	5.75	0.002	
X1	-0.85	-0.43	5.02	-0.09	0.935	1
X2	44.87	22.44	5.02	4.47	0.007	1
X3	52.66	26.33	5.02	5.25	0.003	1
X1*X1	-6.58	-3.29	7.38	-0.45	0.674	1,01
X2*X2	-24.87	-12.44	7.38	-1.68	0.153	1,01
X3*X3	-23.17	-11.58	7.38	-1.57	0.178	1,01
X1*X2	11.36	5.68	7.1	0.8	0.46	1
X1*X3	-22.71	-11.36	7.1	-1.6	0.17	1

Table 3c. ANOVA table for 4-CP removal (continued-model summary)

	Model summary		
S	**R-sq**	**R-sq(adj)**	**R-sq(pred)**
14,1902	92.51%	79.04%	0.00%

this model, the Adj. R^2 sufficient to explain the variability were found to be 79.04% (Tablo 3c).

The residuals are the differences between the observed and the predicted values of the data. It is a diagnostic measure used when evaluating the quality of a model, is known as errors. Residues are important when determining the quality of a model. The residuals are normally distributed. Figure 2 is shown residual plots. The normal probability plot shows

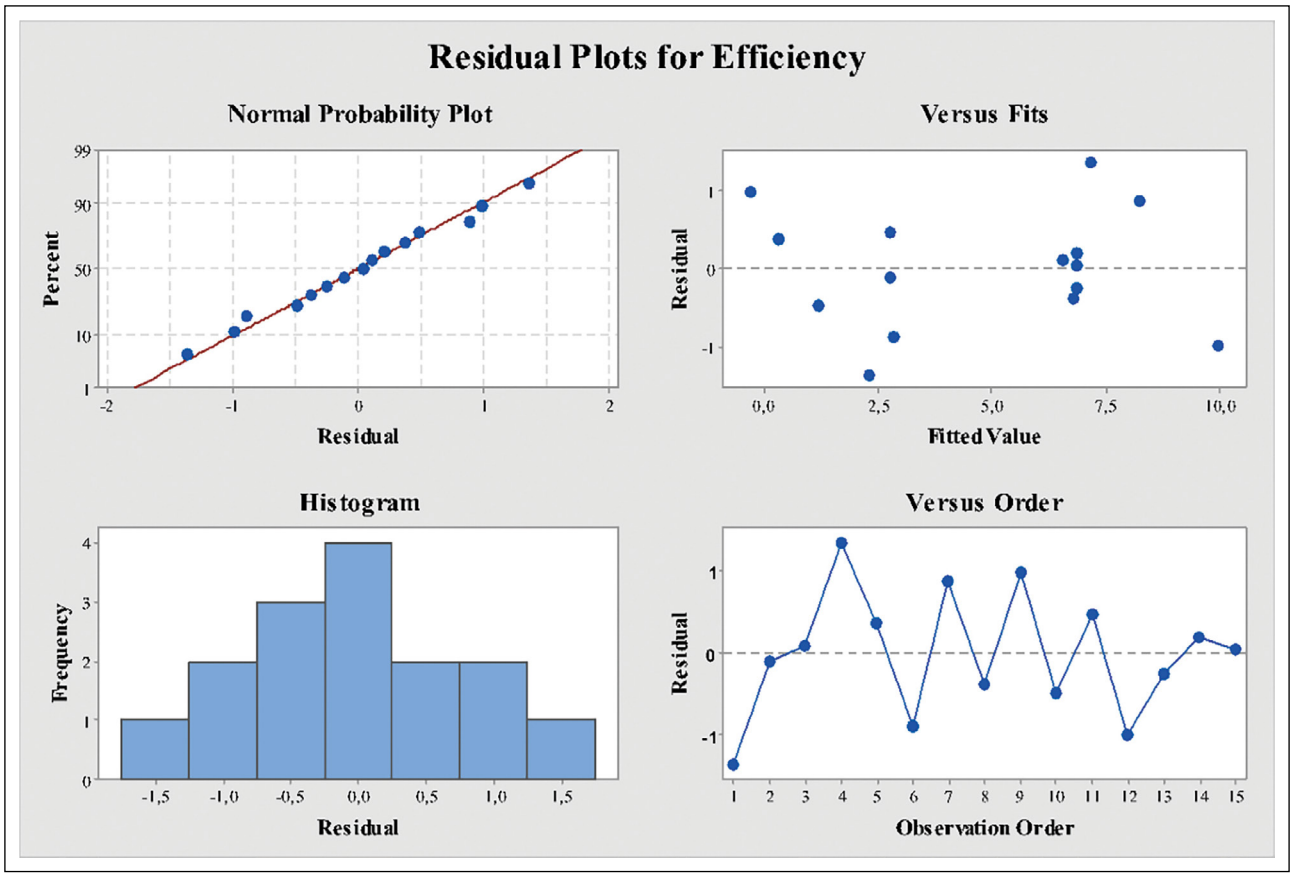

Figure 2. Residual plots for efficiency.

that the data are normally distributed and that variables affect the response. In this model, outliers were not found in the data. The fitted values against the residual values show that the variance is constant and there is a non-linear relationship. The histogram proves that the data is not skewed and that there are no outliers. Residuals by order of data indicate systematic effects on data due to time or order of data collection.

Effects of Operating Parameters

4-CP was removed from the water by floc formation due to oxidation of the anode. This was a three-step process with oxidation of the anode, adsorption/replacement of contaminants, and precipitation of aggregated mass of coagulant with 4-CP. During the initial processing, the anode material changed from coagulant to its hydroxides (insoluble in water). In the second step, 4-CP was adsorbed on the coagulant surface. In the third step, the flocs are precipitated and then removed from the water by filtration. Experiments were conducted at pH 4.0–10.0, under both acidic and alkaline conditions. 4-CP removal was observed in both acidic and basic environments, confirming the hydroxide formation in both cases. The electrochemical reactions of hydroxide formation for copper electrodes are shown below.

Reactions occurring on copper electrodes [24].

Anodic electrochemical dissolution:

$$Cu_{(s)} \rightarrow Cu^{2+}_{(aq)} + 2e^{-} \quad (4)$$

Oxidation of copper ions:

$$Cu^{2+}_{(aq)} + 2H^{+}_{(aq)} + \frac{1}{4}O_{2(g)} \rightarrow Cu^{2+}_{(aq)} + \frac{1}{2}H_2O(I) \quad (5)$$

The hydrolysis reaction:

$$Cu^{2+}_{(aq)} + 2H_2O(I) \rightarrow Cu(OH)_{2(s)} + 2H^{+}_{(aq)} \quad (6)$$

The cathodic electrochemical reaction:

$$2H^{+}_{(aq)} + 2e^{-} \rightarrow H_{2(g)} \quad (7)$$

Overall reaction:

$$2Cu_{(s)} + 3H_2O(I) + \frac{1}{2}O_{2(g)} \rightarrow 2Cu(OH)_{2(s)} + H_{2(g)} \quad (8)$$

The Cu^{2+} and Cu^{3+} ions hydrate and hydrolyses to form monomeric and polymeric species: $Cu(OH)_2^{+}$, $CuOH^{2+}$, $Cu_2(OH)_2^{4+}$, $Cu(OH)_4^{-}$, $Cu(H_2O)_2^{+}$, $Cu(H_2O)_5OH^{2+}$, $Cu(H_2O)_4(OH)_2^{+}$ etc. [25].

Electrical conductivity in metals is a result of the movement of electrically charged particles. Atoms of metal elements are characterized by the presence of valence electrons. It is 'free electrons' that allow metals to conduct an electric current. Copper has high conductivity (6.30×10^7 S/m at 20°C) and less resistivity (1.59×10^{-8} Ω m at 20°C). °C). Energy transfer is strong when there is little resistance. For this reason, it was effective in the removal of 4-CP.

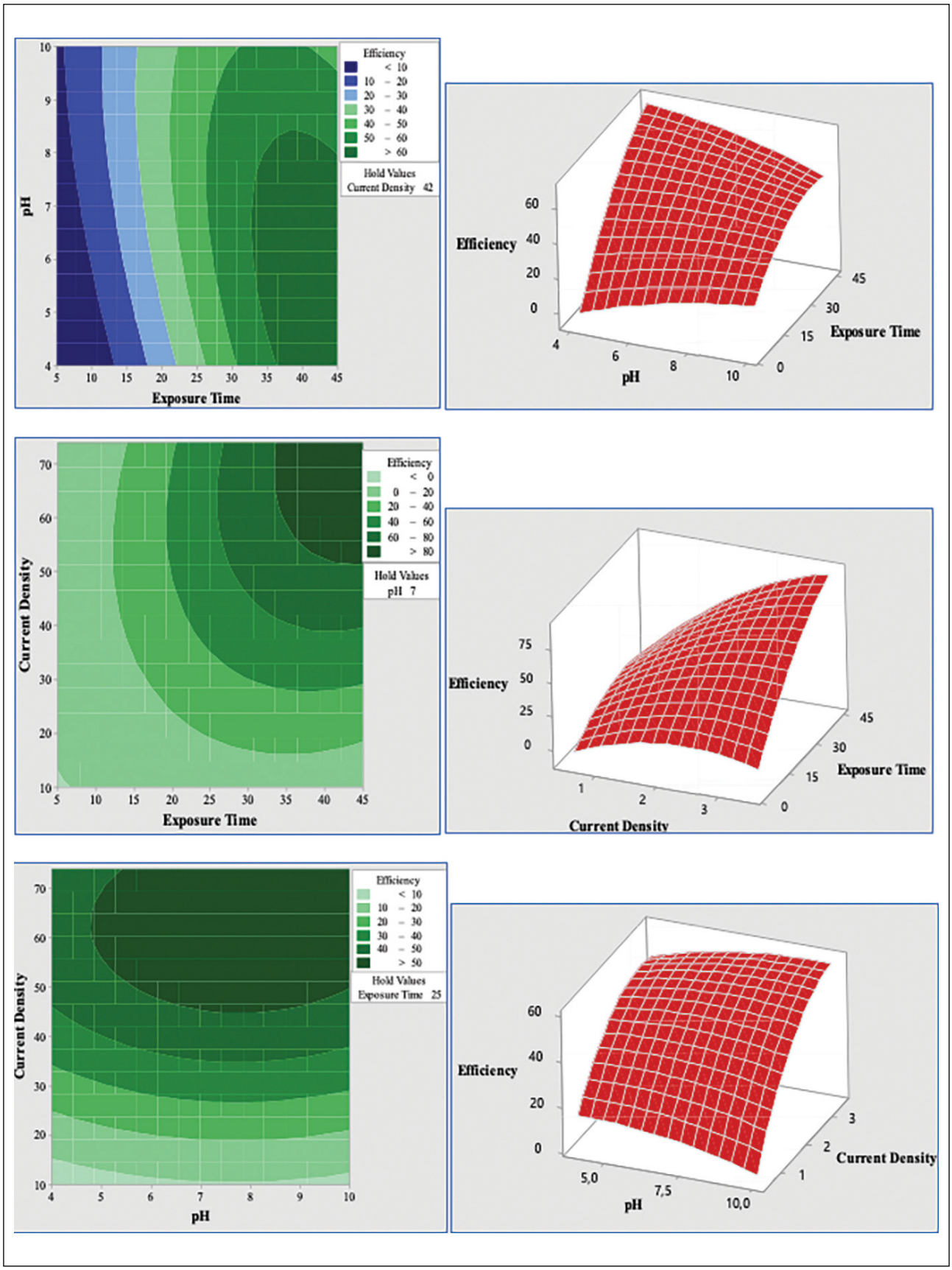

Figure 3. Contour plots and 3D plots.

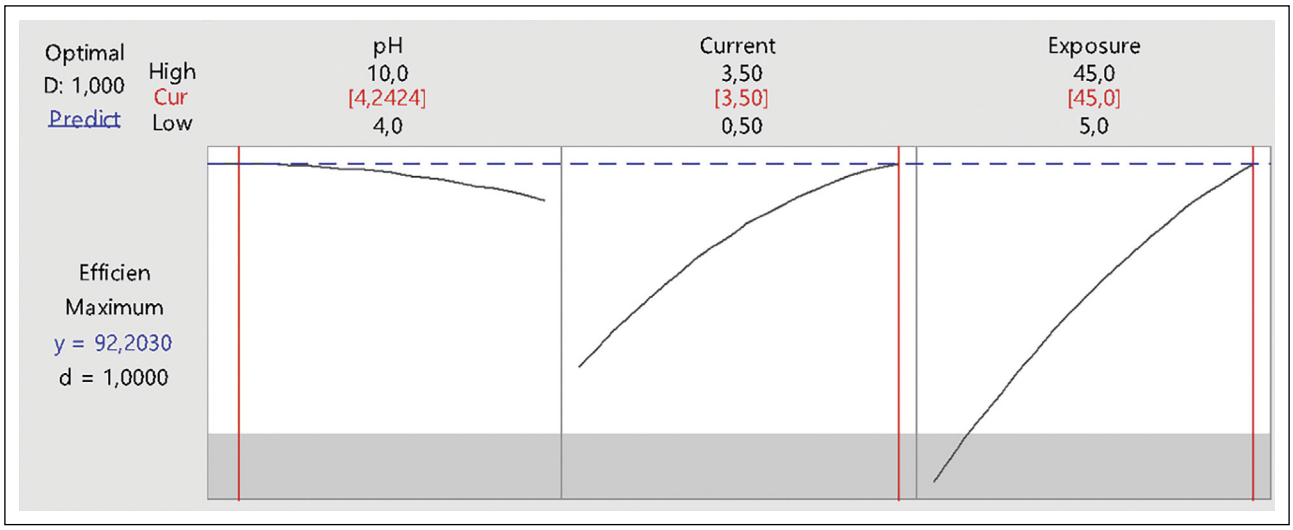

Figure 4. Process optimization for 4-CP removal.

The pH of the EC process is one of the most fundamental factors for controlling the removal of contaminants [26, 27]. To examine the pH effect in the EC, experiments were conducted at various pH values covering acidic, neutral and basic conditions (range 4–10 pH). Maximum 4-CP removal occurred at pH 4–7. The applied current density, on the other hand, directly affects the coagulant dosage rate and bubble generation rate, the current density, which determines the size and growth of the flocs, and affects the removal efficiency of any electrochemical process [28]. Considering the results in Table 2, the increase in the applied current density increased the 4-CP removal, too. The current density produced divalent ion Cu^{2+} and removed it by reacting with 4-CP. Applying the current density for a long time provided ion increase and increased the removal efficiency. 4-CP removal efficiency was 44% in Run 12, while it was 83% in Run 13. After the 25th minute of the exposure time, there was an increase in the removal efficiency.

The combined effects of these 3 factors affecting the EC process were evaluated. For this, the Contour Graph in RSM was used to examine the relationship between a response variable and two predictive variables. In a contour plot, the values of the two predictive variables are represented on the x and y axes, and the values of the response variable are represented by darksome regions called contours. In this study, two-dimensional (2D) contour graphs were drawn representing the interaction effects of pH-Current density, pH-Exposure Time and Current Density-Exposure time on 4-CP removal efficiencies.

In the graphs (Fig. 3), the darker regions show the high removal efficiency achieved by the interaction of the two factors pH and current density. When the contour graph is examined, it is seen that the current density partially interacts with pH and affects the removal efficiency. However, exposure time and current density significantly interact with each other. With the increase of theirs, it was increased to release of copper ions. Thus, easier precipitation of pollutants is ensured and 4-CP removal efficiency is increased. It is indisputable that current density and exposure time greatly affect 4-CP removal with copper electrodes.

Exposure time is one of the most important parameters in the EC. In the EC process, the sufficient time is required for the copper electrodes to dissolve, produce hydroxide, and complete the coagulation. It is seen that the removal efficiency increases with the increase in the study time. This trend can be explained by the greater current supplied to the electrodes, resulting in a greater dosage of coagulant into the water [29].

BBD Optimization

The model was finalized with the multi-response numerical optimization technique. According to the BBD results in Figure 4, the maximum 4-CP removal efficiency was obtained under the following operating conditions at a pH of 4.24, an exposure time of 45 min, and a current density of 74 mA/cm^2. Under these optimal conditions, the 4-CP removal efficiency was 92.20%. It can easily be deduced from this graph that while current density and exposure time have a positive effect, pH removal has not much effect.

As can be seen in Table 4, phenol types removal from real and synthetic wastewater were investigated. The phenol removal efficiencies vary between 100% and 59%. The electrodes used such as aluminum, iron, zinc, steel and metals enriched with different substances. In this study, 4-CP removal was demonstrated using monopolar parallel connected copper electrodes. With the study, approximately 92% phenol removal was achieved. In this study, better efficiency was obtained than many studies in the literature. However, it will be more important to work with real wastewater and achieve the same efficiency in the field.

Table 4. Some studies in literature about removal of phenol types from wastewaters

Wastewater type	Treatment technology	% Phenol removal efficiency	Initial [phenol] (mg L^{-1})	Reference
Phenol wastewater	Persulfate enhanced electrochemical oxidation [EC/PS oxidation ($CuFe_2O_4$/ACF cathode and RuO_2/Ti anode, adding PS)]	97	500	[30]
High salinity waters	Electrochemical advanced oxidation	>70	50	[31]
Synthetic phenol solution	Ti/Pt and MMO (Mixed Metal Oxide) electrodes	84	0.5	[32]
Pistachio processing wastewater (PPW)	The combined electrochemical-assisted fungal treatment process	88.7	3205	[33]
Synthetic phenol solution	Electrochemical filtration carbon membrane (ECM)	91.65	50	[34]
Synthetic phenol solution	Bioelectrochemical Technologies [oxygen-diffused microbial electrochemical systems (MESs)]	59	200	[35]
The simulated and the real wastewater (olive mill)	EC (Zn anode/stainless steel cathode)	84.2–72.3	327–740	[36]
Real refinery wastewater	EC (Al electrode)	100	3	[18]
Synthetic phenol solution	EC (Al and Fe electrode)	94.72–98	5	[37]
Petroleum refinery wastewater	electrochemical oxidation by using boron doped diamond anode (BDD)	98.74	192.9	[29]
Paper mill effluents	EC (Al and Fe electrode)	98–93	0.535	[38]
Synthetic phenol solution	Electrochemical oxidation (ruthenium mixed metal oxide electrode)	99.7	200	[39]
Olive mill wastewater (OMW)	EC (Al electrode)	91	2420	[40]
Synthetic 4-chlorophenol solution	Biochar-load particle electrodes	99.93	500	[41]
Synthetic 4-chlorophenol solution	Two Pd/graphene gas-diffusion cathodes and one Ti/IrO2/RuO2 anode	94.9%	–	[42]
Paper industry wastewater (4-chlorophenol)	Al electrode	100%	0.28	[43]
Paper mill waste water (4-chlorophenol)	Stainless steel (316 L) electrode	99.4%	0.56	[44]
Synthetic phenol solution	EC	92	50	This study

Besides EC, other treatment methods are used efficiently in 4-CP removal [45, 46]. For example, 4-CP removal performances were investigated by synthesizing different carbon adsorbents and 4-CP absorbability was observed as 90% [47]. In a different study, it was proven that 4-CP can be removed 40% from the solution by using composite TiO2 material [48]. Also, over 80% 4-CP removal was achieved with magnetic activated carbon [49]. It is observed from this study that the removal of 4-CP is effective with 92%.

CONCLUSION

In this study, the effect of initial pH, current density and electrolysis time on 4-CP removal efficiency in a reactor using parallel connected copper electrodes was investigated. In the optimization study using the RSM, the maximum phenol removal was found as a function of the current density, reaction time and initial pH value affecting the EC process. The ANOVA results showed the fit of the second-order regression with the experimental data. As a result of this study, it has been determined and optimized that 4-CP is effectively removed from the wastewater with the copper electrodes.

DATA AVAILABILITY STATEMENT

The authors confirm that the data that supports the findings of this study are available within the article. Raw data that support the finding of this study are available from the corresponding author, upon reasonable request.

CONFLICT OF INTEREST

The authors declared no potential conflicts of interest with respect to the research, authorship, and/or publication of this article.

ETHICS

There are no ethical issues with the publication of this manuscript.

REFERENCES

[1] R.Ş. Taşdemir and İ. Koyuncu, "Alternative water supply with membrane technologies: desalination and wastewater recover," Sürdürülebilir Çevre Dergisi, Vol. 1, pp. 18–30.

[2] İ. Koyuncu, "Su/Atıksu Arıtılması ve Geri Kazanılmasında Membran Teknolojileri ve Uygulamaları," Türkiye Çevre Koruma Vakfı, Vol. 1, 2018.

[3] F. Özyonar and B. Karagözoğlu, "Treatment of textile wastewater by electrocoagulation process," Erciyes University Journal of the Institute of Science and Technology, Vol. 28, pp. 29–37, 2012.

[4] M.J. Iskandar, A. Baharum, F.H. Anuar, and R. Othaman, "Palm oil industry in South East Asia and the effluent treatment technology—A review," Environmental Technology & Innovation, Vol. 9, pp. 169–185, 2018. [CrossRef]

[5] F. Sher, A. Malik, and H. Liu, "Industrial polymer effluent treatment by chemical coagulation and flocculation," Journal of Environmental Chemical Engineering, Vol. 1, pp. 684–689, 2013. [CrossRef]

[6] J.M. Dickhout, J. Moreno, P.M. Biesheuvel, L. Boels, R.G.H. Lammertink, and W.M. De Vos, "Produced water treatment by membranes: a review from a colloidal perspective," Journal of Colloid and Interface Science, Vol. 487, pp. 523–534, 2017. [CrossRef]

[7] M.K. Amosa, M.S. Jami, M.F.R. Alkhatib, and T. Majozi, "Studies on pore blocking mechanism and technical feasibility of a hybrid PAC-MF process for reclamation of irrigation water from biotreated POME," Separation Science and Technology, Vol. 51, pp. 2047–2061, 2016. [CrossRef]

[8] G. Boczkaj and A. Fernandes, "Wastewater treatment by means of advanced oxidation processes at basic pH conditions: a review," Chemical Engineering Journal, Vol. 320, pp. 608–633, 2017. [CrossRef]

[9] Y.G. Asfaha, A.K. Tekile, and F. Zewge, "Hybrid process of electrocoagulation and electrooxidation system for wastewater treatment: A review," Cleaner Engineering and Technology, Vol. 4, pp. 100261, 2021. [CrossRef]

[10] Ş. Camcıoğlu, B. Ozyurt, and H. Hapoglu, "pH control of paper wastewater treated with electrocoagulation method," Anadolu University Journal of Science and Technology A- Applied Sciences and Engineering, Vol. 16, pp. 107–115, 2015. (in Turkish). [CrossRef]

[11] C. Cameselle, M. Pazos, and M.A. Sanromán, "Selection of an electrolyte to enhance the electrochemical decolourisation of indigo. Optimisation and scale-up," Chemosphere, Vol. 60, pp. 1080–1086, 2005. [CrossRef]

[12] M.Y.A. Mollah, R. Schennach, J.R. Parga, and D.L. Cocke, "Electrocoagulation (EC)—science and applications," Journal of Hazardous Materials, Vol. 84, pp. 29–41, 2001. [CrossRef]

[13] I. Kabdaşlı, A. Keleş, T. Ölmez-Hancı, O. Tünay, and I. Arslan-Alaton, "Treatment of phthalic acid esters by electrocoagulation with stainless steel electrodes using dimethyl phthalate as a model compound," Journal of Hazardous Materials, Vol. 171, pp. 932–940, 2009. [CrossRef]

[14] M. Bayramoglu, M. Eyvaz, and M. Kobya, "Treatment of the textile wastewater by electrocoagulation: economical evaluation," Chemical Engineering Journal, Vol. 128, , pp. 155–161, 2007. [CrossRef]

[15] B. Coşkun, T.Ö. Hanci, I. Kabdaşli, and O. Tünay, "Treatment of endocrine distrupter dimethyl phthalate by electrocoagulation/Fenton processes," Su Kirlenmesi Kontrolü Dergisi, Vol. 21, pp. 3–12, 2012. (in Turkish)

[16] M. Moradnia, M. Noorisepehr, M. Salari, and M. Darvishmotevalli, "Optimization of 2-chlorophenol removal using ultrasound/persulfate: prediction by rsm method, biodegradability improvement of petrochemical refinery wastewater," Arabian Journal for Science and Engineering, pp. 1–9, 2021. [CrossRef]

[17] J.F. Lewin, and W.T. Cleary, "An accidental death caused by the absorption of phenol through skin. A case report," Forensic Science International, Vol. 19, pp. 177–179, 1982. [CrossRef]

[18] E.S.Z. El-Ashtoukhy, Y.A.El-Taweel, O. Abdelwahab, and E.M. Nassef, "Treatment of petrochemical wastewater containing phenolic compounds by electrocoagulation using a fixed bed electrochemical reactor," International Journal of Electrochemical Science, Vol. 8, pp. 1534–1550, 2013.

[19] H. Çiçek, "The use of beet pulp carbon for the removal of the phenol from aqueous waste solution," Unpublished Master Thesis, Fırat University Graduate School of Natural and Applied Sciences, 2005. (in Turkish)

[20] D. Gümüş, "Elektrokimyasal oksidasyon yöntemi ile fenol ve 4-klorofenol giderimi." Yayınlanmamış Yüksek Lisans Tezi, Ondokuz Mayıs Üniversitesi, Fen Bilimleri Enstitüsü, 2007. (in Turkish)

[21] APHA, "Standard methods for the examination of water and wastewater", APHA American Public Health Association, 1981.

[22] J.P. Maran, V. Sivakumar, K. Thirugnanasambandham, and R. Sridhar, "Artificial neural network and response surface methodology modeling in mass transfer parameters predictions during osmotic dehydration of Carica papaya L.," Alexandria Engineering Journal, Vol. 52, pp. 507–516, 2013. [CrossRef]

[23] S. Jang, A.Y. Lee, A.R. Lee, G. Choi, and H.K. Kim, "Optimization of ultrasound-assisted extraction of

glycyrrhizic acid from licorice using response surface methodology," Integrative Medicine Research, Vol. 6, pp. 388–394, 2017. [CrossRef]

[24] A.K. Prajapati and P.K. Chaudhari, "Physicochemical treatment of distillery wastewater—a review," Chemical Engineering Communications, Vol. 202, pp. 1098–1117, 2015. [CrossRef]

[25] O. Sahu, B. Mazumdar, and P.K. Chaudhari, "Treatment of wastewater by electrocoagulation: a review," Environmental Science and Pollution Research, Vol. 21, pp. 2397–2413, 2014. [CrossRef]

[26] M. Kobya, O.T. Can, and M. Bayramoglu, "Treatment of textile wastewaters by electrocoagulation using iron and aluminum electrodes," Journal of Hazardous Materials, Vol. 100, pp. 163–178, 2003. [CrossRef]

[27] N. Daneshvar, H. Ashassi-Sorkhabi, and A. Tizpar, "Decolorization of orange II by electrocoagulation method," Separation and Purification Technology, Vol. 31, pp. 153–162, 2003. [CrossRef]

[28] M. Kobya, U. Gebologlu, F. Ulu, S. Oncel, and E. Demirbas, "Removal of arsenic from drinking water by the electrocoagulation using Fe and Al electrodes," Electrochimica Acta, Vol. 56, pp. 5060–5070, 2011. [CrossRef]

[29] Y. Yavuz, A.S. Koparal, and Ü.B. Öğütveren, "Treatment of petroleum refinery wastewater by electrochemical methods," Desalination, Vol. 258, pp. 201–205, 2010. [CrossRef]

[30] S. Tian, Y. Tu, J. Chen, G. Shao, Z. Zhou, and Z. Ren, "Persulfate enhanced electrochemical oxidation of phenol with CuFe2O4/ACF (activated carbon fibers) cathode," Separation and Purification Technology, Vol. 279, pp. 119727, 2021. [CrossRef]

[31] B.S. Tawabini, K.V Plakas, M. Fraim, E. Safi, T. Oyehan, and A.J. Karabelas, "Assessing the efficiency of a pilot-scale GDE/BDD electrochemical system in removing phenol from high salinity waters," Chemosphere, vol. 239, pp. 124714, 2020. [CrossRef]

[32] O.T. Can, "Electrooxidation of phenol solution using several electrodes," BEU Journal of Science, Vol. 9, pp. 952–957, 2020. (in Turkish)

[33] Z. Isik, E.B. Arikan, Y. Ozay, H.D. Bouras, and N. Dizge, "Electrocoagulation and electrooxidation pre-treatment effect on fungal treatment of pistachio processing wastewater," Chemosphere, vol. 244, pp. 125383, 2020. [CrossRef]

[34] Z. Pan, F. Yu, L. Li, M. Liu, C. Song, J. Yang, and T. Wang, "Electrochemical filtration carbon membrane derived from coal for wastewater treatment: Insights into the evolution of electrical conductivity and electrochemical performance during carbonization," Separation and Purification Technology, Vol. 247, pp. 116948, 2020. [CrossRef]

[35] L. Zhou, X. Yan, Y. Yan, T. Li, J. An, C. Liao, and X.L. Wang, "Electrode potential regulates phenol degradation pathways in oxygen-diffused microbial electrochemical system," Chemical Engineering Journal, Vol. 381, pp. 122663, 2020. [CrossRef]

[36] A.S. Fajardo, R.F. Rodrigues, R.C. Martins, L.M. Castro, and R.M. Quinta-Ferreira, "Phenolic wastewaters treatment by electrocoagulation process using Zn anode," Chemical Engineering Journal, Vol. 275, pp. 331–341, 2015. [CrossRef]

[37] E. Bazrafshan, H. Biglari, and A.H. Mahvi, "Phenol removal by electrocoagulation process from aqueous solutions," Fresenius Environ. Bull., vol. 21, no. 2, pp. 364–371, 2012.

[38] M. Uğurlu, A. Gürses, Ç. Doğar, and M. Yalçın, "The removal of lignin and phenol from paper mill effluents by electrocoagulation," Journal of Environmental Economics and Management, Vol. 87, pp. 420–428, 2008. [CrossRef]

[39] Y. Yavuz and A.S. Koparal, "Electrochemical oxidation of phenol in a parallel plate reactor using ruthenium mixed metal oxide electrode," Journal of Hazardous Materials, Vol. 136, pp. 296–302, 2006. [CrossRef]

[40] N. Adhoum and L. Monser, "Decolourization and removal of phenolic compounds from olive mill wastewater by electrocoagulation," Chemical Engineering and Processing: Process Intensification, Vol. 43, pp. 1281–1287, 2004. [CrossRef]

[41] S. Xie, M. Li, Y. Liao, Q. Qin, S. Sun, and Y. Tan, "In-situ preparation of biochar-loaded particle electrode and its application in the electrochemical degradation of 4-chlorophenol in wastewater," Chemosphere, Vol. 273, pp. 128506, 2021. [CrossRef]

[42] Q. Shi, H. Wang, S. Liu, Q. Luo, and Z. Bian, "Optimization of a three-electrode system for electrochemical reduction–oxidation of 4-chlorophenol with response surface methodology," Toxicology Environmental Chemistry, Vol. 98, pp. 327–344, 2016. [CrossRef]

[43] D. Kumar and C. Sharma, "Reduction of chlorophenols and sludge management from paper industry wastewater using electrocoagulation process," Separation Science and Technology, Vol. 55(15), pp. 2844–2854, 2020. [CrossRef]

[44] R. Sharma, S. Kumar, and C. Sharma, "Estimation and removal of chlorophenolic compounds from paper mill waste water by electrochemical treatment," International Journal of Chemical and Molecular Engineering, Vol. 10(6), pp. 772–776, 2016.

[45] A.O. Olaniran and E.O. Igbinosa, "Chlorophenols and other related derivatives of environmental concern: properties, distribution and microbial degradation processes," Chemosphere, Vol. 83(10), pp.

1297–1306, 2011. [CrossRef]

[46] A. Kuleyin, "Removal of phenol and 4-chlorophenol by surfactant-modified natural zeolite," Journal of Hazardous Materials, Vol. 144(1–2), pp. 307–315, 2007. [CrossRef]

[47] S. Madannejad, A. Rashidi, S. Sadeghhassani, F. Shemirani, and E. Ghasemy, "Removal of 4-chlorophenol from water using different carbon nanostructures: a comparison study," Journal of Molecular Liquids, Vol. 249, pp. 877–885, 2018. [CrossRef]

[48] S. Silvestri, T.A.L. Burgo, C. Dias-Ferreira, J.A. Labrincha, and D.M. Tobaldi, "Polypyrrole-TiO2 composite for removal of 4-chlorophenol and diclofenac," Reactive Function Polymers Vol. 146, pp. 104401, 2020. [CrossRef]

[49] Z. Duan, W. Zhang, M. Lu, Z. Shao, W. Huang, J. Li, Y. Li, and C. Chen, "Magnetic Fe3O4/activated carbon for combined adsorption and Fenton oxidation of 4-chlorophenol," Carbon N. Y., Vol. 167, pp. 351–363, 2020. [CrossRef]

Environ Res Tec, Vol. 5, Issue. 1, pp. 44–49, March 2022

Environmental Research and Technology
https://ert.yildiz.edu.tr - https://dergipark.org.tr/tr/pub/ert
DOI: https://doi.org/10.35208/ert.1013350

Environmental Research & Technology

Research Article

Life cycle comparison of passenger air and rail transportation

Levent BİLGİLİ[1], Afsin Y. CETİNKAYA[2], S. Levent KUZU[*2]

[1]Department of Naval Architecture and Marine Engineering, Bandırma Onyedi Eylül University, Balıkesir, Türkiye
[2]Department of Environmental Engineering, Yıldız Technical University Faculty of Civil Engineering, İstanbul, Türkiye

ARTICLE INFO

Article history
Received: 22 October 2021
Revised: 22 December 2021
Accepted: 04 January 2022

Key words:
Air transportation; Rail transportation; Life cycle assessment; Social costs

ABSTRACT

Air transportation has an undisputed speed advantage among all other modes. On the other hand, it is known that the environmental metrics of aviation is quite unsatisfactory compared to other transportation types due to its fuel characteristics and the amount of consumed fuel. However, it would be a wrong choice to rely solely on operational processes to make a true comparison. For this reason, a Life Cycle Assessment (LCA) model should be generated by taking into account processes such as production except the operation process and the calculations should be performed with a comprehensive and holistic perspective. In this study, the environmental impacts of air and rail transport types are compared from the life cycle perspective. For this purpose, first, the emissions in the case of one passenger per one km (pkm) transportation by air and rail were calculated. Then, taking into account the production and disposal processes of the aircraft and passenger trains, the LCA cycle was completed and total emissions were calculated. SimaPro version 9.0.0.49 package program and 1.09 version of ReCiPe 2008 method were used for LCA calculations. With the help of the program, emissions generated during both production and one pkm transportation processes of an aircraft, high-speed and normal train were estimated. Accordingly, the greenhouse gas produced one pkm in air transport was 126.8 g in terms of carbon dioxide equivalent (CO_{2eq}), while CO_{2eq} was 0.3 and 0.31 g for high-speed trains and regular trains, respectively. Considering the production processes, 2072.1, 28.72, and 19.07 t of greenhouse gases are produced, respectively for these three transportation modes.

Cite this article as: Levent Bilgili, Afsin Y. Cetinkaya, S. Levent Kuzu. Life cycle comparison of passenger air and rail transportation. Environ Res Tec 2022;5:1:44–49.

INTRODUCTION

In today's society, environmental aspects are important in the transportation sector. The society will presumably change their choice in the transport sector due to changes in the energy/environmental situation in the future [1]. Strategic decisions concerning the development of the transport sector must be based on solid facts concerning both the transport infrastructure and the operation. With the increase in CO_2 emissions, the effects of global warming and climate change, which have accelerated in recent years, have become more evident [2–4]. Understanding the importance of CO_2 provides a new perspective on the discussion of air and rail transport uses [5]. The two transportation modes differ among themselves in terms of supply chain, costs, and energy use. In the literature, each trans-

***Corresponding author.**
*E-mail address: skuzu@yildiz.edu.tr

portation mode was examined individually and has not been compared to any other transportation mode [6–8]. It is important to examine the passenger air and the rail transportation and to compare them with each other.

The LCA method is used to identify, report, and manage environmental impacts at different stages of the life cycle, starting with the acquisition of raw materials that are used in the production of a product or service, including all relevant production, shipment, use by the consumer and disposal as waste [9–12]. LCA evaluates the entire life cycle of a product or service and their connections with each other. As a result, any environmental impact that may arise in all processes from "cradle to grave" of the product or service being evaluated [13, 14]. The railway system represents one of the most resource-efficient answer to the ever-growing demand for transport service. Development trends for the following years project a substantial increase in this sector. Environmental effects caused by railway transport services have been rarely inspected systematically and existing studies focus on single typologies of environmental aspects, like energy consumption and air emissions [15, 16]. A wide summary of LCA based studies showing the transportation sector was provided by Andreoni et al. [17].

In today's world, the aviation industry is becoming more and more important. While it is important in terms of the benefits it creates, it also contributes especially to air pollution and global warming, a problem that the whole world needs to find a solution [18]. Significant contribution to atmospheric pollution was determined in Istanbul Atatürk Airport in Turkey [19]. Some parameters such as NO_X exceeded the air quality threshold value within airport area. The resources used in aviation sector activities directly affect the lives of living things, cause climate change, and create global externalities. The aircraft industry continues to grow as predicted, so reducing emissions is critical. Aviation is responsible for almost 12% of transport related global CO_2 emissions, having approximately 500 Mt annual CO_2 emission [20]. Global passenger and freight air transportation is expected to grow annually at 3–5% per year rate over the next decades [20].

Therefore, this study evaluates the environmental impacts of the railway and the airline transportation through a life cycle analysis, considering CO_2 emissions from both operations and infrastructure construction. A full LCA was conducted to compare modes of transport in terms of their environmental impact.

MATERIALS AND METHODS

LCA is a method that started to be developed about 50 years ago and is now widely used by many industries. LCA examines the environmental impact of a product or service (or, with widespread use, product system) in a holistic way.

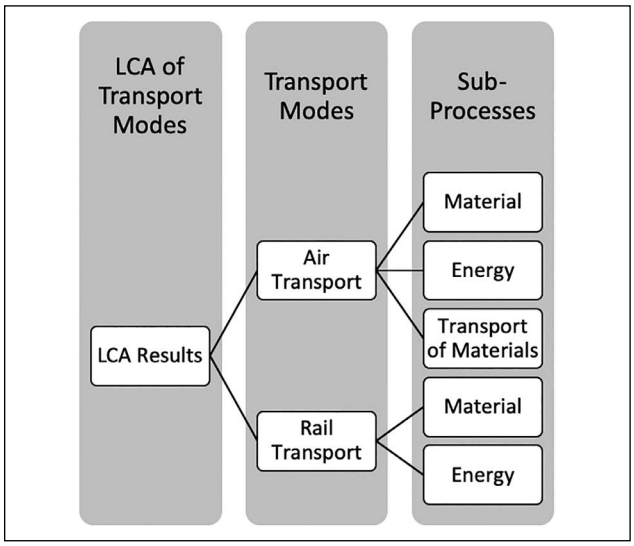

Figure 1. System boundaries.

Unlike traditional methods, the production, transportation, operation, maintenance, and disposal processes of a product system are simultaneously analysed and the results are correlated and then evaluated. This allows a comparison to be made as to which process has a better or worse environmental impact. In addition, thanks to the LCA, a wide variety of previously defined environmental impact categories can be calculated. LCA can also be used to estimate environmental costs [21]. There are many package programs available to make LCA calculations. There are also various methods in these programs. In this study, 9.0.0.49 version of SimaPro package program and 1.09 version of ReCiPe 2008 method were utilised.

In this study, LCA was chosen to make a comparison between product systems and has a holistic perspective on the environmental effects of the product system. The reason for choosing the ReCiPe 2008 method is that it offers up-to-date and comprehensive results. The emissions produced by air transport and regular and high-speed rail transport per 1 pkm, which means the transport of 1 passenger for 1 km, are calculated in this study.

In the calculations of the air transport, the production and operation data of 1 aircraft were used. In the production data; the material consumed during the production, energy and water, and the transportation of the materials by land and rail were considered. In the production data of high-speed and regular train; the production material, the amount of electrical energy and light oil used in production, and the disposal processes of the high-speed train were evaluated. Figure 1 presents the system boundaries for the upstream (manufacturing) processes.

Carbon dioxide (CO_2-biogenic and fossil), carbon monoxide (CO-biogenic and fossil), dinitrogen monoxide (N_2O), waste heat, methane (CH_4-biogenic and fossil), nitrogen

Table 1. Social cost factors (€/kg pollutant)

Pollutant type	Cost factor
CO_2	0.0566
CO	0.0958
N_2O	15
CH_4	1.75
NO_x	34.7
NMVOC	2.1
$PM_{2.5}$	79.5
SO_2	24.9

oxides (NO_x), non-methane volatile organic compounds (NMVOC), particulate matter ($PM_{2.5}$), sulphur dioxide (SO_2) and water vapour (H_2O) were calculated in the LCA. Of these gases, CO_2, N_2O, CH_4, and H_2O are the main contributors of global warming [22]. There are findings that waste heat and $PM_{2.5}$ may contribute to global warming [23–27]. In addition, NO_x, $PM_{2.5}$ and CO have adverse effects on human health and the environment [28]. Unlike the others, CO_2, CO, and CH_4 emissions were examined under both biogenic and fossil emission headings. Biogenic emissions are defined as part of the carbon cycle. Therefore, the net value of biogenic emissions is zero, i.e. the amount of emissions produced and used by nature through photosynthesis is equal [29].

In addition to the emission amounts, the social (or environmental) cost, which expresses the cost spent to reduce the environmental damage caused by the emissions, is also included in the calculations. In this way, the economic, as well as environmental, burden of the emissions can be calculated. Social cost factors are taken from Zevenhoven and Beyene [23] and presented in Table 1.

RESULTS AND DISCUSSIONS

Results obtained as a result of LCA calculations are presented in Figure 2. While Figure 2 includes only the emissions released during the transport process, Figure 3 presents the values obtained as a result of taking the production process into account.

Emissions and waste heat generated during the transport process are quite low for 1 pkm. Figure 2 shows that air transport has higher fossil CO_2 emissions than rail transport. Air transport generates 126.54 g of fossil CO_2 per 1 pkm, while this value is calculated as 0.11 g for rail transport. N_2O and fossil CH_4 production per 1 pkm is higher in railway transportation. Similarly, water vapour production is higher for the rail transportation. However, due to the abundance of CO_2 production, air transport is more unfavourable than the rail transport in terms of greenhouse gas (GHGs) production potential and contribution to global warming. When other emissions are analysed, it

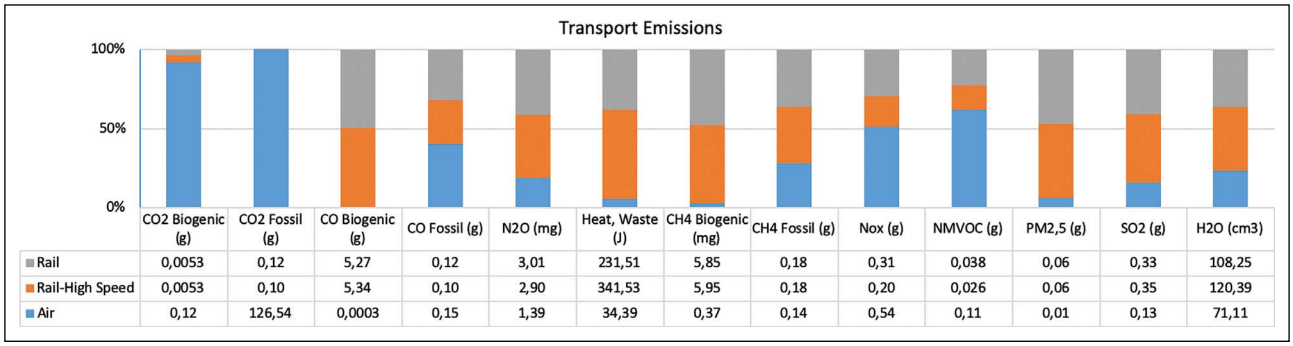

	CO2 Biogenic (g)	CO2 Fossil (g)	CO Biogenic (g)	CO Fossil (g)	N2O (mg)	Heat, Waste (J)	CH4 Biogenic (mg)	CH4 Fossil (g)	Nox (g)	NMVOC (g)	PM2,5 (g)	SO2 (g)	H2O (cm3)
Rail	0,0053	0,12	5,27	0,12	3,01	231,51	5,85	0,18	0,31	0,038	0,06	0,33	108,25
Rail-High Speed	0,0053	0,10	5,34	0,10	2,90	341,53	5,95	0,18	0,20	0,026	0,06	0,35	120,39
Air	0,12	126,54	0,0003	0,15	1,39	34,39	0,37	0,14	0,54	0,11	0,01	0,13	71,11

Figure 2. Transport emissions of air and rail modes.

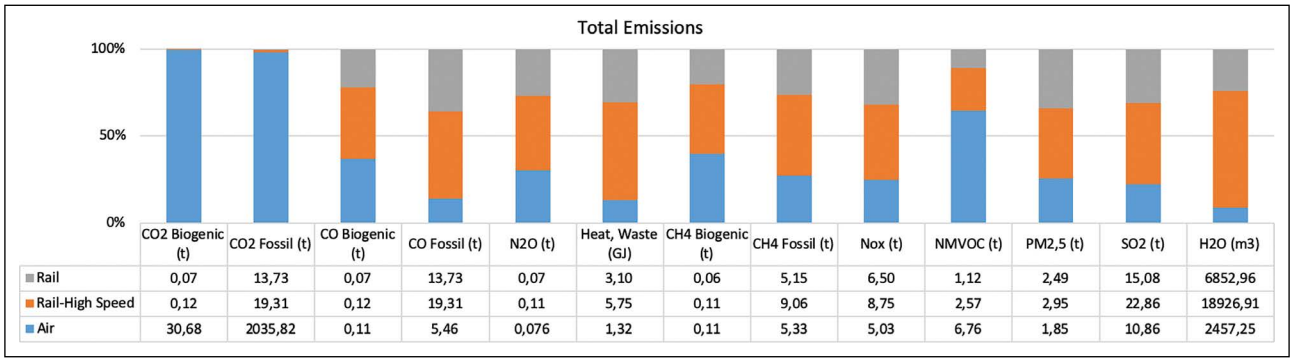

	CO2 Biogenic (t)	CO2 Fossil (t)	CO Biogenic (t)	CO Fossil (t)	N2O (t)	Heat, Waste (GJ)	CH4 Biogenic (t)	CH4 Fossil (t)	Nox (t)	NMVOC (t)	PM2,5 (t)	SO2 (t)	H2O (m3)
Rail	0,07	13,73	0,07	13,73	0,07	3,10	0,06	5,15	6,50	1,12	2,49	15,08	6852,96
Rail-High Speed	0,12	19,31	0,12	19,31	0,11	5,75	0,11	9,06	8,75	2,57	2,95	22,86	18926,91
Air	30,68	2035,82	0,11	5,46	0,076	1,32	0,11	5,33	5,03	6,76	1,85	10,86	2457,25

Figure 3. Total emissions of air and rail modes.

is observed that there is a balanced distribution. For example, air transport is more dominant in the production of biogenic CO_2, fossil CO, NO_x, and NMVOC, while rail transport produces more biogenic CO, $PM_{2.5}$, and SO_2. The values for high-speed and regular train emissions are generally close to each other. Only waste heat is produced much more by high-speed train.

Figure 3 includes the calculations results of production processes to the transportation emissions shown in Figure 2. Air transport is obviously ahead in fossil CO_2 production, when the production processes are also considered. Although rail transport (especially the high-speed train) produces most of other GHGs (N_2O, CH_4 and H_2O), it is possible to admit that the negative contribution of air transport to global warming is higher than that of rail transport. A relatively balanced distribution is observed in other gases. While rail transport is ahead of air transport in the production of fossil CO, waste heat, NO_x, $PM_{2.5}$, and SO_2, air transport surpassed the rail transport in NMVOC production. Since the data in Figure 3 includes the production values of one plane and train, the pkm unit is no more applicable. Since the production values are very high, the values in Figure 2 have decreased to a negligible level.

Social costs caused from emissions were also calculated by multiplying the social cost factors in Table 1 with the values in Figure 3. Accordingly, the total costs of air transport, high-speed train and regular train were calculated as € 355,109, € 288,059, and € 167,898, respectively. According to these values, air transport performed the worst for the environmental costs.

In one of the studies conducted in 2016, environmental performance comparison of airline and high-speed rail transportation was performed [30]. According to the findings of that study, although the general belief is that the high-speed train operations on the same route are more environmentally friendly than the airline operations, the environmentally friendliness of high-speed train operations generally depends on the source from which the energy is obtained, so a definite conclusion cannot be reached. Results of the present study show that the use of the railroad is clearly more environmentally friendly. On the other hand, if a more comprehensive LCA calculation based on country-based energy production studies is made, changes in results are very likely.

In another study conducted in the same year, a comparison was made between a high-speed train operating in Australia and short-distance air transport [26]. CO_2 production per 1 pkm in 2026 was estimated as 104.5 g and 30.3 g for air transport and high-speed rail transport, respectively. These values include the production, maintenance, and operation of the aircraft and the production, maintenance, operation, and disposal processes of the train. According to the results of the study, using high-speed trains instead of airways in short-distance travels in Australia will provide a great reduction in GHG production [26]. In our study, CO_2 values calculated per pkm for air transport and high-speed train are 126.54 g and 0.1 g, respectively. The common point of both studies is that the high-speed train is more environmentally friendly than the air transport.

CONCLUSIONS

Transportation is one of the principal needs of modern people. Different modes of transportation have been developed to meet different demands. These modes of transport have superior and weak characteristics in various areas. Especially in recent years, with the foundation of the concept of sustainability into daily life, the environmental performance of different transport modes has been questioned extensively. LCA is one of the most frequently used methods in these comparisons due to its holistic perspective.

In this study, air and rail modes for 1 pkm transportation were compared with LCA method in terms of environmental performance. Air transport seems to be ahead of the rail transport, especially in GHG production. Air transportation produces 126.54 g of fossil CO_2 per 1 pkm, while the high-speed train produces 0.1 g and the regular train produces 0.12 g of fossil CO_2. Similar results are obtained when the production process is also considered. When the production of one aircraft and the transportation per 1 pkm are examined together, it is seen that 2035.82 t CO_2 is produced. The same values are 19.31 t and 13.73 t for high-speed and regular train. In addition, it is seen that air transportation produces higher social costs compared to rail transport. On the other hand, while air transportation produces more CO, NO_x, and NMVOC during transportation phase, rail transportation modes cause more of them in terms of total emissions. Besides, rail transportation modes are generally responsible for more emissions.

According to these results, it is concluded that air transportation produced worse results for GHGs and thus, for climate change. However, rail transportation is not as environmentally friendly as it is thought when compared to air transport. On the other hand, despite the comparison of the modes of transportation made within the scope of the LCA, more detailed data on the production, operation, maintenance, and disposal processes are required in order to reach more precise conclusions and judgments. The question of 'which mode gives the best solution for the environment' is not easy to answer and because the results of the study provides a limited outcome for a certain comment, it is of great importance to support further studies with a more comprehensive database.

ACKNOWLEDGEMENTS

The authors express their special thanks to Metsims Sustainability Consulting for their support in using the SimaPro program.

DATA AVAILABILITY STATEMENT

The authors confirm that the data that supports the findings of this study are available within the article. Raw data that support the finding of this study are available from the corresponding author, upon reasonable request.

CONFLICT OF INTEREST

The authors declared no potential conflicts of interest with respect to the research, authorship, and/or publication of this article.

ETHICS

There are no ethical issues with the publication of this manuscript.

REFERENCES

[1] J. Koornneef, T. Van Keulen, A. Faaij, and W. Turkenburg, "Life cycle assessment of a pulverized coal power plant with post-combustion capture, transport and storage of CO_2," International Journal of Greenhouse Gas Control, Vol. 2(4), pp. 448–467, 2008. [CrossRef]

[2] R.B. Jackson, C. Le Quéré, R.M. Andrew, J.G. Canadell, G.P. Peters Roy, and L. Wu, "Warning signs for stabilizing global CO_2 emissions," Environmental Reserach Letters, Vol. 12, pp. 110202, 2017. [CrossRef]

[3] F.M. DaMatta, E. Rahn, P. Läderach, R. Ghini, and J.C. Ramalho, "Why could the coffee crop endure climate change and global warming to a greater extent than previously estimated?" Climatic Change, Vol. 152(1), pp. 167–178, 2019. [CrossRef]

[4] V. Hari, O. Rakovec, Y. Markonis, M. Hanel, and Kumar, R. "Increased future occurrences of the exceptional 2018–2019 Central European drought under global warming," Scientific reports, Vol. 10(1), pp. 1–10. 2020. [CrossRef]

[5] Y. Van, S. Perry, J.J. Klemeš, and C.T. Lee, "A review on air emissions assessment: Transportation," Journal of Cleaner Production, Vol. 194, pp. 673–684. 2018. [CrossRef]

[6] V.C. Nneji, A. Stimpson, M. Cummings, and K.H. Goodrich, "Exploring concepts of operations for on-demand passenger air transportation," In 17th AIAA Aviation Technology, Integration, and Operations Conference, pp. 3085, 2017. [CrossRef]

[7] B. Cox, W. Jemiolo, and C. Mutel, "Life cycle assessment of air transportation and the Swiss commercial air transport fleet," Transportation Research Part D: Transport and Environment, Vol. 58, pp. 1–13. 2018. [CrossRef]

[8] S. Kaewunruen, J. Sresakoolchai, and J. Peng, "Life cycle cost, energy and carbon assessments of Beijing-Shanghai high-speed railway," Sustainability, Vol. 12(1), pp. 206, 2020. [CrossRef]

[9] A.Y. Çetinkaya, "Life cycle assessment of environmental effects and nitrate removal for membrane capacitive deionization technology," Environmental Monitoring Assessment, Vol. 192(8), pp. 1–8, 2020. [CrossRef]

[10] M. N. Nwodo, and C.J. Anumba, "Review of life cycle assessment of buildings using a systematic approach," Building and Environment, Vol. 162, pp. 106290, 2019. [CrossRef]

[11] L. Bilgili, S.L. Kuzu, A.Y. Çetinkaya, and P, Kumar, "Evaluation of railway versus highway emissions using LCA approach between the two cities of Middle Anatolia," Sustainable Cities Society, Vol. 49, pp.101635, 2019. [CrossRef]

[12] C. Lee, J.Y. Lee, W.S. Jung, and Y.W. Hwang, "A study on the characteristics of environmental impact in construction sector of high-speed railway using LCA," Journal of Korean Society Railway, Vol. 17, pp. 178–185. 2014. [CrossRef]

[13] S. Saxe, and D. Kasraian, "Rethinking environmental LCA life stages for transport infrastructure to facilitate holistic assessment," Journal of Industrial Ecology, Vol. 24(5), pp. 1031–1046, 2020. [CrossRef]

[14] J. Vespermann, and A. Wald, "Much do about nothing? – An analysis of economic impacts and ecologic effects of the EU-emission trading scheme in the aviation industry," Transporation Research Part A Policy Practice, Vol. 45, pp. 1066–1076, 2011. [CrossRef]

[15] L. Bilgili, S.L. Kuzu, A.Y. Çetinkaya, and P. Kumar. "Evaluation of railway versus highway emissions using LCA approach between the two cities of Middle Anatolia," Sustainable Cities and Society, Vol. 49, pp. 101635, 2019. [CrossRef]

[16] M. Banar, and A. Özdemir, "An evaluation of railway passenger transport in Turkey using life cycle assessment and life cycle cost methods," Transportation Research Part D: Transport and Environment, Vol. 41, pp. 88-105, 2015. [CrossRef]

[17] V. Andreoni, A. Miola, and A. Perujo, "Cost effectiveness analysis of the emission abatement in the shipping sector emissions," JRC Scientific and Technical Reports, 2008.

[18] A.Y. Çetinkaya, L. Bilgili S., and L. Kuzu, "Life cycle assessment and greenhouse gas emission evaluation from aksaray solid waste disposal facility," Air Quality Atmosphere Health, Vol. 11, pp. 549–558, 2018. [CrossRef]

[19] S.L. Kuzu, "Estimation and dispersion modeling of landing and take-off (LTO) cycle emissions from Atatürk International Airport," Air Quality Atmosphere Health, Vol. 11, pp. 153–161, 2018. [CrossRef]

[20] ICAO, International Civil Aviation Organization Environmental Report 2013.

[21] S, De Bruyn, M. Bijleveld de Graaff, L.E. Schep, A. Schroten, R. Vergeer, and S. Ahdour, "Environmental Prices Handbook EU28 Version - Methods and numbers for valuation of environmental impacts," CE Delf, 2018.

[22] M.Z. Hauschild, R.K. Rosenbaum, and S.I. Olsen (Eds.), "Life cycle assessment: Theory and practice," 1st ed. Springer, Cham, Switzerland, 2018.

[23] R. Zevenhoven, and A. Beyene, "The relative contribution of waste heat from power plants to global warming," Energy, Vol. 36, pp. 3754–3762, 2011. [CrossRef]

[24] S. Kollamthodi, C. Brannigan, M. Harfoo, I. Skinne, C. Whall, L.Lavric, R, Noden, D. Lee, Ø. Buhaug, K. Martinussen, R. Skejic, I. Valberg, J.C. Brembo, V. Eyring, and, J. Faber, "Greenhouse gas emissions from shipping: Trends, projections and abatement potential: Final report to the Committee on Climate Change (CCC)," AEA Technology, 2008.

[25] A. Miola, B. Ciuffo, M. Marra, and E. Giovine, Analytical framework to regulate air emissions from maritime transport, European Commission Joint Research Centre Institute for Environment and Sustainability, 2010.

[26] S. Robertson, "The potential mitigation of CO_2 emissions via modal substitution of high-speed rail for short-haul air travel from a life cycle perspective - An Australian case study," Transporation Research Part D Transporation Environment, Vol. 46, pp. 365–380, 2016. [CrossRef]

[27] M. Schreier, H. Mannstein, and V. Eyring, and H. Bovensmann, "Global ship track distribution and radiative forcing from 1 year of AATSR data," Geophysical Research Letters, Vol. 34(17), 2007. [CrossRef]

[28] M.W. Khan, Y. Ali, F. De Felice, A. Salman, and A. Petrillo, "Impact of brick kilns industry on environment and human health in Pakistan," Science of the Total Environment, Vol. 678, pp. 383–389, 2019. [CrossRef]

[29] M. Head, P. Bernier, A. Levasseur, R. Beauregard, and M. Margni "Forestry carbon budget models to improve biogenic carbon accounting in life cycle assessment," Journal of Cleaner Production, Vol. 213, pp. 289–299, 2019. [CrossRef]

[30] T. D'Alfonso, C. Jiang, and V. Bracaglia, "Air transport and high-speed rail competition: Environmental implications and mitigation strategies," Transporation Research Part A Policy Practice, Vol. 92, pp. 261–276, 2016. [CrossRef]

Environ Res Tec, Vol. 5, Issue. 1, pp. 50–55, March 2022

Environmental Research and Technology
https://ert.yildiz.edu.tr - https://dergipark.org.tr/tr/pub/ert
DOI: https://doi.org/10.35208/ert.1009790

Environmental Research & Technology

Research Article

Extraction of some heavy metal ions from aquatic solution by banana peel-based biosorbents

Doğu RAMAZANOĞLU*[1], Zaman Adnan MOHAMMED[1], Khalid Ali MAHER[2]

[1]*Zakho University, Scientific Research Center, Zakho, Iraq*
[2]*Department of Chemistry, Zakho University, Zakho, Iraq*

ARTICLE INFO

Article history
Received: 14 October 2021
Revised: 31 December 2021
Accepted: 31 January 2022

Key words:
Banana peel; Density of biosorbents; Extraction; Heavy metal

ABSTRACT

In this work, economic, natural, and eco-friendly biosorbent want to be advised instead of traditional methods. For that reason, banana peel-based biosorbents were been done to remove Cu^{2+}, Ni^{2+}, and Co^{2+} ions from the solution by batch method. Moreover, how their natural assets like density, water intake, solubility, and heavy metal extraction performance were affected by their starch and oil contents had been determined. Flame atomic absorption spectroscopy (FAAS) having been using for the analysis of biosorbents uprooting performance. The density of the biosorbents had worked according to ASTM D 792 standards. As a result, the untreated banana peel-based biosorbents had transported 4.87 mg of Co^{2+} ions, 4.73 mg of Ni^{2+} ions, and 4.29 mg of Cu^{2+} ions from 25 ml 7 ppm of each heavy metal ions solution with 175 rpm agitation speed at 24°C during half-hour.

Cite this article as: Ramazanoğlu D, Mohammed ZA, Maher KA. Extraction of some heavy metal ions from aquatic solution by banana peel-based biosorbents. Environ Res Tec 2022;5:1:50–55.

INTRODUCTION

Processing of heavy metals had been beginning since antics time without awareness of their toxicity. The usage amount of heavy metal-containing coals that causes air pollution also develop industrialization. Water pollution is the thinnest point for damage to the food chain for that reason, the studies about extraction of organic and inorganic contaminants from wastewater are so valuable [1–8]. Numerous organic and inorganic studies have been done and suggested for wastewater treatment methods like as, electrochemical treatment, ion exchange, reverse osmosis, and chemical precipitate. These traditional methods have low performance, are expensive, and are unsuitable for large-scale processing [9–12]. Hence, an alternative method has been desiring.

Nowadays, the biosorbents have been shined like an alternative method instead of these traditional ones. Biosorption is a natural potential of biomaterials to the extraction of heavy metal ions from water metabolically or physiochemically [13]. Non-living biomass like shrimp, bark, crab shell, etc.; were used as traditional biosorbent [14]. In this study, banana peels have operated as an alternative biosorbent because of their abundance and low cost [15, 16]. As a biosorbent, they have the potential for reducing toxic metal ions like Cu^{2+}, Ni^{2+}, and Co^{2+} from urban environ-

***Corresponding author.**
*E-mail address: doguramazanoglu@hotmail.com

mental problems as well as metal-contaminated industrial effluent treatment expenses.

Banana is one of the most enjoyed fruits around the world. Although, its peels do not have specific usage. For that reason, the banana peels were tested as adsorbents of metal ions. This biomass has polymeric groups such as proteins, pectin lignin, cellulose, and hemicellulose which take a role in the adsorption of metal ions [17].

Besides these, it has other chemical groups like carboxylic acid, phosphate, and hydroxyl group attach to metals ions [18]. Figure 1 shows the chemical groups of banana peels; (a) carboxyl, (b) hydroxyl, (c) phosphate, and metal ions. In this study, 6 different biosorbents were supplied from banana peels to extract Cu^{2+}, Ni^{2+}, and Co^{2+} ions from the aquatic. Lastly, how their content affects their extraction performance during 30 minutes of contact time at room temperature investigated.

MATERIALS AND METHODS

Materials

Corn and wheat starch, apple cider vinegar (4–5% acetic acid), sunflower oil, Banana has bought from a local grocery store in Zaho. Cobalt (II) Acetate $C_4H_6CoO_4$, Nickel (II) Nitrate Hexahydrate $Ni(NO_3)_2.6H_2O$, and Copper (II) chloride dihydrate $CuCI_2.2H_2O$ has provided from (Merck, Germany).

Methods

Am Scope brand microscope has trained for taking surface images at the biology lab at Zakho university. Atomic absorption spectroscopy (FAAS) that (PerkinElmer, Turkey) brand has applied for a measured left of the concentration of solution after treatment with biosorbents in the scientific research center. Banana (Musa) peels having dried for two days at 103±2°C. Dried peels had been granulated by a coffee pulverizing machine.

Preparation of Biosorbents

The component of the banana peel-based biosorbents cornstarch, banana, sunflower oil having weighed and placed in a 500 ml beaker as given in Table 1. 25 ml of pure water summed to the beaker. Later, 3 ml of acetic acid was added and stirred to break the long-chain molecules of the starch. After, 1–2 ml of sunflower oil was combined as a plasticizer to re-crystallize to depolymerized polymer chains. It having mixed and fired at 75°C until gelation proceeds. Then, they left in the oven for 45 minutes at 103±2°C as shown in Figure 2.

Solubility Test (%)

The solubility test had found in 1992 by Gontard et al. [17]. Samples have taken in the oven for 24 hours at 103±2°C.

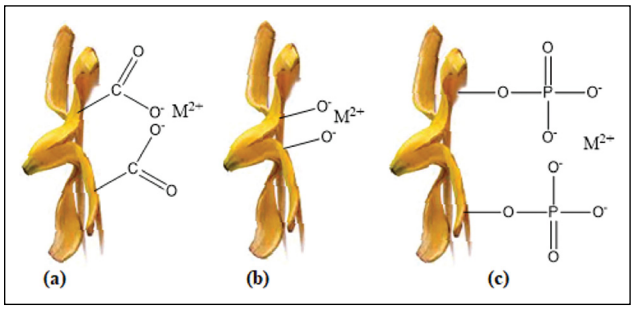

Figure 1. Interactions between the metal ions (M^{2+}) and the chemical groups present in the banana peel; **(a)** carboxyl, **(b)** hydroxyl, and **(c)** phosphate groups [10].

Table 1. Content of biosorbents

B1	B2	B3	B4	B5	B6
1g.B/ 2g.S	1.5g.B/ 1.5g.S	2g.B/ 1g.S	1g.B/ 2g.S	1.5g.B/ 1.5g.S	2g.B/ 1g.S
0.5 ml Oil	0.5 ml Oil	0.5 ml Oil	1 ml Oil	1 ml Oil	1 ml Oil

Then, they were weighed (Wi) and washing with 50 ml of purified water at 175 rpm for a day. After the rinsing step, they have balanced again. Finally, the solubility of the biosorbents had determined according to the equation given in (1).

$$S=(Wi-Wf)/Wix100 \quad (1)$$

Wi: Initial mass; Wf: Final mass.

Water Intake (%)

The water intake (%) values of biosorbents kept in pure water for 24 hours have determined according to the formula is given in (2).

$$SW=[(Mw-Md)/Md]x100 \quad (2)$$

Md=Sample initial weight (g); Mw=The weight of the sample after immersion in water (g); SW=water uptake rate (%).

Density Test (g/cm³)

The Air-dry weights of the samples were found and recorded. Then, they were immersed in water and weighed. The density of those samples had calculated concerning the equation in (3).

$$Density\ (g/cm^3)=[Ma/Mw] \quad (3)$$

Here, Ma=weight of the sample in the air (g). Mw=The weight of the sample in water (g) is given.

Batch Experiment

$CuCI_2.2H_2O$, $Ni(NO_3)_2.6H_2O$, and $C_4H_6CoO_4$ were used for preparing 25 ml 7 ppm of Cu^{2+}, Co^{2+}, and Ni^{+2} heavy metal ions solutions. Then, 25 mg of biosorbent was separated for the adsorption of each solution. Adsorption circumstances have adjusted to 175 rpm of stir speed, at 24°C for 30

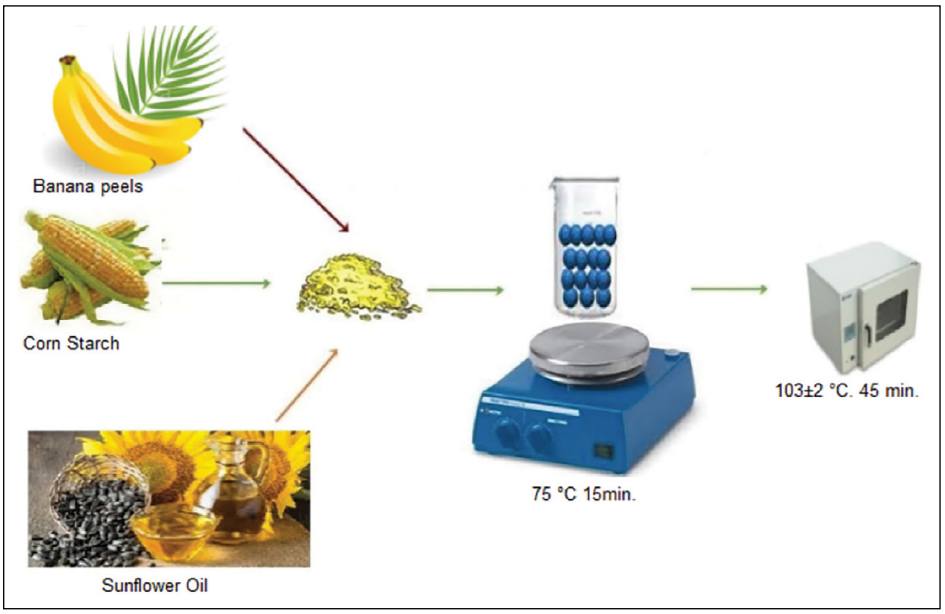

Figure 2. Preparation of biosorbents.

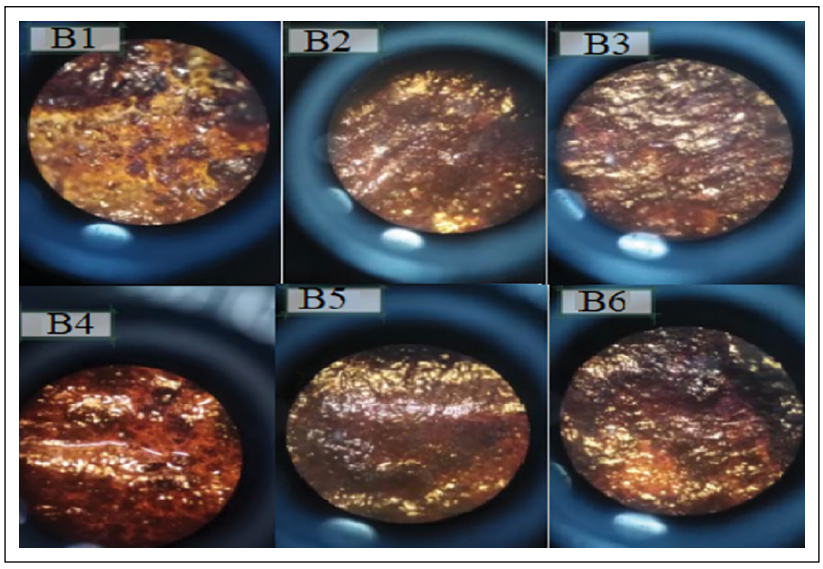

Figure 3. Banana peels-based biosorbents. Banana peels, starch, and oil content ratio of biosorbent (1/2/0.5) for B1, (1.5/1.5/0.5) for B2, (2/1/0.5) for B3, (1/2/1) for B4, (1.5/1.5/1) for B5, (2/1/1) for B6 respectively.

minutes. The performances have been obtained from the equation in (4).

$$Q=[(Co-Ce).V]/ m \quad (4)$$

Where; Co (mg/L) is an initial concentration, and Ce (mg/L) is the final concentration. V is the volume in a liter (L) unit, and m is biosorption in gram (g) units.

Morphology of Biosorbents

The surface photographs of biosorbents having taken by microscope in Figure 3. The biosorbents have different ingredients that make appearing not the same.

RESULTS AND DISCUSSION

Water Intake Analysis of Biosorbents

Banana peels-based biosorbents solubilities are calculated according to the equation in (1). Also, water intake values are shown in Figure 4.

The bar diagram trades with the water intake capacity of banana peel-based biosorbents. When, water intake was being decreased from B1 to B3 with an increasing quantity of banana peels contents [18, 19]. While the starch amount was raising biosorbents, the water adsorption capacity was diminishing. The chart has separated into

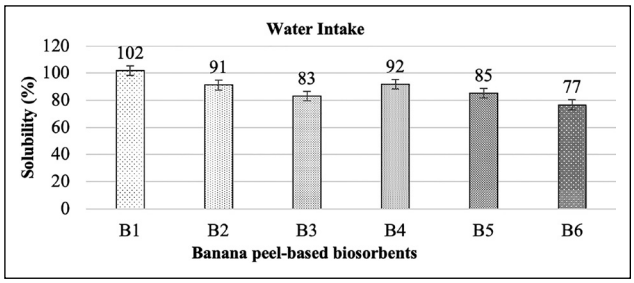

Figure 4. Water-intake of banana peels-based biosorbents. Banana peels, starch, and oil content ratio of biosorbent (1/2/0.5) for B1, (1.5/1.5/0.5) for B2, (2/1/0.5) for B3, (1/2/1) for B4, (1.5/1.5/1) for B5, (2/1/1) for B6 respectively.

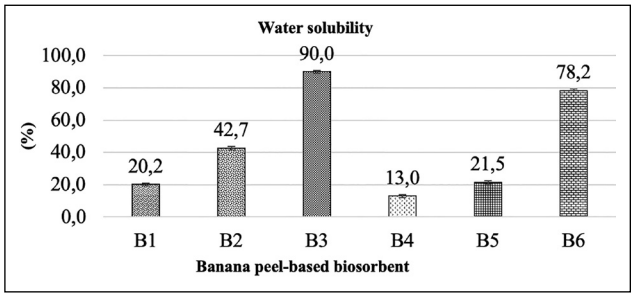

Figure 5. Solubility of banana peel-based biosorbents. Banana peels, starch, and oil content ratio of biosorbent (1/2/0.5) for B1, (1.5/1.5/0.5) for B2, (2/1/0.5) for B3, (1/2/1) for B4, (1.5/1.5/1) for B5, (2/1/1) for B6 respectively.

two groups referring to their oil contents. The first group of biosorbents had B1, B2, and B3. The second group had B4, B5, and B6.

Water Solubility Analysis of Biosorbents

The solubility of banana peel-based biosorbent was measured and given in Figure 5. The increasing amount of starch in biosorbent causes more solubility. However, the increased oil contents for B4, B5, and B6 show us how to decrease the solubility percentage. Hence, the B4 was the least water-soluble banana peel-based biosorbent with a 13.0% value and the B3 had the highest solubility value with 90.0%. There is just one difference between B1, B2, and B4, B5 that double oil content which decreased to solubility nearly 50%. On the other hand, B3 and B6 nearly lose the solubility ratio 10 percent. It showed how starch content negatively affects the solubility of biosorbents.

Density of Biosorbents

The bar chart has given in Figure 6 deals with the density of banana peel-based biosorbents. While the density of biosorbents was diminishing, starch content was rising. The elevated sunflower oil causes a slight uptick in mass [18–21]. The frequency of biosorbent had been directly equivalent to banana barks content.

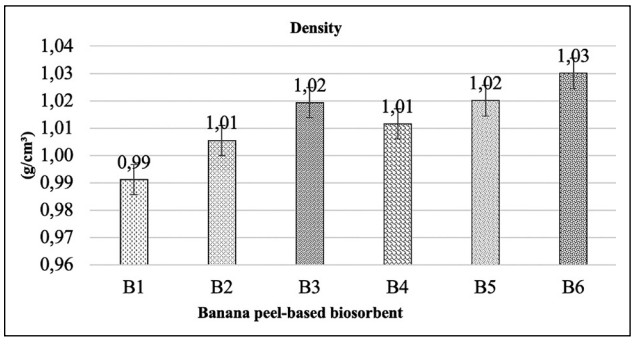

Figure 6. Density of banana peel-based biosorbents. Banana peels, starch, and oil content ratio of biosorbent (1/2/0.5) for B1, (1.5/1.5/0.5) for B2, (2/1/0.5) for B3, (1/2/1) for B4, (1.5/1.5/1) for B5, (2/1/1) for B6 respectively.

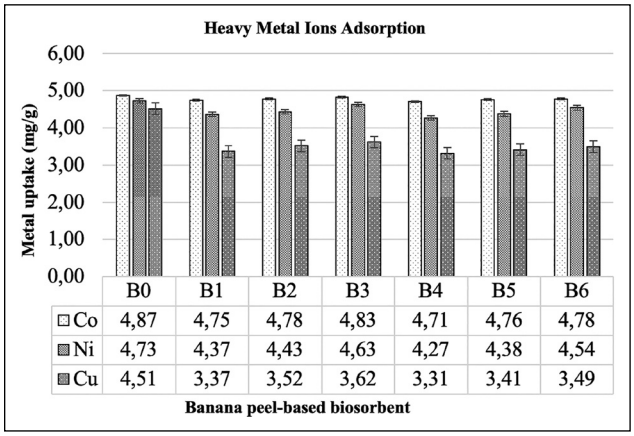

	B0	B1	B2	B3	B4	B5	B6
Co	4,87	4,75	4,78	4,83	4,71	4,76	4,78
Ni	4,73	4,37	4,43	4,63	4,27	4,38	4,54
Cu	4,51	3,37	3,52	3,62	3,31	3,41	3,49

Figure 7. Heavy metal ions adsorption capacity of banana peels-based biosorbents; Banana peels, starch, and oil content ratio of biosorbent (1/2/0.5) for B1, (1.5/1.5/0.5) for B2, (2/1/0.5) for B3, (1/2/1) for B4, (1.5/1.5/1) for B5, (2/1/1) for B6 respectively.

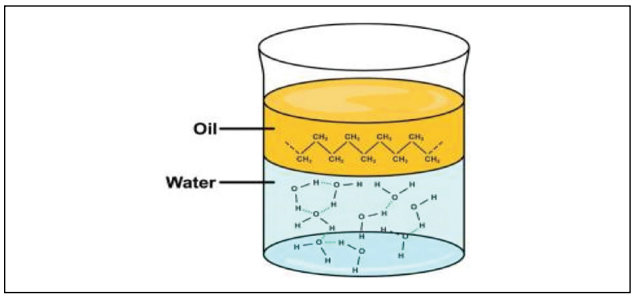

Figure 8. Interaction between water and oil molecules [22].

Adsorption Studies of Biosorbents

The adsorption studies of banana peel-based biosorbents having evaluated at the same condition for all heavy metal ions. The adsorption amount of Co^{2+}, Ni^{2+}, and Cu^{2+} heavy metal ions have given in Figure 7.

It has been obtained from the chart that untreated biosorbent has more adsorption capacity. Also, an expanded

volume of biomass content boosted the sorption capacity. Generally, biosorbents had double the amount of sunflower oil ingredients that have less adsorption capacity than others. That might be explained better by the interaction between water and oil molecules in Figure 8.

Oil has non-polar molecules. As we know, the electronegativity of non-polar molecules atoms is equal. But water has polar molecules that mean their electronegativity is not stable. Because of these polarity distinctions, might be cause for the adsorption capacity diminished. The other reason why untreated biosorbent performed better adsorption than other bio-composites is because of the chemical group's abundancy like carboxyl, hydroxyl, and phosphate groups present on banana peels which includes less from others.

The untreated biosorbent; B0 was the highest biosorption among them with the values of 4.87 mg/g, 4.73 mg/g and 4.51 mg/g for Co^{2+}, Ni^{2+}, and Cu^{2+} heavy metals ions respectively during half hour, at 24°C and 175 rpm agitation speed.

CONCLUSION

1. In the water intake analysis, the water intake amount decreases with increasing oil content. When the amount of banana peels content has increased, intake of water has diminished. Moreover, the surged starch content was inversely proportional to the water intake of banana peel-based biosorbent.
2. In the water solubility study, the raised sunflower oil content having decreased the solubility of all biosorbents. The B3 was observed as the highest soluble one with value of 90% among its groups. The B4 was recognized as the least soluble with value of 13.0%. The increasing amount of biomass enhances the solubility of biosorbents. Moreover, expanded biomass inversely proportions with a starch content have not been saved in a bioform. That is why the diminished starch amount grows the solubility.
3. In the density analysis, the booming oil content improves density for all biosorbents. Biosorbent that has the highest densities in its group was B6 determined as 1.03 g/cm^3. The biosorbent B1 was found as lowest one with the value of 0.99 g/cm^3.
4. In the adsorption step, untreated Banana peels has the highest Co^{2+}, Ni^{2+} and Cu^{2+} ions adsorption among others. Moreover, the increased sunflower oil reduced the heavy metal ion adsorption. Additionally, decreasing the amount of starch content also lessened adsorption capacity. Oppositely, the raised amount of biomass improves the adsorption performance. The density of all biosorbents was directly proportional to adsorption capacities.

According to results, banana peels can be used as biosorbent directly instead of other expensive water treatment methods. Further studies can be about to determination of the optimum condition of biosorbents and their carbonized form.

ACKNOWLEDGEMENTS

The corresponding author is glad to say thanks to the biology department of Zakho University for the visualization of synthesized biosorbents. Also, the authors thank reviewers for their contribution to this study.

DATA AVAILABILITY STATEMENT

The authors confirm that the data that supports the findings of this study are available within the article. Raw data that support the finding of this study are available from the corresponding author, upon reasonable request.

CONFLICT OF INTEREST

The authors declared no potential conflicts of interest with respect to the research, authorship, and/or publication of this article.

ETHICS

There are no ethical issues with the publication of this manuscript.

REFERENCES

[1] M.C.S. Minello, A.L. Paçó, M.A.U. Martines L. Caetano, A.D. Santos, P.M. Padilha, and G.R. Castro, "Sediment grain size distribution and heavy metals determination in a dam on the Paraná River at Ilha Solteira, Brazil," Journal of Environmental Science and Health, Part A, Vol.44, no 9, pp. 861–865, 2009. [CrossRef]

[2] M.C.S. Minello, A.L. Pac, R.S.D. Castro, L. Caetano, P.M. Padilha, G. Ferreira, M.A.U. Martines, and G.R. Castro, "Evaluation of heavy metal availability in contaminated sediments from the ilha solteira hydroelectric dam on the parana river at ilha solteira SP, Brazil," Fresenius Environmental Bulletin, Vol. 19, pp. 2210, 2010.

[3] N. Abdullah, N. Yusof, W.J. Lau, J. Jaafar, and A.F. Ismail, "Recent trends of heavy metal removal from water/wastewater by membrane technologies," Journal of Industrial and Engineering Chemistry, Vol. 76, pp. 17–38, 2019. [CrossRef]

[4] J.O. Duruibe, M.O.C. Ogwuegbu, and J.N. Egwurugwu, "Heavy metal pollution and human biotoxic effects," International Journal of Physical Science, Vol. 2, pp. 112–118, 2007.

[5] S.O. Lesmana, N., Febriana, F.E, Soetaredjo, J, Sunarso, and S. Ismadji. "Studies on potential applications of biomass for the separation of heavy metals from water and wastewater," Biochemistry Engineering Journal, Vol. 44, pp. 19–41, 2009. [CrossRef]

[6] F. Fu, and Q. Wang, "Removal of heavy metal ions from wastewaters: A review," Journal of Environment Management, Vol. 92, pp. 407–418, 2011. [CrossRef]

[7] D. Purkayastha, U. Mishra, S. Biswas. "A comprehensive review on Cd(II) removal from aqueous solution," Journal of Water Process Engineering, Vol. 2, 105–128, 2014. [CrossRef]

[8] M. Gavrilescu, "Removal of heavy metals from the environment by biosorption," Engineering Life Science, Vol. 4, 219–232, 2004. [CrossRef]

[9] N.P. Raval, P.U. Shah, and N.K. Shah, "Adsorptive removal of nickel (II) ions from aqueous environment: A review," Journal of Environment Management, Vol. 179, pp. 1–20, 2016. [CrossRef]

[10] C.L. Massocatto, E.C. Paschoal, N. Buzinaro, T.F. Oliveria, C.R.T. Tarley, J. Caetano, A.C. Gonçalves, D.C. Dragunski, and K.M. Diniz, "Preparation and evaluation of kinetics and thermodynamics studies of lead adsorption onto chemically modified banana peels," Desalination Water Treatment, Vol. 51, 5682–5691, 2013. [CrossRef]

[11] J. Anwar, U. Shafique, W. Zaman, M. Salman, A. Dar, and S. Anwar. "Removal of PB (II) and CD (II) from water by adsorption on peels of banana," Bioresearch Technology, Vol. 101 pp. 1752–1755, 2010. [CrossRef]

[12] J.R. Memona, S.Q. Memonb, M.I. Bhangera, G.Z. Memonc, A. El-Turki, and G.C. Allend, "Characterization of banana peel by scanning electron microscopy and FT-IR spectroscopy and its use for cadmium removal," Colloids and Surfaces B: Biointerfaces, Vol. 66, pp. 260–265, 2008. [CrossRef]

[13] Q. Yu, and P. Kaewsarn, "Binary adsorption of copper (ii) and cadmium (ii) from aqueous solutions by biomass of marine algadurvillaea potatorum," Separation Science and Technology, Vol. 34, pp. 1595–1605, 1999. [CrossRef]

[14] M. Zhao, J. Duncan, and H.R. Van, "Removal and recovery of zinc from solution and electroplating effluent using Azolla filiculoides," Water Research, Vol. 33, pp. 1516–1522, 1999. [CrossRef]

[15] E. Fourest, and J.C. Roux, "Heavy metal biosorption by fungal mycelial by-products: mechanisms and influence of pH," Applied Microbiology and Biotechnology, Vol. 37, pp. 399–403, 1992. [CrossRef]

[16] M. Ahmaruzzaman, "Industrial wastes as low-cost potential adsorbents for the treatment of wastewater laden with heavy metals," Advances in Colloid and Interface Science, Vol. 166, pp. 36–59, 2011. [CrossRef]

[17] N. Gontard, S. Guilbert, and J.L. Cuq. "Edible wheat gluten films: influence of the main process variables on film properties using response surface methodology," Journal of Food Science and Technology, Vol. 57, pp. 190–195, 1992. [CrossRef]

[18] R. Apiratikul and P. Pavasant, "Batch and column studies of biosorption of heavy metals by caulerpa lentillifera," Bioresource Technology, Vol. 99, 2766–2777, 2008. [CrossRef]

[19] F. Özdemir, and D. Ramazanoğlu, "Production of wood-based eco-friendly bioplastic composites using waste banana peel, pepper stalk and red pine wood flour," Turkish Journal of Forestry, Vol. 20, pp. 267–273, 2019. (in Turkish). [CrossRef]

[20] F. Özdemir, and D. Ramazanoğlu, "Production of bioplastic composite and wood bioplastic composite with starch from different biomasses," Journal of Bartin Faculty of Forestry, Vol. 21, pp. 377–385, 2019.

[21] ASTM D 792 2004. Density and specific gravity (relative density) of plastics by displacement, ASTM International, West Conshohocken, PA.

[22] D. Rosenthal, "Lubricant Chemistry and Oil/Water Separator Performance," Available: https://www.airbestpractices.com/technology/air-treatmentn2/lubricant-chemistry-and-oilwater-separator-performance. Accessed on Dec 30, 2021.

Environ Res Tec, Vol. 5, Issue. 1, pp. 56–71, March 2022

Environmental Research and Technology
https://ert.yildiz.edu.tr - https://dergipark.org.tr/tr/pub/ert
DOI: https://doi.org/10.35208/ert.1000739

Environmental Research & Technology

Research Article

Developing a GMDH-type neural network model for spatial prediction of NO_x: A case study of Çerkezköy, Tekirdağ

Can Burak ÖZKAL*[1], Özkan ARSLAN[2]

[1]*Department of Environmental Engineering, Tekirdağ Namık Kemal University, Tekirdağ, Türkiye*
[2]*Department of Electronics and Communication Engineering, Tekirdağ Namık Kemal University, Tekirdağ, Türkiye*

ARTICLE INFO

Article history
Received: 25 September 2021
Revised: 06 January 2022
Accepted: 24 January 2022

Key words:
Air pollutant; Artificial intelligence; GMDH; NO_x; NO_x prediction; Self-organizing deep learning

ABSTRACT

Air pollution-induced issues involve public health, environmental, agricultural and socio-economic aspects. Therefore, decision-makers need low-cost, efficient tools with high spatiotemporal representation for monitoring air pollutants around urban areas and sensitive regions. Air pollution forecasting models with different time steps and forecast lengths are used as an alternative and support to traditional air quality monitoring stations (AQMS). In recent decades, given their eligibility to reconcile the relationship between parameters of complex systems, artificial neural networks have acquired the utmost importance in the field of air pollution forecasting. In this study, different machine learning regression methods are used to establish a mathematical relationship between air pollutants and meteorological factors from four AQMS (A-D) located between Çerkezköy and Süleymanpaşa, Tekirdağ. The model input variables included air pollutants and meteorological parameters. All developed models were used with the intent to provide instantaneous prediction of the air pollutant parameter NOx within the AQMS and across different stations. In the GMDH (group method of data handling)-type neural network method (namely the self-organizing deep learning approach), a five hidden layer structure consisting of a maximum of five neurons was preferred and, choice of layers and neurons were made in a way to minimize the error. In all models developed, the data were divided into a training (80%) and a testing set (20%). Based on R^2, RMSE, and MAE values of all developed models, GMDH provided superior results regarding the NOx prediction within AQMS (reaching 0.94, 10.95, and 6.65, respectively for station A) and between different AQMS. The GMDH model yielded NOx prediction of station B by using station A input variables (without using NOx data as model input) with R^2, RMSE and MAE values 0.80, 10.88, 7.31 respectively. The GMDH model is found suitable for being employed to fill in the gaps of air pollution records within and across-AQMS.

Cite this article as: Özkal CB, Arslan Ö. Developing a GMDH-type neural network model for spatial prediction of NOx: A case study of Çerkezköy, Tekirdağ. Environ Res Tec 2022;5:1:56–71.

***Corresponding author.**
*E-mail address: cbozkal@nku.edu.tr

INTRODUCTION

Air pollutants can be categorized as primary (SO_2, NO_X, CO, hydrocarbons, particle matter) and secondary (ozone) pollutants. NOx can be represented by the most commonly found NO_2 form generated as a result of reaction between combusted hydrocarbons due to industrial and traffic emissions and atmospheric oxygen. NO_x are responsible for the formation of tropospheric ozone (bad ozone). Nitrogen oxides likewise SO_2, ammonia and volatile organic carbons are responsible for the formation of $PM_{2.5}$. and have been subject a to numerous research on the basis of monitoring, prediction [1, 2] and mitigation methodologies development [3]. The spread and transport of air pollutants that are released into the atmosphere is influenced by weather and climatic factors [4, 5]. Interaction of meteorological factors, mainly wind speed and wind direction with the air pollutants bring along variations in spatial distribution, spatiotemporal variation of air pollutants. Numerous research have demonstrated regional transport of air pollutants interpretation with the main meteorological factors; Humidity, temperature, pressure, wind direction and wind speed, dew point [6].

Recently, a city air quality determination study has gained importance. Thus, the periodic and spatial dimensions of pollution necessitate accurate determination. In order to overcome observed deficiencies, higher maintenance and repair expenses in air quality monitoring stations (AQMS) and provide supplementary data, solutions including increasing prevalence of AQMS, use of mobile AQMS and low cost sensors (LCS) are widely applied [7, 8]. Up to date, research have emphasized the modeling approaches for temporal and spatial prediction [9] and forecasting of air pollution [10].

Monitoring of air quality and air pollution parameters is performed by static, mobile AQMS and establishment of low cost sensors (LCS). Regulatory pollutants (carbon monoxide, nitrogen oxides, ozone and particulate matter are measured by certified reference instruments at static AQMS. Those stations and sensors are large and expensive, also necessitate strict calibration and maintenance routines in order to provide high quality data and comparability between different region and stations [7, 8, 11]. Sensors and low cost sensors are able to monitor a range of air pollutants but mostly they are unable to meet the Air Quality Directive - Data quality objectives criteria and under effect of chemical interferences and environmental conditions [7, 12]. According to framework and legal requirements described in air quality directive 2008/50/EC for ambient air quality assessment and management, the reference measurement methods are applied in the stable AQMS in Europe. The data provided by LCS are usually less accurate than AQMS [11]. The Air Quality Directive also pave the way for alternative and supplementary techniques such as air quality models for air quality and air pollution management.

Recent research accordingly have hypothesized to estimate air pollutants concentrations through their association/ interpretation with meteorological parameters [13], landscape data, environmental information [14] and other measured air pollutants [15, 16]. Underlie the spatiotemporal correlations between air pollutants emission and diffusion mechanisms, mechanistic or a non-linear model must be considering those correlation and/or able to realize non-linear mechanism of air pollutants spread, diffusion, transport and interaction under environmental, meteorological and atmospheric conditions [16].

Air quality management includes monitoring and timely application of foreseen preventions related to extreme air quality scenarios. Therefore, short and mid-term forecasting of air pollution and air quality indexes became the focus of numerous research [2]. There are many gaps encountered in air pollution data series of stable AQMS, during their observation period [17]. The research method for predictive determination of air pollution parameters and air quality mainly based on statistical or deterministic approaches [16]. The emission and diffusion of pollutant is related both with interaction of pollutants and the meteorological factors. As a result it is prerequisite to use sufficient number of meteorological and air quality parameters in an air pollution prediction model. Similar approach was applied via Pearson correlation, support vector regression (SVR) with or without principal component analysis, for the purpose of decision making on keeping the most correlated pollutant parameters in the data set [9, 16]. According to recent literature findings, modelling approaches including artificial neural network (ANN) methods were found eligible to be employed to fill in the gaps of air pollution records by deep learning based prediction of $PM_{2.5}$, LSTM based estimation of air pollutant concentrations that cannot be directly measured by the air quality monitor and ANN based forecasting of the spatial–temporal profile of pollutant concentrations and air quality determinants in specific cases of power outages, negative and wrong records of pollutants [11, 13, 16].

Most generally, machine learning (ML) methods and mostly ANN application are proposed to forecast the spatial-temporal pollutant concentration profiles during extreme scenarios be it; power outage, maintenance, sensor repairmen and replacement, negative and faulty pollutant records. Also recent research have reported successful application of various modelling techniques developed with intent to eliminate high number of monitoring stations requirement and become an alternative for advanced representation of air pollution spatial variability; where Feed forward neural networks and Long short-term memory deep learning techniques were applied with intent to provide data at currently unmonitored locations [11, 18].

Traditional linear models or deterministic models descriptive of chemical dispersion and transportation re-

main limited as a result of the high degree of non-linearity between different air pollutants and weather conditions [2]. As it was reported in recent literature, the nonlinear mechanism of atmospheric phenomenon can be realized by ANN [17, 19] and excellent prediction performance can be achieved [16]. For the very reason air pollutant parameters prediction using ANN is found superior to multi-linear regression [17, 20].

Conventional recurrent neural networks (RNN) and long short-term memory (LSTM) is suitable option to be applied on time series thereby applied in various research topics from various disciplines [11]. These methods mostly conform with the cases where the values of concern are related to their previous situation like traffic flow prediction, air pollution prediction, solar irradiation scenarios [11]. For the case of interpolation and extrapolation based estimation, model inputs are selected from a group of monitoring stations. Model training is performed by historical data of limited number of station with LSTM method, therefore the model was proposed to be suitable in small cities where only a few monitoring stations are established [11]. Besides the reported high performance of LSTM application in research related to air pollution, concentration prediction is the common field of research area [16, 21].

Recently, soft computation artificial intelligence (AI) techniques have been used successfully in the prediction of air pollution parameters such as NOx. Because of the many parameters that affect NOx, the results predicted from empirical models do not match well with the measured results. Therefore, it is necessary to develop models that provide more accurate prediction of NOx under various air pollution and meteorological conditions. Group Method of Data Handling (GMDH), an AI-based method, is a self-organizing technique that can be used to solve complex problems in nonlinear system with large degrees of complexity. The GMDH technique, which is a multi-layered structure, uses only neurons that can provide the most effective and accurate results unlike traditional machine learning methods. Thus, it is ensured that the most efficient input variables are used instead of using all input variables for the predictive model output. In this regard, the GMDH approach requires less data training compared to classical ANN methods and facilitates the interpretation of model input and output parameters. In air pollution prediction applications, it is very important to determine the pollutant (emission) sources and to determine the prevailing wind direction [19]. Demonstrated through preliminary research on AQMS of Tekirdağ and literature findings, deficiencies are observed in the AQMS data, with measurements either not being performed or not being shared on numerous occasions during the course of the year [13, 18, 22]. In order to overcome these shortcomings, GMDH-type neural networks using a non-linear structure can be preferred for the estimation of the NOx parameter.

In this study, we hypothesize the employment of GMDH-type neural network as an alternative technique in prediction (forecast length equal to 0) of NO_x air pollutant concentrations within the AQMS and spatial prediction of air pollutant concentration between different stations. The developed model provided prediction of NOx within a certain station by using data from a total number of four different weather stations and taking one station as reference. It has been observed that the GMDH-type neural network model minimizes the error rates under certain NOx prediction states within a station and between different stations.

MATERIALS AND METHODS

Location of Interest

Tekirdağ is located at European part of Turkey, in the Thrace region surrounded by Marmara Sea, Greece and Bulgaria. The city is located within the Ergene basin and is the center of population growth (predominated by the industrial development in the eastern part of the city, Çerkezköy and Çorlu districts) and air pollution as a result of heating, traffic and industrial activity. Tekirdağ constitutes the western border of İstanbul and the northern border of the Marmara Sea. Süleymanpaşa is the biggest district of Tekirdağ. There many organized industrial zones (OIZ) located at Çorlu, Çerkezköy, Kapaklı, Velimeşe, Ergene districts, as indicated in Figure 1. Tekirdağ host over 1100 factories (with the frequency of occurrence; textile, paper, packaging, chemical and metal industries respectively). In Tekirdağ, there a total of 14 organized industrial zones, while 5 of them established around Çorlu district and its immediate surroundings. 4 of the organized industrial zones (OIZ) are lined up in the west-east direction along Çorlu, the Velimeşe OIZ is located between Çerkezköy and Çorlu (North south direction) and more than 500 facilities operate. Çorlu is the area where the new settlement is located and the traffic is concentrated while Çerkezkoy host an OIZ under which more than 270 facilities operate and it one of Turkey's largest OIZs [23, 24]. The topographical properties of the location of interest (as indicated in Figure 1) can be described as land appearance in the form of wavy plains and is uneven, with low to mid slope values. Çorlu is under the influence of a transition type climate where Black Sea, Mediterranean and continental climate characteristics are encountered together. Cold air masses descending from the north and humid-warm air currents coming from the south, the Mediterranean and the Aegean affect the climate structure of the region. Typically, the wind blows at Tekirdağ dominantly from the directions of NNE-NE and rarely from the directions of SW-SSW [24].

Air Quality Monitoring Stations

In this study, urban and industrial AQMS located on the Çerkezköy-Çorlu-Tekirdağ line were selected as

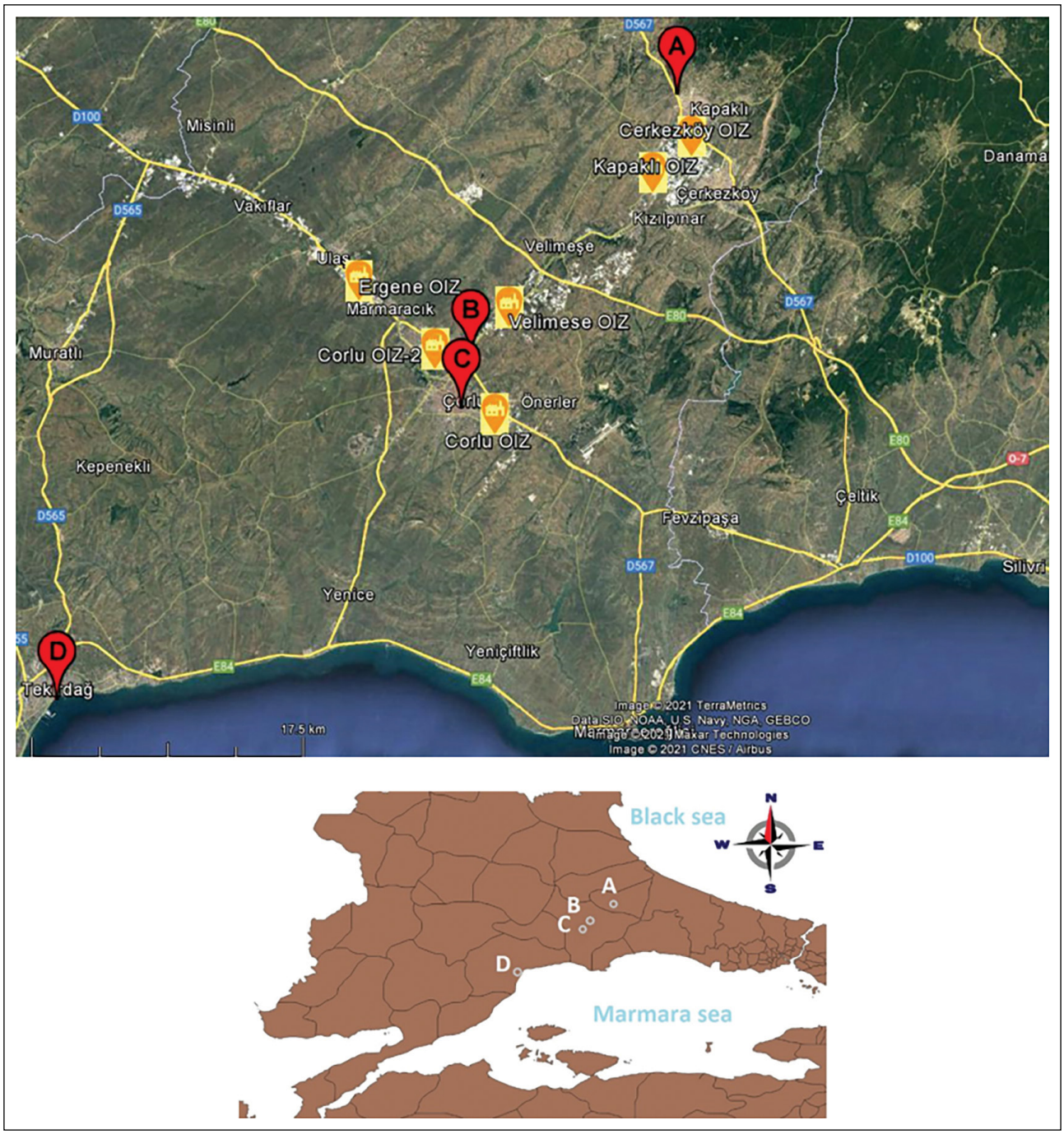

Figure 1. AQMS locations for stations; A: Çerkezköy, B: Çorlu, C: Çorlu Center, D: Tekirdağ center.

data source. Air quality of Çorlu is monitored through 2 AQMS; an urban AQMS located in town center (as a result of its distance from industrial activity) and an industrial AQMS located between town center and Çerkezköy (Fig. 1). For the case of Tekirdağ (Suleymanpasa center city) air quality is monitored at two different stations. The exact location, coordinates and bird flight (BF) distance between selected stations in Tekirdağ-Suleymanpasa, Çorlu and Çerkezköy are described in Figure 1 and AQMS distances between stations are given in Table 1.

Between studied dates, northern winds were prevalent around station A. For station B and C, the direction of wind could be described as spreaded over a wider range (as a result of E-SE winds prevalence), as it is demonstrated in Figure 2. Station B has distinctly strong winds where the average is above the meteorological upper limits reported for mild winds. Those strong winds are reported to trigger air pollutants transport and dispersal mechanisms [16]. Air pollutants at regions where mountain-valley and land-sea breezes cycles are dominant

Table 1. AQMS distances for stations

BF Distances between AQMS of interest	
AQMS # (stations separated by-)	**Distance in km**
Ed A-B	≈21
A-C	≈23
A-D	≈54
B-C	≈3
B-D	≈34
C-D	≈31

Letter Code/Name of AQMS. A: Çerkezköy; B: Çorlu; C: Çorlu Center; D: Tekirdağ center.

wind systems, are not easily transported from emission sources and accumulate. Also, WS over 5 m/s may create unstable weather conditions which increase PM and SO_2, NO_x distribution [4, 17].

Data Acquisition

The air pollutant and meteorological data source is the official Air Quality Monitoring Network website of the Ministry of Environment and Urbanization. Daily average values were used and taken as references all along the study. PM_{10}, SO_2, NO_x data as air pollutant parameters and air temperature (T), wind direction (WD), wind speed (WS), relative humidity (RH) and Air pressure (AP) were used as meteorological model variables for the period between December 2017 – December 2018.

It can be figured out from the correlation coefficients (depicted in Figure 4) of 0.79, 0.26, 0.43 and 0.91 for stations A, B, C, and D between targets output NOx and input variable PM, the PM parameter will be effective in NOx prediction for all stations. The PM_{10} and SO_2 are amongst the sole parameters continuously measured at each AQMS in common. Therefore, the choice of using PM10 and SO_2 as model inputs for NO_X prediction could be reasoned based on theory; the relation between air pollutant parameters as a result of their complex and interacting formation mechanisms. Nitrogen oxides likewise SO_2, ammonia and volatile organic carbons are responsible for the formation of particulate matter.

In the Nox prediction model, 174-day air pollution and meteorological data were used, which were recorded for 1 year. The statistical distributions of these data are shown in Figure 2 and can be summarized as; PM_{10}, SO_2 and NO_x data of station D shows a wider distribution compared to station A-

C. The distribution of annual temperature data did not differentiate between stations. Higher average wind-speed values were measured at Station C. A substantial difference of wind direction distribution was not observed at the stations. Average RH were reported to be the highest and lowest for station A and B respectively. Average AP values were distinctively higher at station D.

Regression Methods

Various machine learning regression methods are used to establish a mathematical relationship between the inputs which are air pollutants (PM_{10}, NO_X and SO_2) and meteorological parameters (T, WD, WS, RH and AP) and the target output. The predicted output is calculated by training the data in all models for different air quality measurement stations. In this study, various regression methods that provide a relationship between target NO_X and inputs are given below.

Linear Regression

Linear regression is one of the simplest methods that provide a mathematical relationship between the input parameters and the target output. It is often preferred because of the simple and convenient mathematical structure. In this regression method, the mathematical equation of the target based on the inputs is obtained with a slope and intercept value. The relationship between the target NO_X and the input variables is expressed by linear regression as:

$$Y = a_0 + a_1x_1 + a_2x_2 + \cdots + a_nx_n \quad (1)$$

where Y is output, $x_1, x_2, \ldots, x_n$ are input variables and $a_1, a_2, \ldots, a_n$ are coefficients obtained from the model.

Random Forest Regression

Random forest (RF) regression is one of the machine learning models that can be effective in predictive analysis under conditions where the output and input parameters are in a non-linear relationship. In this method, which reduces over fitting in model training, the predictions of all decision trees are combined to obtain more accurate and stable results. The forest tree diversity increases the robustness of the model obtained by regression [25].

Multilayer Perceptron Regression

Multilayer perceptron (MLP) is an artificial neural network method frequently used in regression. MLP method, which is also considered as the early stage of deep learning, consists of an input, multiple hidden and an output layer. In MLP neural networks, the first layer contains the input parameters and the output layer makes a prediction about the input. Hidden layers are used as a computational tool between the input and output layers [26].

MLP regression method is often used in supervised learning applications that involve the training phase for certain target and input parameters are used in all hidden layer neurons. In this method, which is based on the training of inputs and output, a model based on correlation between input and output is learned. In the training phase, the parameters and weight coefficients of the model that minimize the error are obtained.

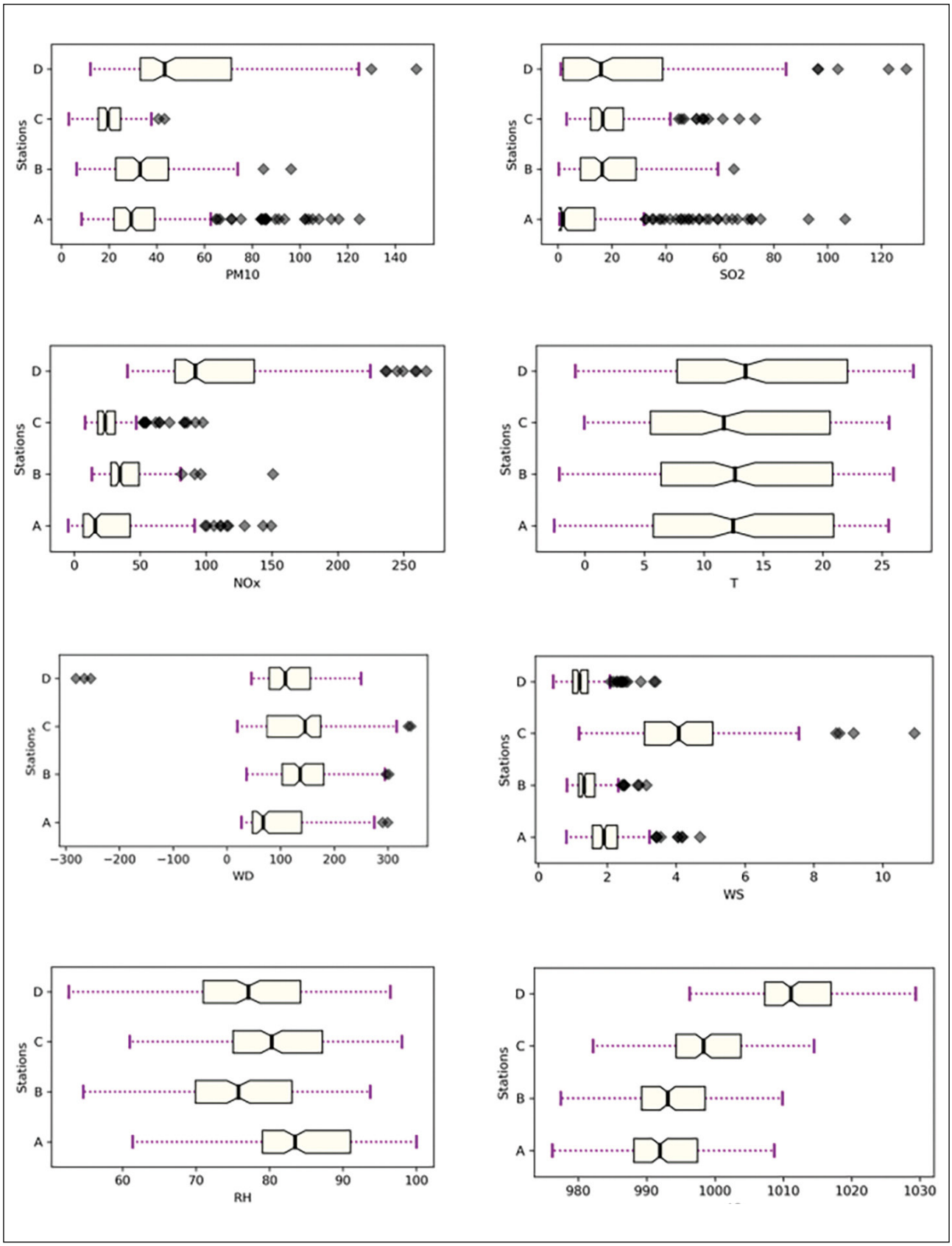

Figure 2. Boxplot data summary of PM_{10}, SO_2, NO_X, T, WD, WS, RH and AP parameters for stations A-WD: Wind direction (degrees), WS: Wind speed (m/s), RH: relative humidity (%), AP: Atmospheric pressure (hPa).

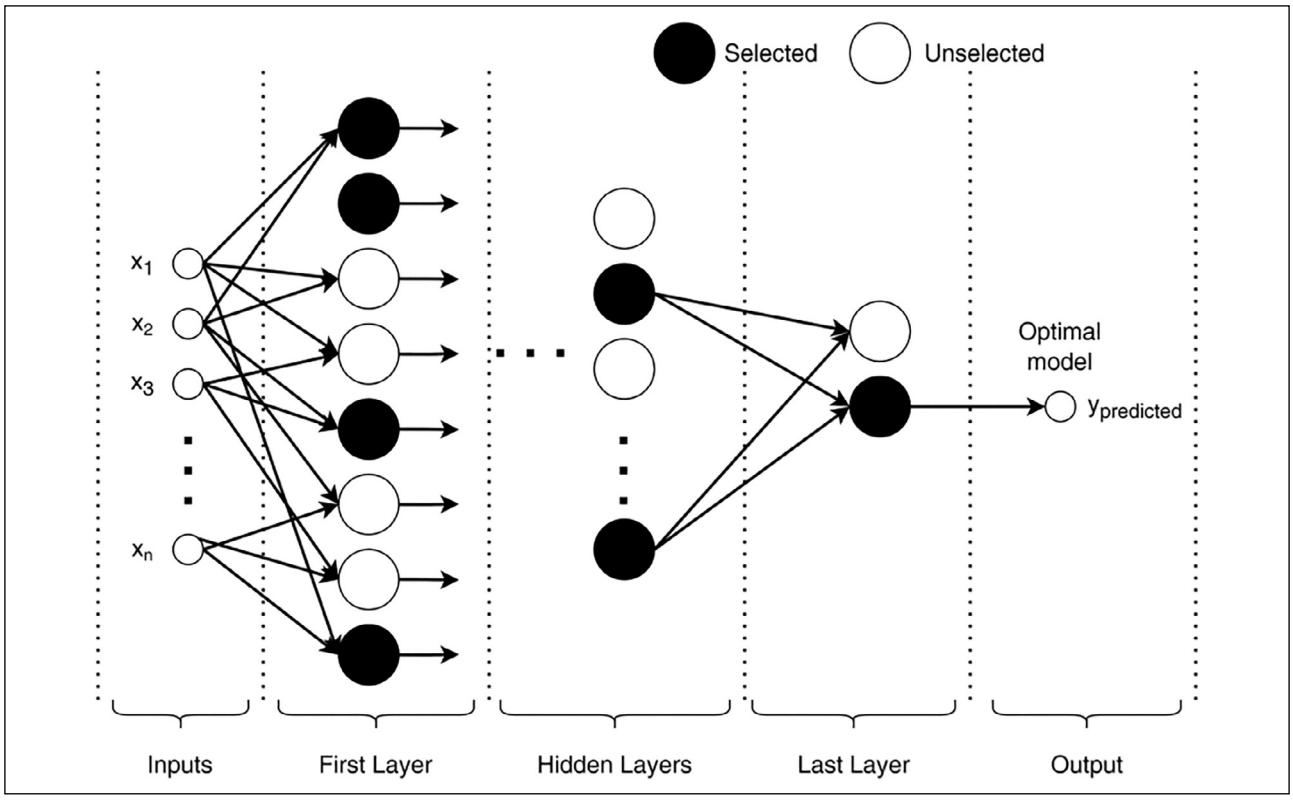

Figure 3. General structure of GMDH-type neural network.

GMDH-type Neural Network Regression

Group Method of Data Handling (GMDH), which is a self-organizing network model that behaves according to the input data, is preferred in regression analysis applications, unlike MLP artificial neural network models where the inputs are used on all neurons in the hidden layer [27]. The use of input parameters in all neurons may cause over fitting and performance degradation in regression models. In addition, there are difficulties and shortcomings in adjusting the bias and weight coefficients for a small number of datasets.

GMDH-type neural networks are one of the best methods for model estimation in complex structured problems. This neural network model is a multi-layered structure and uses only neurons that can provide the most effective and accurate results. Each layer consists of independent neurons and these neurons are used in pairs. In this network model, a quadratic polynomial function is used as the activation function. The neurons in the hidden layers work independently and neuron outputs which minimize the error rate are used. Thus, a multilayer neural network model consisting of optimal layers and neurons is designed instead of using all neurons in the layers [28]. Figure 3 shows the general structure of GMDH-type neural network.

GMDH-type neural networks are defined as a relationship between input and output parameters expressed in the form of a stepwise complex Kolmogorov-Gabor polynomial function. This relationship is expressed as a nonlinear form of the Kolmogorov-Gabor function [29].

$$\bar{y} = \alpha_0 + \sum_{i=1}^{n} \alpha_i x_i + \sum_{i=1}^{n}\sum_{j=1}^{n} \alpha_{ij} x_i x_j + \sum_{i=1}^{n}\sum_{j=1}^{n}\sum_{k=1}^{n} \alpha_{ijk} x_i x_j x_k + \cdots \quad (2)$$

where $\bar{y}$ and α are predicted output and the coefficients of the quadratic polynomial, respectively. The number n is the degree of polynomial function and $i, j, k \in (1, 2, \ldots, n)$. In this study, the number n was chosen as 2. The polynomial operation is performed in three steps for i={0, 1 and 2}.

The Kolmogorov-Gabor polynomial, which has a nonlinear structure, is expressed in the form of a quadratic polynomial consisting of two variables as follows:

$$\bar{y} = G(x_i, x_j) = \alpha_0 + \alpha_1 x_i + \alpha_2 x_j + \alpha_3 x_i x_j + \alpha_4 x_i^2 + \alpha_5 x_j^2 \quad (3)$$

The GMDH-type neural network estimates the output for each set of input parameters (x_i and x_j) and is used to estimate the α_i coefficients that minimize the mean squared error between the predicted and the actual output. This process is called self-organization of models, and neurons with minimum error calculated by the least squares method are selected.

In the GMDG-type neural network model, the coefficient vector of the quadratic polynomial is calculated and the neurons that increase the error are eliminated. The objective function (OF), which is a selection criterion, is used for elimination process and OF is expressed as:

$$OF = \frac{1}{n}\sum_{i=1}^{n}\left(y_{pre} - y_{mea}\right)^2 \quad (4)$$

where y_{pre}, y_{mea} and n are the predicted, measured values and total number of dataset, respectively.

Evaluation of Models

The performance of a regression model is evaluated by calculating the error rate of the predicted output obtained by the model. In addition, the fit of the regression line to the data set is also used as a criterion in model evaluation. The correlation coefficient (R^2), root-mean square error (RMSE) and mean absolute error (MAE) are used to calculate between the predicted and actual values. The R^2 value is between 0 and 1, and a larger value indicates a better fit between the predicted and the actual values. The R^2 is a good measure to determine how well the model fits the dependent variables and is expressed as:

$$R^2 = 1 - \frac{\sum_{i=1}^{n}\left(y_{mea} - y_{pre}\right)^2}{\sum_{i=1}^{n}\left(y_{mea} - y_m\right)^2} \quad (5)$$

The RMSE is calculated as the sum of the square of the error by subtracting the predicted from the actual value, then divided by the total number of data and the square root is taken. The RMSE, which is widely used in the evaluation of models, is expressed as follows:

$$RMSE = \sqrt{\frac{\sum_{i=1}^{n}\left(y_{mea} - y_{pre}\right)^2}{n}} \quad (6)$$

The mean absolute error (MAE), a measure similar to the mean squared error (MSE), is defined as the sum of the absolute value of the error and is expressed mathematically as follows:

$$MAE = \frac{1}{n}\sum_{i=1}^{n}\left|y_{mea} - y_{pre}\right| \quad (7)$$

where y_{mea}, y_{pre}, y_m and n represent the measured, predicted, the average of measured values and the total number of dataset, respectively.

Model Development Setup

Many empirical models have been developed to estimate the air pollution parameter NO_X values using air pollution and meteorological parameters. Recent research have focused on instant prediction of target pollutant parameter value [13]. Machine learning regression methods are extensively used to derive empirical equations. However, the application of ANN models in larger spatial dimensions would bring along a significant decline in the model's performance for places far away from the station (data of which was used for model training), as was hypothesized in recent studies [9, 11, 30]. This study aims to develop empirical models based on not only pollution conditions, but also depend on meteorological conditions for NOx prediction. In this study, different regression methods such as linear, RF, MLP, and GMDH-type NN were analyzed for the NOx prediction model. The influences of different parameters, including air pollutants (PM_{10}, SO_2) and meteorological parameters (T, WD, WS, RH, and AP), on the prediction of NOx within station and across different stations were investigated. In the experimental setup, the parameters of the regression methods were set as follows: the number of forest trees was taken as 500 for RF, five hidden layer structures consisting of 20 neurons was established for MLP and 0.01 learning rate, rectified linear unit activation function, Adam optimization were chosen. In the GMDH-type neural network, a five hidden layer structure consisting of a maximum of five neurons was preferred and, layers and neurons that minimized the error were used. In all developed models, the data were split into a training (80%) and a testing set (20%). R^2, RMSE, and MAE values were calculated to obtain the most effective and accurate empirical model that can be used in the prediction of NO_X.

RESULTS AND DISCUSSIONS

In this study, pollution and meteorological parameters were used as input variables in different regression methods for the NO_x prediction model and it was aimed to obtain a model that provides the best prediction. Figure 3 shows the correlation between the parameters used as input variables and the output NO_x, and the correlation values between these parameters. As can be seen from Figure 4, it has been observed that target output NO_x has a high correlation with PM and SO_2 parameters at all stations. It can be said that the obtained correlation results are compatible with the literature. A similar hypothesis was proposed in recent research in the Marmara region; were correlations between SO_2 and PM_{10} values reported for residential areas (with solid fuel use) were higher than it is determined for industrial areas [31].

There are correlation coefficients of 0.79, 0.26, 0.43 and 0.91 for stations A, B, C, and D between targets output NO_x and input variable PM, respectively. These results show that the PM parameter will be effective in prediction the output NO_x for stations A and D. Similarly, the correlation between output NOx and SO_2 is 0.83, 0.73, 0.11 and 0.89 for stations A, B, C, and D, respectively. It is concluded that the SO_2 parameter will have a negative effect on the prediction of the NO_X parameter for station C. In addition, it can be said that there is no high correlation between meteorological parameters and NO_x for all stations. However, the use of meteorological parameters in the prediction of target output NO_X is important to obtain a more robust model.

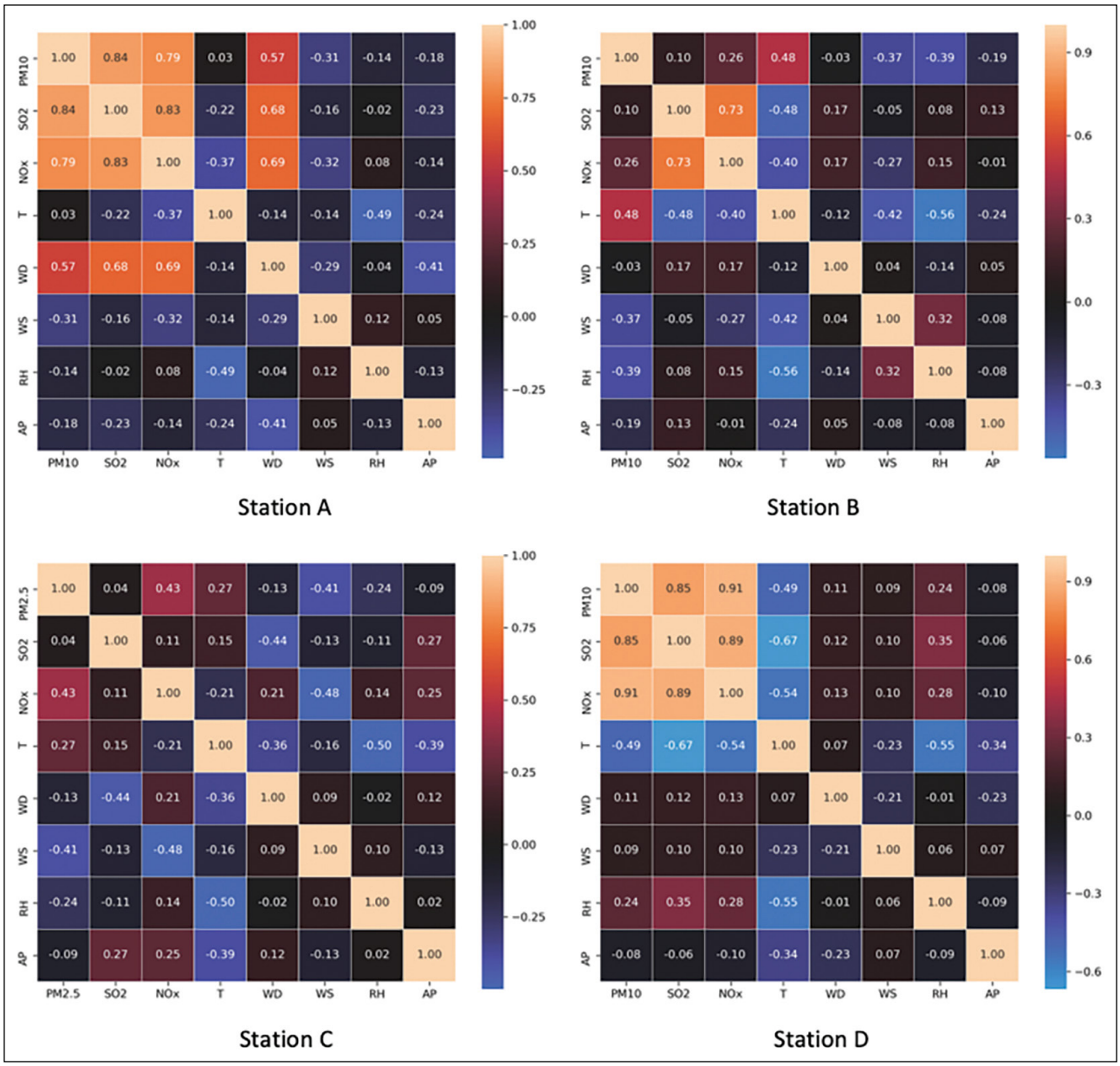

Figure 4. Pearson's correlation coefficients of air pollutant and meteorological parameters for stations A, B, C, D.

The Prediction Approach

Due to the non-linear relationship between NO_X and input parameters, linear regression methods were found ineligible for modelling. All the cells in the layers are used in MLP neural network-based modelling, resulting in an excessive training problem and a recession in model performance. RF modelling is one of the machine learning models that can be efficient in predictive analysis even in non-linear relations, have lower regression and higher error rates compared to the GMDH method. GMDH neural network prefer the most appropriate cells and pathways that minimize the error rate in the estimation.

As a result the GMDH method performed better for estimating NO_X as compared to other methods. In this method, the number of hidden layers and the number of cells in those layers are optimally obtained based on the input parameters. The NO_X prediction within a certain station by the GMDH-type neural network model resulted with regression coefficients (Table 2) ranging from 0.87 to 0.94. For the case of using meteorological and air pollution data of station A as model inputs; the regression coefficient of NO_x prediction by the GMDH-type models were found to be 0.85, 0.54, and 0.65 for station B, C, D (as shown in Table 4), respectively.

In another research, it was emphasized to use ANN algorithms for predicting hourly concentrations of O_3, NO_2, PM_{10}, $PM_{2.5}$, SO_2, CO with correlation coefficient (R^2) between measured and predicted values and root-mean-

Table 2. Prediction of each station's NOX for input parameters (PM_{10}, SO_2, T, WD, WS, RH and AP)

Station	Machine learning techniques											
	Linear regression			Random forest regression			MLP regression			GMDH regression		
	R^2	RMSE	MAE	R^2	RMSE	MAE	R^2	RMSE	MAE	R^2	RMSE	MAE
A	0.85	15.16	10.72	0.91	11.61	8.03	0.82	16.32	10.76	0.94	10.95	6.65
B	0.59	16.52	8.18	0.52	17.92	9.21	0.57	32.48	20.69	0.87	8.99	6.10
C	0.46	12.96	10.00	0.77	8.40	5.68	0.64	22.57	16.75	0.88	7.19	5.44
D	0.89	17.42	13.26	0.84	21.45	15.23	0.83	22.08	17.03	0.93	18.68	13.60

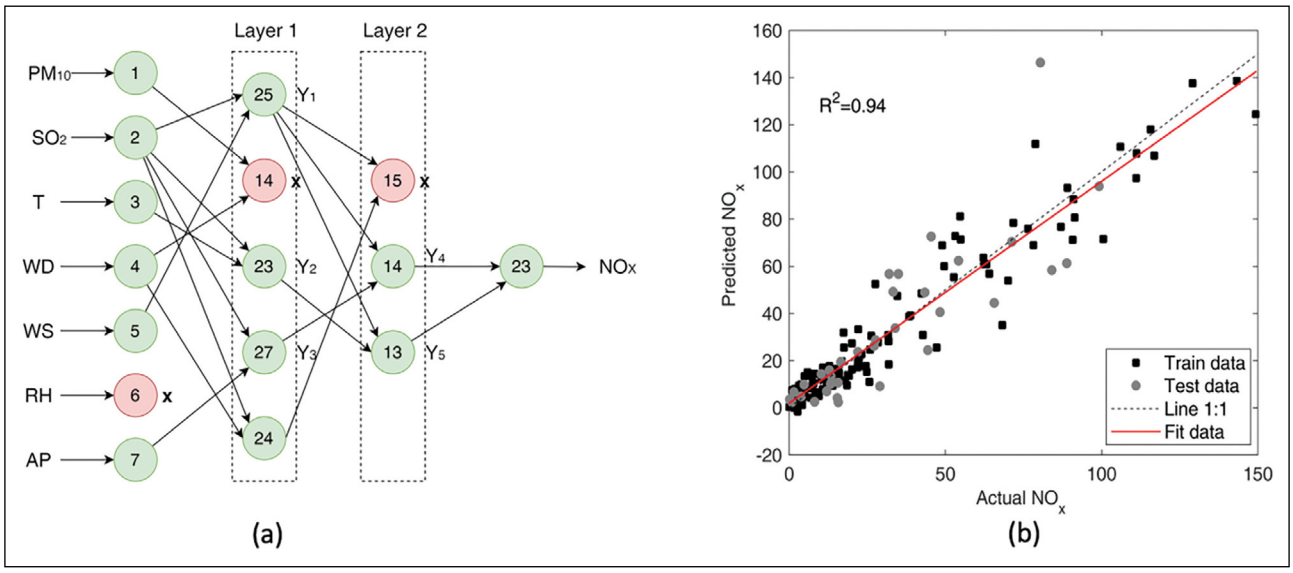

Figure 5. The prediction of NO_X in station A. **(a)** structure of double hidden GMDH layers; **(b)** actual and predicted NOX by GMDH model.

square (RMSE) values of 0.87 and 59.5 respectively [13]. It was reported by another research group that, using the WS, WD, and temperature as input variables, and ANN, ANFIS models have provided SO_2 prediction with R^2 values between 0.20 and 0.50 [32], and in another study with R^2 >0.70 [33]. Recent research have proposed using both the meteorological factors and air pollutant parameters as input variables and reported that the ANN model produced a $PM_{2.5}$ prediction with R^2>0.92 [34]. Another study revealed that the use of NO_X and meteorological parameters as input variables and the ANFIS model provided O_3 predictions with R^2>0.94 [35]. Based on findings of a recent study, using weather factors and air visibility as input variables is feasible for the ANFIS model and CO-NO_2, PM_{10}, SO_2 – O_3 were predicted with R^2 between 0.65–0.89 [10].

Prediction of NO_x Parameter Within a Station

In this study, the NO_X prediction was obtained by various regression methods using the PM_{10}, SO_2, T, WD, WS, RH, and AP of each station as input factors. Table 2 shows the calculated R^2, RMSE, and MAE values of linear, RF, MLP and GMDH-type regression algorithms for all stations. Regarding R^2, RMSE and MAE values, the prediction of NO_X within a certain station by the GMDH-type neural network have provided better results.

NO_x prediction at station A has been provided by the GMDH-type neural network with the design demonstrated in Figure 5a. This designed network structure consists of an input layer with 7 neurons, two hidden layers with 5 and 3 neurons, respectively, and an output layer with a single neuron. In this network structure, neuron outputs that minimize the error rate between predicted and actual output were selected. As a result, at station A the NO_X was predicted with R^2=0.94, RMSE=10.95, and MAE=6.65, (Fig. 5b). Similarly, prediction of NO_x in stations B, C, and D by the GMDH-type neural network model have ended up with regression coefficients of 0.87, 0.88, and 0.93, respectively.

The prediction of NO_X is formulated using the optimal neuron outputs of the network structure shown in Figure 5. Each polynomial equation obtained with active neuron outputs and finally the NO_X prediction equation is given in Table 3. Relative humidity (RH), one of the input layer pa-

Table 3. Parameters and coefficients used in neuron equations for the prediction of NO_X in station A

Equation	No.
$Y_1 = 54.76 + 3.06\,SO_2 - 37.49\,WS - 0.02\,SO_2{}^2 + 6.47\,WS^2 - 0.17\,SO_2 \cdot WS$	
$Y_2 = 15.54 + 2.58\,SO_2 - 0.56\,T - 0.02\,SO_2{}^2 - 0.003\,T^2 + 0.04\,SO_2 \cdot T$	
$Y_3 = [3.99 - 0.0008\,SO_2 - 0.0081\,AP] \cdot 10^4$	
$Y_4 = -6.09 + 0.77\,Y_1 + 0.69\,Y_3 + 0.014\,Y_1{}^2 + 0.004\,Y_3{}^2 - 0.02\,Y_1 \cdot Y_3$	
$Y_5 = -6.96 + 0.75\,Y_1 + 0.8\,Y_2 + 0.02\,Y_1{}^2 + 0.009\,Y_2{}^2 - 0.04\,Y_1 \cdot Y_2$	
$NO_x = 0.26 - 0.43\,Y_4 + 1.39\,Y_5 + 0.04\,Y_4{}^2 + 0.03\,Y_5{}^2 - 0.08\,Y_4 \cdot Y_5$	(8)

Table 4. Prediction of B, C and D station's NOX for input parameters (PM_{10}, SO_2, NO_X, T, WD, WS, RH and AP) of station A

Station	Machine learning techniques											
	Linear regression			Random forest regression			MLP regression			GMDH regression		
	R^2	RMSE	MAE	R^2	RMSE	MAE	R^2	RMSE	MAE	R^2	RMSE	MAE
B	0.56	17.25	9.31	0.63	15.83	8.44	0.55	17.36	9.69	0.85	9.45	6.16
C	0.11	16.66	9.78	0.22	15.54	9.54	0.08	16.92	10.30	0.54	13.24	8.19
D	0.29	44.85	33.44	0.38	41.94	28.62	0.25	46.25	32.66	0.65	38.63	29.15

rameters, is deactivated because it increases the error rate in the NO_X prediction model. The output of PM_{10} and WD polynomial pair in the first hidden layer, and the output of SO_2 and WD polynomial pair and Y1 output in the second hidden layer are not included in the model because they increase the error rate in the NO_X prediction. Thus, the NO_X prediction is modelled as a polynomial function using the selected optimal neuron outputs.

Prediction of NOX Across Stations

The NOX prediction of stations located at different distances and directions were performed using station A data as input parameters via various machine learning regression methods. Table 4 shows the NO_X prediction results of stations B, C, and D. The NO_X values are also used as input data of station A which is accepted as a source station. The results show that the GMDH-type neural network provides higher R^2, lower RMSE, and MAE values than other methods for all stations. It has been observed that the prediction performance of the proposed model is more successful at station B than at other stations. This result is due to the fact that reference station A, whose data is used as input, is closer to station B than to other stations.

The GMDH-type neural network model designed for the prediction of NO_X values at station B using data from station A and the regression fit line of this model are shown in Figure 6. In the double hidden layer model designed in Figure 6a, the input parameters WD and RH were deactivated because they increased the error between the predicted and actual output. The PM_{10} and NO_X polynomial pair output from the data of station A in the first hidden layer and output polynomial pair Y_1 and Y_2 in the second hidden layer were not used because they adversely affected the NO_X prediction of station B.

The NO_X prediction at station B is modelled as a polynomial function via the remaining optimal neuron outputs and the fit line of model is shown in Figure 5b. The model equations were obtained by using the optimal neuron outputs of the GMDH-type neural network. The design is demonstrated in Figure 5a, and the equations are given in Table 5. As a result, Eq. (9) is obtained for the case that neuron outputs are used as polynomial pairs in the NO_X prediction model of station B.

Prediction of NOX Across Stations without Using NO_x as Input Variable

The NO_X prediction across stations that are located at different distances and directions was performed using meteorological and air pollution data of station A data (the NO_X is excluded) as input parameters via linear, RF, MLP and GMDH-type neural network regression methods. The R^2, RMSE and MAE results of these regression methods including all stations were listed in Table 6. According to the analysis of NO_X prediction results of stations B, C and D (without using the NO_X data of station A, that was taken as the reference station). It is apparent that GMDH-type

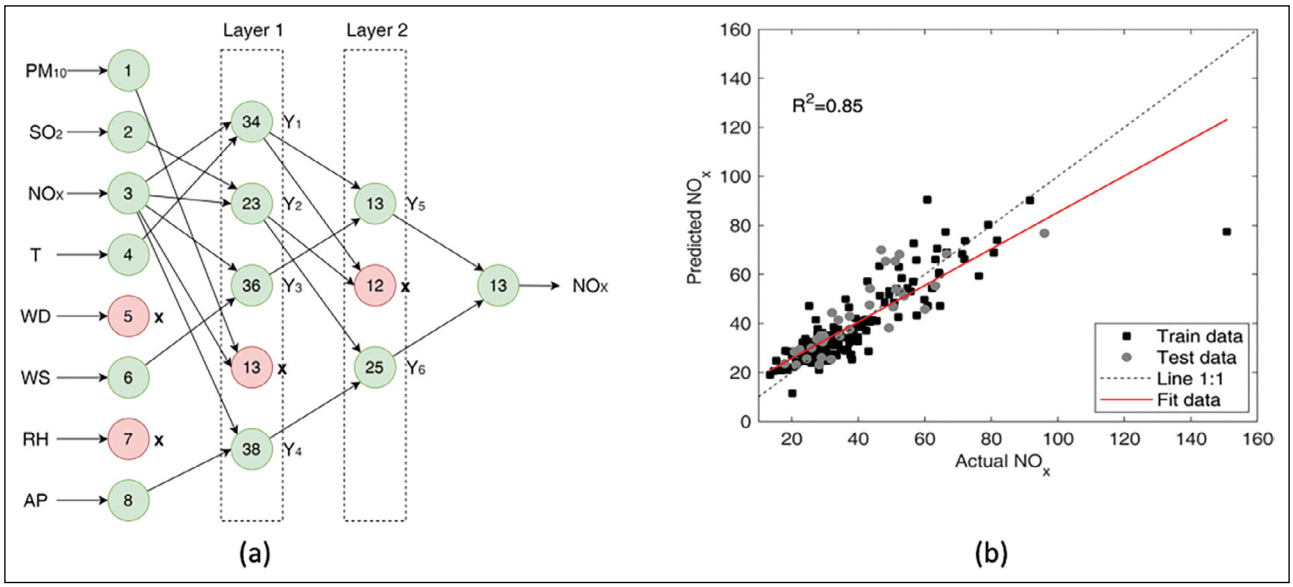

Figure 6. The prediction of NO_X in station B using NO_X of station A. **(a)** structure of double hidden GMDH layers; **(b)** actual and predicted NO_X by GMDH model.

Table 5. Parameters and coefficients used in neuron equations for the prediction of NO_X in station B using NOX of station A

Equation	No.
$Y_1 = 15.43 + 1.08\,NO_x + 0.76\,T - 0.03\,NO_x{}^2 - 0.01\,T^2 - 0.03\,NO_x \cdot T$	
$Y_2 = 21.5 - 0.52\,SO_2 + 1.003\,NO_x + 0.0002\,SO_2{}^2 - 0.005\,NO_x{}^2 + 0.04\,SO_2 \cdot NO_x$	
$Y_3 = 4.51 + 1.11\,NO_x + 16.59\,WS - 0.004\,NO_x{}^2 - 3.64\,WS^2 - 0.11\,NO_x \cdot WS$	
$Y_4 = [-1.05 + 0.0004\,NO_x + 0.0021\,AP] \cdot 10^4$	
$Y_5 = 0.27 + 0.94\,Y_1 + 0.05\,Y_3 - 0.06\,Y_1{}^2 - 0.05\,Y_3{}^2 + 0.11\,Y_1 \cdot Y_3$	
$Y_6 = 7.03 - 0.52\,Y_2 + 1.17\,Y_4 + 0.006\,Y_2{}^2 - 0.02\,Y_4{}^2 + 0.01\,Y_2 \cdot Y_4$	
$NO_x = -1.08 + 0.45\,Y_5 + 0.59\,Y_6 - 0.01\,Y_5{}^2 - 0.02\,Y_6{}^2 + 0.03\,Y_5 \cdot Y_6$	(9)

Table 6. Prediction of NO_x for station B, C and D station's by using (PM_{10}, SO_2, T, WD, WS, RH and AP) input parameters of station A

Station	Machine learning techniques											
	Linear regression			Random forest regression			MLP regression			GMDH regression		
	R^2	RMSE	MAE	R^2	RMSE	MAE	R^2	RMSE	MAE	R^2	RMSE	MAE
B	0.49	18.58	9.01	0.54	17.64	9.68	0.50	18.27	10.19	0.80	10.88	7.31
C	0.17	16.04	9.71	0.23	15.50	9.63	0.16	16.14	10.16	0.48	13.69	8.51
D	0.34	43.38	32.45	0.38	41.91	29.35	0.20	47.62	35.10	0.71	35.90	26.13

neural network has higher R^2 values; 0.80, 0.48 and 0.71 for stations B, C, and D compared to other methods, respectively. Therefore, empirical models for prediction of NO_X were obtained via GMDH-type neural networks.

The GMDH-type neural network model designed for the prediction of NO_X values at station B using station A data (not including NO_x) and the regression fit line of this model are shown in Figure 7. In the double hidden

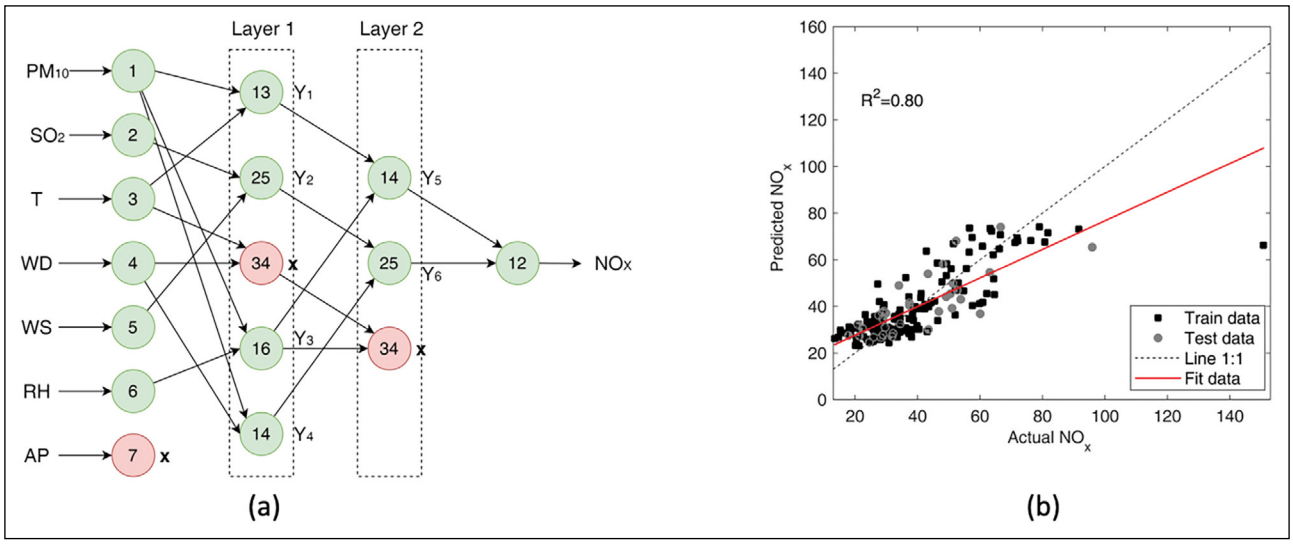

Figure 7. The prediction of NO_X in station B without NO_X of station A. **(a)** structure of double hidden GMDH layers; **(b)** actual and predicted NO_X by GMDH model.

Table 7. Parameters and coefficients used in neuron equations for the prediction of NO_X in station B without NO_X of station A

Equation	No.
$Y_1 = 13.51 + 1.47\,PM_{10} + 0.28\,T - 0.003\,PM_{10}{}^2 + 0.01\,T^2 - 0.06\,PM_{10} \cdot T$	
$Y_2 = 49.94 + 1.49\,SO_2 - 11.5\,WS - 0.01\,SO_2{}^2 + 0.79\,WS^2 + 0.009\,SO_2 \cdot WS$	
$Y_3 = 307.35 - 1.73\,PM_{10} - 6.48\,RH - 0.0002\,PM_{10}{}^2 + 0.04RH^2 + 0.03\,PM_{10} \cdot RH$	
$Y_4 = 27.84 - 0.16\,PM_{10} + 0.1\,WD - 0.005\,PM_{10}{}^2 - 0.0008\,WD^2 + 0.007\,PM_{10} \cdot WD$	
$Y_5 = -1.58 + 1.12\,Y_1 - 0.1\,Y_3 - 0.01\,Y_1{}^2 - 0.007\,Y_3{}^2 + 0.02\,Y_1 \cdot Y_3$	
$Y_6 = 1.61 + 1.42\,Y_2 - 0.5\,Y_4 + 0.003\,Y_2{}^2 + 0.01\,Y_4{}^2 - 0.02\,Y_2 \cdot Y_4$	
$NO_x = -13.96 + 0.82\,Y_5 + 0.8\,Y_6 - 0.02\,Y_5{}^2 - 0.02\,Y_6{}^2 + 0.04\,Y_5 \cdot Y_6$	(10)

layer model shown in Figure 7a, the AP input parameter was not used because it increases the error between the predicted and actual NO_X values. The T and WD polynomial pair output was not used in the first hidden layer. In the second hidden layer, as they may pose an adverse effect on NO_x prediction, the polynomial pair output and the polynomial output formed by the Y_3 output were not used.

The NO_x prediction of station B is modelled in terms of polynomial function by using the optimal neuron outputs and the data fit line is shown in Figure 7b. The equations of the model obtained by using the optimal neuron outputs of the GMDH-type neural network, are given in Table 7. And the network structure was demonstrated in Figure 7a. As a result, Eq. (10) is obtained for the case that the neuron outputs are used as polynomial pairs in the NO_X prediction model of station B.

The results show that the predicted NO_x output at stations B, C and D varies depending on the distance and direction from the source station A. The stations B, C and D are located 21, 23 and 54 km from source station A, respectively. The correlation coefficient R^2 of the GMDH model proposed for stations B, C and D is 0.85, 0.54 and 0.65, respectively when source station A NO_x parameter is used. The station B, which is closest to the source station, has the highest correlation coefficient. Similarly, when the source station A station NO_x parameter is not used, the correlation coefficient R^2 of the GMDH model proposed for the stations B, C and D is 0.80, 0.48 and 0.71, respectively (prediction accuracy negatively affected for station D). Although the station D is at the farthest distance from source station A, the correlation coefficient results of the prediction model are higher than station C. That can be interpreted to the influence of local air pollution sources (point and/or linear

sources like industry and traffic) on measured NOX values rather than the level of effect ascribed to near surrounding environment. In order to carry out an ascendant evaluation and sort out such entangled issues, air pollution trajectory and dispersion model and their outputs can be used as helpful tools and useful source of information for specific periods of time [4, 36].

The developed model provided prediction of NO_x within a certain station by using data from a total number of four different weather stations and taking one station as reference. For the specific cases of NO_x prediction within a station and across different stations, the GMDH like neural network model results have been increased as a means of enhancing accuracy and minimizing error rates (lower error rates obtained).

CONCLUSIONS

This study presents a case study of application of machine learning algorithms to predict NO_X concentrations using both air pollution and meteorological parameters. To accurately predict the NO_X parameter, data of a certain station and across different stations were compiled and new models were derived. The GMDH model produced a precise prediction of NO_X within stations and across stations (station to station) with/without using NO_X as the model input variable. The key findings can be emphasized below:

(1) The results show that meteorological parameters significantly affect the NO_X air pollution parameter and that the effects of meteorological parameters change with distance between stations.

(2) The proposed empirical models provide a rapid assessment of air quality and the prediction of NO_X with an acceptable range of accuracy (R^2={0.94, 0.85, 0.80} within station A, B via source station data and B via source station not including NO_X).

(3) Results obtained through GMDH models exhibit a high degree of accuracy for NO_X prediction values and significantly outperform conventional methods. The proposed model provides the opportunity to evaluate the effect of each input parameter on the model output. It has been observed that relative humidity (RH) increases the error rate and is disabled in the derivation of empirical models.

(4) The proposed GMDH-type neural network model uses air pollution parameters (PM_{10} and SO_2) and meteorological parameters (T, WD, WS, RH and AP) as inputs to estimate NO_X air pollution values.

(5) The obtained model is region specific, but for a wide range of spatial representations and validity, data can be gathered from multiple stations at certain distance.

(6) As a future scope, GMDH-type neural network and proposed approach can be used to support decision makers and engineers in planning stages including but not limited to optimization of total number and spatial distribution of AQMS to be set-up in a specific region.

DATA AVAILABILITY STATEMENT

The authors confirm that the data that supports the findings of this study are available within the article. Raw data that support the finding of this study are available from the corresponding author, upon reasonable request.

CONFLICT OF INTEREST

The authors declared no potential conflicts of interest with respect to the research, authorship, and/or publication of this article.

ETHICS

There are no ethical issues with the publication of this manuscript.

REFERENCES

[1] Y. Dokuz, A. Bozdağ, and B. Gökçek, "Use of machine learning methods for estimation and spatial distribution of air quality parameters," Nigde Omer Halisdemir University Journal of Engineering Sciences, Vol. 9, pp. 37–47, 2020. (in Turkish)

[2] S.M. Cabaneros, J.K. Calautit, and B.R. Hughes, A review of artificial neural network models for ambient air pollution prediction, Environmental Modelling & Software, Vol. 119, pp. 285–304, 2019. [CrossRef]

[3] A. Yakın, and R. Behçet, "Effect of different types of fuels tested in a gasoline engine on engine performance and emissions," International Journal of Hydrogen Energy, Vol. 46, pp. 33325–33338, 2021. [CrossRef]

[4] H. Zhang, Y. Wang, J. Hu, Q. Ying, and X.M. Hu, "Relationships between meteorological parameters and criteria air pollutants in three megacities in China," Environment Reseach Vol. 140, pp. 242–254, 2015. [CrossRef]

[5] H.K. Elminir, "Dependence of urban air pollutants on meteorology," Science of the Total Environment, Vol. 350, pp. 225–237, 2005. [CrossRef]

[6] E. Demirci, and B. Cuhadaroglu, "Statistical analysis of wind circulation and air pollution in urban Trabzon," Energy Building, Vol. 31, pp. 49–53, 2000. [CrossRef]

[7] S. Munir, M. Mayfield, D. Coca, S.A. Jubb, and O. Osammor, "Analysing the performance of low-cost air quality sensors, their drivers, relative benefits and calibration in cities—a case study in Sheffield," Environmental Monitoring and Assessment, Vol. 191, Article 94, 2019. [CrossRef]

[8] N. Castell, F.R. Dauge, P. Schneider, M. Vogt, U. Lerner, B. Fishbain, D. Broday, and A. Bartonova, "Can commercial low-cost sensor platforms contribute to air quality monitoring and exposure estimates?," Environment International, Vol. 99 pp. 293–302, 2017. [CrossRef]

[9] M. Castelli, F.M. Clemente, A. Popovič, S. Silva, and L. Vanneschi, "A machine learning approach to predict air quality in California," Complexity, Vol. 2020, Article 8049504, 2020. [CrossRef]

[10] K. Prasad, and A.K. Gorai, P. "Goyal, Development of ANFIS models for air quality forecasting and input optimization for reducing the computational cost and time," Atmospheric Environment, Vol. 128, pp. 246–262, 2016. [CrossRef]

[11] N. Liu, X. Liu, R. Jayaratne, and L. Morawska, "A study on extending the use of air quality monitor data via deep learning techniques," Journal of Cleaner Production, Vol. 274, Article 122956, 2020. [CrossRef]

[12] R. Dongol, "Evaluation of the usability of low-cost sensors for public air quality information," [Unpublished Master Thesis], Universitetet I Oslo Department of Informatics Programming and Networks, 2015.

[13] H. Maleki, A. Sorooshian, G. Goudarzi, Z. Baboli, Y. Tahmasebi Birgani, and M. Rahmati, "Air pollution prediction by using an artificial neural network model," Clean Technologies and Environmental Policy, Vol. 21, pp. 1341–1352, 2019. [CrossRef]

[14] S.R. Shams, A. Jahani, S. Kalantary, M. Moeinaddini, and N. Khorasani, "Artificial intelligence accuracy assessment in NO2 concentration forecasting of metropolises air," Scientific Reports, Vol. 11, pp. 1–9, 2021. [CrossRef]

[15] J. Xu, Y. Xu, H. Wang, C. Guo, H. Qiu, Y. He, Y. Zhang, X. Li, and W. Meng, "Occurrence of antibiotics and antibiotic resistance genes in a sewage treatment plant and its effluent-receiving river," Chemosphere, Vol. 119, pp. 1379–1385, 2015. [CrossRef]

[16] U. Pak, J. Ma, U. Ryu, K. Ryom, U. Juhyok, K. Pak, and C. Pak, "Deep learning-based PM2.5 prediction considering the spatiotemporal correlations: A case study of Beijing, China," Science of the Total Environment, Vol. 699, Article 133561, 2020. [CrossRef]

[17] H.K. Cigizoglu, K. Alp, and M. Kömürcü, "Estimation of air pollution parameters using artificial neural networks," Advances in Air Pollution Modeling for Environmental Security, pp. 63–75, 2005. [CrossRef]

[18] A. Alimissis, K. Philippopoulos, C.G. Tzanis, and D. Deligiorgi, "Spatial estimation of urban air pollution with the use of artificial neural network models", Atmospheric Environment, Vol. 191, pp. 205–213, 2018. [CrossRef]

[19] F. Kunt, Z.C. Ayturan, and S. Dursun, "Used some modelling applications in air pollution estimates," Journal of International Environment Applied Science Vol. 11, pp. 418–425, 2016.

[20] Y.A. Ayturan, Z.C. Ayturan, H.O. Altun, C. Kongoli, F.D. Tuncez, S. Dursun, and A. Ozturk, "Short-term prediction of pm2.5 pollution with deep learning methods," Global Nest Journal, Vol. 22, pp. 126–131, 2020.

[21] M. Krishan, S. Jha, J. Das, A. Singh, M.K. Goyal, and C. Sekar, "Air quality modelling using long short-term memory (LSTM) over NCT-Delhi, India," Air Quality, Atmosphere & Health Vol. 12, 899–908, 2019. [CrossRef]

[22] G. Varol, B. Tokuç, S. Ozkaya, and Ç. Çağlayan, "Air quality and preventable deaths in Tekirdağ, Turkey," Air Quality, Atmosphere & Health, Vol. 14, pp. 843–853, 2021. [CrossRef]

[23] Thrace Development Agency, Thrace Region Plan (Rep.), 2019. Available at: https://www.trakya-ka.org.tr/upload/Node/33264/xfiles/trakya_bolge_%0Aplani_2014-2023.pdf. Accessed on Feb 2022, 06.

[24] A. Vardar, R. Okursoy, and Y. Tekin, "Local wind characteristics for east Thrace, Turkey," Energy Sources, Part B: Economics, Planning, and Policy, Vol. 7, pp. 1–9, 2012. [CrossRef]

[25] A. Liaw, and M. Wiener, "Classification and regres-sion by random forest," R News, Vol. 2, pp. 18–22, 2002.

[26] F. Murtagh, "Multilayer perceptrons for classification and regression," Neurocomputing, Vol. 2, 183–197, 1991. [CrossRef]

[27] T. Kondo, "GMDH neural network algorithm using the heuristic self-organization method and its application to the pattern identification problem," In Proceedings of the 37th SICE Annual Conference. International Session Papers, IEEE, pp. 1143–1148, 1998.

[28] S.-K. Oh, and W. Pedrycz, "The design of self-organizing polynomial neural networks," Information Sciences, Vol. 141, pp. 237–258, 2002. [CrossRef]

[29] S.J. Farlow, "Self-organizing methods in modeling: GMDH type algorithms," CRC Press, Florida, 2020. [CrossRef]

[30] J. Ma, Y. Ding, J.C.P. Cheng, F. Jiang, and Z. Wan, "A temporal-spatial interpolation and extrapolation method based on geographic Long Short-Term Memory neural network for PM2," Journal of Cleaner Production, Vol. 237, Article 117729, 2019. [CrossRef]

[31] Ö. Akyürek, O. Arslan, ve A. Karademir, "SO2eV PM10 hava kirliliği parametrelerinin CBS ile konumsal analizi: Kocaeli örneği, TMMOB Coğrafi Bilgi Sistemleri Kongresi, Cilt 12, 2013.

[32] M. Savic, I. Mihajlovic, and Z. Zivkovic, "An anfis–based air quality model for prediction of SO2 concentration in urban area," Serbian Journal of Management, Vol. 8, pp. 25–38, 2013. [CrossRef]

[33] A.B. Chelani, C.V.C. Rao, K.M. Phadke, and M.Z. Hasan, "Prediction of sulphur dioxide concentration using artificial neural networks," Environmental Modelling & Software, Vol. 17, pp. 159–166, 2002. [CrossRef]

[34] G. Asadollahfardi, H. Zangooei, and S.H. Aria, "Predicting PM 2.5 concentrations using artificial neural networks and markov chain, a case study Karaj City," Asian Journal of Atmospheric Environment, Vol. 10 pp. 67–79, 2016. [CrossRef]

[35] L. Rafati, M. Ehrampoush, A. Talebi, and M. Mokhtari, Z. Kheradpisheh, H. Dehghan, "Modelling the formation of Ozone in the air by using Adaptive Neuro-Fuzzy Inference System (ANFIS) (Case study: city of Yazd, Iran)," Desert, Vol. 19, pp. 131–135, 2014.

[36] S. Teixeira, P. Pereira, and F. Ferreira, "Co-creating data based on human nose perceptions to study odour nuisance from an oilseed industry," 16th International Conference on Environmental Science and Technology, 2019.

Environ Res Tec, Vol. 5, Issue. 1, pp. 72–83, March 2022

Environmental Research and Technology
https://ert.yildiz.edu.tr - https://dergipark.org.tr/tr/pub/ert
DOI: https://doi.org/10.35208/ert.973270

Environmental Research & Technology

Research Article

Morphogenesis, physico-chemical properties, mineralogical composition and nature of parent materials of some alluvial soils of the Lower Niger River plain, Nigeria

Achimota DICKSON[1], Joseph ARULEBA[2], Joseph Oyinbrakemi TATE[*1]

[1]Department of Soil Science, Niger Delta University Faculty of Agriculture, Yenagoa, Bayelsa State, Nigeria
[2]Department of Soil Science, Ekiti State University, Ado Ekiti, Ekiti State, Nigeria

ARTICLE INFO

Article history
Received: 13 August 2021
Revised: 08 January 2022
Accepted: 31 January 2022

Key words:
Floodplain soils; Lower niger river; Mineralogical composition; Morphogenesis; Soil characteristics

ABSTRACT

Nine pedons of alluvial origin in the Lower Niger River floodplains of Nigeria were examined for morphogenesis, physicochemical properties, mineralogical composition, and heterogeneity of the parent materials. The soils were stratified with redoximorphic features observed in the different layers reaching A-horizon with subsurface grayization. Soils that received annual alluvial enrichment were found to be structurally weak while others were moderately strong. Soil characteristics showed varying degrees of heterogeneity with source of parent materials and degrees of hydromorphism, moulding morphogenesis and gleization as major soil-forming processes. Silt loam was the predominant soil texture except ELM3 and TFN3 dominated by sandy loam and loamy sand textures. Soils were strongly acid to neutral [pH (H_2O), 4.94–7.00], having very low to medium organic matter (0.13–4.02 %), and low to very high K (0.1–2.13 cmol kg^{-1}). Quartz dominated the identified mineral phases followed by kaolinite, indicating the dominance of low activity clays and low ferromagnesian minerals presence. The presence of several K-bearing minerals in the pedons (micas and feldspars) suggest that the K pool could naturally be replenished. Textural diversity between the different SMUs is ascribed to different sources of the water-borne sediments and the flow rate of the floodwater at the time of deposition of the parent materials. Organic carbon distribution patterns indicated stratification and heterogeneity of parent materials. Wetness, flooding, and soil chemical and physical fertility were major constraints to increased and sustainable crop production in the Lower Niger River floodplain soils.

Cite this article as: Dickson A, Aruleba J, Tate JO. Morphogenesis, physico-chemical properties, mineralogical composition and nature of parent materials of some alluvial soils of the Lower Niger River plain, Nigeria. Environ Res Tec 2022;5:1:72–83.

INTRODUCTION

Floodplain soils, worldwide, are very useful for agricultural production as they constitute a huge reserve of available nutrients for utilization by crop plants [1]. The agricultural potentials of alluvial soils however, have not been fully exploited because of lack of understanding of their physical and chemical properties and the changes they undergo under intensive cultivation [2]. For instance, greyish colouration at lower depths have been associated with ground water influence or poor drainage [3, 4] while [5] associated clear and smooth horizon boundaries with some diffuse, wavy,

***Corresponding author.**
*E-mail address: j.o.tate@ndu.edu.ng

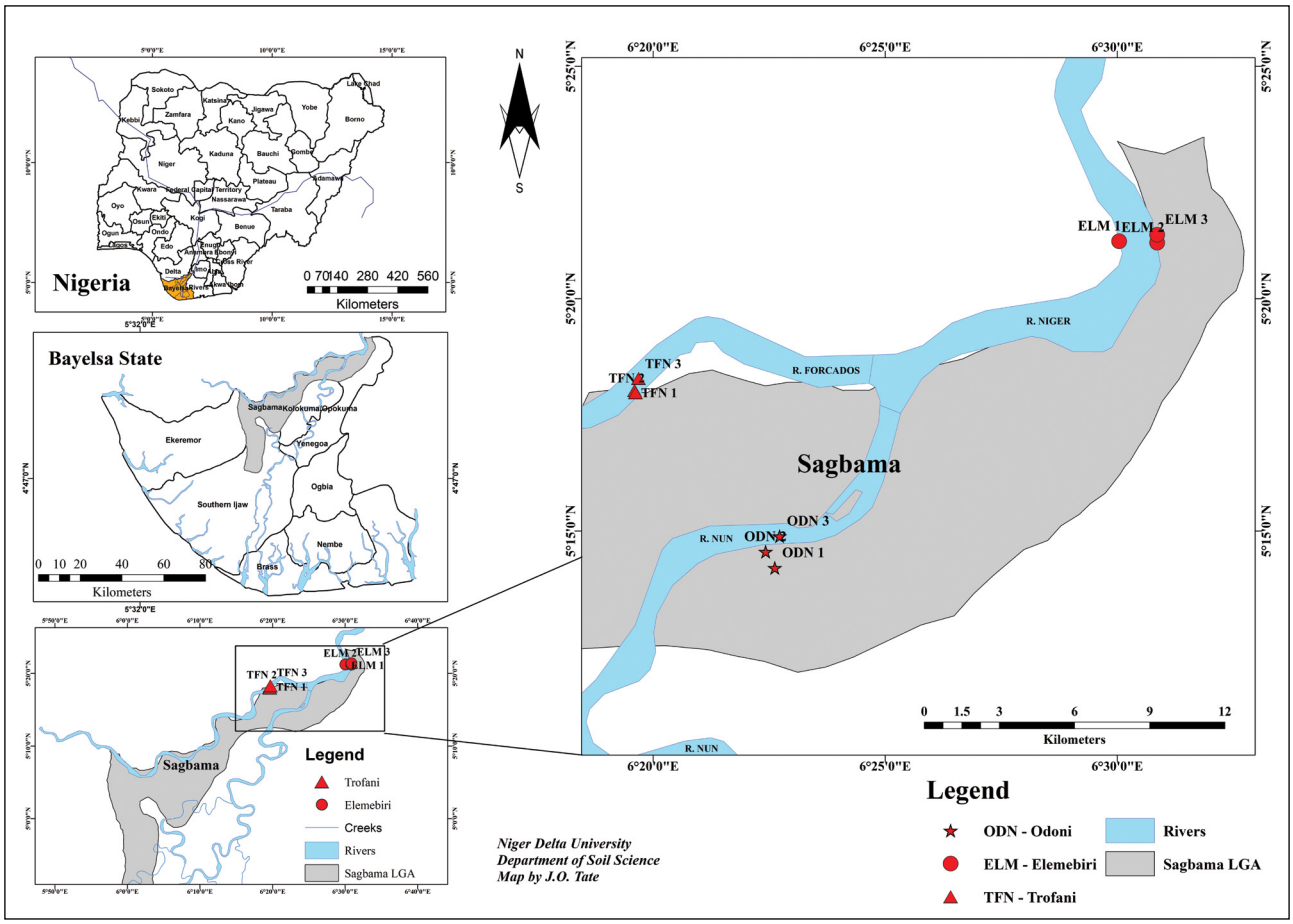

Figure 1. Map showing soil mapping units for the study.

and gradual boundaries to recentness of the soils and young soil development or rejuvenation processes. Two dominant factors appeared to condition kaolinization process under tropical conditions which included composition of the soil solution in the weathering environment and mineralogical composition of the weathering soil or parent rock. However, warm soil temperatures are believed to cause marked dissociation of soil water leading to a build-up of hydrogen ions or lowering of the pH of the soil solution. Under such condition, hydrolytic or H-weathering of silicates to kaolinite progresses rapidly [6]. Texture, organic carbon distribution and clay mineralogy are features commonly used as pointers to the homogeneity or otherwise of the parent materials. Again, the very fine sand and fine sand proportions are used to indicate lithologic discontinuities. Though, it is believed that the floodplain soils of Bayelsa state have high agricultural potentials, current information and knowledge on the dominant soil forming processes, soil characteristics including mineralogical composition, and the homogeneity of parent materials or otherwise are inadequate. For instance, [7] characterization and classification of alluvial soils of the Nun River floodplains did not supply information on the morphogenesis and/or mineralogical status of Bayelsa State soils. Similarly, [8] classification of Ogochie River floodplain soils in Imo State, Nigeria did not provide sufficient morphogenetic information that could be resourceful as an indicator for proper policy formulation by government. Hence, the efficient management of the soils for increase and sustainable crop production is constrained. The situation is further exacerbated by smallholder farmers' poor management practice of low to sub-optimal use of fertilizer inputs [9–11] that neither mitigate the nutrient mining process nor adequately guarantee the restoration of the fertility status [12]. With the present drive of the world towards food security, the state cannot be left behind and government is working towards agricultural intensification in various parts of the state which cannot be achieved with the present level of information and knowledge on the soils. The aim of this study, therefore, is to examine the morphogenetic features, physico-chemical, mineralogical properties and nature of the parent materials of soils of some selected communities earmarked by the Bayelsa State government for agricultural intensification.

MATERIALS AND METHODS

Description of the Study Areas

This study was carried out in Bayelsa State in the Niger Delta region, Southern Nigeria. The study locations lie

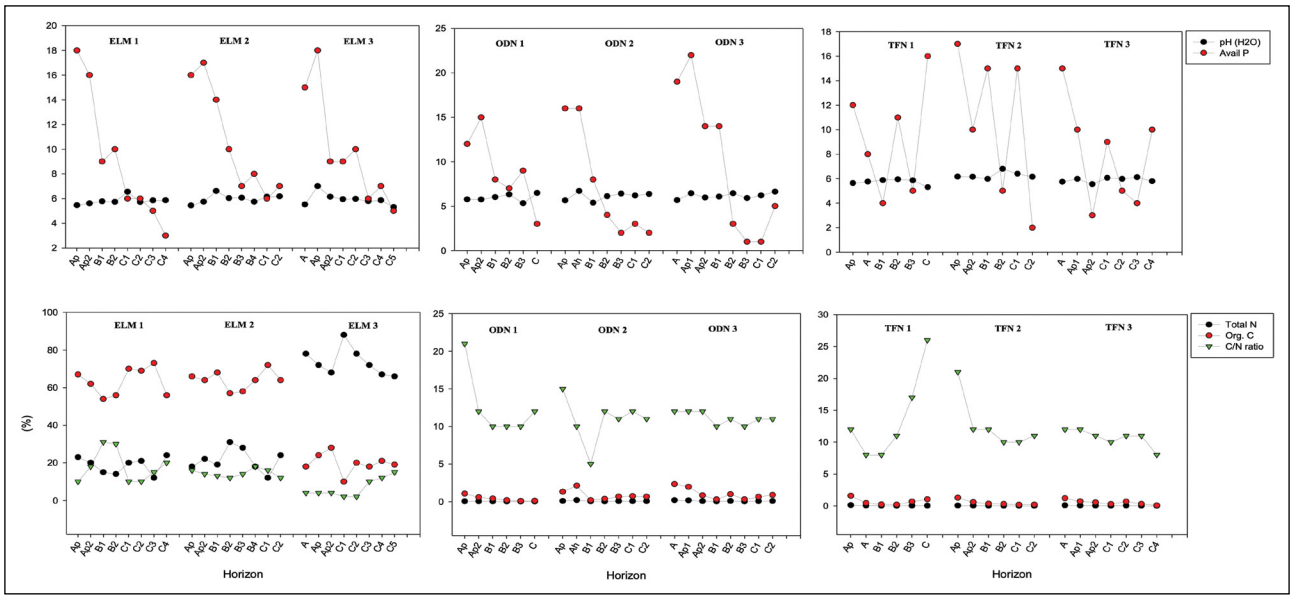

Figure 2. Scattered plot showing the distribution of soil pH, Available P, Total N, Organic C and C/N ratio of Elemebiri, Odoni and Trofani soils.

between latitude 05° 22' 03.9" N and 04° 59' 08.9" N and longitude 006° 30' 21.1" E and 006° 06' 54.1" E. The Niger River traverses Nigeria in a North-western to Southern direction with the attendant sediment load ensuring that the delta platform ends up as flat terrain, making it a unique geologic environment. The Niger River flows southward and breaks up into two- the Forcados and Nun Rivers in Bayelsa State, the Nun River, running north and south down the middle of the Bayelsa State, which remains the most direct tributary of the Niger while Forcados River demarcates the western borders of the state. The Elemebiri community by the Lower Niger River, Odoni by Nun River and Trofani by the Forcados River (Figure 1) were chosen for the study due to the proposed agricultural intensification.

Soil Sampling and Analyses

Following a detailed soil survey conducted on agricultural lands from Elemebiri (ELM), Odoni (ODN) and Trofani (TFN) using rigid grids, the SMUs were examined for morphogenetic features, physico-chemical properties, mineralogical composition and heterogeneity of parent materials. The designation of the soil mapping units (SMUs) were ELM1, ELM2 and ELM3 for Elemebiri, ODN1, ODN2, and ODN3 for Odoni soils and TFN1, TFN2 and TFN3 for Trofani, representing levee crest, levee slope and floodplain, soil profiles described following the procedures prescribed by the USDA Soil Taxonomy [13] and the World Resource Base. Three representative soil pedons were dug per location, one each on the levee crest, levee slope and flood plain or recent alluvial soils in the channel of the present active river. The soils were morphologically described in-situ and samples collected from the different horizons for physico-chemical properties following standard procedures. Using the geographic positioning system (GPS), coordinates of each SMU boundaries and profile pit locations were taken during the field survey. The soil samples collected were air-dried, crushed and sieved to pass through a 2 mm mesh. Soil analyses were carried out in the Green River Project laboratory of the Nigerian Agip Oil Company and Zadell laboratory, Port Harcourt, Nigeria. Standard laboratory methods were used to determine the physical and chemical properties of the soil samples. Soil particle size analysis was determined using [14] method, popularly known as hydrometer method. Soil pH both in water and CaCl2 (1:2 ratio) was determined using glass electrode pH meter and electrical conductivity determined using conductivity meter [15]. Organic carbon was determined using the modified dichromate oxidation method of Walkley-Black as described by [15] and the values obtained multiplied by 1.724 to obtain organic matter, total N was determined using macro-kjeldahl digestion-distillation method as described by [16] and available P by Bray P-1 method [17]. Exchangeable acidity was extracted with 1M KCl and determined by titration with NaOH solution using phenolphthalein indicator [18] and exchangeable Al with 0.01 M HCl [19]. Exchangeable cations were extracted with neutral normal ammonium acetate solution as described by [15] and potassium and sodium in the extract measured by flame photometry and calcium and magnesium by atomic absorption spectrophotometry. Cation exchange capacity (CEC) was by the summation method [20]. The mineralogical study on the clay fraction of the soils was carried out based on random powder analysis using A PANalytical X'Pert Pro instrument (XRD) [21].

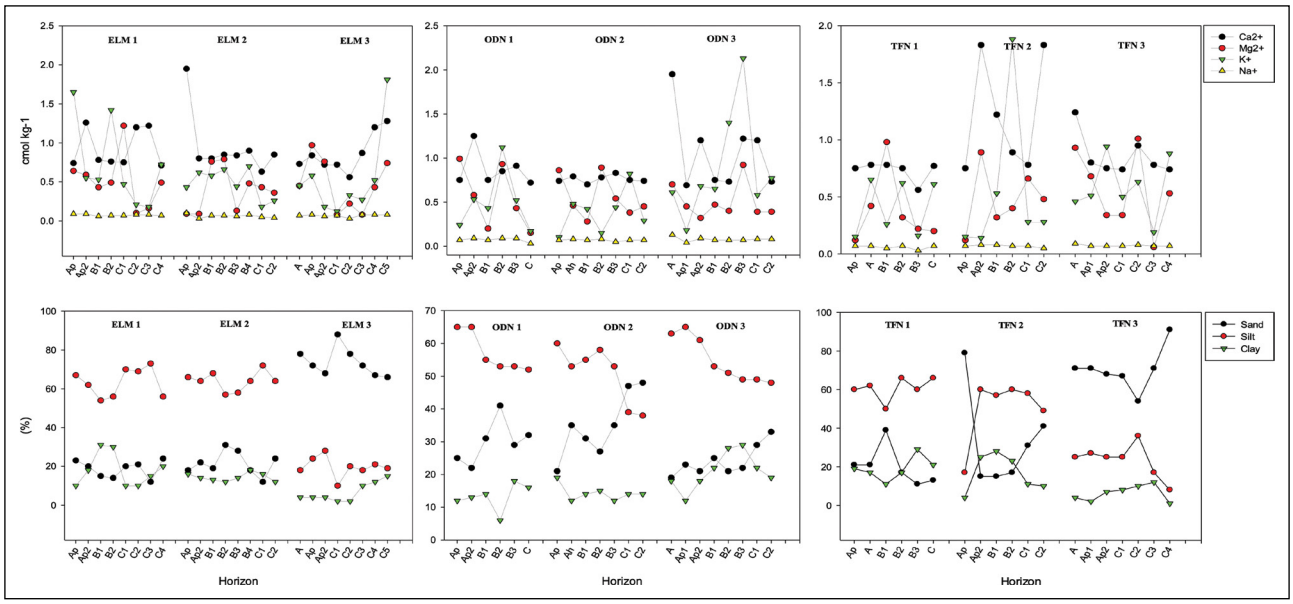

Figure 3. Scattered plot showing the distribution of Exchangeable bases and particle distribution of Elemebiri, Odoni and Trofani soils.

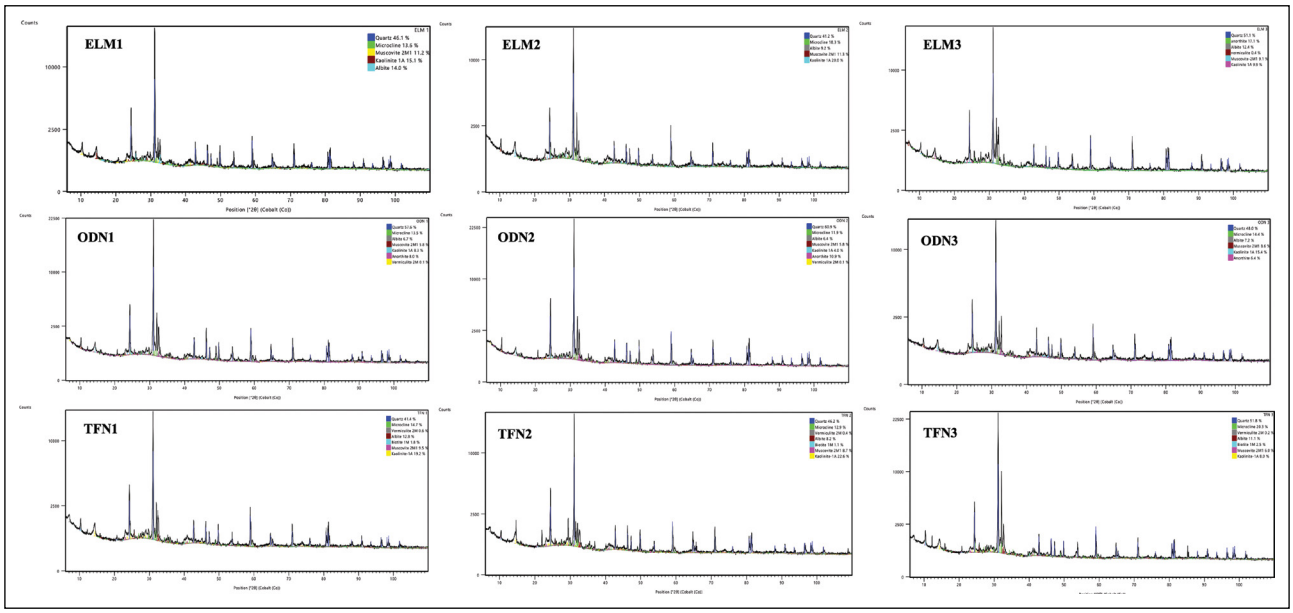

Figure 4. X-ray diffractogram of Elemebiri, Trofani and Odoni soils.

RESULTS AND DISCUSSIONS

Morphological Properties

Morphological characteristics of the Elemebiri, Odoni and Trofani soils are presented on Tables 1, 2, and 3, respectively. The soils were generally deep, no much variation in soil colour as most of the SMUs have Hues of 10 YR except some SMUs in Odoni dominated by hues of 7.5 YR. At the 18–31cm depth of the ELM3, few, medium, distinct 2.5 YR 3/3 mottles were observed and at the 38–69 cm depth of TFN3, many, medium, distinct, 10 YR 3/3 mottles were observed. The zone of water saturation during the flood season was at the soil surface for ELM3, ODN3 and TFN3, about 40 cm from the mineral soil surface for ELM2, ODN2 and TFN2, and at about 118 cm for ELM1, 117cm for ODN1 and 140cm for TFN1 (Tables 1, 2, and 3). All the studied profiles were considered hydromorphic because of the presence of mottles except ELM3 and TFN3. Since there was no perched water table below the 18–31cm depth of ELM3 and the 38–69 cm depth of TFN3, which were the observed mottled layers and no mottles occurred below them, the mottling in these layers was ascribed to

Table 1. Morphological characteristics of the Elemebiri soils and their classification

Horizon	Depth (cm)	Soil colour	Mottles		Texture	Structure	Consistence		Concr.	Boundary
			Colour	Pattern			Moist	Wet		
ELM1 *(Aquic Dystrudepts/Fluvic Cambisol)*										
Ap	0–8	10YR3/2			fsil	Cr to WSAB	fr	Ss, Sp		cs
Ap2	8–21	10YR3/3			fsilcl	WSAB	sfi	Ss, Sp		cs
B1	21–34	10YR3/4			fsilcl	SAB	mfi	Ss, Sp		cs
B2	34–65	10YR3/4			fsil	SAB	mfi	Ss, Sp	C	cs
C1	65–90	10YR4/4			fsil	SAB	sfi	Ss, Sp		cs
C2	90–118	10YR4/4			fsilcl	SAB	sfi	Ss, Sp		cs
C3	118–150	10YR5/4	7.5YR5/6	F2D	fsil	SAB	sfi	Ss, Sp		cs
C4	150–200	10YR5/3	5YR4/6	C2D	fsil	SAB	sfi	Ss, Sp		
ELM2 *(Typic Epiaquepts/Fluvic Cambisol)*										
Ap	0–11	10YR2/2			fsil	Cr to WSAB	fr	ss, sp		cs
Ap2	11–19	10YR3/3			fsilcl	SAB	mfi	ss, sp		cs
B1	19–32	10YR3/2			fsilcl	SAB	mfi	ss, sp		cs
B2	32–42	10YR4/3			fsil	SAB	sfi	ss, sp		cs
B3	42–57	10YR5/3	7.5YR4/3		fsil	SAB	sfi	ss, sp		cs
B4	57–88	10YR5/2	7.5YR3/4	M2D	fsilcl	SAB	sfi	ss, sp		cs
C1	88–106	10YR5/2	7.5YR4/6	M2D	fsil	SAB	sfi	ss, sp		cs
C2	106–190	10YR5/1	7.5YR4/6	M2D	fsil	SAB	sfi	ss, sp		
ELM3 *(Eutric Udifluvents/Haplic-Fluvic Fluvisol)*										
A	0–18	10YR3/6			fsl	Cr	vfr	ns, np		cs
Ap1	18–31	10YR3/3	2.5YR3/3	F2D	fsl	Sg	fr	ns, np		c
Ap2	31–44	10YR6/4	–	–	ls	Sg	fr	ns, np		c
C1	44–68	10YR4/6	–	–	sl	Sg	fr	ns, np		cs
C2	68–81	10YR5/4	–	–	sl	Sg	fr	ns, np		cs
C3	81–123	10YR3/4	–	–	ls	VWSAB	sfr	ns, np		cs
C4	123–160	7.5YR4/4	–	–	ls	SAB	sfr	ns, np		g
C5	160–200	7.5YR2.5/3	–	–	ls	VWSAB	fr	ns, np		

Mottle pattern- The first letter denotes abundance (F=few; C=common; M=many); The center number denotes size (1=fine; 2=medium; 3=coarse); The second letter denotes contrast (D=distinct; P- prominent).; colour: YR=yellowish red; structure: Cr=crumbly, VWSAB=very weak sub angular blocky, WSAB=weak sub angular blocky, SAB=sub angular blocky, crumb=crumbly, sg=single grain; Texture: fsil=fine silt loam, sl=sandy loam, ls=loamy sand, fsl=fine sandy loam, fsicl=fine silty clay loam, Consistence: ns=non sticky, np=non plastic, ss=slightly sticky, sp=slightly plastic, fr=friable, vfr=very friable, sfi=slightly firm; mfi=moderately firm; concretion: c=carbon concretions; boundary: cs=clear smooth; g=gradual; *=all belong to iso-hyperthermic temperature regime.

Table 2. Morphological characteristics of the Odoni soils and their classification

Horizon	Depth (cm)	Soil colour	Mottles		Texture	Structure	Consistence		Concr.	Boundary
			Colour	Pattern			Moist	Wet		
ODN1 *(Humic Dystrudepts/Fluvic Cambisol)*										
Ap	0–23	7.5YR3/2			fsil	VWSAB	sfi	ss, sp	–	cs
Ap2	23–30	7.5YR4/4			fsil	WSAB	sfi	ss, sp	–	cs
B1	30–63	7.5YR4/4			fsil	SAB	mfi	ss, sp	–	dw
B2	63–117	7.5YR4/6			sil	SAB	mfi	ss, sp	–	dw
B3	117–160	7.5YR4/3	5YR4/4	M3D	sil	SAB	mfi	ss, sp	–	dw
C	160–200	7.5YR4/6	5YR4/6	M3P	sil	SAB	mfi	ss, sp	–	
ODN2 *(Typic Epiaquepts/Fluvic Cambisol)*										
Ap	0–20	10YR3/4			fsil	Cr	fr	ns, np	–	cs
A	20–40	10YR5/4			l	WSAB	sfi	ss, sp	–	cs
B1	40–110	10YR5/3	5YR6/4	F2D	sil	SAB	sfi	ss, sp	–	cs
B2	110–141	7.5YR5/4	5YR4/4	M3D	sil	SAB	Sfi	ss, sp	–	dw
B3	141–180	7.5YR5/2	5YR3/4	M3P	sil	SAB	sfi	ss, sp	–	cs
C	180–200	10YR5/1	5YR3/4	M3P	sil	SAB	sfi	ss, sp	–	
ODN3 *(Fluvaquentic Epiaquepts/Fluvic Cambisol)*										
A	0–5	7.5YR3/2			fsil	WSAB	sfi	ss, sp	–	dg
Ap1	5–11	7.5YR4/4	5YR5/3	C2D	sil	WSAB	Sfi	ss, sp	–	dw
Ap2	11–25	7.5YR4/4	5YR6/4	C2D	sil	SAB	sfi	ms, mp	–	dg
B1	25–41	7.5YR6/2	5YR6/1	C2D	sil	SAB	mfi	ms, mp	Fe-Mn	cs
B2	41–48	7.5YR4/4	5YR5/2	C2D	sicl	SAB	mfi	ms, mp	Fe-Mn	cs
B3	48–56	7.5YR5/4	5YR4/4	M3P	cl	SAB	mfi	ms, mp	–	cs
C1	56–122	7.5YR5/6	5YR4/4	M3P	l	SAB	mfi	ms, mp	–	cs
C2	122–200	7.5YR4/6	5YR4/6	M3P	l	SAB	mfi	ms, mp	–	

Mottle pattern- The first letter denotes abundance (F=few; C=common; M=many); The centre number denotes size (1=fine; 2=medium; 3=coarse); The second letter denotes contrast (D=distinct; P- prominent).; colour: YR=yellowish red; structure: Cr=crumbly, VWSAB=very weak sub angular blocky, WSAB=weak sub angular blocky, SAB=sub angular blocky, crumb=crumbly, sg=single grain; Texture: fsil=fine silt loam, sl=sandy loam, ls=loamy sand, fsl=fine sandy loam, fsicl=fine silty clay loam, Consistence: ns=non sticky, np=non plastic, ss=slightly sticky, sp=slightly plastic, fr=friable, vfr=very friable, sfi=slightly firm; mfi=moderately firm; concretion: c=carbon concretions; boundary: cs=clear smooth; g=gradual; *=all belong to iso-hyperthermic temperature regime.

Table 3. Morphological characteristics of Trofani Soils and their classification

Horizon	Depth (cm)	Soil colour	Mottles		Texture	Structure	Consistence		Concr.	Boundary
			Colour	Pattern			Moist	Wet		
TFN1 *(Aquic Dystrudepts/Fluvic Cambisol)*										
Ap	0–14	10YR3/4			fsil	SAB	sfi	ss, sp		cs
A	14–31	10YR3/4			fsil	SAB	sfi	ss, sp		cs
B1	31–55	10YR3/4			fsil	SAB	mfi	ss, sp		cs
B2	55–140	10YR3/6			fsil	SAB	mfi	ss, sp		cs
B3	140–150	10YR4/2	2.5YR3/4	C2D	fsilcl	SAB	mfi	ms, mp	C	cs
C	150–200+	10YR4/4	5YR4/6	M3P	fsil	SAB	mfi	ms, mp		
TFN2 *(Typic Epiaquepts/Fluvic Cambisol)*										
Ap	0–11	7.5YR3/3			fls	Cr	fr	ns, np		cs
Ap2	11–35	10YR4/4			fsil	SAB	sfi	ss, sp	C	cs
B1	35–44	10YR5/2			fsilcl	SAB	mfi	ss, sp		cs
B2	44–70	10YR5/3	5YR5/6	C2D	fsil	SAB	sfi	ss, sp		cs
C1	70–126	10YR5/2	5YR3/3	M3P	fsil	SAB	sfi	ss, sp		dg
C2	126–200+	10YR6/2	5YR3/3	M3P	l	SAB	sfi	ss, sp		
TFN3 *(Aquic Udifluvents/Haplic Fluvisol)*										
A	0–13	10YR3/3			fsl	M	sfi	ss, sp		dw
Ap1	13–23	10YR3/4			sl	Gr	fr	ns, np		dw
Ap2	23–38	10YR5/4			sl	Gr	fr	ns, np		cs
C1	38–52	10YR3/3	10YR3/3	M2D	sl	Gr	fr	ns, np		cs
C2	52–69	10YR4/6	10YR3/3	M2D	sl	Gr	fr	ns, np		cs
C3	69–83	10YR3/3			ls	Sg	l	ns, np		cs
C4	83–200+	10YR6/3			s	Sg	l	ns, np		

Mottle pattern- The first letter denotes abundance (F=few; C=common; M=many); The center number denotes size (1=fine; 2=medium; 3=coarse); The second letter denotes contrast (D=distinct; P- prominent); colour: YR=yellowish red; fil=fine silt loam, fsilcl=fine silty clay loam, l=loam, fsl=fine sandy loam, sl=sandy loam, ls=loamy sand; s=sand; Structure: cr=crumbly, SAB=sub angular blocky, gr=granular, sg=single grain; Consistence=friable, vfr=very friable, l=loose, sfi=slightly firm, mfi=moderately firm; ns=non sticky, np=non plastic, ss=slightly sticky, sp=slightly plastic, ms=moderately plastic, mp=moderately plastic; Concretions: c=carbon; Boundary: cs=clear smooth, dw=diffuse wavy, dg-diffuse gradual.

Table 4. Percentage distribution of clay mineral types in the soil mapping units

SMU	Percentage mineral in the soil									
	Quartz	Kaolinite	Vermiculite	Biotite	Muscovite	Microline	Albite	Anorthite	Chlorite	Zeolite
ELM1	46.1	15.1	nd	nd	11.2	13.6	14	nd	nd	nd
ELM2	41.2	20	nd	nd	11.3	18.3	9.2	nd	nd	nd
ELM3	51.1	9.9	0.4	nd	9.1	nd	12.4	17.1	nd	nd
ODN1	57.6	8.3	0.1	nd	5.8	13.5	6.7	8	nd	nd
ODN2	60.9	4	0.1	nd	5.8	11.9	6.4	10.9	nd	nd
ODN3	48	15.4	nd	nd	8.6	14.4	7.2	6.4	nd	nd
TFN1	41.4	19.2	0.6	1.8	9.5	14.7	12.8	nd	nd	nd
TFN2	46.2	22.6	0.4	1.1	8.7	12.9	8.2	nd	nd	nd
TFN3	51.8	8	0.2	2.5	6	20.3	11.1	nd	nd	nd

nd: Not detectable.

the parent materials of the specific layers which indicated heterogeneity in parent materials of the specific SMUs. No saturation zone was found in any of the profiles during the dry season. All the profiles therefore were considered to be influenced by an annual cycle of wet/dry soil moisture regimes which qualified as 'udic' moisture regimes [13]. The drainage condition of the profiles was dictated by the rainy season and the annual Niger River floods. Subsurface greyization (gleys) was a notable morphometric feature in the levee slope soils (ELM2, ODN2 and TFN2) and ODN3 of the flood plain. Regular decrease of organic carbon down the profiles with hydromorphism within the surface 50 cm was observed for ELM2, ODN2 and TFN2 and within 5 cm for ODN3. The presence of mottles in these soils indicated fluctuation of ground water table while the presence of gleys in the lower horizons of ELM2, ODN2 and TFN2 indicated perennial hydromorphism as noted previously by [5]. Greyish colouration at lower depths is associated with ground water influence or poor drainage [3] and/or such soil layer is subject to groundwater influence in most part of the year [4]. The pedons showed mostly clear and smooth horizon boundaries with some diffuse, wavy, and gradual boundaries, reflecting the recentness of the soils and young soil development or rejuvenation processes [5] and different seasons of deposition of the parent materials. Moreover, no clay movement from A to B horizon was noticed confirming young soil development or rejuvenation processes. Similarly, cutans (clay skins) were absent on ped surfaces as there was no illuvial accumulation of clays in the pedons. The presence of many mica flakes in the profiles corroborated the incipient nature of the soils. Surface and subsurface texture of the SMUs was fairly uniform, dominated by silt loam and silty clay loam except ELM3 and TFN3 dominated by sandy loam and loamy sand. The ELM3 and TFN3 SMUs, of recent alluvial soils in the channels of present active rivers received annual alluvial materials enrichment from the yearly floods and were structurally weak. Structural development in the other SMUs was moderately strong.

Physico-Chemical Properties

The texture of the soils was dominantly silt loam followed by silty clay loam and loam except ELM3 and TFN3, dominated by loamy sand and sandy loam (Figure 3). The dominance of sand in ELM3 and TFN3 (Figure 3) indicated that the SMUs have high infiltration rate and low water holding capacity with possibility of moisture stress during dry months [22, 23]. The clay distribution within ELM1, ELM2, ODN1, ODN2, ODN3, TFN1 and TFN2 SMUs was irregular. Reported [24] irregular distribution of clay within the subsoil of three pedons, characteristic of cambic horizon. Though the distribution of silt/clay ratio was also irregular with depth, silt/clay ratios generally increased with increase in silt content and vice versa. Higher silt/clay ratio in the surface layers reflected annual alluvial enrichment of the surface through deposition by the annual floods. Report [25] indicated that soils with silt/clay ratios below 0.15 indicated that such soils are of old parent material, while those above 0.15 are of young parent materials with low degree of weathering. Recorded [24] silt/clay ratio of <1.00 in Southern Guinea Savanna soils in Nigeria and concluded that the soils have undergone ferralitic pedogenesis. All the SMUs recorded silt/clay ratios far above unity confirming that the soils are young with weatherable minerals and have not gone through ferralitic pedogenesis.

The SMUs were moderately acidic to neutral, pH (water) ranging from 5.31 to 7.00 for Elemebiri soils, 5.33–6.70 for Odoni soils and 5.30–6.80 for Trofani soils, respectively (Figure 2). The pH of the soils generally increased with soil depth due to less H+ ions released from organic matter decomposition as organic matter decreased irregularly (Figure 2) with increase in depth [26]. Reported [27] pH of 6.0 to 7.0 as the optimum pH for most agricultural crops while [28] and [29] gave 5.5 to 7.0 as the preferred range for most crops. Among the SMUs, the surface layers of ELM1 and ELM2 fall below the FAO preferred pH range as reported by [28]. This is an indication that the SMUs need some form

of soil amendments. Attributed [5] increase in soil pH with depth to ferrolysis which is acidification of topsoil caused by continual displacement of bases by ferrous ion during the reduction phase associated with annual flooding. The study area is prone to high rainfall and flooding therefore, there is possibility of ferrolysis. Usually, ΔpH value is used to estimate the presence of negatively charged clay colloids in soils [30]. Positive ΔpH values were obtained for all the soils indicating that the soils were all negatively charged.

Organic matter content of the soils, generally, was low to moderate, ranging from 0.19–3.88%, 0.13–4.02% and 0.37–2.76% for the Elemebiri, Odoni and Trofani soils, respectively (Figure 2). Generally, organic carbon and indeed organic matter levels decreased irregularly with soil depth which agreed with the reports of previous authors in Nigeria [31, 32] and [30] in Ethiopia. Also reported [5] organic C decrease with soil depth for Bangladeshi soils and low organic C content was attributed to rapid decomposition of organic matter under hyperthermic temperature regime. For the soils under consideration, low organic matter concentration was attributed to low biomass return to the soils owing to short fallow periods coupled with the cultural practice of bush burning which destroys organic materials. It is necessary to note that organic matter mineralization rate in the soils is high due to high temperatures and heavy rainfall as the SMUs belong to the iso-hyperthermic soil temperature regime. Low N values was traced to high rate of organic matter decomposition and mineralization as well as leaching, coupled with intermittent flooding and drying which is known to favour N loss through nitrification-denitrification processes [29]. Reported [33] that soils with less than 0.07% total N have limited N mineralization potential, whereas those having values greater than 0.15% would be expected to mineralize sufficient amount of N during the succeeding crop cycle. Based on this, the surface layers of ELM1, ELM2, ODN2, ODN3, TFN1, and TFN3 are likely to have reasonable mineralization potential while the mineralization potential of ELM3, ODN1 and TFN2 was low.

Available P distribution apparently decreased with depth in ELM and ODN with an inconsistent distribution pattern in TFN soils. Available P concentration in ELM and ODN agreed with the results of [34] in a study of soils along a toposequence in Ethiopia that reported available P showing an increasing trend down topographic position and a decreasing trend with depth which they attributed to increase in clay content and decrease in soil organic matter content. Whilst the inconsistency in distribution of available P in TFN with an expected distribution pattern of organic matter in the same SMU, the result, however, could be attributed to the differences in source of parent material. Similar variations were observed in ELM soils where organic matter was seen to be inconsistent with available P distribution. Moreover, the distribution of P within the profiles showed no regular pattern of decrease which agreed with the findings of [35]. This could be due to P fixing capacity and the slow release by the soils as a result of the relatively high level of iron and aluminum oxides in the soils. Low P availability in tropical soils can as well be attributed to the nature of the chemical forms of soil P and the high content of oxides of Fe and Al which are associated with high P fixation.

Exchangeable K varied from 0.18–1.81 cmol kg^{-1} in Elemebiri, 0.10–2.13 cmol kg^{-1} in Odoni and 0.14–1.88 cmol kg^{-1} in the Trofani soils (Figure 3). Also, the ECEC values were low, ranging from 1.49–6.11 cmol kg^{-1} in Elemebiri soils, 2.47–8.06 cmol kg^{-1} in Odoni soils, and 2.79–6.37 cmol kg^{-1} in Trofani Exchangeable Ca^{2+} dominated the exchange complex of the SMUs followed by Mg^{2+}. Cation ratios are helpful in identifying soil structural problems. In the SMUs, Ca^{2+}/Mg^{2+} ratio of most of the layers was above unity. Reported [5] Ca^{2+}/Mg^{2+} ratios of less than unity in Bangladeshi soils, attributing this development to loss of Ca^{2+} due to gleization. Reported [26] that Ca^{2+}/Mg^{2+} ratio in soils decreases with increasing maturity. The low Ca^{2+}/Mg^{2+} ratios recorded in the SMUs was rather ascribed to the inherently low concentration of ferromagnesian minerals that supply Ca and to a lesser extent, possible loss of Ca by gleization as noted previously by [5]. Low exchangeable bases in soils (Ca, Mg, K and Na) have been attributed to acidifying properties of organic matter, high aluminium concentration and leaching loss of exchangeable bases [36]. The low exchangeable Ca and Mg in these soils was attributed to the inherently low concentration of ferromagnesian minerals, low nutrient retentive capacity, high exchangeable Al and leaching losses due to the high rainfall. Based on the categorisation of [28], it is obvious that K in most layers of the pedons was medium to very high.

The exchange acidity of 45% of the soils was 2.0 cmol kg^{-1} and above suggesting that 45% of the soils were slightly to strongly acidic [8], Odoni soils having higher total exchange acidity.

MINERALOGICAL COMPOSITION

Table 4 shows the variation in the composition of clay mineral assemblage in the pedons. Ten different mineral phases were identified in the nine locations, kaolinite, quartz, muscovite ($KAl_2(AlSi_3O_{10})(OH,F)_2$ and albite ($NaAlSi_3O_8$) identified in all the locations. Quartz was the dominant mineral in the locations while kaolinite was easily detectable and dominated the clay fraction. Microline was detected in all the locations except ELM3. The occurrence of vermiculite and biotite was low, vermiculite, detected only in ELM1, ELM2 and ODN3 and biotite, in Trofani soils (TFN1, TFN2 and TFN3) only. The X-ray diffractograms of the pedons are presented in Figure 4. The dominance of silt-sized quartz fraction in the clay mineral assemblage further confirmed the assertion that the soils were recent in origin. Kaolinite, muscovite, microline ($KAlSi_3O_8$) and albite of the

plagioclase group were also prominent (Table 4). Anorthite [Ca $(Al_2Si_2)O_8$], another mineral of the plagioclase group was present in ELM3 out of the nine locations. There was also vermiculite, an interstratified clay mineral, present in six (ELM3, ODN1, ODN2, TFN1, TFN2, and TFN3) SMUs though not in large quantities and biotite [$K(Mg.Fe)_2(AlSi_2O_{10})(OH,F)_2$] in TFN1, TFN2, and TFN3. These findings corroborate an earlier report by [37]. It was further reported that kaolinite, quartz, mica, vermiculite and interstratified or mixed layer silicates were present in the clay fractions of Mbiama-Kaiama soils of the same meander belts region of Bayelsa State. Similarly [38], identified quartz, kaolinite, illite, smectite, vermiculite and interstratified types as common minerals in the silt-clay fraction of floodplain soils in Kogi State. In the [39] characterization of clays in Odukpani, South-eastern Nigeria reported that Kaolinite is the dominant clay mineral.

Another major observation in the clay mineralogy of the soils was the near absence of ferromagnesian minerals in the soils. The only minerals of the ferromagnesian family were vermiculite and biotite (Table 4) whose quantities were low. This may account for the low levels of basic cations such as Mg and Ca in the soils. Consequently, Mg:K ratio in the soils was low which placed most of the pedons in the marginally suitable class for oil palm production. However, the presence of several K bearing minerals in the pedons such as the micas (biotite and muscovite) and the feldspars suggest that the K pool in the pedons could naturally be replenished. This agreed with the medium to high K concentration results recorded in most of the pedons.

Among the silicate clay minerals, kaolinite was dominant (Table 4) which agreed with findings of [39]. Kaolinization, therefore, is the dominant clay forming process in these pedons hence the dominance of kaolinite among silicate clays in all the pedons. Vermiculite and biotite, the only ferromagnesian minerals detected were low and were not detected in most of the pedons which could be evidence that parent materials are heterogenous. The near absence of ferromagnesian minerals in the clay mineralogical composition of the soils and the dominance of kaolinite implied that the soils are dominated by low activity clays (LAC) and can easily be eroded. Consequently, split application of recommended fertilizers rates is suggested to avert leaching loss of nutrients when applying fertilizer. In addition, cultural practices such as bush burning that destroy soil organic matter should be avoided to maintain organic matter levels in the soils.

Soil Properties and Nature of the Parent Materials

Texture (Figure 3), organic carbon distribution (Figure 2) and clay mineralogy (Table 4 and Figure 4) are features commonly used as indicators of the homogeneity or otherwise of the parent materials. The very fine sand and fine sand proportions are used to indicate lithologic discontinuities within individual soil profiles because these two size fractions form the greatest percentage of the sand fraction, and are assumed to be made up of quartz and other resistant primary minerals. Though sand was not separated into fine, medium and coarse in this study, the distribution pattern of sand in some of the SMUs presented a lot about the parent materials. Figure 3 indicated significant change and differences in the distribution pattern of sand in the different horizons of ELM3, ODN1, ODN2, TFN2, TFN3, and to a lesser extent, ODN3 and TFN1. Similar observation was made in the distributional pattern of silt and in particular clay in the soils. The textural diversity observed between the different SMUs was ascribed to differences in the sources of the water-borne sediments and flow rate of the flood water at the time of deposition of the parent materials. Whereas the parent materials of ELM3 and TFN3 were deposited during the period of high flood as they are recent alluvial soils from the channels of present active Niger and Forcados Rivers and dominantly constituted by sand-sized particles (sandy loam, loamy sand and sand), other profiles were dominated by silt loam, silty clay loam and loam. The finer soil particles, in suspension, probably were transported for longer period of time over greater distances and deposited at low flood period when there was less turbulence than the case of ELM3 and TFN3, deposited during the high flood water under high current. Reported [24] higher amount of silt in JG3 profile of Southern Guinea Savannah of Nigeria and linked it to the seasonal depositional effect of the seasonal stream and the Suleja water reservoir inundating the JG3 area. The 0–11 cm layer of ELM2 seems to be of different parent material from the rest of the horizons as the proportion of sand in this layer was 79% as compared to other horizons with 40% or less sand. The high concentration of sand in this layer cannot be ascribed to clay eluviation or surface erosion. The dominance of sand in the two bottom layers of ODN2 also showed that these layers were of different parent material (Figure 3).

Organic carbon distribution pattern in the soils (Figure 2) indicated stratification. Irregular decrease in organic matter content with depth was consistent with the properties of fluvents [13]. The organic C distribution pattern in ELM1, ELM2, ELM3, ODN2, ODN3, TFN1, TFN2 and TFN3 did not suggest uniform parent materials with the observed abrupt increase in organic C in some horizons down the profile of some SMUs. As shown on Figure 2, organic C abruptly increased from 0.7% in the 90–118 cm layer to 1.07% in the 150–200 cm layer of ELM1, 0.11% in the 42–57 cm layer to 0.16% in the 88–106 cm layer of ELM2, 0.2% in the 21–37 cm layer to 0.73% in the 79–149 cm layer of ODN2, 0.31% in the 25–41 cm layer to 0.99% in the 41–48 cm layer and 0.31% in the 48–56 cm layer to 0.86% in the 122–200 cm layer of ODN3, 0.21% in the 55–140 cm layer to 1.04% in the 150–200 cm layer of TFN2 and 0.30% in the 38–52 cm layer to 0.68% in the 52–69 cm layer of TFN3 which probably indicated heterogeneity.

CONCLUSIONS

The floodplain soils of the Lower Niger River and the two major tributaries (Nun and Forcados) showed some degree of differences in morphological, physical, chemical and mineralogical characteristics, as well as heterogeneity of parent materials. The source of parent materials and degree of hydromorphism, being the major factors moulding morphogenesis. Parent materials were of mixed origin and the soils were at an initial stage of development. Seasonal inundation by the flood water and dryness in the dry season set the stage for alternate oxidation and reduction, providing the most distinguishing feature of the pedochemical environment. Subsurface grayization was a notable morphometric feature and gleization, a major soil forming process. The SMUs were dominated by quartz and low activity clays, kaolinization, being the dominant clay mineral forming process. The study, however, found out that flooding, wetness and soil fertility are major constraints to agricultural intensification that must be addressed should government desire achievable results for sustainable crop production. The findings therefore, provides a robust and reliable guide for the Bayelsa State government to draw effective agricultural policies not only for sustainable crop production ventures within these affected areas but for the state at large as soils of the entire state are likely to have similar parent materials. Further morphological and mineralogical studies are therefore recommended on a larger scale so as to provide both State and the Federal governments the needed information for proper agricultural intensification programmes.

DATA AVAILABILITY STATEMENT

The authors confirm that the data that supports the findings of this study are available within the article. Raw data that support the finding of this study are available from the corresponding author, upon reasonable request.

CONFLICT OF INTEREST

The authors declared no potential conflicts of interest with respect to the research, authorship, and/or publication of this article.

ETHICS

There are no ethical issues with the publication of this manuscript.

REFERENCES

[1] A. U. Akpan-Idiok and P. O. Ogbaji, "Characterization and classification of Onwu River floodplain soils in Cross River State, Nigeria," International Journal of Agricultural Research, Vol. 8, pp. 107–122, 2013. [CrossRef]

[2] G. S. Effiong and T. O. Ibia, "Characteristics and constraints of some river flood plains soils to crop production in Southeastern Nigeria," Agricultural Journal, Vol. 4, pp. 103–108, 2009.

[3] I. Esu, "Soil characterization, classification and survey," HEBN Publishers Plc, Lagos, 2010.

[4] M. M. Hossain, Z. H. Kpan, M. S. Hussain and A. R. Mazumder, "Characterisation and classification of some intensively cultivated soils from the Ganges river floodplain of Bangladesh," Dhaka University Journal of Biological Sciences, Vol. 20, pp. 71–80, 2011. [CrossRef]

[5] Z. H. Khan, M. S. Hussain and F. Ottner, "Morphogenesis of three surface water gley soils from the megna floodplain of Bangledesh," Dhaka University Journal of Biological Sciences, Vol. 21, pp. 17–27, 2012. [CrossRef]

[6] A. Ojanuga, "Clay mineralogy of soils in the nigerian tropical savanna regions," Soil Science Society of America Journal, Vol. 43, pp. 1237–1242, 1979. [CrossRef]

[7] A. A. Dickson, J. O. Kamalu, O. J. Tate and P. T. Ogboin, "Characterization and classification of some Alluvial soils of the Lower Niger River floodplains in Bayelsa State, Nigeria," Bulgarian Journal of Soil Science Agrochemisty and Ecology, Vol. 55, pp. 45-62, 2021.

[8] C. I. Ernest and E. U. J. Onweremadu, "Classification of soils along Ogochie River Floodplain in Niger-Okpala, Imo State,Southern Nigeria," Journal of Global Research, Vol. 2, pp. 78–83, 2016.

[9] R. Lal, "Managing world soils for food security and environmental quality," Advances in Agronomy, Vol. 74, pp. 155–192, 2001.[CrossRef]

[10] F. R. Kutu, J.A.N. Asiwe, "Assessment of maize and dry bean productivity under different intercrops and fetilizer regimes," African Journal of Agricultural Research, Vol. 5, no. 13, pp. 1627–1631, 2010.

[11] F. R. Kutu and M. L. Diko, "Mineralogical considerations in soil fertility management on selected farmlands in Limpopo and northwest provinces, South Africa," in In An innovative perspective on the role of clays and clay minerals and Geophagia Book of conference proceeding of the first international conference of clays and clay minerals in Africa and second international conference on Geophagia in Southern Africa, South Africa, 2011.

[12] C. A. Shisanya, M. W. Mucheru, D. N. Mugendi and J. B. Kung'u, "Effect of organic and inorganic nutrient sources on soil mineral nitrogen and maize yields in central highlands of Kenya," Soil and Tillage Research, Vol. 103, no. 2, pp. 239–246, 2009. [CrossRef]

[13] D.W. Smith, "Soil survey staff, keys to soil taxonomy," 11th ed., United State Department of Agriculture, Natural Resource Conservation Service, Washington D.C., pp. 372, 2010.

[14] P. Day, "Particle fractionation and particle size analysis," Methods of soil analysis," American Society of Agronomy, Madison, 1965.

[15] G. Estefan, R. Sommer and J. Ryan, "Methods of soil, plant and water analysis: A manual for the West Asia and North Africa," International Center for Agricultural Research in thee Dry Areas (ICARDA), Beirut, 2013.

[16] V. J. G. Houba, J. J. Van Der Lee and I. Novozamsky, "Soil and plant analysis, part 5B soil analysis procedures, other procedures, Wagnengin University, Wageningen, 1995.

[17] R. Bray and L. Kurtz, "Determination of total, organic and available forms of phosphorus in soils," Soil Science, Vol. 59, no. 1, pp. 39–45, 1945. [CrossRef]

[18] J. Anderson and J. Ingram, "Tropical Soil biology and fertility: A handbook of methods," CAB International, Oxford, pp. 12–21, 1993.

[19] M. E. Sumner and B. A. Stewart, "Soil crusting: chemical and physical processes, 1st ed.: Lewis Publishers, Athens, Georgia, p. 372, 1992.

[20] E. Kamprath, Soil acidity and liming, In P.A. Sanchez (Ed.). "A Review of Soil Research in Tropical Latin America," North Carolina Experimental Station, North Carolina, 1970.

[21] M. Loubser and S. Verryn, "Combining XRF and XRD analyses and sample preparation to solve mineralogical problems," South African Journal of Geology, Vol. 111, no. 2-3, pp. 229–238, 2008. [CrossRef]

[22] B. Senjobi, "Comparative assessment of the effect of land use and land use type on soil degradation and productivity in Ogun State," Ibadan, 2007.

[23] B. A. Senjobi, R. T. Idehen, O. O. Oduntan and J. K. Adesodun, "Characterization and morphogenetic variability of soils under organic-based oil palm plantations in Southwestern Nigeria," Journal of Organic Agriculture and Environment, Vol. 4, no. 1, pp. 17–27, 2016.

[24] B. A. Lawal, A. G. Ojanuga, P. A. Tsado and A. Mohammed, "Characterization, classification and agricultural potentials of soils of toposequence in southern Guinea Savanna of Nigeria," World Academy of Science, Engineering and Technology International Journal of Agricultural and Biosystems Engineering, Vol. 7, no. 5, pp. 148–152, 2013.

[25] C.N. Egbuchua and S. Ojobor, "Characterization of some hydric soils in the Niger Delta region of Nigeria for land evaluation purposes," International journal of Advanced Biological Research, Vol. 1, no. 1, pp. 77–82, 2011.

[26] S. W. Buol, R. J. Southard, R. C. Graham and P. A. McDaniel, "Soil genesis and classification, 6 ed., John Wiley & Sons, New York, pp. 560, 2011. [CrossRef]

[27] J. W. C. Wong, K. M. Lai, D. S. Su and M. Fang, "Avilability of heavy metals for Brassica Chinensis grown in an acidic loam soil amended with domestic and sewage sludge," Water, Air and Soil Pollution, Vol. 128, pp. 339–353, 2001. [CrossRef]

[28] R. Jahn, H. P. Blume, V. B. Asio, O. Spaargaren and P. Schad, "Guidelines for soil description," Food and Agricultural Organization of the United Nation," FAO, Rome, 2006.

[29] N. Brady and R. Weil, "The nature and properties of soils," 14 ed., Pearson Princeton Hills, New Jersey, 2008.

[30] Y. Alemayehu, H. Gebrekidan and S. Beyene, "Pedological characteristics and classification of soils along landscapes at Abobo, southwestern lowlands of Ethiopia," Journal of Soil Science and Environmental Management, Vol. 5, no. 6, pp. 72–82, 2014.

[31] S. Idoga and D. E. Azagaku, "Characterization and classification of Janta Area, Plateau State of Nigeria," Nigerian Journal of Soil Science, Vol. 15, pp. 116–122, 2005.

[32] S. O. Atofarati, B. S. Ewulo and O. Ojeniyi, "Characterization and classification of SWoils on two toposequence at Ile-Oluji, Ondo State, Nigeria," International Journal of Agricultural Science, Vol. 2, pp. 642–655, 2012.

[33] T. K. Hartz, "Soil testing for nutrient availability: Procedures and interpretation for california vegetable crop production," University of California, Davis, 2007.

[34] A. Abate, K. Kibret, H. Gebrekidan and A. Esayas, "Determination of physico-chemical properties and agricultural potentials of soils in Tembaro District, KembataTembaro Zone, Southern Ethiopia," Eurasian Journal of Soil Science, Vol. 8, no. 2, pp. 118–130, 2019. [CrossRef]

[35] B. O. Nuga, N. C. Eluwa, G. E. Akinbola and C. C. Nwokocha, "Characterization and Classification of soils along a toposequence in Ikwano Local Government Area of Abia State, Nigeria," Agriculture Journal, Vol. 1, pp. 192–197, 2006.

[36] S. L. Tisdale, W. L. Nelson, J. D. Beaton and J. L. Havlin, "Soil fertility and fertilizers", 5th ed., Prentice Hall, New Delhi, 2004.

[37] P. Loganathan, A.A. Dickson, and N.O.Isirimah, "Potassium supplying capacity of soils formed on different geological deposits in the Niger Delta region of Nigeria," Geoderma, Vol. 65, pp. 109–120, 1995. [CrossRef]

[38] M. Ukubiala, "Characterization and classification of river benue floodplain soils in bassa local government area of Kogi State," Kogi State University, Kogi, 2012.

[39] V. N. Osobor, P. C. Okafor, K. A. Ibe and A. A. Ayi, "Characterization of clay minerals in Odukpani, Southeastern Nigeria," African Journal of Pure and Applied Chemistry, Vol. 13, pp. 79–85, 2009.

Environ Res Tec, Vol. 5, Issue. 1, pp. 84–93, March 2022

Environmental Research and Technology
https://ert.yildiz.edu.tr - https://dergipark.org.tr/tr/pub/ert
DOI: https://doi.org/10.35208/ert.1010295

Environmental Research & Technology

Research Article

Waste management practices towards low carbon cities

Ümmü Ayca BİLGİ*, Ece Ümmü DEVECİ

Department of Environmental Engineering, Niğde Ömer Halisdemir University, Niğde, Türkiye

ARTICLE INFO

Article history
Received: 18 October 2021
Revised: 16 December 2021
Accepted: 24 January 2022

Key words:
Greenhouse gas emissions; Low carbon city; Waste management

ABSTRACT

Urbanization has increased rapidly in the world. It uses an intensive resource consumption for urbanization and the expanding economy. The consequences of unconscious consumption of these resources, which constitute the thermodynamic system of cities, are solid wastes, wastewater and air pollution. As a result of improper management of these wastes in cities, it increases the effect of climate change by producing greenhouse gas emissions directly or indirectly. The most innovative approach in controlling these effects is "low-carbon city" studies. Turkey should give priority to low-carbon city applications that comply with the European Green Deal and transition to a green economy. In this context, with this study, applications and solutions were examined together to become a low-carbon city in Turkey. Considering policies and commitments, the roadmap is drawn in this way, the study will be a reference for many cities.

Cite this article as: Bilgi ÜA, Deveci EÜ. Waste management practices towards low carbon cities. Environ Res Tec 2022;5:1:84–93.

INTRODUCTION

It has become a living area with intense immigration and a crowded population with the increase in the need for manpower of the industry and the service sector [1]. Cities have the capacity to support their population. When this capacity is exceeded, various problems occur for the city and its inhabitants. The growth of cities is giving way to inefficient layouts that consume large amounts of energy and water, technologies and significant amounts of waste problems [2]. In cities that do not have waste management, many problems arise such as leaving the wastes in various areas with wild storage, decreasing the air quality due to the fossil fuels used in the city, and climate change due to the increase in greenhouse gases [3]. In order to find solutions to these problems, new urban concepts emerged which have been on the agenda in recent years and on which studies have increased [4].

a. Sustainable cities,

b. Ecological cities,

c. Low carbon cities,

d. Livable cities,

e. Smart cities,

f. Digital cities.

Although these terms and their meanings are different, their goals are the same. Each approach aims to find solutions to the city's problems.

***Corresponding author.**
*E-mail address: aycabilgii@gmail.com

As centers of population, industry, transport and infrastructure, cities are responsible for 70% of global CO_2 emissions. With the gradual acceleration of urbanization and industrialization processes, a series of environmental regulations are needed to reduce greenhouse gas emissions in world cities [5]. The biggest cause of global warming has been identified as the increase in carbon dioxide emissions. This situation has drawn attention to carbon emissions and a low-carbon city strategy has been developed as an effective reduction method [6]. Low carbon city; It is a concept that will reduce the carbon footprint by providing the increasing energy need in cities from renewable energy sources and help increase the quality of life with high efficiency [4]. Low carbon city; it is a concept that focuses on the amount of carbon in order to prevent climate change, reduce greenhouse gas emissions and continue the carbon cycle in the atmosphere. This focal point is included in the solutions of the city's problems, and the contribution of the solutions to the carbon cycle is important. The concept of a low-carbon city differs from other definitions in this respect.

The Latest Status of Waste Management

According to the IPCC 1.5 degree report, they stated that sectors such as energy, transportation, food and waste should switch to low carbon practices in order to take the right steps in the fight against climate change. With the increase in the urban population, the growth in every area causes an increase in the amount of waste produced [7]. Integrated waste management has an important place in the formation of low-carbon cities. This has economic, environmental and social consequences. Inaccuracies and deficiencies in the management of waste negatively affect the environment and constitute 3% of the total greenhouse gas emissions in the atmosphere [8]. Waste management; it is to minimize the effect of the elimination of wastes generated in the system on the environment and economy [9]. The waste management hierarchy has been accepted as in Figure 1 as the opposite of the waste hierarchy that was given and taught before [10]. According to this figure; the importance of waste management hierarchy to prevent waste; by devoting the largest part of the pyramid to waste prevention, it supports savings and emphasizes the minimization of the materials used. In order for this pyramid to function well, first of all, the materials considered as waste should be reduced, and then the benefits that can be obtained from the waste such as reuse, recycling and recovery of the waste ones should be maximized. In the end, it is desired to minimize the amount of waste that will come to the last item by including the disposal item [11]. While in the previous strategy, most of the waste was sent to landfills as disposal, in the new strategy, minimal disposal is accepted in accordance with the zero-waste philosophy.

Turkey now accepts this newly created waste hierarchy and puts the necessary legal regulations into practice. The legislation required for waste management in Turkey is shown in Figure 2.

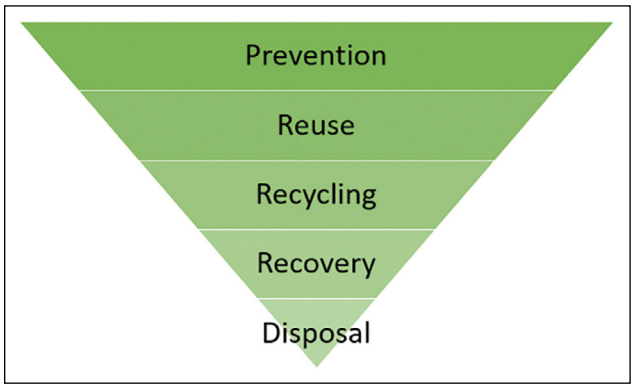

Figure 1. Waste management hierarchy [10].

The Waste Management Regulation published on 02.04.2015 regulates waste management. Among the purposes of this regulation; ensuring the management of wastes from generation to disposal without harming the environment and human health, reducing waste generation, reducing the use of natural resources and ensuring waste management through ways such as reuse, recycling and recovery of wastes [12].

"National Waste Management and Action Plan" was prepared in Turkey in 2015 and this plan, the current state of Turkey's current waste management and the elements that need to be improved and developed by determining the current situation were determined, and investments in waste management and 2023 targets were set [13].

The Zero Waste Regulation, which started to work in our country in 2017, entered into force in 2019. The implementation of the Zero Waste Principle, which includes protecting our resources, preventing waste, reducing the amount of waste, collecting waste separately at the source and recycling waste, is very important in terms of leaving a clean and livable world to future generations [14].

Although the regulations issued for Turkey, which tends to bury more than 65% of its wastes under the ground, show the efficient management of waste, there is a long way to go in waste management practices. Particularly, the problems experienced by municipalities in reaching the households, the increase in street collectors over time and the inefficient development of public awareness on this issue make the management of waste difficult. The Turkish economy, similar to other developing and developed economies, operates on a linear buy-use-dispose resource model that generates significant amounts of waste. It is inevitable that over the years, Turkey's economic and population growth, the increase in resource and energy use, and the waste generation are pending a solution. Turkey is facing the risk of raw material shortages to meet the production and consumption demand, together with the difficulties in waste disposal with increasing urbanization. Similar trends apply on a global scale.

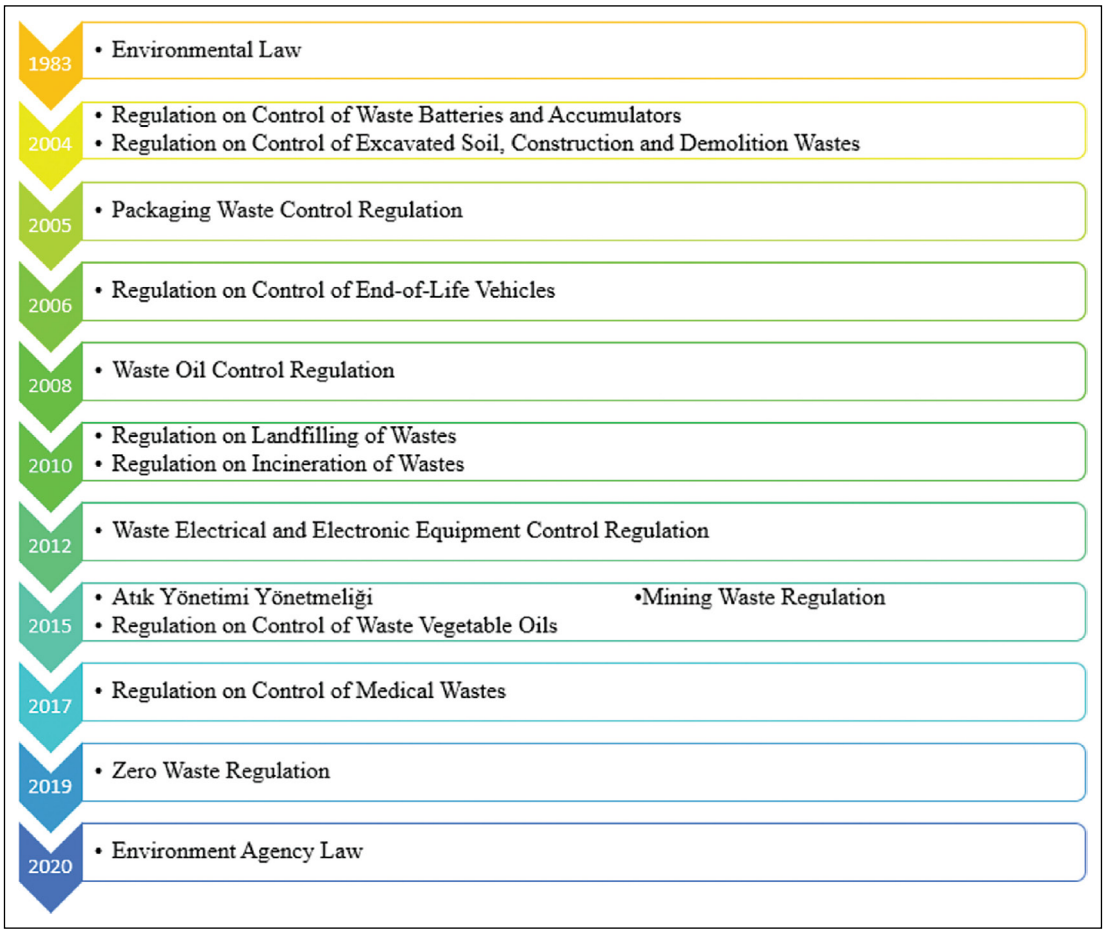

Figure 2. Waste legislation.

Within the scope of the Eleventh Development Plan (2019–2023), waste management under the title of "Livable Cities, Sustainable Environment", provided detailed information. In addition, statements are included "Public awareness will be raised in the recycling of solid wastes. Zero Waste Project practices will be expanded. Technical standards for the recovered secondary product will be developed, incentive and guidance legislation will be improved. A separate collection system of wastes will be expanded." In addition, it was stated in the Eleventh Development Plan that the domestic solid waste recycling and disposal facility projects and the transfer station projects of the local governments with insufficient financial power would be financially supported. In this context, 2023 targets are also included in the plan [15].

Greenhouse gas emissions and climate change are also mentioned in the Eleventh Development Plan. It has been stated that studies will be carried out within the framework of the Intended National Contribution for the emission control of the sectors that cause greenhouse gas emissions. It has been stated that in order to adapt to climate change, regional and city-based needs and solutions will be determined according to these needs, and Climate Change Action Plans will be prepared for this purpose [15].

Inadequate waste management; It supports global warming by producing methane gas, and the leachate flowing from wild storage areas causes pollution of underground and surface waters and endanger human health [16]. Waste production globally has been determined to have increased from 635 million tons in 1965 to 1999 million tons in 2015 and is estimated using modeling techniques to reach 3539 million tons by 2050 [17]. In the studies carried out, 1385 million tons of CO_2 emission value obtained from the solid waste collected in the city in 2018 alone constitutes 3.7% of the global CO_2 emissions of that year [17].

In Turkey, the total greenhouse gas emissions from the waste sector in 2016 are 16.2 million tons of CO_2 equivalent and constitute 3.3% of the total greenhouse gas emissions. There is an increase of 45.9% in greenhouse gas emissions from waste compared to 1990. As seen in Figure 3, the main source of greenhouse gas emissions from the waste sector is solid waste disposal and wastewater discharge and treatment. In 2016, 72.2% of the greenhouse gas emissions from waste were caused by solid waste disposal and 27.7% by wastewater discharge and treatment [18].

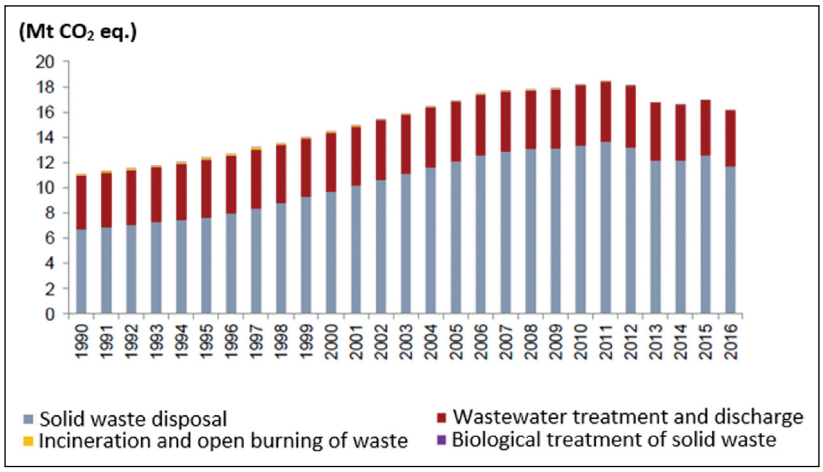

Figure 3. Greenhouse gas emissions from the waste sector, 1990–2016 [18].

Depending on the population growth, waste disposal in regular waste storage and disposal sites is also increasing. As seen in Figure 4, approximately 28.5 million tons of waste was dumped in the landfill in 2015 and 68% of this amount was stored in managed landfills [18].

As the amount of waste sent to the landfills increases, the amount of waste stored in the wild decreases and the greenhouse gas emission rate from the landfills decreases [18]. Solid waste has many negative environmental effects, including increasing greenhouse gas emissions and nitrogen pollution [17]. The rapid increase in the amount of waste and its impact on climate change show that waste management will become more important in the future [19]. Intelligent waste management by efficient application and energy saving; It prevents the formation of gases such as carbon dioxide in the air that can cause air pollution and global warming, making the city and nature more livable and cleaner [4].

Mitigation and Adaptation in Climate Change and Waste Management

In order to contribute to global efforts in the fight against climate change in Turkey, changes and transformations are observed in legal, institutional and policy frameworks. This transformation begins with the establishment of the Climate Change Coordination Board (CCCB) in 2001, with the responsibility of coordinating Turkey's efforts on climate change. In 2013, its name was changed to the Climate Change and Air Management Coordination Board (CCAMCB), and its scope and responsibilities were expanded. The Board is responsible for the coordination of the activities under the United Nations Framework Convention on Climate Change (UNFCCC) and the protocols subject to these agreements and the relevant national policy and legislation [18]. Turkey created the National Climate Change Strategy in 2010 and the National Climate Change Action Plan in 2011. The Regulation on the Monitoring of Greenhouse Gas Emissions was published in the Official Gazette dated 17 May 2014 and numbered 29003 and entered into force. Apart from these, it has been a side too and contributed to international agreements and protocols. The signed or signed agreements/protocols are listed in Table 1 chronologically.

Studies to be carried out to reduce greenhouse gas emissions from waste in Turkey are included in the Intended Nationally Determined Contribution document submitted in 2015 for the Paris Climate Agreement. This document is a document put forward by our becoming a party to the Paris Climate Agreement. In addition, the practices made for the reduction committed by Turkey on behalf of the waste sector are given below. In order for these commitments to be fulfilled and everything not to remain on the writing, it is necessary to carry out various applications. It is clearly seen that Turkey has determined strategies beyond the tasks it has undertaken with it becoming a party to the agreement.

Another important development for Turkey is that it ceased to be a party to the Paris Climate Agreement on 5 October 2021 and was ratified with parliamentary approval, which was signed by many countries in 2015. In this way, while paving the way for green development, the number of tasks to be done has increased while the way for additional budgets has been opened due to the implementation and implementation of many climate-compatible studies. These increases will enable the opening of new business lines.

With the approval of the Paris Climate Agreement, it is important that the public correctly understands this agreement. Therefore, in the fight against climate change, the adaptation of people's lifestyles to the climate comes first. For this, municipalities take the first place in adapting living spaces to climate. Efficient collection and recycling of waste have an important role in reducing a city's

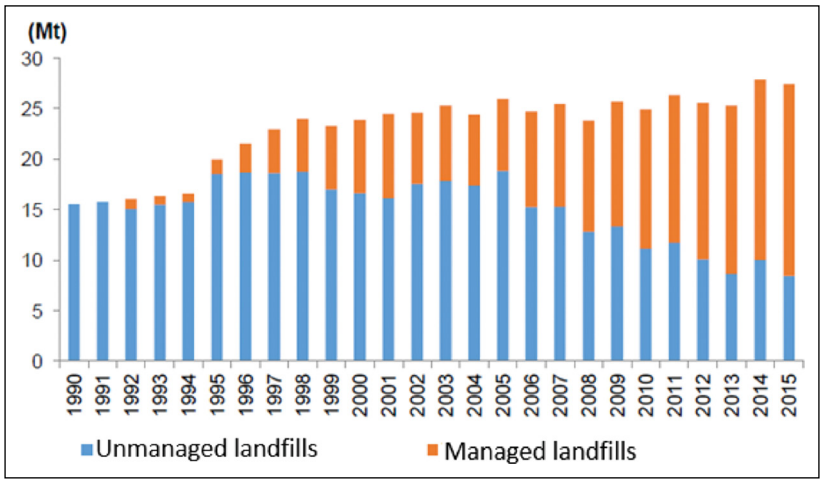

Figure 4. Annual waste disposal at solid waste disposal sites, 1990–2015 [18].

Table 1. Agreements/protocols related to the reduction of greenhouse gas emissions in Turkey [20]

Agreement/Protocol	Acceptance - Effective date	Turkey's Situation
Montreal Protocol on Substances that Deplete the Ozone Layer	Accepted D.: 1987 Effective D.: 1 January 2019	It became a party on 19 December 1991 and accepted all the amendments introduced by the Protocol.
United Nations Framework Convention on Climate Change (UNFCCC)	Accepted D.: 3-14 June 1992 Effective D.: 21 Mart 1994	Joined on 24 May 2004. Turkey is the only country within the scope of Annex-1 that does not have a transition economy and whose "special conditions" were accepted by the resolutions of the Conference of the Parties.
Kyoto Protocol	Accepted D.: 1997 Effective D.: 16 February 2005	It became a party on 26 August 2009. Turkey, which was not a party to the UNFCCC when the Protocol was adopted, was not included in the Annex-B list of the Protocol. Therefore, there is no quantified emission limitation/reduction commitment.
Paris Climate Agreement	Accepted D.: 5 October 2016 Effective D.: 4 November 2016	It was signed on April 22, 2016, but it was not a party. The National Intended Statement of Contribution was submitted on 30 September 2015. According to Turkey's national contribution statement, a reduction of 18% to 21% is foreseen in 2030 compared to the increase in greenhouse gas emissions compared to the reference scenario.
Paris Climate Agreement	Approval D.: 5 October 2021	It was unanimously approved by the parliament. A zero emission target has been set for 2053.

carbon footprint and CO_2 emissions. For this reason, it is necessary for municipalities to carry out many studies and to prepare training programs in order to increase public awareness. It is necessary to carry out intensive practices in order to convey environmental awareness within social activities, to create public service announcements about recycling and to ensure that everything is not at the educational level. Giving priority to encouraging ways in practices has an important place in ensuring public participation.

The items regarding the waste sector of the Intended Nationally Determined Contribution, which Turkey has committed with our becoming a party to the Paris Climate Agreement, are examined in detail below.

- Sending solid wastes to landfills

There were 15 landfills in Turkey until 2003, and there were 89 facilities in 2019. According to the data of the Ministry of Environment and Urbanization for 2019, the ratio of the population served by landfill facilities to the total municipal population is 82%. This situation has been determined by increasing the proportion of the population provided with waste disposal service to 100% by 2023 as a near target, and by spreading the zero-waste management system as a distant target by 2050. In this way, the landfills will be completed gradually, wild landfills will be prevented and projects will be put into effect upon sending less waste [21].

- Reuse, recycling and other processes to obtain secondary raw materials, to be used as an energy source or to be disposed of the waste

The zero-waste management system, which started with the separation of wastes at the source, has made Waste Derived Fuel (WDF) facilities widespread in the waste industry. Waste-derived fuel (WDF) is an alternative solid fuel type that takes the remaining non-recyclable materials as raw materials after the recyclable materials (plastic, glass, metal, etc.) of domestic or industrial solid wastes are separated. End-of-life vehicle tires, wastepaper, waste oils, wood waste, treatment sludge, plastics are WDF raw materials. When WDF and coal are compared, WDF; It is advantageous because it is cleaner, more energy efficient, environmentally friendly and less dusty [22].

- Reducing the amount of biodegradable waste to be stored in 2015 to 75% by weight of the total amount of biodegradable waste produced in 2005, 50% in 2018 and 35% in 2025. Accordingly, the establishment of pre-treatment facilities in order to reduce the amount of biodegradable waste to be stored in 2025 to 35%,

The final product of organic wastes, which is subjected to microbial degradation (decomposition) under aerobic or anaerobic conditions, is called compost [23]. Green garden wastes (leaves, grass, pruning wastes, wood, bark) resulting from the works of the parks, gardens and afforestation units of the municipalities can be converted into compost with the appropriate composting method. Social responsibility projects on compost production have started to become widespread in Turkey [24].

- Ensuring energy recovery from waste by subjecting wastes to processes such as material recovery, bio-drying, biomethanization, compost, advanced thermal processes or incineration,
- Realization of methane recovery from landfill gas originating from regular and irregular landfills,

Methane gases, which cause an increase in greenhouse gas emissions 25 times more than carbon dioxide, are converted into electrical energy by burning after they are collected from the gas collection channels opened in the landfills [25]. Between January and February 2021, 96,358 megawatt-hours of electricity were produced by recovering methane from landfill gas. 52% of this amount was obtained from Odayeri Landfill Gas Power Plant and Seymen Landfill Gas Power Generation Facility [26].

- The industrial symbiosis approach that allows the wastes from industry to be used as alternative raw materials or fuel in another sector, and the waste from one sector to be the raw material of another sector,

Industrial Symbiosis is the union formed by turning the by-product or output of one of the industrial facilities into the raw material of another. Iskenderun Bay (Adana, Mersin, Osmaniye, Iskenderun) Industrial Symbiosis Project; It was carried out by the Technology Development Foundation of Turkey (TTGV) between 2011–2014 [27]. In this project, industrial production on animal feed production from fruit pulp, energy production from agricultural and animal waste, bioremediation product production from cottonseed waste, electricity production from waste oil, granule production from end-of-life tires, lead recovery from scrap batteries and the use of slag from iron and steel production in road construction, symbiosis studies were carried out [28].

- Carrying out appropriate studies for the evaluation of wastes from livestock and poultry farms,

Animal waste is seen as an ideal source for biogas (65% CH4, 35% CO_2) production. The obtained biogas is an important energy input for electricity and heat production. In addition, manure, which is a by-product, is used in agriculture [29]. Establishing facilities such as biogas and biodiesel for the evaluation of animal waste in the world creates a sustainable cycle by preventing the damage of wastes to the environment and human health [30]. In addition, the establishment of meat and bone meal production facilities for the evaluation of animal waste and by-products occurring in slaughterhouses is among the studies evaluated [31].

- Rehabilitation of irregular landfills and ensuring the disposal of wastes in landfills,

Rehabilitation (rehabilitation) by closing the areas where irregular storage is made has been legalized with the "Regulation on Regular Storage of Wastes", which was published in the Official Gazette dated 26.03.2010 and numbered 27533 [32].

In order to fulfill the commitments made regarding the waste sector, the above-mentioned studies are carried out and success is achieved in many areas. It is envisaged that the commitments in all titles will be completed by 2030. In addition to all these studies, strategies are being developed by further studies on waste.

The Paris Climate Agreement, which was signed in 2015 on the mitigation, adaptation and financing of climate change within the scope of the United Nations Framework Convention on Climate Change, entered into force in 2016. Among the countries that did not ratify the agreement, such as Eritrea, Iran, Iraq, Libya, Turkey and Yemen, Turkey was the 191st country to sign the agreement as of 2021. Paris Climate Agreement; It sheds light on what should be done to reduce greenhouse gases that cause global warming and climate change in the world. It aims to limit global warming to 1.5^{o}C. It presents a perspective that aims to reduce greenhouse gas emissions from coal, oil or all other fossil fuels. The living now sees the problem of climate change. For a solution, it is necessary to switch to climate change adaptation policies. The difference of the Paris Climate Agreement from other agreements; The country's need to align its policies, economy and industry with climate change. The Ministry

of Industry and Technology, metropolitan municipalities and local governments will take quick steps, which will ensure that Turkey is less affected by the provisions of the Green Agreement and the Paris Climate Agreement. A resource is created to transfer money from developed countries to poor countries in order to reduce greenhouse gas emissions and adapt to climate change. An annual budget of around 100 billion dollars is envisaged for this resource, which is called the green climate fund.

Waste Management for Low Carbon Cities

Data collection and analysis are a priority for creating low-carbon city strategies [33]. In order to find solutions to the problems, there must be data belonging to the problems. Finding the most appropriate solution over these data is also possible with data analysis. Data analysis is based on organizing the collected data with various methods and eliminating unnecessary, redundant data that will affect the accuracy of the result. When the data analysis is done correctly, it will highlight the appropriate solution [34]. A few of the waste management practices made in Europe in order to achieve the goal of becoming a low-carbon city are listed below.

CO_2 emissions; mostly from the use of fossil fuels or from industrial processes. Renewable energy sources should be used to prevent CO_2 formation. For industrial processes where we cannot prevent CO_2 formation, it is necessary to prevent CO_2 emissions and to ensure CO_2 recovery. Carbon dioxide capture and storage processes are applied to the places where carbon dioxide is produced the most and consist of three stages. These are handling, transport and storage. The process of separating CO_2 from the flue gas formed during the capture phase is carried out. In the transportation phase, there are two options as pipeline or ship transportation. The storage stage is the process of injecting carbon dioxide into an underground rock formation by compressing it. In the storage phase, there are three alternatives: geological storage, oceanic storage and mineral carbonization [35].

One of the most used methods to reduce carbon emissions in the waste sector is biogas plants. Established biogas facilities both meet the city's heat and natural gas needs as a renewable resource and provide fertilizer support to be used in agricultural lands. This method prevents the landfills from exceeding their capacity, thus contributing to the storage of less waste and making fewer landfills and economically contributing to the country [36].

Cities that want to reduce their carbon emissions through waste management focus on new projects by making use of technology. The use of smart waste management systems and the collection of waste with electric vehicles reduce carbon emissions in both the transportation and waste management sectors. Routes created automatically according to the occupancy rate of the waste bins prevent unnecessary vehicle circulation and carbon emissions in the city [11]. The implementations on the so-called Climate Street in Amsterdam demonstrate the contribution of waste management to the low-carbon city. The collection of waste from the city with electrical waste separation vehicles prevents the carbon emissions emitted by the waste vehicles [37]. In addition, another exemplary application seen on the same street is energy-saving waste bins working with solar energy. By compressing the waste with solar energy, it has more waste capacity than a normal waste bin. Thus, the filling time of the waste bins is extended and the working time of the waste vehicles is shortened [38].

In Songdo city of South Korea, the system where waste is sent directly from waste bins to the recycling facility, energy generation or underground waste facility for incineration with pneumatic tube systems is one of the applications where waste management and carbon emissions are minimized. There are no waste and waste vehicles in the city [39].

The Relationship of Waste Management with Carbon Tax

Another method applied to reduce carbon emissions and raise awareness is the carbon tax. It is a consumption tax per ton of coal, per barrel of oil or emissions. Although it is a method that has been applied globally for years, it was first put into effect by Finland in 1990 [40].

According to the Evaluation of Market-Based Emission Reduction Policy Options in Turkey Final Report published by the Ministry of Environment and Urbanization in 2017, priority areas in emission reduction were determined and studies to be carried out on these areas were compiled. It has been stated that the energy, process emissions and transportation sectors will be subject to tax at the first stage, while the agriculture and waste sectors will be exempted from the tax at the first stage. It is stated that it is exempted due to the complexity of emission measurement in the waste and land-use sectors and the need to further develop appropriate methodologies [41].

CONCLUSIONS

The increase in human needs with industrialization in cities has led to population density in cities. The fact that the cities are not ready for such a population leads to the fact that every person living in the city cannot be provided with the same quality of life. Green areas are given up for housing rights and trees are given up for road construction. The lack of adequate infrastructure reveals the most concrete evidence of environmental pollution in rapidly growing cities. Industrialization, which is not controlled against the environment and human health, has ceased to be a problem only for cities.

In recent years, the whole world has started to see how big problems climate change has caused and will cause. It is understood that the absorption of carbon emissions should be provided by human-made solutions. Reducing carbon emissions, which is the starting point of low-carbon cities, can be achieved by reaching all cities. The new regulations that emerged with the Paris Climate Agreement, where the green economy is related to waste management, and these new regulations need to be pointed out in order to reach low-carbon cities.

The legal regulations made by the government in the waste sector in Turkey were examined and the signed/approved agreements/contracts on carbon reduction were listed and it was revealed how much of the commitments were made. It is seen that feasibility studies and legal regulations regarding the reduction of carbon emissions are about to be completed. It is seen that the practices that still need to be done in the waste sector for the reduction at the level committed with the Paris Climate Agreement do not cover 100% of the population in the country. Carbon reduction methods for the waste sector and the work that can be done on behalf of other sectors are explained with examples from abroad. While determining its strategies for the future, Turkey needs to closely follow and realize the changes in the world. This work; forms the basis for many studies on low-carbon cities.

DATA AVAILABILITY STATEMENT

The authors confirm that the data that supports the findings of this study are available within the article. Raw data that support the finding of this study are available from the corresponding author, upon reasonable request.

CONFLICT OF INTEREST

The authors declared no potential conflicts of interest with respect to the research, authorship, and/or publication of this article.

ETHICS

There are no ethical issues with the publication of this manuscript.

REFERENCES

[1] S. Yıldız, S. Kıvrak, and A. B. Gültekin, "Sosyal Sürdürülebilirliğe Katkı Veren Bir Yapılı Çevre İçin Kentsel Dönüşüm Çalışmalarında Dikkate Alınması Gereken Tasarım Unsurları," in SBE16 İSTANBUL - Uluslararası Sürdürülebilir Yapılı Çevre Konferansı, 2016, pp. 190–199, Available at: http://www.sbeistanbul.com/assets/SBE16_Bildiri_TR-24-10-2016.pdf. Accessed on Oct 10, 2021.

[2] S. E. Bibri, "The eco-city and its core environmental dimension of sustainability: green energy technologies and their integration with data-driven smart solutions," Energy Informatics, Vol. 3, Article 4, 2020. [CrossRef]

[3] E. Kaya, H. Şentürk, O. Danış, and S. Şimşek, modern kent yönetimi i. Okutan Yayıncılık, İstanbul, 2007.

[4] S. Sınmaz, "The concept of 'smart settlement' and basic principles in the framework of new developing planning approaches," Megaron, Vol. 8, pp. 76–86, 2013. (in Turkish). [CrossRef]

[5] H. Chen, W. Guoc, X. Fenga, W. Weiad, H. Liue, Y. Fengf, and W. Gongb, "The impact of low-carbon city pilot policy on the total factor productivity of listed enterprises in China," Resources, Conservation & Recycling, Vol. 169, Article 105457, 2021. [CrossRef]

[6] Y. Yu, and N. Zhang, "Low-carbon city pilot and carbon emission efficiency: Quasi-experimental evidence from China," Energy Economics, Vol. 96, Article 105125, 2021. [CrossRef]

[7] H. Khandelwal, H. Dhar, A. K. Thalla, and S. Kumar, "Application of life cycle assessment in municipal solid waste management: A worldwide critical review," Journal of Cleaner Production Vol. 209, pp. 630–654, 2019. [CrossRef]

[8] IPCC, "IPCC Fourth Assessment Report: Climate Change 2007," 2007.

[9] A. A. Gündüzalp, and S. Güven, "Waste and waste types, waste management, recycling and consumer: Çankaya municipality and instance of neighbourhood consumers," Hacettepe Üniversitesi Sosyolojik Araştırmalar Dergisi, pp. 1–19, 2016.

[10] F. Ercan, "Atık Yönetimi Mevzuatı," Ankara, 2015. [Online]. Available at: http://www.pagcev.org/upload/files/Funda Ercan Atik Yonetimi Mevzuati.pdf. Accessed on Oct 10, 2021.

[11] A. Söylemez, "Waste management in smart cities and smart waste management samples in the world," Yasama Dergisi, Vol. 13, no. 37, pp. 87–100, 2018. (in Turkish).

[12] Çevre ve Şehircilik Bakanlığı, Atık Yönetimi Yönetmeliği. Ankara: Resmî Gazete, 2015.

[13] Çevre ve Şehircilik Bakanlığı, "Ulusal Atık Yönetimi ve Eylem Planı (2016-2023)," Ankara, 2017. Available at: https://webdosya.csb.gov.tr/db/cygm/haberler/ulusal_at-k_yonet-m--eylem_plan--20180328154824.pdf. Accessed on Oct 10, 2021.

[14] Çevre ve Şehircilik Bakanlığı, "Sıfır atık el kitapçığı," Ankara, 2017. Available at: https://webdosya.csb.gov.tr/db/sifiratik/icerikler/k-tapc-k-2017-1-20180129130757.pdf. Accessed on Oct 10, 2021.

[15] Türkiye Cumhuriyeti Cumhurbaşkanlığı Strateji ve Bütçe Başkanlığı, "Onbirinci Kalkınma Planı 2019-

2023," Ankara, 2019. Available at: https://www.sbb.gov.tr/wp-content/uploads/2019/07/OnbirinciKalkinmaPlani.pdf. Accessed on Oct 10, 2021.

[16] S. Güleç Solak, and Ş. Pekküçükşen, "Municipal solid waste management in Turkey: a comparative analysis, MANAS Journal of Social Studies, Vol. 7, pp. 653–683, 2018. (in Turkish)

[17] D. M. C. Chen, B. L. Bodirsky, T. Krueger, A. Mishra, and A. Popp, "The world's growing municipal solid waste: trends and impacts," Environmental Research Letters, Vol. 15, 2020. [CrossRef]

[18] Çevre ve Şehircilik Bakanlığı, "Türkiye'nin Yedinci Ulusal Bildirimi," 2018. Available at: https://webdosya.csb.gov.tr/db/cygm/icerikler/yed-nc--ulusal-b-ld-r-m-20190909092640.pdf. Accessed on Oct 10, 2021

[19] E. Irbaş, and F. Dadaşer-Çelik, "Evsel katı atık yönetim senaryolarının yaşam döngüsü analizi: Melikgazi ilçesi (Kayseri) örneği," Doğal Afetler ve Çevre Dergisi, Vol. 7, pp. 266–277, 2021. [CrossRef]

[20] Dışişleri Bakanlığı, "İklim Değişikliğiyle Mücadelenin Önemi," Dışişleri Bakanlığı, 2021. Available at: https://www.mfa.gov.tr/iklim-degisikligiyle-mucadelenin-onemi.tr.mfa. Accessed on Oct 10, 2021.

[21] Çevre ve Şehircilik Bakanlığı, "Çevresel Göstergeler," Çevre ve Şehircilik Bakanlığı, 2021. Available at: https://cevreselgostergeler.csb.gov.tr/atik-duzenli-depolama-tesis-sayisi-belediye-sayisi-hizmet-verilen-nufus-i-85750 Accessed on Oct 10, 2021

[22] Doğu Akdeniz Kalkınma Ajansı, "Osmaniye İlinde AYT Potansiyelinin Araştırılmasına Yönelik Fizibilite Raporu," 2015. Available at: https://www.dogaka.gov.tr/assets/upload/dosyalar/www.dogaka.gov.tr_899_AS8W82MW_Osmaniye-ilinde-ATY-Potansiyelinin-Arastirilmasina-Yonelik-Fizibilite-Raporu.pdf. Accessed on Oct 10, 2021.

[23] E. Erdin, "Katı Atıkların Kompostlaştırılması," İzmir, 2005. Available at: http://web.deu.edu.tr/erdin/tr/ders/kati_atik/ders_not/katiatiklarinkompostlastirilmasi.pdf. Accessed on Oct 10, 2021.

[24] Buğday Ekolojik Yaşamı Destekleme Derneği, "Belediyeler için Kompost Rehberi," 2017. [Online]. Available at: http://www.turkeycomposts.org/dosya/kaynaklar/Belediyeler_Icin_Kompost_Rehberi.pdf. Accessed on Oct 10, 2021.

[25] T. Kankılıç and H. Topal, "Production of solid biogas and energy in sanitary landfill from municipal waste," Mühendis ve Makina, Vol. 56, pp. 58–69, 2015. (in Turkish)

[26] D. Kumtepe, "Enerjisini Üreten Fabrikalar," Enerjisini Üreten Fabrikalar, 2021. Available at: https://www.stendustri.com.tr/enerjisini-ureten-fabrikalar/yeni-tesislerle-cop-gazindan-elektrik-uretimi-artti-h112872.html. Accessed on Oct 10, 2021.

[27] Türkiye Teknoloji Geliştirme Vakfı, "İskenderun Körfezi'nde Endüstriyel Simbiyoz Projesi Uygulama Aşaması, Sonuçlar ve Kazanımlar," 2015. Available at: http://www.endustriyelsimbiyoz.org/wp-content/uploads/2014/09/İskenderun-Körfezinde-Endüstriyel-Simbiyoz-Sonuç-Broşürü.pdf. Accessed on Oct 10, 2021.

[28] A. Özkan, Z. Günkaya, A. Özdemir, and M. Banar, "Industrial symbiosis approach towards cleaner production and circular economy in industry: a review," Anadolu University Journal of Science and Technology B - Theoretical Sciences, Vol. 6, pp. 84–97, 2017.

[29] M. Tolay, H. Yamankaradeniz, S. Yardımcı, and R. Reiter, "Hayvansal Atıklardan Biyogaz Üretimi," 2008. Available at: https://biyogazder.org/makaleler/mak18.pdf. Accessed on Oct 10, 2021.

[30] T. Kaufmann, "Sustainable livestock production: Low emission farm – The innovative combination of nutrient, emission and waste management with special emphasis on Chinese pig production," Animal Nutrition, Vol. 1, pp. 104–112, 2015. [CrossRef]

[31] J. Bujak, and P. Sitarz, "Incineration of animal by-products - The impact of selected parameters on the flux of flue gas enthalpy," Waste Management, Vol. 50, pp. 309–323, 2016. [CrossRef]

[32] Çevre ve Orman Bakanlığı, Atıkların Düzenli Depolanmasına Dair Yönetmelik. Turkey: Resmî Gazete, 2010.

[33] E. Papargyropoulou, S. Colenbrander, A. H. Sudmant, A. Gouldson, and L. C. Tin, "The economic case for low carbon waste management in rapidly growing cities in the developing world: The case of Palembang, Indonesia," Journal of Environment Management, Vol. 163, pp. 11–19, 2015. [CrossRef]

[34] B. Kıral, "Nitel bir veri analizi yöntemi olarak doküman analizi," Siirt Üniversitesi Sosyal Bilimler Enstitüsü Dergisi, Vol. 8, pp. 170–189, 2020.

[35] E. R. Arslan, "Karbondioksit Tutum ve Depolaması Özel Raporu," 2005. Available at: https://www.ipcc.ch/site/assets/uploads/2021/03/sum-policy-tr.pdf. Accessed on Oct 10, 2021.

[36] B. Gürel, "Determination of current biomass potential in turkey and calculation of sectoral and total combustion energy values for wastes which are a good alternative for energy production by combustion," Mühendislik Bilimleri ve Tasarım Dergisi, Vol. 8, pp. 407–416, 2020. (in Turkish) [CrossRef]

[37] S. Sauer, "Do smart cities produce smart entrepreneurs?," Journal of Theoretical and Applied Electronic Commerce Research, Vol. 7, pp. 63–73, 2012. [CrossRef]

[38] G. Nair, "The reconstruction of urban life in light of information an communication technologies and an example from Anatolia, Turkey: Smart city applica-

tions of sivas municipality," MANAS Journal of Social Studies, Vol. 8, pp. 531–550, 2019. [CrossRef]

[39] E. Katier, "Akıllı kent uygulama incelemeleri ve Edirne için bir model önerisi," [Yayınlanmamış Yüksek Lisans Tezi], Trakya Üniversitesi, 2019. (in Turkish)

[40] N. Işık, and E. C. Kılıç, "The relationship between CO2 emissions and energy R&D expenditures in the transport sector," Sosyoekonomi, Vol. 22, 2014. (in Turkish) [CrossRef]

[41] Çevre ve Şehircilik Bakanlığı, "Türkiye'de Piyasa Temelli Emisyon Azaltım Politika Seçeneklerinin Değerlendirilmesi Nihai Rapor," Ankara, 2017. Available at: https://pmrturkiye.csb.gov.tr/wp-content/uploads/2018/12/nihai-rapor-6.pdf. Accessed on Oct 10, 2021.

Environ Res Tec, Vol. 5, Issue. 1, pp. 94–100, March 2022

Environmental Research and Technology
https://ert.yildiz.edu.tr - https://dergipark.org.tr/tr/pub/ert
DOI: https://doi.org/10.35208/ert.1026602

Environmental Research & Technology

Research Article

The effect of atmospheric deposition on potassium accumulation in several tree species as a biomonitor

Kaan IŞINKARALAR[*1], Ramazan ERDEM[2]

[1]*Department of Environmental Engineering, Kastamonu University, Kastamonu, Türkiye*
[2]*Kastamonu University Forestry and Forestry Products, Araç Rafet Vergili Vocational School, Kastamonu, Türkiye*

ARTICLE INFO

Article history
Received: 21 November 2021
Revised: 17 January 2022
Accepted: 31 January 2022

Key words:
Atmospheric deposition; Biomonitors; Nutrient element potassium; Trees

ABSTRACT

Minimizing air, water, and soil pollution are very important for a sustainable environment. Particularly, ensuring the continuity of soil fertility without deteriorating the soil structure is very important. This objective can be achieved only by determining the physical, biological, and chemical properties of atmospheric deposition and taking the required measures in agricultural lands. Trees and plants reflect the soil quality and especially they take both beneficial and harmful materials in their bodies owing to Saharan dust and using fossil fuel. Among them, nutrient elements have specific importance since it was determined that many factors including texture, irrigation method, organic matter, lime concentration, plant species and age, pH, and ion balance play effective roles in the growth or degradation of plants' productivity. Being one of the major nutrient elements taken by plants, potassium (K^+) is of vital importance for trees and plants. Its concentration, which varies depending on the species of plant, is influenced by the mutual interaction between tree development and environmental/genetic factors. The scope of this study was to evaluate and rank the contribution of atmospheric potassium (K^+) deposition flows to organs of *Robinia pseudoacacia* L., *Cupressus arizonica* G., and *Platanus orientalis* L. trees as biomonitors.

Cite this article as: Işınkaralar K, Erdem R. The effect of atmospheric deposition on potassium accumulation in several tree species as a biomonitor. Environ Res Tec 2022;5:1:94–100.

INTRODUCTION

Rapidly increasing world population and consequent increase in urbanization, industrialization, and unawares use of agricultural lands resulted in deterioration of many forests and fertile agricultural lands [1–3]. Minimizing air, water, and soil pollution is very important for a sustainable environment [4]. Particularly, ensuring the continuity of the urban environment without deteriorating the air and soil structure is very important for a sustainable environment [5]. Although the quality of the soil belongs to the region where it is located, atmospheric precipitation plays a role in global cases [6]. This is dust transport, emissions from nearby inert sources, and acid rain, which is formed as a result of the reactions of pollutants released due to the use of fossil fuels and their effects on plants [7]. Atmospheric potassium deposition can affect the physical, biological, and chemical properties of soil and take the required measures in agricultural lands via wet, dry, and total deposition [8]. Thus, plants need fundamental

***Corresponding author.**
*E-mail address: kisinkaralar@kastamonu.edu.tr

nutrient elements from the soil to grow and to maintain their metabolic activities. The potassium (K^+) is one of the most abundant elements that represent the amount of potassium defined in a spatial and temporal [9]. It is a nutrient influencing many biochemical and physiological processes [10]. It founds in dust and rainfall that likely comes from terrestrial sources that can quickly be re-deposited or be transported for large distances [11].

The K^+ is a fundamental nutrient allowing plants to survive various biotic and abiotic stresses (diseases, insects, drought, salinity, cold, frost, and flood) [12]. It is important for developmental crops and activation enzymes [13]. It was stated in previous studies that each plant has various concentration values and different levels of need for K element that is the vital impact for enzyme activation, protein synthesis, photosynthesis, energy transfer, stoma movement, osmoregulation, phloem transfer, and cation-anion balance [14]. The most well-known source of K in the soil minerals such as feldspar and mica although it is found in dust and rainfall likely comes from terrestrial sources [15]. The effects of differences in presence of K in different plants on species' anatomy, morphology, and plant metabolism couldn't be explained yet and they are still debated [16]. It was shown that the presence of K allowed the trees to overcome the stress conditions. In previous studies, it was reported that trees and plants primarily need mineral nutrients to overcome biotic and abiotic stress conditions [17–19]. The presence of K in fertilizers used in herbal production increases the quality of fertilizer. It was determined in many studies that the second-most important nutrient for plant development is potassium, following nitrogen. Previous studies showed that plant fertilizer has a positive correlation with crop development and quality. However, potassium deficiency can also be seen in some cases. Potassium deficiency is observed especially in acidic soils with ample water and high salinity levels [20]. Several negativities are observed in the development of plants and trees in such soils. Intake of potassium by plants and trees occurs via roots and the intake levels vary [21]. On the contrary other soil nutrients, K is available in the soil as only a K^+, which supports the plant productivity and environmental services, depending on the deficiency and abundance of nutrients [22]. Besides that, the optimum benefit can be obtained from the fertilization process, which is performed by having accurate knowledge about the chemical and physical properties [23]. For this purpose, many studies were carried out to determine the productivity levels of different regions and soils, to foreknow the potential nutritional problems, and to increase the crop quality [24]. The K^+ is one of the elements used by the plants in the soil at a higher concentration in comparison to the others [25]. Although there are many studies about the accumulation, transport, and levels of The K^+ is one of the elements used by the plants in the soil at higher concentrations of potassium, they could not calculate the amount of potassium that passes from the atmosphere to the soil [26]. For the determination of the available potassium amount, inputs (atmospheric deposition, plant residue, and animal manures, commercial fertilizers, minerals, etc.) and outputs (removal of plant, leaching, erosion, fixation, etc.) of potassium sources should be well known as ecosystem services [27, 28].

Plants and trees are great bioindicators of atmospheric metals deposition including trace and toxic metals due to their effective adsorption capacity of them [29, 30]. The main sources of potassium and other elements are atmospheric inputs as wet, dry, and total deposition [31]. There are also some studies on the atmospheric trace metals transport and deposition on plants from anthropogenic sources [32–35]. The amount of potassium is increased with acid rain and precipitation because trace metals and other pollutants oxides form chemical compounds on terrestrial ecosystems [36]. Biomonitoring with plants ensures inexpensive knowledge on the composition and quantity of the deposition of trace and toxic metals [37]. In this study, the atmospheric potassium deposition was examined in the organs of trees for years. The K^+ concentrations were inspected in the rings of 3 different trees growing in the Kocaeli industrial zone via years and organs. The organs of trees used for this purpose *Robinia pseudoacacia* L., *Cupressus arizonica* G., and *Platanus orientalis* L. were selected because they are widespread on the terrestrial ecosystem for resistance to air pollution. The concentrations of K^+ were analyzed in the outer bark, inner bark, and wood fractions of trees. It was aimed to determine how the K^+ concentration in the annual rings of trees changed over the years.

MATERIALS AND METHODS

Study Area and Sampling Site

The study area is located around the organized zone of Kocaeli city, Türkiye. Significant factors of air pollutants are released from many industrial activities and fuel combustion. Air pollutants may contain heavy metals and toxic elements including macronutrients. Organs (wood, inner bark, and outer bark) of four dominant tree species were used *Robinia pseudoacacia* L., *Cupressus arizonica* G., and *Platanus orientalis* L. in an industrial area and were collected no more than 4 km from the site of the organized zone. All samples were taken from the main trunk of trees. After sampling, wood, inner bark, and outer bark were urgently placed in a glass vessel and transferred to the lab for preparation of analysis.

Preparation of Tree Species Sampling

The tree rings were determined to be 30 years old (between 1991 and 2020) in three years. The species had an almost same trunk diameter and height around 1 m above the ground. All samples were rinsed with acetone (Merck, Ger-

Table 1. Change of K^+ concentrations (ppm) based on species

	Species			
Organ	***Robinia pseudoacacia* L.**	***Cupressus arizonica* G.**	***Platanus orientalis* L.**	**F value**
Wood	776.7 Aa	472 Aa	1439.2 Ba	15.8*
Inner bark	1976 Ba	783.9 Aa	6187.1 Cb	48537.8*
Outer bark	3216.8 Bb	1909.8 Ab	6458 Cb	50096.1*
F value	12.2*	36.2*	160.2*	

*: Significant at $p<0.001$. Upper and lower letters differ significantly based on the Duncan test.

many) then they were divided into groups for the age ranges. All samples taken into glass vessels were kept at 50°C for 7 days. The samples were taken as 0.5 g weighed and 6 mL of 65% nitric acid (HNO_3) and 2 mL of 30% hydrogen peroxide (H_2O_2) were added to glass vessels. According to USEPA 3052 Method, the combustion process was carried out in the microwave oven at 200°C for 15 minutes [38]. The resulting samples were made up to 50 mL with ultrapure water and potassium analyzes were made in by Inductively Coupled Plasma-Optical Emission Spectrometry (ICP-OES) with a plasma source device (SpectroBlue, Spectro). Analytical grade chemicals were used for the research.

Statistical Analyses

All measurements were repeated as in triplicate. Analysis of variance (ANOVA) and Duncan test was conducted to identify the significance of atmospheric potassium deposition in species by using the SPSS 22.0 statistical package program for Windows.

RESULTS

The biomonitoring organ of plants was chosen outer bark, inner bark, and wood of a *Robinia pseudoacacia* L., *Cupressus arizonica* G., and *Platanus orientalis* L. which, due to its widely used and readily available in local terrestrial ecosystem. It has been proven that it can provide information on the presence of the K^+ element in Table 1.

According to the results of variance analysis (ANOVA) that the change in the concentration of K^+ element on an organ basis in all three species is statistically significant ($p<0.001$). Considering the Duncan test results, the lowest values are obtained in the wood and the highest values were obtained in the outer bark, the values obtained in the wood and inner bark of *Platanus orientalis* L. are in the same group, and in other species, each organ formed a separate group. Considering the Duncan test results, the inner bark and wood were in the same groups in *Robinia pseudoacacia* L. and *Cupressus arizonica* G. also, the inner bark and the outer bark of *Platanus orientalis* L. were in the same groups. It is noteworthy that the values obtained in the outer bark are many times higher than the values obtained in the inner bark and wood in all three species. The lowest value in the outer bark is obtained in *Cupressus arizonica* G. with 1909.8 ppm, the highest value is obtained in *Robinia pseudoacacia* L. with 3216.8 ppm, the highest value in the inner bark is obtained in *Platanus orientalis* L. with 6187.1 ppm, and the lowest value is obtained in *Cupressus arizonica* G. with 783.9 ppm. In the wood part, the lowest value is obtained in *Cupressus arizonica* G. with 472 ppm, and the highest value is obtained in *Platanus orientalis* L. with 1439.2 ppm. According to these results, it can be said that the lowest values are obtained in *Cupressus arizonica* G. and the highest values are obtained in *Platanus orientalis* L. The change in the K^+ concentration in woods depending on the age range and direction is given in Table 2.

When the values showing the change of K element according to the age range are examined, it is seen that the highest value in *Robinia pseudoacacia* L. is obtained with 3520.9 ppm in 2018–2020, the lowest value with 379.9 ppm in 1994–1996, the lowest value in *Cupressus arizonica* G. in 1997–1999 with 256.8 ppm, the highest value is obtained in the years 2015–2017 with 778.5 ppm, the highest value in *Platanus orientalis* L. with 3069.2 ppm in the years 2018–2020, and the lowest value with 982.1 ppm in the years 1997–1999. According to the analysis of variance results, it is determined that the variation of K concentration depending on the species is statistically significant at least 99.9% confidence level ($p<0.001$) in all age ranges. When the values are examined, it is very difficult to say that the K^+ concentration changes regularly based on species or year. This situation can be interpreted as the change of K^+ concentration in plants does not change primarily depending on the species or year, and other factors are more dominant.

DISCUSSION

In regions, where four seasons are observed, it was determined that the development of trees increased in parallel with several intakes of potassium (K) in their bodies [39]. Regarding this point, providing data about the nutrient accumulation in trees, tree rings and organs can give important information about the chronology of the atmospheric elements deposition in its ecosystem [40]. Although there are

Table 2. The K^+ concentration (ppm) age interval and species change of in wood

	Species			
Years	***Robinia pseudoacacia* L.**	***Cupressus arizonica* G.**	***Platanus orientalis* L.**	**F value**
2018–2020	3520.9 Cg	762.4 Ag	3069.2 Bh	34256.8*
2015–2017	610.2 Af	778.5 Bh	2093.0 Cg	44693.2*
2012–2014	562.6 Ae	773.4 Bh	1688.0 Cf	11214.3*
2009–2011	404.4 Abc	637.2 Be	1160.8 Ce	8293.5*
2006–2008	487.2 Ad	722.8 Bf	1064.6 Cc	2267.6*
2003–2005	591.6 Bf	449.0 Ad	999.9 Cb	15820.5*
2000–2002	393.6 Bab	339.6 Ac	1100.3 Cd	4085.8*
1997–1999	396.1 Bab	256.8 Ab	982.1 Ca	7985.1*
1994–1996	379.9 Ba	123.6 Aa	1169.8 Ce	6713.1*
1991–1993	420.2 Bc	125.8 Aa	1064.2 Cc	28405.3*
F Value	22130.5*	8467.0*	12896.2*	

*: Significant at $p<0.001$. Upper and lower letters differ significantly based on the Duncan test.

studies on the usability of accumulation in the rings of trees, there are few studies on the transfer of elements between the organs of trees [41]. The changes in the concentration of K^+ in organs of 3 different trees grown in the intense industrial zone in Kocaeli province by organs. They were determined by making use of *Robinia pseudoacacia* L., *Cupressus arizonica* G., and *Platanus orientalis* L. in the present study. It was aimed to evaluate the level of atmospheric K^+ accumulation in the inner bark, outer bark, and wood segments of the tree and to interpret if the K^+ concentrations in rings and organs varied by year. In this study, the change of potassium concentration in barks and wood of three species was found to be 783.9 ppm of *Cupressus arizonica* G. but to be 6187.1 ppm in that of *Platanus orientalis* L. in the inner bark. Similarly, the K^+ concentration was found to be 472 ppm in *Cupressus arizonica* G. but 1439.2 ppm in *Platanus orientalis* L. in wood. Accordingly, it can be stated that K^+ concentration significantly varied between the species.

In previous studies carried out on this subject, it was determined that the concentrations of many elements significantly varied by the species [42]. The accumulation of elements within the bodies of plants is closely related to the plant habitus and development [43]. Plant development is shaped by the mutual interaction between genetic structure and environmental conditions [44]. Hence, the factors influencing the genetic structure of plants directly influence the intake and accumulation of elements in plants and, since different species have different genetic structures, it is normal for species to have different levels of element accumulation [45]. Another important result achieved in this study is that the concentration of potassium significantly varied by organs in all the species. Examining all three species, the highest values were found in the outer bark and the lowest values in the inner bark.

Many studies reported that the element accumulations differed between the organs of the same plant [46]. Moreover, it was also determined that the differences between the organs could reach very high levels [47]. In previous studies, the lowest concentrations were generally found in wood and the highest ones in outer bark [48]. The reason for higher element concentration in outer barks when compared to other organs was reported to mainly be the structure of the organ, particle matters, and the contamination of these particles by elements. It was determined in studies carried out before, it was determined that the elements in air adhered to the surface of particles and enriched them in elements, and these elements adhered to the plant organs and increased the element concentrations in these organs. The rough surface of the outer bark makes it easier for particles to hold on these surfaces [49].

The atmospheric potassium deposition significantly varied between the woods forming in subsequent years and the difference can reach very high levels. For instance, the potassium concentration in the woods of *Robinia pseudoacacia* L. forming from 2015 to 2017 was found to be 610.2 ppm, whereas it was 3520.9 ppm for the woods forming from 2018 to 2020. This finding suggests that the transfer of the K element in wood can be very limited. Among the species examined in this study, the lowest proportion of change was observed in *Platanus orientalis* L. and the highest one in *Robinia pseudoacacia* L. on atmospheric potassium deposition. It suggests that, among these species, the species that is most suitable for monitoring the change of potassium concentration is *Robinia pseudoacacia* L. in an industrial area. The knowledge about the transfer of elements between the organs is, however, very limited in plants.

CONCLUSIONS

Plants are the main indicator of urban environmental pollution and they fulfill many ecologic, economic, and social functions in ecosystem services. Development and phenotypic characters of plants are shaped by the genetic structure and edaphic factors such as soil's structure and nutrient content and soil, as well as climatic factors such as light, temperature, and atmospheric deposition-precipitation. Hence, to understand regional pollution which spatial distribution information links to existing or future policy with regards to sustainable environmental pollution including air and soil. Atmospheric deposition influences plant development, it is necessary to determine the intake and accumulation of elements directly from the surrounding environment. Atmospheric deposition contains quantities of K^+ which can significantly affect the structure and development of plants. Biomonitoring the deposition of atmospheric K^+ concentration is the crucial method to present levels of other metals and toxic metals in the territorial environment. The result of this study provides biomonitoring of atmospheric metals deposition on plants that tell the level of their accumulation. Future research on atmospheric other metals deposition for the suitability of some commonly found species for biomonitoring should be investigated the spatial and temporal variation of industrial and high traffic areas.

DATA AVAILABILITY STATEMENT

The authors confirm that the data that supports the findings of this study are available within the article. Raw data that support the finding of this study are available from the corresponding author, upon reasonable request.

CONFLICT OF INTEREST

The authors declared no potential conflicts of interest with respect to the research, authorship, and/or publication of this article.

ETHICS

There are no ethical issues with the publication of this manuscript.

REFERENCES

[1] G.S. Cumming, A. Buerkert, E.M Hoffmann, E. Schlecht, S. von Cramon-Taubadel and T. Tscharntke, "Implications of agricultural transitions and urbanization for ecosystem services," Nature, Vol. 515, pp. 50–57, 2014. [CrossRef]

[2] D. Yılmaz and Ö. Işınkaralar, "Climate action plans under climate-resilient urban policies", Kastamonu University Journal of Engineering and Sciences, Vol. 7, pp. 140–147, 2021

[3] D. Yılmaz and Ö. Işınkaralar, "How Can Natural Environment Scoring Tool (Nest) be Adapted for Urban Parks?" Kastamonu University Journal of Engineering and Sciences, Vol. 7, pp. 127–139, 2021

[4] G. M. Barinova, D. V. Gaeva, and E. V. Krasnov, "Hazardous chemicals and air, water, and soil pollution and contamination," Good Health and Well-Being, pp. 255-266, 2020. [CrossRef]

[5] D. Hou, D. O'Connor, A.D. Igalavithana, D.S. Alessi, J. Luo, D.C. Tsang, D.L. Sparks, Y. Yamauchi, J. Rinklebe, and Y. S. Ok. "Metal contamination and bioremediation of agricultural soils for food safety and sustainability.," Nature Reviews Earth & Environment, Vol. 1(7), pp. 366–381, 2020. [CrossRef]

[6] X. Zhong, S. Joimel, C. Schwartz, and T. Sterckeman, "Assessing the future trends of soil trace metal contents in French urban gardens," Environmental Science and Pollution Research, Vol. 29, pp. 3900–3917, 2021. [CrossRef]

[7] A.R. Baker, M. Kanakidou, A. Nenes, S. Myriokefalitakis, P.L. Croot, R.A. Duce, Y. Gao, C. Guieu, A. Ito, T.D. Jickells, N.M. Mahowald, R. Middag, M.M.G. Perron, M.M. Sarin, R. Shelley, and D. Turner, R. "Changing atmospheric acidity as a modulator of nutrient deposition and ocean biogeochemistry," Science Advances, Vol. 7(28), pp. eabd8800, 2021. [CrossRef]

[8] E.A. Mikhailova, G.C. Post, M.P. Cope, C.J. Post, M.A. Schlautman, and L. Zhang, "Quantifying and mapping atmospheric potassium deposition for soil ecosystem services assessment in the United States," Frontiers in Environmental Science, Vol. 7, pp. 74, 2019. [CrossRef]

[9] C. Hafsi, A. Debez, and C. Abdelly, "Potassium deficiency in plants: effects and signaling cascades," Acta Physiologiae Plantarum, Vol. 36(5), pp. 1055-1070, 2014. [CrossRef]

[10] D. T. Britto, and H. J. Kronzucker, "Cellular mechanisms of potassium transport in plants," Physiologia Plantarum, Vol. 133(4), pp. 637–650, 2008. [CrossRef]

[11] M. Nieves-Cordones, R. Ródenas, A. Lara, V. Martínez, and F. Rubio, "The combination of K^+ deficiency with other environmental stresses: what is the outcome?" Physiologia Plantarum, Vol. 165(2), pp. 264–276, 2019. [CrossRef]

[12] S. Shabala, and I. Pottosin, "Regulation of potassium transport in plants under hostile conditions: implications for abiotic and biotic stress tolerance," Physiologia Plantarum, Vol. 151, pp. 257–279, 2014. [CrossRef]

[13] V. Römheld, and E.A. Kirkby, "Research on potassium in agriculture: needs and prospects," Plant and Soil, Vol. 335(1), 155–180, 2010. [CrossRef]

[14] J. Sardans, and J. Peñuelas, "Potassium: a neglected nutrient in global change," Global Ecology and Biogeography, Vol. 24(3), pp. 261–275, 2015. [CrossRef]
[15] E. Mikhailova, M. Cope, G. Groshans, C. Post, M. Schlautman, and L. Zhang, "Contribution of atmospheric deposition to soil provisioning ecosystem services in the contiguous United States: Part 1 Calcium," ProScience, Vol. 5, pp. 58–68, 2018.
[16] A.N.M. Roseli, T.F. Ying, and N. Osman, "Changes in leaf thickness, chlorophyll content, and gas exchange of a landscape tree, Xanthostemon Chrysanthus, treated with paclobutrazol and potassium nitrate," Arboriculture & Urban Forestry, Vol. 47(2), 2021. [CrossRef]
[17] M. Wang, Q. Zheng, Q. Shen, and S. Guo, "The critical role of potassium in plant stress response," International Journal of Molecular Sciences, Vol. 14(4), pp. 7370–7390, 2013. [CrossRef]
[18] P. Shults, P. Nzokou, and I. Koc, "Nitrogen contributions of alley cropped Trifolium pratense may sustain short rotation woody crop yields on marginal lands," Nutrient Cycling in Agroecosystems, Vol. 117(2), pp. 261–272, 2020. [CrossRef]
[19] I. Koc, "Using Cedrus atlantica's annual rings as a biomonitor in observing the changes of Ni and Co concentrations in the atmosphere," Environmental Science and Pollution Research, pp. 1-7, 2021.
[20] J. Guo, Y. Jia, H. Chen, L. Zhang, J. Yang, J. Zhang, and Y. Zhou, "Growth, photosynthesis, and nutrient uptake in wheat are affected by differences in nitrogen levels and forms and potassium supply," Scientific Reports, Vol. 9(1), pp. 1–12, 2019. [CrossRef]
[21] D.K. Jaiswal, J.P. Verma, S Prakash, V.S. Meena, and R.S. Meena, "Potassium as an important plant nutrient in sustainable agriculture: a state of the art," Potassium Solubilizing Microorganisms for Sustainable Agriculture, pp. 21-29, 2016. [CrossRef]
[22] A. Wakeel, M. Farooq, M. Qadir, and S. Schubert, Potassium substitution by sodium in plants. Critical reviews in plant sciences, Vol. 30(4), pp: 401-413, 2011. [CrossRef]
[23] Y. Xing, J. Bubier, T. Moore, M. Murphy, N. Basiliko, S. Wendel, and C. Blodau, "The fate of 15 N-nitrate in a northern peatland impacted by long term experimental nitrogen, phosphorus and potassium fertilization," Biogeochemistry, Vol. 103(1), pp. 281–296, 2011. [CrossRef]
[24] C. Zörb, M. Senbayram, and E. Peiter, "Potassium in agriculture–status and perspectives," Journal of Plant Physiology, Vol. 171(9), pp. 656–669, 2014. [CrossRef]
[25] D.W. Dibb, and W.R. Thompson Jr, "Interaction of potassium with other nutrients," Potassium in Agriculture, pp. 515–533, 1985. [CrossRef]
[26] D.A. Manning, "Mineral sources of potassium for plant nutrition. A review," Agronomy for Sustainable Development, Vol. 30(2), pp. 281–294, 2010. [CrossRef]
[27] N. C Brady, and R.R. Weil, "The nature and properties of soils," 13th ed., Pearson Education, London, 2002.
[28] F. Bilias, and N. Barbayiannis, "Potassium availability: an approach using thermodynamic parameters derived from quantity-intensity relationships," Geoderma, Vol. 338, pp. 355–364, 2019. [CrossRef]
[29] I.E. Bruteig, "The epiphytic lichen Hypogymnia physodes as a biomonitor of atmospheric nitrogen and sulphur deposition in Norway," Environmental Monitoring and Assessment, Vol. 26(1), pp. 27–47, 1993. [CrossRef]
[30] H. Schulz, P. Popp, G. Huhn, H.J. Stärk, and G. Schüürmann, "Biomonitoring of airborne inorganic and organic pollutants by means of pine tree barks. I. Temporal and spatial variations," Science of the Total Environment, Vol. 232, 49–58, 1999. [CrossRef]
[31] L., Morselli, E., Bernardi, I., Vassura, F., Passarini, and E. Tesini, "Chemical composition of wet and dry atmospheric depositions in an urban environment: local, regional and long-range influences," Journal of Atmospheric Chemistry, Vol. 59(3), pp. 151–170, 2008. [CrossRef]
[32] K. Isinkaralar, and R. Erdem, "Landscape plants as biomonitors for magnesium concentration in some species," International Journal of Progressive Sciences and Technologies, Vol. 29(2), 468-473, 2021.
[33] W.E.O Ghoma, H. Sevik, and K. Isinkaralar, "Using indoor plants as biomonitors for detection of toxic metals by tobacco smoke," Air Quality, Atmosphere & Health, 2022. [CrossRef]
[34] K. Işınkaralar and R. Erdem, "Changes of calcium content on some trees in Kocaeli", Kastamonu University Journal of Engineering and Sciences, vol. 7, pp. 148–154, 2021
[35] M. Çetin, H. Şevik, A. Türkyılmaz and K. Işınkaralar, "Using abies's needles as biomonitors of recent heavy metal accumulation," Kastamonu University Journal of Engineering and Sciences, Vol. 7, pp. 1–6, 2021.
[36] N. M. Mahowald, R. Scanza, J. Brahney, C.L. Goodale, P.G. Hess, J.K. Moore, and Neff, J. "Aerosol deposition impacts on land and ocean carbon cycles," Current Climate Change Reports, Vol. 3(1), pp. 16–31, 2017. [CrossRef]
[37] B. Wolterbeek, "Biomonitoring of trace element air pollution: principles, possibilities and perspectives," Environmental Pollution, Vol. 120(1), pp. 11-21, 2002. [CrossRef]
[38] USEPA E (1996) Method 3052: Microwave assisted acid digestion of siliceous and organically based

matrices. United States Environmental Protection Agency, Washington, DC USA.

[39] B. Nemzer, F. Al-Taher, and N. Abshiru, "Phytochemical composition and nutritional value of different plant parts in two cultivated and wild purslane (Portulaca oleracea L.) genotypes," Food Chemistry, Vol. 320, pp. 126621, 2020. [CrossRef]

[40] M. E. Conti, and G. Cecchetti, "Biological monitoring: lichens as bioindicators of air pollution assessment—a review," Environmental Pollution, Vol. 114(3), pp. 471–492, 2001. [CrossRef]

[41] A. Turkyilmaz, H. Sevik, K. Isinkaralar and M. Cetin, "Using Acer platanoides annual rings to monitor the amount of heavy metals accumulated in air," Environmental Monitoring and Assessment, Vol.190, pp. 578, 2018. [CrossRef]

[42] B. Aricak, M. Cetin, R. Erdem, H. Sevik and H. Cometen, "The change of some heavy metal concentrations in Scotch pine (Pinus sylvestris) depending on traffic density, organelle and washing," Applied Ecology and Environmental Research, Vol. 17(3), pp. 6723–6734, 2019. [CrossRef]

[43] D. Güney, E. Seyis, F. Atar, A. Bayraktar and İ. Turna, "Effects of some nitrogen-fixing plants on seedling growth of scotch pine," Turkish Journal of Forestry, Vol. 20(4), pp. 284-289, 2019. [CrossRef]

[44] D. Güney, Z. Yahyaoglu, A. Bayraktar, F. Atar and I. Turna, "Genetic diversity of Picea orientalis (L.) Link populations in Turkey," Šumarski list, Vol. 143(11-12), pp. 539–547, 2019. [CrossRef]

[45] H. Sevik, M. Cetin, H.U. Ozel, H.B. Ozel, M.M.M. Mossi and I.Z. Cetin, "Determination of Pb and Mg accumulation in some of the landscape plants in shrub forms," Environmental Science and Pollution Research, Vol. 27(2), pp. 2423–2431, 2020. [CrossRef]

[46] T. Karacocuk, H. Sevik, K. Isinkaralar, A. Turkyilmaz and M. Cetin, "The change of Cr and Mn concentrations in selected plants in Samsun city center depending on traffic density," Landscape and Ecological Engineering, Vol. 18(1), pp. 75–83, 2022. [CrossRef]

[47] D.S. Savas, H. Sevik, K. Isinkaralar, A. Turkyilmaz and M. Cetin, "The potential of using Cedrus atlantica as a biomonitor in the concentrations of Cr and Mn," Environmental Science and Pollution Research, Vol. 28, pp. 55446–55453, 2021. [CrossRef]

[48] A. Turkyilmaz, M. Cetin, H. Sevik, K. Isinkaralar and E.A.A. Saleh, "Variation of heavy metal accumulation in certain landscaping plants due to traffic density," Environment, Development and Sustainability, Vol. 22(3), pp. 2385–2398, 2020. [CrossRef]

[49] H. Sevik, "The variation of chrome consantration in some landscape plants due to species, organ and traffic density," Turkish Journal of Agriculture-Food Science and Technology, Vol. 9(3), pp. 595-600, 2021. [CrossRef]

Environ Res Tec, Vol. 5, Issue. 1, pp. 101–110, March 2022

Environmental Research and Technology
https://ert.yildiz.edu.tr - https://dergipark.org.tr/tr/pub/ert
DOI: https://doi.org/10.35208/ert.969400

Environmental Research & Technology

Research Article

Use of a convolution neural network for the classification of *E. Coli* and *V. Cholara* bacteria in wastewater

Tohid IRANI[1], Hamid AMIRI*[2], Sama AZADI[3], Mohsen BAYAT[4], Hedieh DEYHIM[1]

[1]*Department of Civil Engineering, Shiraz Payam Noor University, Shiraz, Iran*
[2]*Department of Civil and Environmental Engineering, Tarbiat Modares University, Tehran, Iran*
[3]*Department of Civil and Environmental Engineering, Ferdowsi University, Mashhad, Iran*
[4]*Department of Electronic Engineering, National University of Ireland, Maynooth, Ireland*

ARTICLE INFO

Article history
Received: 11 July 2021
Revised: 25 January 2022
Accepted: 31 January 2022

Key words:
Classification; Convolution neural network; *E. coli*; *V. cholera*; Wastewater bacteria

ABSTRACT

Identifying the microbial population and type of them is a crucial measure in the water and wastewater treatment processes, reuse of wastewater, and sludge treatment system. Todays, manual methods are usually used to count and detect the type of bacteria in water and sewage laboratories which mostly suffer from human errors. This study aims at presenting an accurate method based on image analysis through the convolution neural network (CNN) to classify *Escherichia coli* (*E. coli*) and *Vibrio cholera* (*V. cholera*) bacteria, in wastewater. About 9,000 Red-Green-Blue (RGB) microscopic images of the sewage sample containing the stained bacteria were used as the input datasets. The results showed that the bacteria would be classified and counted with the accuracy of 93.01% and 97.0%, respectively. While CNN performed pretty well in counting the number of bacteria for both RGB and grayscale color models, its classification performance is only satisfactory in the RGB images. The sensitivity analysis of CNN illustrated that the Gaussian noise enhancement caused to the increment in the standard deviation (σ) that proportionally decreased the CNN accuracy.

Cite this article as: Irani T, Amiri H, Azadi S, Bayat M, Deyhim H. Use of a convolution neural network for the classification of *E. Coli* and *V. Cholara* bacteria in wastewater. Environ Res Tec 2022;5:1:101–110.

INTRODUCTION

Contamination identification, efficiency evaluation of the wastewater treatment system, and reusability of treated wastewater are basic principles of the microbial monitoring in the contaminated water resources with human wastewater [1–4]. In fact, according to the world health organization (WHO) guidelines, the main goal is preventing the water resources from contaminating by any type of pathogenic bacteria. One effective solution to this issue is the indicator microorganisms' contamination tests. For instance, existing the *E. coli* bacteria in the water samples has been considered as a fecal pollution indicator due to its ease and rapid detection [5, 6]. Traditionally, the manual method is used

***Corresponding author.**
*E-mail address: hamid64amiri@gmail.com

to count the number of cultured colonies to determine the amount of fecal pollution in water samples [7]. This method not only is time and energy consuming, but also suffers from the human errors [8]. Large number of samples as well as small size and overlapping on colonies, and diversity and large number of colonies formed in a sample are the most common reasons to make errors in this method [8–10].

Recently, employing the convolution neural network (CNN) along with the computer processing power has been playing an increasing role in the field of deep learning [11]. Some interesting applications of this method are in the environmental science, cancer detection, medical image processing. The interesting results in these applications are provided by the possibility of employing deeper layers in comparison with other artificial neural networks (ANN) [4, 12–15]. So far, CNN in measuring the concentration of cyanobacteria in water [16], pollution of the water distribution network [17], detection of water impurities [18], classification of urban wastewater microbeads [19], etc. have been studied. Akbarian Mymand et al. (2014), studied the feasibility of using an image processing method for the count of bacteria in the mixture of Quail flora, sourdough, and kefir drinks. They compared this method with colony counter method in the different dilution proportions. The results of this study indicated a significant difference between the numbers of counted bacterial in samples with low dilution proportion [20]. Huang and Wu (2018) classified the clinical bacterial colonies with different morphologies into 18 categories by a deep neural network (DNN)-based classifier. They obtained over 90% identification and classification accuracy of each bacterium category [21]. Yurtsever and Yurtsever (2018) achieved 89% accuracy to classify microbeads in the wastewater by CNN [19]. Shaily and Kala (2020) classified various shapes of bacterial particles in 20 different categories with more than 99% accuracy [22]. According to a previous study, CNN effectively improves the detection and counting accuracy of the bacterial particles [23].

In this study, by employing the capabilities of this method, we try to obtain a very high accurate classifier to identify the aforementioned bacteria in sewage. For this purpose, we design a two-part network which exploits the K-means and new data producing methods to prepare images which followed by a CNN to classify the data. First, the input images contain three components of RGB images with the resolution of 749x1000 pixels are used as the primary datasets for both bacteria. About 150 images per bacterium are considered as an initial number for the training set, which is increased to 9,000 to have more generalized dataset. One way of overfitting prevention is increasing the data which is obtained by some specific operations, such as adding Gaussian noise, rotating images at a 90o angle, upside down flip, left right flip and so on. Then, K-means clustering algorithm is used to image segmentation and masking. Finally, the prepared images are exploited as the input dataset to the CNN, and the reliability of this method is evaluated by the sensitivity analysis.

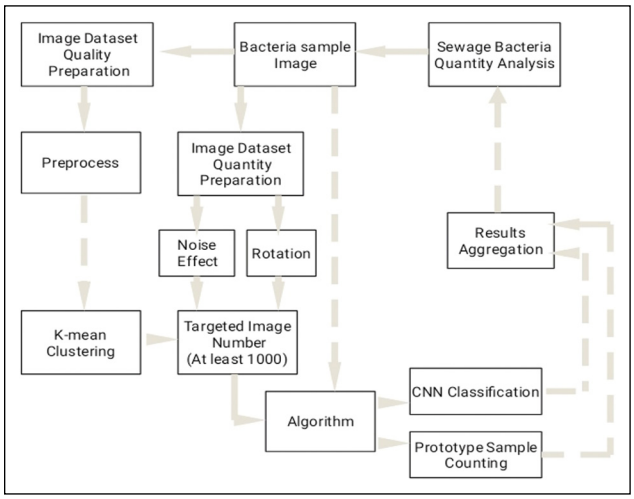

Figure 1. Main steps diageram.

METHOD AND MATERIAL

Overview

In this study, the *E. coli* and *V. cholera* bacteria image dataset is obtained from the central water and wastewater laboratory of Ardabil University of medical science. These images are 1000×749-pixel sized in the RGB color model. The main steps of this study are shown in Figure 1. K-means clustering algorithm is employed to sparse and keep only few meaningful features in the input images as an input unit for the next network (Fig. 2). This helps to have a clear separation between features which makes the classification more accurate. Furthermore, different techniques, such as image 90° rotation, upside-down flip, left-right flip, and Gaussian noise are used to generate new input images in the datasets for training and validation of CNN. Then, the input layer in the CNN will be a multidimensional array including 1000x749x3 units that will be employed to train the network for the bacteria classification and counting. It is worth noting that the applied images are in both RGB and Grayscale models that generalizes the proposed method for different color models.

Bacteria Specifications

E. coli is an anaerobic Gram-negative bacterium considered as an indicator to identify fecal pollution in the water resources. It is also applied to evaluate the performance of the disinfection system in the wastewater treatment plants and reusing effluent for irrigation. According to the WHO guideline, the allowable limit of this pollutant varies depending on the type of usage. For example the maximum acceptable level of *E. coli* for recreation water use and general irrigation, recommended less than 385 and 1000 MPN/100ml, respectively [24]. The morphology of *E. coli* similar to most of the gram-negative bacteria bacillus is in rod shape (Fig. 3).

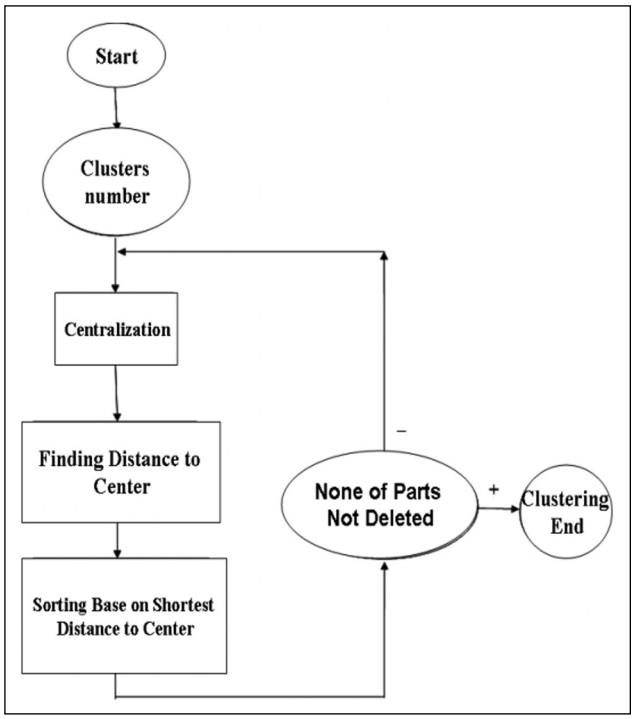

Figure 2. K-means clustering algorithm.

V. cholera is a Gram-negative comma shape bacterium which has been widely distributed in the water environment [25, 26]. Figure 3 shows a *V. cholera* bacterium with a length and width of 2.7-3.5 μm and 0.36-0.4 μm, respectively. This bacterium can be transmitted to the human intestine through fruits and vegetables irrigated with water polluted with this bacterium.

Image Preprocessing

Generally, image is a matrix that pixels are its entries that the values of these entries show the intensity of each pixel in the image. Image processing includes methods to enhance the quality of an image, and search to extract the relevant information in order to the following analysis in an algorithm. Firstly, the quality of image is improved by filtering unwanted effects, such as noises, lights, etc. Noise capturing filters are mostly categorized from the simple average and median filters to the more complicated Gaussian and adaptive filters [27]. Next step is image segmentation to keep the most meaningful information in it. There are also several approaches to image segmentation and masking, such as K-means clustering, threshold algorithm, watershed algorithm, neural network, and deep learning methods [23]. Since this study is aimed on two categories of bacteria, preprocessed images of each category imported as the input data to the CNN. In this study, the gram-negative bacteria considered as red/violet-color cells. All images used in RGB (Red, Green, and Blue) and grayscale modes and operations repeated for each mode. MATLAB 2015 Image Processing Toolbox used for CNN operation while supported with the Visual Studio 2013.

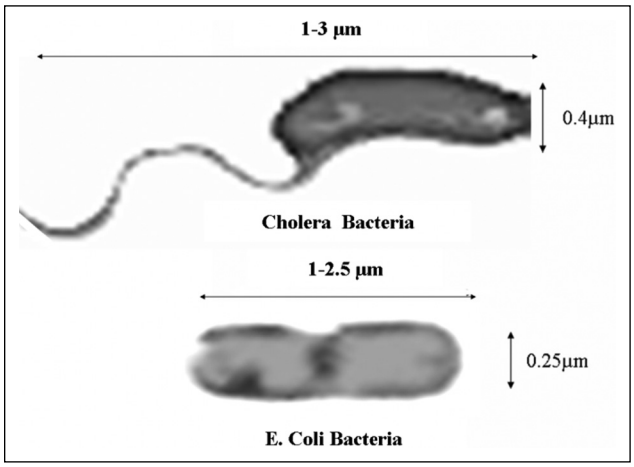

Figure 3. *E. coli* and *V. cholera* bacteria morphology.

K-means Clustering

The approach of clustering is partitioning a set of data to some clusters. K-means clustering labels each pixel of the image to a cluster with the nearest mean or shortest distance to the center of that cluster. In fact, it finds the optimum point of data by minimizing the following error function.

$$J = \sum_{i} D^2.(X, C_i), \quad (1)$$

where D is the distance of C_i as the center of i^{th} cluster in the data group X. Different distance measures, such as Euclidean and Manhattan distances can be exploited in the K-means clustering [28]. Generally, K-means clustering algorithm includes four following steps:

1- Inserting random means within the data.

2- Calculating distance of each data to the means and assigning the data to the nearest group.

3- Calculating the new mean of each group.

4- Repeating the steps 2 and 3 to converge to the target.

K-means here is applied for segmenting and masking bacteria shapes within the images. All images are segmented and masked with K-means clustering algorithm accurately. Particularly, each image is divided into two separated background and foreground parts which the former is bacteria-shaped area, and the latter is black-colored area. The bacteria-shaped area contains intensity and position of each pixel which will be used as the input of CNN for both categories of bacteria. Figure 4 shows image masking in the RGB and grayscale modes.

Convolution Neural Network (CNN)

Convolution neural network as a kind of feed forward neural network and deep learning method uses a Perceptron network with some changes on classic operation. This network is based on four characteristics which have

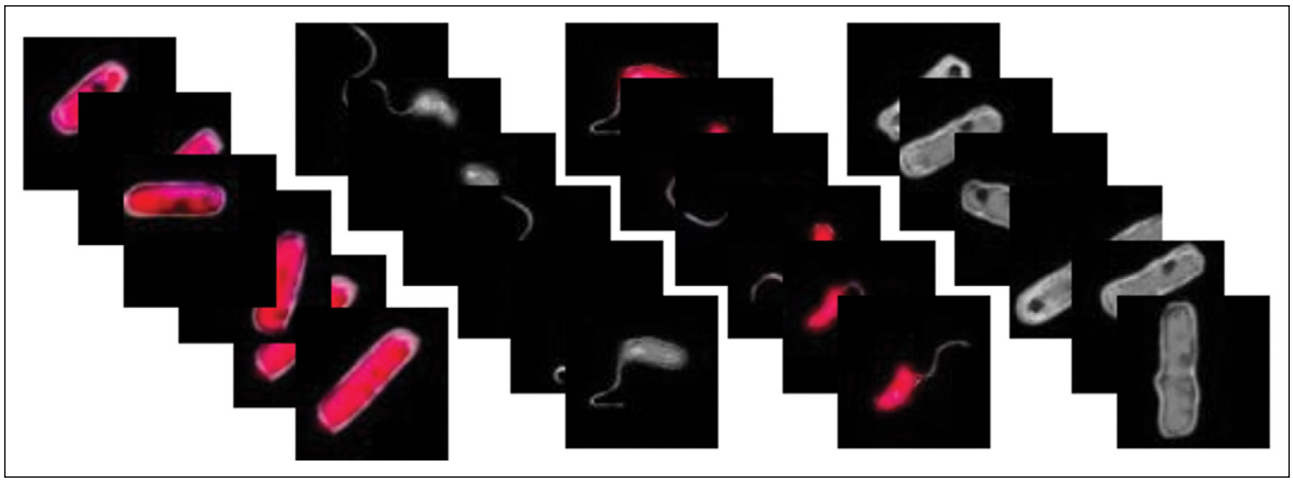

Figure 4. Masked and segmented bacteria images (RGB, grayscale).

been implied from natural signals. Therefore, CNN can be applied to the process of natural signals and multi-dimensional matrices. This characteristic includes neurons near communications, layer common weights, using numbers of layer and polling ability [29]. CNN formed in layers includes convolution layers, polling layer and fully connected layer and sub layers. Each layer connects to prier layers base on the weight. Non-linear functions and activation functions include sigmoid function or ReLU functions applied to import sum of neurons' weight in each layer. These layers extract near specification of images or in other situation continuity of common specifications. Maximum values of vicinity choice to reduce the dimension of data and summarize extracted image specifications. Each CNN contains layers for the convolution and polling operation. Layers exploit ReLU non-linear functions. Each weight of layers calculates by back propagation method [30]. Dense layer with the fully connected layer used for this study to extract specifications and assorting the data. Finally, the classified results of the dense layer are considered as the outputs. The CNN with seven major layers and sub-layers used for this study CNN structure, see Figure 5.

Equation 2 defines CNN output layer operation function (f)

$$Y_{w,h,m} = f(Y_{w,h,m}) = f\left(\sum_{i=(w-1)s+1}^{(w-1)s+k} \sum_{j=(h-1)s+1}^{(h-1)s+k} \sum_{K=1}^{N} W_{k,m} x_{i,j,k} + b_m\right), \quad (2)$$

where $Y_{w,h,m}$ regards as convolution output layer with the dimension of h, w and m. Parameters bm and $W_{k,m}$ are neurons bios and weights, respectively. The input of the network is $x_{i,j,k}$ as $(i,j)^{th}$ pixel of the k^{th} component of an RGB image.

A pooling layer as a sub-sampling layer is exploited after every convolution layer to summarize specifications and bold characteristics of the previous layer. In fact, accuracy in characteristics improves the training operation accuracy. In this regard, two possible sub-sampling strategies in this layer are maximum pooling and average pooling.

RESULTS AND FINDING

Images and CNN Layers

The images after noise reduction and removing unwanted lights rectified by the average filter. Then, the preprocessed images masked and segmented by the K-means clustering algorithm. In this step, 150 extracted bacteria units extracted to categorize each bacterium. Furthermore, the number of images in the primary dataset increased to train and validate the CNN. Rotation process employing 90° rotation, upside-down flip, and left-right flip, in collaboration with Gaussian noise addition used to increase the number of images in the dataset, see Fig 6 and 7. The resulted 9,000 units of data in the size of 85×85-pixel considered as the input layer in the CNN.

Input image dataset included both RGB and grayscale modes. Size of images regarded 85×85 pixels while other image sizes like 64×64-pixel and 125×125-pixel had relatively poor results. In fact, the dimension of the images in the input layer for RGB and grayscale modes are subsequently 85×85×3 and 85×85×1.

Counting algorithm is employed to count the number of bacteria in each microscopic image. In addition to the input layer, the network has three convolutional, pooling, fully connected layers. The trend of CNN operation includes epochs of training, frequency of validation and rate of learning. The algorithm chose 70.0% of the dataset for the training procedure including 6300 images per each labeled category of *E. coli* and *V. cholera*. It also selected 30.0% or 2700 images of the dataset as the validation set. Furthermore, for counting the number of bacteria, image ingredient counting algorithm used in the CNN.

Classification

Primary results of the CNN revealed that although the grayscale images due to the smaller size had a faster training/validation, the accuracy of that was poor. However, the

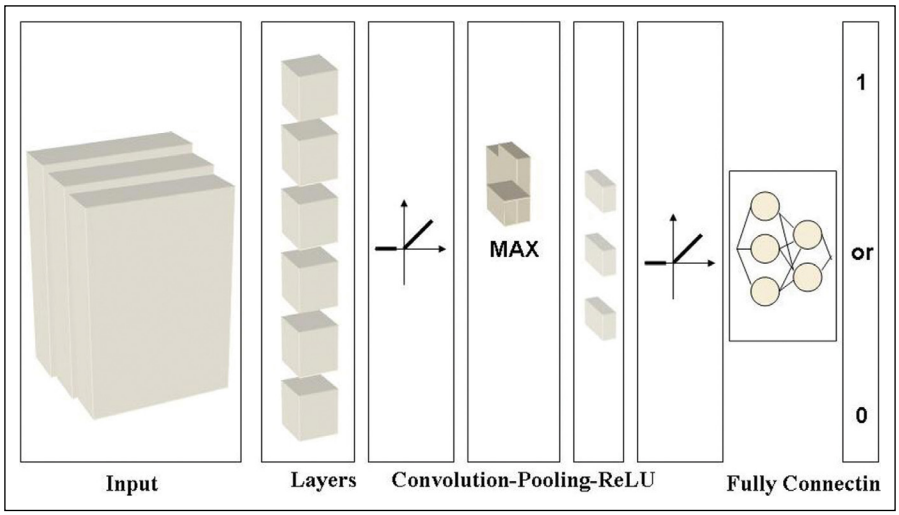

Figure 5. CNN structure.

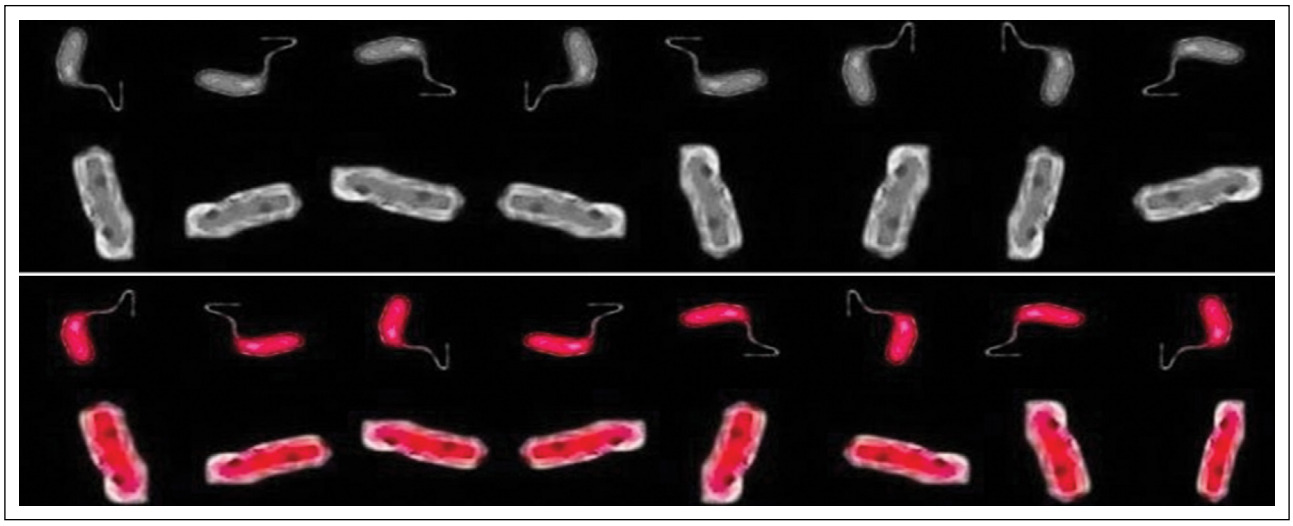

Figure 6. Masked and segmented images rotation.

RGB mode provided more data in the different color channels which resulted in higher accuracy in the cost of higher training/validation time. Color model of the images as the basic parts of this procedure are determinative factor for the bacteria classification. Since the RGB images contain more data, it provides better performance in the classification. Thus, training/validation in the grayscale space achieved 59.0% accuracy while RGB mode provides higher performance in the training/validation with accuracy of 93.01%. These results show the outstanding performance of the CNN in the classification of wastewater bacteria for the RGB images. Table 1 presents the training/validation results.

CNN training set exploited 6300 images for each bacterium and totally 12,600 images in the training procedure. CNN reached to the best point of the training in the 246th repetition. Results show that the CNN operation accuracy achieves 93.01% with least squares error (LSE) of 0.087 in the RGB mode. Figure 8 shows how the proposed method meets the highest accuracy in the RGB mode classification. Last optimizing point achieved in 246th training and validation repetitions. Figure 9 illustrates the LSE convergence of the method which is saturated at the 246th iteration with the error of 0.087.

Table 1. Training and validation results

Parameter	RGB	Grayscale
Accuracy (training - validation)	93.01%	59%
Error (training - validation)	0.087	1.9

Table 2. CNN counting results

Parameter	RGB	Grayscale
Accuracy	97%	97%
Error	0.03%	0.03%

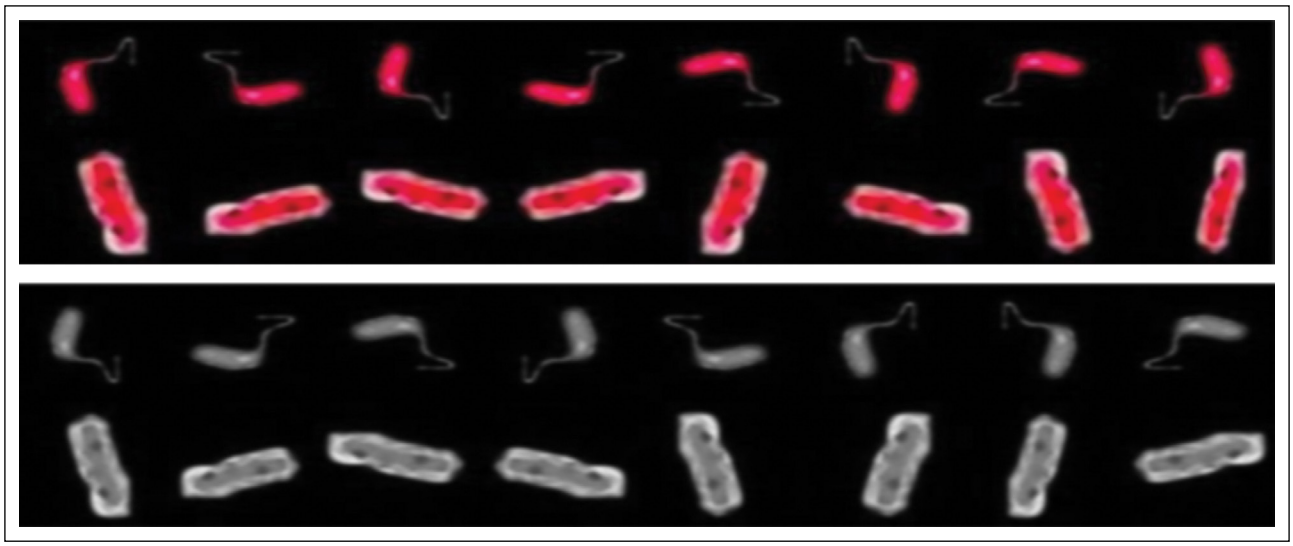

Figure 7. Adding Gaussian noise (σ=30) to images after rotation.

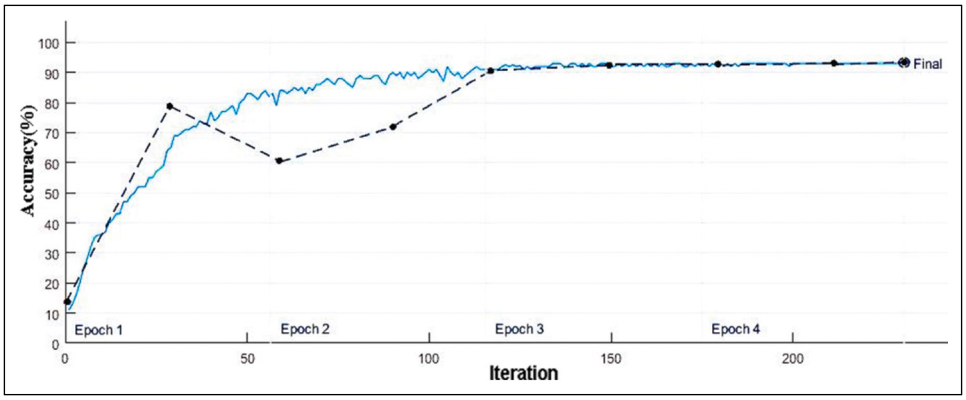

Figure 8. Procedure of accuracy optimizing (RGB), training, validation.

Counting Sample Bacteria

Images ingredient counting algorithm used to count the number of bacteria in the CNN. This algorithm employs "Morphological opening" operations to keep each bacteria shape skeleton. Per each defined morph of bacteria up counter counted to add number to counter clipboard. Procedure is repeating for all morphs to the end. Total values of counter regarded as number of the bacteria for each microscopic image of bacteria. Figure 10 and 11 show the counting procedure of the microscopic sample image. This section of CNN operation's result achieved 97.0% of accuracy. Related results are presented in the Table 2.

Sensitivity Analysis

Sensitivity analysis used to evaluate the effects of the images' quality on the accuracy. Different situation regarded as changes in primary image to increase numbers to 9,000 images for each category. These situations including normal images, image 90° rotation, upside-down flip images, and left-right flip images while Gaussian's noise (σ) added to them. Accuracy of results evaluated for each situation. Enhancing the Gaussian noise caused to higher standard deviation (σ) per pixel. Standard deviation relates directly to the histogram width or variance of the dataset. Figure 12 shows noise enhancement and histogram changes and the results of the sensitivity analysis are in the Table 3.

Figure 13 illustrates the effect of the Gaussian noise on four states of the images. The result reveals the inverse relation between the Gaussian noise and system accuracy. Generally, enhancing the gaussian noise totally decreases the CNN accuracy.

DISCUSSION

According to this study, microbial monitoring is used to analysis water, wastewater, and other water resources with high efficiency. Furthermore, evaluating wastewater treatment analysis efficiency is important. CNN model helps to analysis wastewater ingredients through the image processing methods. Monitoring the ingredients helps to analysis the qualities and effects of waste-

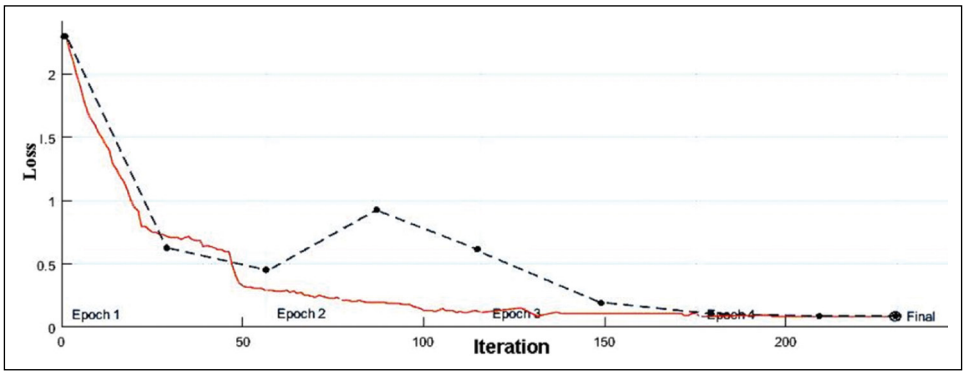

Figure 9. Procedure of error optimizing (RGB), training, validation.

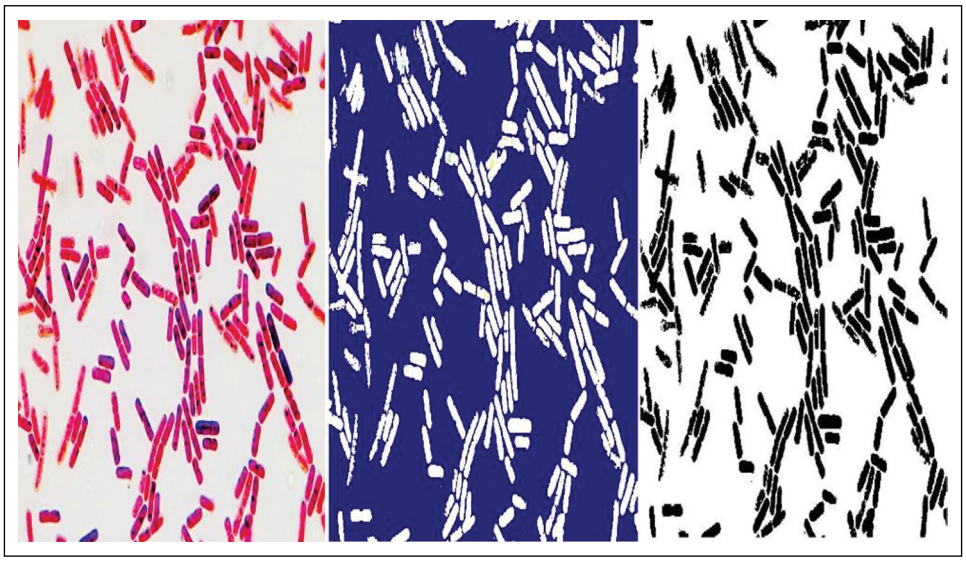

Figure 10. *E. coli* counting processing procedure.

water secondary uses on the environment and human. In this study, CNN analysis used as the major approach to classify and count the bacteria in the wastewater. All operations in the CNN have been used in a fast and inexpensive manner while results achieved to high accuracy. Along with the computer processing improvement and in combination with the artificial intelligent development, new methods are competing as well with classic approaches and even are advance rather than classic approaches. This study used classification and counting bacteria simultaneously as a new method for the RGB and grayscale modes dataset. All operations are applicable to other types of the bacteria as well.

Using two categories of bacteria improves the CNN promptitude in comparison to high number of the bacteria categories. This point regarded to evaluate the CNN operation fast and remake it for better operation. Grayscale mode achieved poor accuracy in comparison to the RGB mode while counting results were equal. Increasing the number of images will improve the performance of the CNN. Clear images in the large datasets of bacteria are ideal cases but in common situations different sort of images in variety range of qualities are available. Hence, removing Gaussian noise will be such as overfit results with high accuracy of classification only in the high-quality image datasets. Therefore, providing a variety of different images in the dataset will be logical solution to elate the deep learning procedure.

The CNN used in this study made in seven layers and sub-layers, and the operation showed flexible performance in comparison to the pre-trained CNN, such as AlexNet, VGGNet, ResNet, etc. Pre-trained CNN uses more layer of convolution to achieve high accuracy of classification. These kinds of the convolution neural networks are not easily adaptable to the different cases of datasets and require more time and high-performance hardware to train and validate the datasets.

Result of sensitivity analysis verified the Gaussian noise has an inverse relation with the accuracy. Upside-down flip images took most effect of the Gaussian noise with poor accuracy of 58.0% while left-right flip images had most similar results to the normal images.

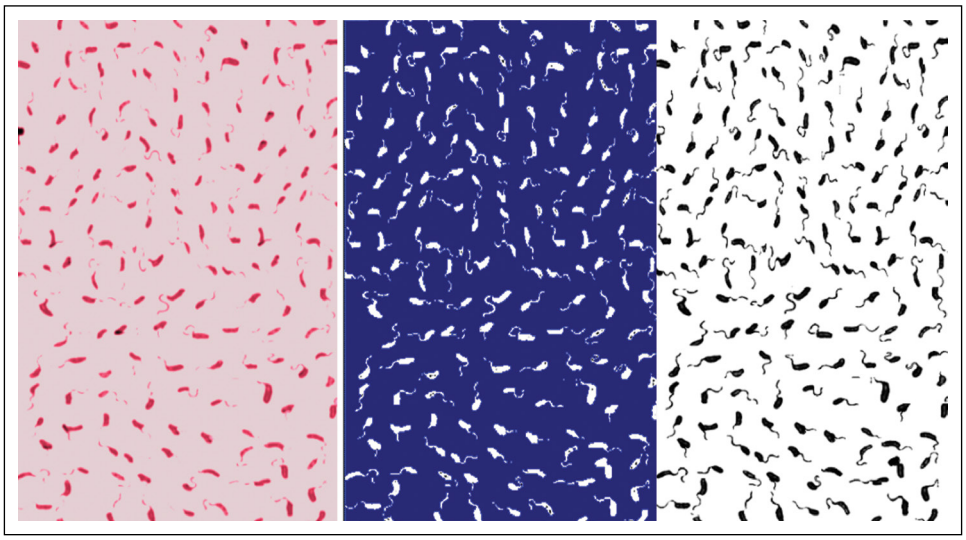

Figure 11. *V. cholera* counting processing procedure.

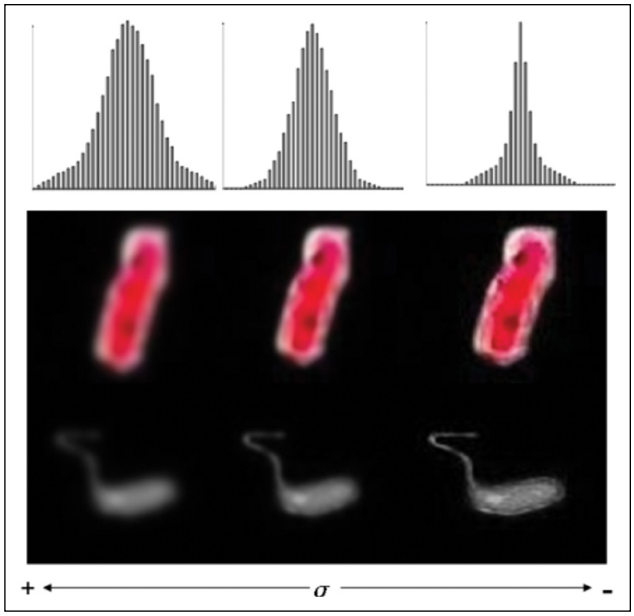

Figure 12. Gaussian noise histogram.

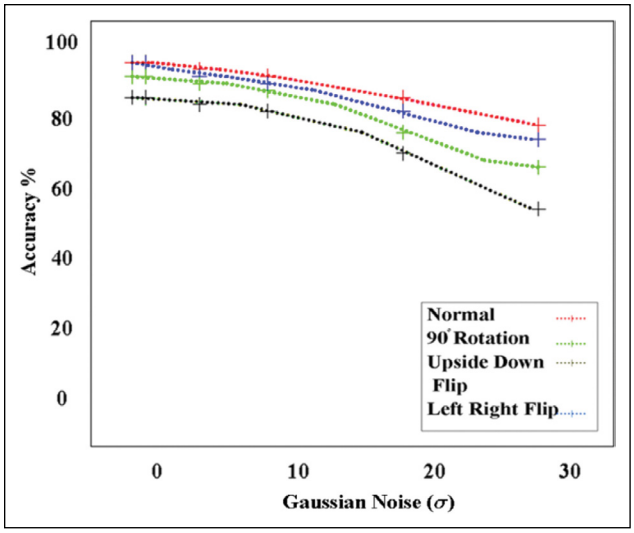

Figure 13. Plot of the sensitivity analysis.

CONCLUSION

This study used an image processing-based method through a CNN model in seven layers and sub-layers to classify and count bacteria in the RGB and grayscale images. *E. coli* and *V. cholera* bacteria considered as the most common bacteria and wastewater indicators.

From a computational viewpoint, this study verified the CNN performance for combining duties of classification and counting bacteria. The results revealed that the CNN model in the RGB mode achieved high efficiency with the accuracy of 93.01% and LSE of 0.087 to classify the bacteria. Also, counting results verified the CNN counting efficiency with accuracy of 97.0% for both RGB and grayscale images. The used method in this study can classify and count other bacteria which confirms the high flexibility of the model. Accuracy of 93.01% verifies high efficiency of classification in comparison with the pre-trained CNN with high number of layers and greater dataset. Moreover, all operations are faster and simple in use with low GPU system requirements.

Results of the sensitivity analysis indicated that Gaussian noise affects the performance of the CNN model. In the presence of the additive Gaussian noise (σ=30), upside-down flip images took most effect of that which resulted in decreasing the accuracy to 58.0%. Left-right flip and 90°-rotated images had most similar results to the normal images with the accuracy of 78.0% and 75.0%, respectively.

In principle, our study presents an inexpensive, fast, rather simple image processing-based method by employing the CNN. This method can be used to classify and count the

number of bacteria in the wastewater, and in the similar approach sort the microbial. Adapting the used CNN for the classification and counting samples can be beneficial in the wastewater treatment, education, and microbial researchers.

DATA AVAILABILITY STATEMENT

The authors confirm that the data that supports the findings of this study are available within the article. Raw data that support the finding of this study are available from the corresponding author, upon reasonable request.

CONFLICT OF INTEREST

The authors declared no potential conflicts of interest with respect to the research, authorship, and/or publication of this article.

ETHICS

There are no ethical issues with the publication of this manuscript.

REFERENCES

[1] S. Abtahi, R. Seyed Sharifi, and F. Qaderi, "Influence of nitrogen fertilizer rates and seed inoculation with plant growth promoting rhizobacteria (PGPR) on yield, fertilizer use efficiency, rate and effective grain filling period of soybean (Glycine max L.) in second cropping," Journal of Agricultural Science and Sustainable Production, Vol. 24, pp. 112–129, 2014.

[2] G. Medema, "Assessing microbial safety of drinking water," IWA Publishing, London, 2003.

[3] F. Qaderi, B. Ayati, and H. Ganjidoust, "Role of moving bed biofilm reactor and sequencing batch reactor in biological degradation of formaldehyde wastewater," Iranian Journal of Environmental Health Science and Engineering, Vol. 8, pp. 295–306, 2011.

[4] F. Qaderi, and E. Babanezhad, "Prediction of the groundwater remediation costs for drinking use based on quality of water resource, using artificial neural network," Journal of Cleaner Production, Vol. 161, pp. 840–849, 2017. [CrossRef]

[5] S.T. Odonkor, and J.K. Ampofo, "*Escherichia coli* as an indicator of bacteriological quality of water: an overview," Microbiology Research, Vol. 4, pp. 5–11, 2013. [CrossRef]

[6] F. Edition, "Guidelines for drinking-water quality," WHO Chronicle, Vol. 38(4), pp. 104-108, 2011.

[7] G. Bitton, "Wastewater microbiology," John Wiley & Sons, New York, 2005. [CrossRef]

[8] B. Jarvis,"Errors associated with colony count procedures," in Statistical Aspects of the Microbiological Examination of Foods. (Third Edition), Academic Press, pp. 119-140, 2016. [CrossRef]

[9] P. Houpikian, and D. Raoult, "Traditional and molecular techniques for the study of emerging bacterial diseases: one laboratory's perspective," Emerging Infectious Diseases Vol. 8, pp. 122, 2002. [CrossRef]

[10] B. Jarvis, A.J. Hedges, and J.E. Corry, "The contribution of sampling uncertainty to total measurement uncertainty in the enumeration of microorganisms in foods," Food Microbiology, Vol. 30, pp. 362–371, 2012. [CrossRef]

[11] A. Sayeed, Y. Choi, E. Eslami, Y. Lops, A. Roy, and J. Jung, "Using a deep convolutional neural network to predict 2017 ozone concentrations, 24 hours in advance," Neural Networks, Vol. 121, pp. 396–408, 2020. [CrossRef]

[12] F. A. Azis, H. Suhaimi, and E. Abas, "Waste Classification using Convolutional Neural Network," Conference Paper, ITCC 2020: 2020 2nd International Conference on Information Technology and Computer Communications, pp. 9–13, 2020. [CrossRef]

[13] J. Kalajdjieski, E. Zdravevski, R. Corizzo, P. Lameski, S. Kalajdziski, I.M. Pires, N.M. Garcia, and V. Trajkovik, "Air pollution prediction with multi-modal data and deep neural networks," Remote Sensing, Vol. 12, pp. 4142, 2020. [CrossRef]

[14] H. Pratt, F. Coenen, D.M. Broadbent, S.P. Harding, and Y. Zheng, "Convolutional neural networks for diabetic retinopathy," Procedia Computer Science, Vol. 90, pp. 200–205, 2016. [CrossRef]

[15] D. Tamiev, P.E. Furman, and N.F. Reuel, "Automated classification of bacterial cell sub-populations with convolutional neural networks," PloS One, Vol 15, Article e0241200, 2020. [CrossRef]

[16] A. Bahrani, B. Majidi, and M. Eshghi, Coral Reef Management in Persian Gulf Using Deep Convolutional Neural Networks, pp. 200-204, IEEE, 2019. [CrossRef]

[17] L. Sun, H. Yan, K. Xin, and T. Tao, "Contamination source identification in water distribution networks using convolutional neural network," Environmental Science and Pollution Research, Vol. 26, pp. 36786–36797, 2019. [CrossRef]

[18] A. Gupta, and E. Ruebush, "Aquasight: Automatic water impurity detection utilizing convolutional neural networks," arXiv preprint arXiv:1907.07573, 2019.

[19] M. Yurtsever, and U. Yurtsever, "Use of a convolutional neural network for the classification of microbeads in urban wastewater," Chemosphere, Vol. 216, 271–280, 2019. [CrossRef]

[20] J. Akbarian Mymand, S. Farji Kafshgari, A. Sadeghi Mahounak, S.A. Hoseyni Sharghi, and M. Vatan Khah, "Investigate the feasibility of using image processing method for the count of bacteria and comparison with Colony Counter," Iranian Journal of Medical Microbiology, Vol. 8, pp. 8–13, 2014.

[21] L. Huang, and T. Wu, "Novel neural network application for bacterial colony classification, Theoretical Biology and Medical Modelling, Vol. 15, pp. 1-16, 2018. [CrossRef]

[22] T. Shaily, and S. Kala, "Bacterial image classification using convolutional neural networks," IEEE 17th India Council International Conference (INDICON), pp. 1–6, 2020. [CrossRef]

[23] M. Talo, "An automated deep learning approach for bacterial image classification," arXiv preprint arXiv:1912.08765, 2019.

[24] R.S. Fujioka, H.M. Solo-Gabriele, and M.N. Byappanahalli, and M. Kirs, "US recreational water quality criteria: a vision for the future," International Journal of Environmental Research and Public Health Vol. 12, pp. 7752–7776, 2015. [CrossRef]

[25] S. Naidoo, and A.O. Olaniran, "Treated wastewater effluent as a source of microbial pollution of surface water resources," International Journal of Environmental Research and Public Health, Vol. 11, pp. 249–270, 2014. [CrossRef]

[26] P. Asadi, H.A. Rad, and F. Qaderi, "Comparison of Chlorella vulgaris and Chlorella sorokiniana pa. 91 in post treatment of dairy wastewater treatment plant effluents," Environmental Science and Pollution Research, Vol. 26, 29473–29489, 2019. [CrossRef]

[27] B. NIK, "Intensity Transformations and Spatial Filtering," 2005.

[28] J.A. Hartigan, and M.A. Wong, "AK-means clustering algorithm," Journal of the Royal Statistical Society: Series C (Applied Statistics), Vol. 28, pp. 100–108, 1979. [CrossRef]

[29] YJ Zhang, "A survey on evaluation methods for image segmentation," Pattern Recognition, Vol. 29, 1335–1346, 1996. [CrossRef]

[30] Y. LeCun, Y. Bengio, and G. Hinton, "Deep learning," Nature, Vol. 521, pp. 436–444, 2015. [CrossRef]